

Doctoral thesis

Doctoral theses at NTNU, 2024:141

Osama Abdelfattah Shawky Aly Hegeir

Moment-resisting timber frames combined with cross laminated timber walls for multistorey timber buildings

NTNU
Norwegian University of Science and Technology
Thesis for the Degree of
Philosophiae Doctor
Faculty of Engineering
Department of Structural Engineering



Norwegian University of
Science and Technology

Osama Abdelfattah Shawky Aly Hegeir

Moment-resisting timber frames combined with cross laminated timber walls for multistorey timber buildings

Thesis for the Degree of Philosophiae Doctor

Trondheim, April 2024

Norwegian University of Science and Technology
Faculty of Engineering
Department of Structural Engineering



Norwegian University of
Science and Technology

NTNU

Norwegian University of Science and Technology

Thesis for the Degree of Philosophiae Doctor

Faculty of Engineering

Department of Structural Engineering

© Osama Abdelfattah Shawky Aly Hegeir

ISBN 978-82-326-7876-1 (printed ver.)

ISBN 978-82-326-7875-4 (electronic ver.)

ISSN 1503-8181 (printed ver.)

ISSN 2703-8084 (online ver.)

Doctoral theses at NTNU, 2024:141

Printed by NTNU Grafisk senter

Preface

The present doctoral thesis has been submitted to the Norwegian University of Science and Technology (NTNU) in partial fulfilment of the requirements for the degree of Philosophiae Doctor (Ph.D.). This work has been carried out at the Department of Structural Engineering, NTNU, Trondheim. The work was supervised by Associate Professor Haris Stamatopoulos and Professor Kjell Arne Malo.

The author declares that this thesis and the appended papers have been written by him, and the related experiments and simulations have been conducted by him. The thesis contains no material that has previously been submitted for a degree at this university or any other institution.

This thesis is paper-based and contains three parts. Part I is an introductory part, Part II includes six appended papers, and Part III includes four appendices.

Osama Abdelfattah Hegeir

Trondheim, December 2023

Acknowledgments

My Ph.D. journey at the Norwegian University of Science and Technology (NTNU) has been an extraordinary experience, one that has not only shaped me but also put my capabilities to the test. Throughout my Ph.D., I have been fortunate to receive unwavering support from a multitude of individuals at NTNU, whose guidance and assistance I will always cherish.

I would like to express my deep gratitude to my supervisors Associate Professor Haris Stamatopoulos and Professor Kjell Arne Malo for giving me the valuable opportunity to carry out this interesting research. Their doors have always been open for questions and discussions, which has greatly facilitated my progress. I also thank them for improving the quality of my research and the knowledge imparted during my time at NTNU. Additionally, I extend my gratitude to all the members of the Timber Structures group at NTNU, Trondheim.

I am deeply grateful to my wife, daughter, mother, father, and brothers and sisters for their exceptional support. Their continuous encouragement has been instrumental in my success, and I am forever indebted to them for their presence throughout this journey.

Experimental work has been a significant component of this Ph.D. thesis, and I would like to express my sincere appreciation to all laboratory technicians who have provided invaluable help and assistance. Special thanks to Gøran Loraas, Terje Petersen, Johan Fagervold, Christian Jensen, Trond Auestad, and the laboratory manager Ragnar Moen. Their contributions have been vital to the successful execution of the experimental work.

Last but not least, I would like to appreciate the contribution of students Elisabeth Frette, Amund Heggheim, Thomas Munkeby, Haakon Flaten, Ulrik Sæther Langvik, Simen Kåre Bokalrud, Marius Bjørnholm, and Baktash Sadat in the preparation and the execution of the experiments.

Abstract

The increase in the world population results in higher urbanization, which poses a significant challenge due to the substantial contribution of construction industry to greenhouse gas emissions. The increased urbanization results in further increase in greenhouse gas emissions, leading to adverse environmental impacts. Consequently, the incorporation of sustainable building materials becomes imperative. Timber, as a renewable material, offers a viable alternative to concrete and steel in reducing the adverse environmental impact of construction activities.

Timber has a very good strength-to-weight ratio, attributed to its lightweight nature. However, the lightweight and moderate stiffness characteristics of timber buildings result in serviceability issues, particularly excessive lateral displacements and accelerations under service-level wind loading. Excessive lateral displacements can impact the functionality of buildings and cause damage to non-structural elements, while large accelerations may result in discomfort for occupants. Therefore, it is crucial to ensure that displacements and accelerations are within acceptable limits.

Lateral displacements can be reduced by increasing the lateral stiffness of the building, such as using stiffer connections. Wind-induced accelerations can be reduced by increasing the lateral stiffness of the building, the mass of the building, the damping, or a combination of these.

Lateral bracing with diagonal elements is widely used to provide the lateral stiffness for multistorey timber buildings. However, this requires substantial bracing elements that extend throughout the height of the building, potentially limiting architectural flexibility. A common alternative is the use of Cross Laminated Timber (CLT) walls as lateral load-resisting elements. Nevertheless, buildings with CLT walls tend to be material-intensive and characterized by cellular configurations.

Moment-Resisting Timber Frames (MRTFs) offer a viable option as a lateral load-resisting system for multistorey timber buildings. In MRTFs, the beam-to-column Moment-Resisting Connections (MRCs) provide the necessary lateral stiffness. Compared to buildings with diagonal bracing or CLT walls, MRTFs offer increased

open space and architectural flexibility. Additionally, incorporating stiff connections in timber floors can enhance their performance with respect to human-induced vibrations. Nevertheless, the use of MRTFs is less common in timber construction, mainly due to their flexibility. The stiffness of MRTFs can be enhanced by use of stiffer beam-to-column connections, thus making them more practical and feasible.

A feasibility study (Vilguts et al. 2021) of MRTFs using Glued Laminated Timber (glulam) has shown that they can hardly be used for more than 8 storeys with a small out-of-plane spacing (2.40 m) between adjacent frames due to increased wind-induced accelerations and lateral displacements. The use of MRTFs in combination with CLT walls (i.e. dual frame-wall) can allow for greater number of storeys and larger out-of-plane spacing between the frames. Moreover, stairs and elevators always exist in multistorey buildings, and are often surrounded by walls, hence employing CLT walls in combination with MRTFs presents a practical consideration. In this thesis, a parametric study was performed to investigate the feasibility of a dual frame-wall structural system. The feasibility of employing outriggers in combination with the dual frame-wall system was also explored.

An extensive database was created for MRTFs with and without CLT walls, by use of linear elastic Finite Element Analysis (FEA). The FEA database was used to derive simplified analytical expressions for the fundamental frequency, mode shape, top-floor displacement, inter-storey drift, and top-storey wind-induced acceleration by use of nonlinear regression. The FEA database was also used to train Artificial Neural Networks (ANNs) that can be used to predict the aforementioned response parameters with an improved accuracy. The derived expressions and the ANNs can be used for preliminary assessment of MRTFs (with and without CLT walls) considering serviceability requirements.

Experimental studies on pullout behaviour of threaded rods screwed into glulam have demonstrated their high strength and stiffness. As a result, these rods can be utilized in timber connections that demand high capacity and stiffness. Research conducted on pullout behaviour of threaded rods screwed into CLT elements is limited. In this thesis, a series of experiments was conducted on threaded rods

screwed into the narrow face of CLT elements to evaluate their withdrawal properties. Penetration length, loading type (tension, compression, and fully reversed), loading configuration (pull-pull and pull-push), and angle to the grain (parallel and perpendicular) were varied during the testing. The use of self-tapping screws as reinforcement was also explored. Rods inserted perpendicular to the grain have demonstrated high withdrawal capacity and stiffness. Rods inserted parallel to the grain have shown high withdrawal stiffness, but the withdrawal capacity exhibited significant variability.

Timber MRCs can be realized by either laterally-loaded or axially-loaded fasteners. Although MRCs with laterally-loaded fasteners typically exhibit high ductility, testing of such connections shows low stiffness and considerable pinching under cyclic loading. In contrast, MRCs with axially-loaded fasteners, such as screwed-in threaded rods, exhibit higher stiffness and lower pinching.

MRCs using threaded rods screwed into glulam have demonstrated the possibility of stiff connections. However, the failure mode was brittle splitting. CLT comprises timber boards in two orthogonal directions, which may prevent the splitting reported in the MRCs made with glulam and achieve a higher capacity.

In this thesis, an innovative slip-friction connection that can be used in combination with screwed-in threaded rods, featuring ease of assembly and disassembly, high stiffness under service-level loading, and damage-free ductility via friction sliding under ultimate-level loading is presented. Four full-scale, beam-to-column, MRCs with CLT and screwed-in threaded rods have been tested. All specimens have been subjected to service-level cyclic loading, followed by a destructive cyclic loading. The connection demonstrated high stiffness in the range of 10000-20000 kNm/rad (under service-level loading) and high moment capacity in the range of 164-180 kNm (under destructive loading).

In view of the results of the performed parametric studies (no seismic design) and the full-scale tests of the developed MRCs, the dual frame-wall system can be used for multistorey timber buildings up to 10-12 storeys with 5.0 m out-of-plane spacing between adjacent frames. Employing outriggers can allow for up to 16 storeys.

Keywords: moment-resisting connection, friction connection, cross laminated timber, threaded rod, withdrawal stiffness, withdrawal capacity, rotational stiffness, ductility, energy dissipation, damping, multistorey timber building, moment-resisting timber frame, dual frame-wall, outrigger, wind-induced acceleration, serviceability of timber buildings, stiffness variability, artificial neural network.

Table of contents

Preface.....	i
Acknowledgments.....	iii
Abstract.....	v
Table of contents.....	ix
Abbreviations.....	xiii
Part I:	
1 Introduction.....	1
1.1 Background, motivation, and problem statement.....	1
1.2 Scope and objectives.....	4
1.3 Limitations.....	6
1.4 Structure of the thesis.....	7
2 Structural systems for multistorey timber buildings.....	8
2.1 Platform-type construction.....	8
2.2 Post and beam construction.....	10
2.3 3D modular construction.....	15
3 Serviceability of dual frame-wall structural system: challenges and mitigation techniques.....	16
3.1 Structural system, materials, and finite element analysis.....	16
3.2 Calculation of wind-induced acceleration and lateral displacements.....	18
3.2.1 Wind-induced acceleration.....	18
3.2.2 Lateral displacements.....	19
3.3 Acceptance criteria.....	20
3.3.1 Wind-induced acceleration.....	20
3.3.2 Lateral displacements.....	20

3.4	Performance of the dual frame-wall structural system.....	21
3.5	Mitigation techniques.....	24
3.6	Ultimate limited state considerations.....	29
3.7	Stiffness variability.....	31
3.7.1	SLS response parameters.....	32
3.7.2	ULS response parameters.....	33
4	Moment-resisting connections for multistorey timber buildings.....	36
4.1	Connections with laterally-loaded fasteners.....	36
4.2	Connections with axially-loaded fasteners.....	37
4.3	Slip-friction moment connection using threaded rods and CLT.....	41
4.3.1	Slip-friction connections: background and general concept.....	42
4.3.2	The developed connection: components and assembly.....	45
4.3.3	Experimental work.....	48
4.3.4	Analytical modelling.....	54
4.4	Screwed-in threaded rods.....	58
4.4.1	Background.....	58
4.4.2	Threaded rod inserted into CLT: experimental work.....	59
5	Summary of the appended papers.....	66
5.1	Paper I.....	66
5.2	Paper II.....	68
5.3	Paper III.....	69
5.4	Paper IV.....	69
5.5	Paper V.....	70
5.6	Paper VI.....	71
6	Suggestions for future work.....	72
	References.....	75

Part II: Appended papers:

Paper I: *Experimental investigation on axially-loaded threaded rods inserted perpendicular to grain into cross laminated timber.*

Paper II: *An innovative slip-friction moment-resisting connection using screwed-in threaded rods in cross laminated timber and steel coupling parts: An experimental study*

Paper III: *Serviceability performance of timber dual frame-wall structural system under wind loading*

Paper IV: *Parametric analysis of moment resisting timber frames combined with cross laminated timber walls and prediction models using nonlinear regression and artificial neural networks*

Paper V: *Feasibility of outrigger structural system for tall timber buildings: A numerical study*

Paper VI: *Analysis and design aspects of moment-resisting, beam-to-column, timber connections with inclined threaded rods: from fastener level to construction level*

Part III: Appendices:

Appendix A. Analytical modelling of moment-resisting timber connection with inclined threaded rods

Appendix B. Experimental work on rods inserted parallel to grain into the narrow face of CLT elements

Appendix C. Friction shims: experimental work

Appendix D. Additional journal paper published during the Ph.D.

Abbreviations

GHG	Greenhouse Gas
LCA	Life Cycle Analysis
LLRSs	Lateral Load-Resisting Systems
CLT	Cross Laminated Timber
MRTFs	Moment-Resisting Timber Frames
MRCs	Moment-Resisting Connections
Glulam	Glued Laminated Timber
<i>C/C</i>	Centreline-to-Centreline
SLS	Serviceability Limit State
ULS	Ultimate Limit State
ANNs	Artificial Neural Networks
FEA	Finite Element Analysis
GLRS	Gravity Load-Resisting System
LVL	Laminated Veneer Lumber
IDR	Inter-storey drift
OR	Outrigger
EYM	European Yield Model
STS	Self-tapping screws
GiRs	Glued-in Rods
CoV	Coefficient of Variation
SFCs	Symmetric Friction Connections
AFCs	Asymmetric Friction Connections
RSFJ	Resilient Slip Friction Joint
HSBs	High Strength Bolts
LVDTs	Linear Variable Differential Transducers

Part I

Introduction, background, and overview of the
present work

1 Introduction

1.1 Background, motivation, and problem statement

The global population is continuously growing, leading to an increased demand for urbanization. However, the construction sector contributes significantly to Greenhouse Gas (abbr. GHG) emissions worldwide. The construction sector ranks as the second largest emitter of carbon dioxide, responsible for approximately 33% of the total global carbon dioxide emissions [1]. These emissions are associated with the critical issue of climate change and its adverse environmental impacts, including extreme temperatures, heavy precipitation, and droughts [2]. Given the simultaneous need for increased urbanization and for reducing GHG emissions from construction, the use of environmentally-friendly construction materials is significant.

Timber is an environmentally-friendly and renewable material that can be used as an alternative to concrete and steel. A comparative Life Cycle Analysis (abbr. LCA) conducted by Eliassen et al. [3] has shown that the utilization of timber can lead to a reduction of GHG of 13% when compared to reinforced concrete and steel. An LCA study conducted by Skullestad et al. [4], focusing on buildings up to 21 storeys, has shown that timber buildings have a climate change impact that is 34%-84% lower than that of reinforced concrete buildings with similar load-carrying capacity.

While the environmental benefits of utilizing timber in construction are evident, the effectiveness of timber as a sustainable construction material depends heavily on its management beyond the lifespan of the structure [5]. Therefore, there is a need for innovative structural solutions that enable the reuse of timber structural elements and connections. Unfortunately, the common practice involves the incineration of wood waste for energy recovery. In 2022, approximately 87% of wood waste in Norway was incinerated [6]. The incineration of wood waste after the demolition of timber structures leads to substantial GHG emissions, thereby reducing the positive environmental impact associated with using timber in construction.

Despite the favourable environmental impact of using timber as a construction material, timber buildings, due to their lightweight and moderate stiffness, are often susceptible to excessive accelerations and lateral displacements under wind loads [7-13]. Large lateral displacements can cause damage to non-structural elements and may impact the functionality of buildings. Increased wind-induced accelerations may lead to discomfort for the occupants. Thus, it is important to keep lateral displacements and accelerations within acceptable limits to ensure acceptable performance of buildings under service loads.

Reducing lateral displacements of buildings can be achieved by increasing the lateral stiffness, such as by use of stiffer connections or larger cross-sections [7-10]. Wind-induced accelerations can be reduced by increasing the lateral stiffness of the building [7-10], the mass of the building [7, 8, 10], the damping [14], or a combination of these.

Various Lateral Load-Resisting Systems (abbr. LLRSs) can be used to provide the lateral stability for multistorey timber buildings. Multistorey timber buildings employing diagonal bracing are prevalent, such as *Treet* [11] and *Mjøstårnet* [15] in Norway. Another common LLRS is based on Cross Laminated Timber (abbr. CLT) walls. Examples for buildings that employ CLT walls are *Stadthaus* [16] in London, and *Moholt 50/50* [17] in Trondheim. However, both structural systems impose architectural restrictions and space limitations.

Moment-Resisting Timber Frames (abbr. MRTFs) can also be used as a LLRS for multistorey timber buildings. In MRTFs, the lateral stability is provided by the beam-to-column, Moment-Resisting Connections (abbr. MRCs). Compared to buildings with diagonal bracing and CLT walls, MRTFs provide more open space and less architectural limitations. Moreover, the use of MRCs can improve the performance of floors against human-induced vibrations [7, 18]. Despite the aforementioned advantages of MRTFs, their use is less common in practice due to their flexibility. The stiffness of MRTFs can be greatly enhanced by incorporating stiffer connections. However, such stiff connections are not commonly available in practice.

A parametric study of MRTFs [8], assuming Glued Laminated Timber (abbr. glulam) beams and columns, highlighted the feasibility of MRTFs for multistorey timber buildings. However, under high wind velocities, the MRTFs can hardly be used for more than 8 storeys with limited out-of-plane spacing (Centreline-to-Centreline, abbr. C/C) of 2.4 m between adjacent frames [8]. This is due to increased wind-induced accelerations and lateral displacements [8].

To realize MRTFs with greater number of storeys and larger C/C distance, it is necessary to use larger column cross-sections than those provided by standard glulam dimensions. CLT panels are currently produced with standard dimensions up to 3.5 m by 16.0 m, making them suitable for achieving these larger dimensions. Moreover, multistorey buildings have stairs and elevators, and walls typically surround the staircase and elevator shaft. Therefore, employing CLT walls in combination with MRTFs (i.e. dual frame-wall) presents a practical consideration.

Full-scale testing of MRCs employing threaded rods screwed into glulam beams and columns has shown the possibility of stiff connections [19, 20]. However, the failure mode in these connections was brittle splitting, either in the beam or the panel zone of the column, due to high shear and tensile stresses perpendicular to grain. CLT comprises timber boards in two orthogonal directions. The presence of timber boards in two orthogonal directions can potentially prevent the splitting cracks reported in [19, 20] for MRCs made with glulam and achieve a higher capacity and a more ductile behaviour.

Without reinforcement, timber is inherently brittle in bending, shear, and tension [21]. However, ductility and greater energy dissipation can be achieved by the use of ductile and dissipative connections [21]. By using ductile connections and timber elements that are capacity-designed, post-elastic deformation and damage occur primarily at the connections, resulting in a ductile behaviour of the structure [21]. This is a desirable property in earthquake-prone regions, where structures must be designed to absorb and dissipate seismic energy. Ductile behaviour can also increase the robustness of the structure [21], and allow for redistribution of stresses in

indeterminate structures, resulting in a higher capacity compared to the capacity estimated based on elastic analysis [21].

A conventional approach to dissipate seismic energy in timber connections is through embedment and yielding of the fasteners [22]. However, this approach leads to irreversible damage, requiring the rehabilitation of structural elements and connections following a seismic event. To minimize such irreversible damage, it is necessary to incorporate damage-free energy dissipation mechanisms.

Slip-friction connections have been shown to be effective damage-free connections [23, 24]. These connections dissipate seismic energy through friction slip under cyclic loading. While slip-friction connections have been successfully implemented in steel structures [24-27], their application in timber connections is currently limited.

1.2 Scope and objectives

This Ph.D. thesis aims to develop structural concepts and connections with enhanced mechanical properties for multistorey timber buildings. Special emphasis is given to stiffness, load-carrying capacity, and ductility. The Ph.D. thesis focuses on dual frame-wall structural system, which combines MRTFs with CLT walls. A 3D view of an example multistorey timber building with dual frame-wall system is shown in Figure I.1. The dual system is parallel to X direction.

In the framework of this Ph.D. thesis, the following objectives were outlined:

1. To investigate the feasibility of dual frame-wall system for multistorey timber buildings. The feasibility is evaluated in terms of lateral displacements and wind-induced accelerations (Serviceability Limit State, abbr. SLS). However, Ultimate Limit State (abbr. ULS) considerations are also discussed. This objective was addressed in Paper III.
2. To investigate the feasibility of using outriggers in combination with the dual frame-wall system for multistorey timber buildings. This objective was addressed in Paper V.

3. To develop simplified analytical expressions and Artificial Neural Networks (abbr. ANNs) that can be used for preliminary assessment of the dual frame-wall system with respect to SLS. This objective was addressed in Paper IV.
4. To evaluate the influence of stiffness variability on the performance of MRTFs. This objective was addressed in Paper VI.
5. To investigate, through experimental testing, the mechanical properties (stiffness, energy dissipation, and capacity) of threaded rods inserted into CLT elements. This objective was addressed in Paper I and Appendix B.
6. To investigate, through full-scale testing, the possibility of utilizing threaded rods screwed into CLT to construct beam-to-column MRCs with enhanced stiffness, capacity, and ductility. This objective was addressed in Paper II.

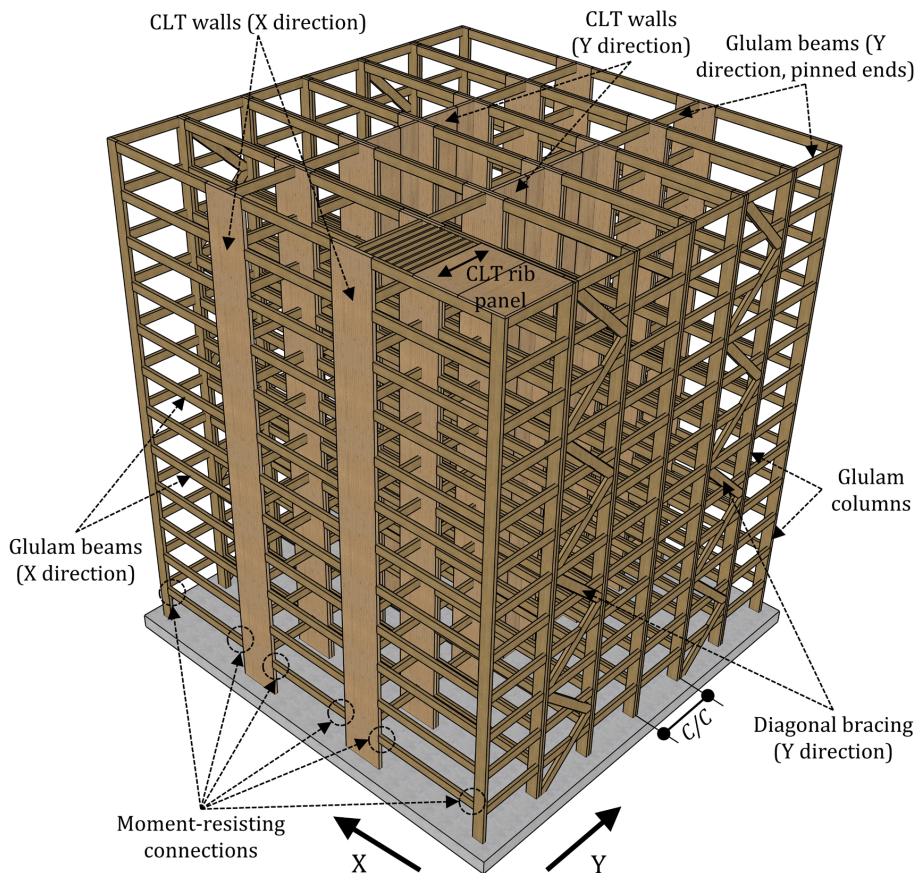


Figure I.1 Example multistorey timber building with dual frame-wall system in X direction

1.3 Limitations

The work in this this Ph.D. is subject to the following limitations:

1. The Finite Element Analysis (abbr. FEA) was limited to linear elastic analysis. This limitation is relevant for Paper III, Paper IV, Paper V, and Paper VI.
2. Wind-induced acceleration was calculated using the method described in Annex B of EN 1991-1-4 [28]. This method is based on gust factor approach. Dynamic analysis, such as time-history, was not considered in this thesis. This limitation is relevant for Paper III, Paper IV, Paper V, and Paper VI.
3. The feasibility of the dual frame-wall structural system and the outriggers was mainly evaluated with respect to SLS, with some ULS considerations. However, seismic design was not included in the evaluation. This limitation is relevant for Paper III and Paper V.
4. The analytical expressions and the ANNs were developed based on an assumption of a simplified building layout. This simplification may not accurately capture the complexities and variations found in practical buildings. This limitation is relevant for Paper IV.
5. The experimental testing in this Ph.D. was limited to short-term loading conditions only. As a result, this thesis does not address issues related to long-term loading effects, moisture dependency, or fatigue behaviour. This limitation is relevant for Paper I and Paper II.
6. The material used for experimental testing was stored in a climate room with controlled temperature and relative humidity of 20 °C and 65%, respectively, leading to a moisture content within the range of 10%-12%. This limitation is relevant for Paper I and Paper II.
7. The experiments performed on threaded rods inserted into CLT were limited to rods inserted parallel and perpendicular to grain, other angles to grain were not investigated. Furthermore, the tests were performed using 3-layer, non-edge glued CLT elements, and the rods were inserted to a maximum penetration length of 20 times the outer thread diameter of the used threaded rod. This limitation is relevant for Paper I.

1.4 Structure of the thesis

This Ph.D. thesis is divided into 3 parts:

Part I: This part includes six introductory chapters for the Ph.D. thesis. The 1st chapter presents the background and motivation to this Ph.D. thesis, identifies the problem statement, and outlines the scope, objectives, and limitations of this Ph.D. thesis. The 2nd chapter provides an overview of various structural systems for multistorey timber buildings. The 3rd chapter introduces the dual frame-wall system, presents the serviceability requirements considered in this thesis, and discusses the challenges and mitigation techniques to meet these requirements. ULS considerations and the influence of stiffness variability are also discussed in the 3rd chapter. The 4th chapter discusses moment-resisting connections for multistorey timber buildings, with emphasis on connections with threaded rods. The 5th chapter presents brief summaries of all appended papers. The 6th chapter outlines suggestions for future research.

Part II: This part includes six appended papers.

Part III: This part includes four appendices.

2 Structural systems for multistorey timber buildings

There are different approaches to categorize the various structural systems used for multistorey timber buildings, see e.g. [29-32]. In this chapter, only structural systems relying on timber as the main material for the load-bearing structural system are considered, i.e. hybrid structural systems are not included.

Common structural categories for multistorey timber buildings are platform, post and beam, and 3D modular construction. Each category is briefly discussed in this chapter.

2.1 Platform-type construction

Platform-type timber structures are built using slabs and load-bearing walls, usually made of CLT. In this type of construction, the vertical continuity of the CLT walls is interrupted at each floor level by inserting CLT slabs between the consecutive CLT walls, confer Figure I.2.

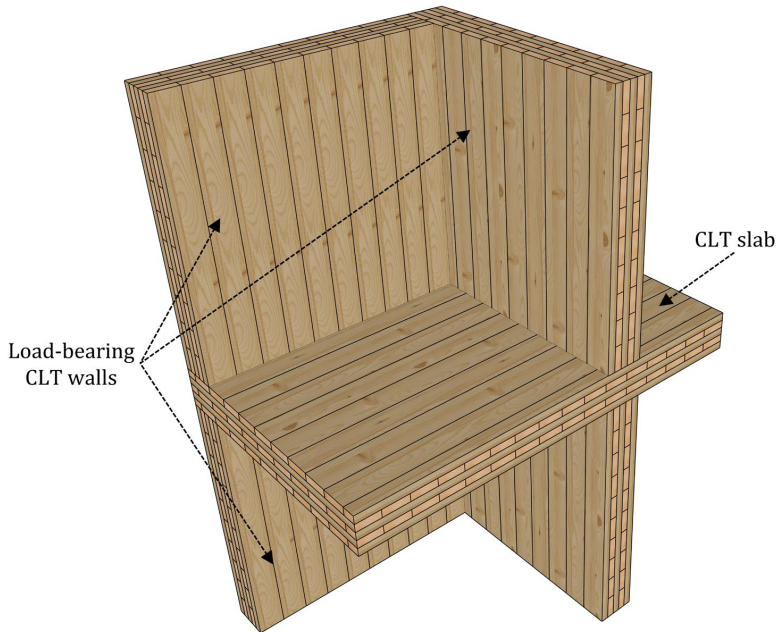


Figure I.2 Platform-type construction

Buildings built using platform-type construction can resist lateral load given the large number of walls. Under lateral loads, the CLT slabs act as diaphragms, transferring the lateral forces to the walls. Research has shown that the connections between the CLT walls and the foundation (or the CLT slab below), and the connections between adjacent CLT walls are the main contributors to the CLT wall deformations, see e.g. [33, 34]. The CLT walls themselves behave mostly as rigid bodies. Therefore, the strength and stiffness of CLT walls, and therefore the whole building, are governed by the connections.

Despite the advantage of using the CLT slabs as platforms, allowing for easier assembly and erection of the structural elements at upper storeys, there are several disadvantages associated with the use of this construction type:

1. Placing CLT slabs between CLT wall elements at each floor results in high stresses perpendicular to grain on the CLT slabs at the lower storeys. Loading timber perpendicular to the grain is unfavourable due to its lower strength and stiffness compared to loading it parallel to the grain. This leads to limitations on the number of storeys that can be built with this construction method.
2. The increased number of connections between the vertical CLT elements (i.e. walls) leads to an overall flexible lateral behaviour. This also sets limitations on the maximum height of buildings due to increased lateral displacements and wind-induced accelerations.
3. The load-bearing CLT walls are typically carrying low stresses, leading to material-intensive constructions.
4. The extensive use of CLT slabs and walls results in cellular buildings with less architectural flexibility and open space.

Despite the aforementioned disadvantages, platform-type construction is widely used for low and mid-rise CLT buildings. This may be attributed to their easy and fast construction. Example buildings are *Stadthaus* [16] in London, and *Moholt 50/50* [17, 35] in Norway, see Figure I.3. Significant research has been conducted on the performance of platform-type CLT buildings, see e.g. [36-40], leading to the development of design standards, e.g. CSA O86 [41].

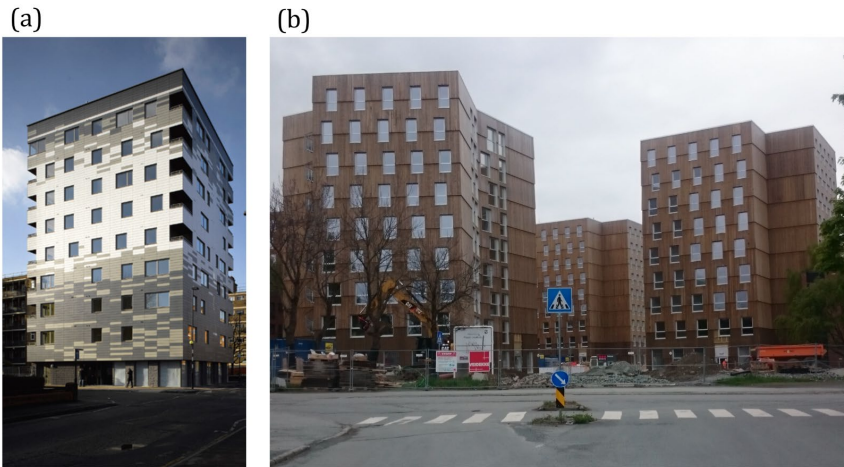


Figure 1.3 (a) Stadthaus [16] and (b) Moholt 50/50 [35]

2.2 Post and beam construction

Post and beam construction is a construction method where the vertical support of the building consists of beams and columns. Unlike platform construction, post and beam construction is characterized by fewer load-bearing walls, allowing for more open space and flexible architecture.

Post and beam structures consist of four main components, see Figure 1.4:

a) Floors

The characteristics of the flooring system (span, thickness, one-way spanning, two-way spanning, etc) can have an impact on the layout of the building. Common flooring systems include CLT slabs, CLT rib panels, composite timber floors [42, 43], and timber-concrete composite floors [44].

b) Beams

Beams are a component of the Gravity Load-Resisting System (abbr. GLRS), carrying the floors and transferring their loads to the columns. In such case, the beam-to-column connections are usually pinned connections. However, in the case of MRTFs, the beam-to-column connections are moment-resisting, and are an integral

component of the LLRS [8] in addition to the GLRS. The most common types of beams are glulam and Laminated Veneer Lumber (abbr. LVL) beams.

c) Columns

Similar to the beams, columns are a component of the GLRS, transferring the loads from the beams to the foundation. Columns can also be part of the LLRS, e.g. in MRTFs [8] and outrigger structures [45]. The most common type of columns are glulam columns.

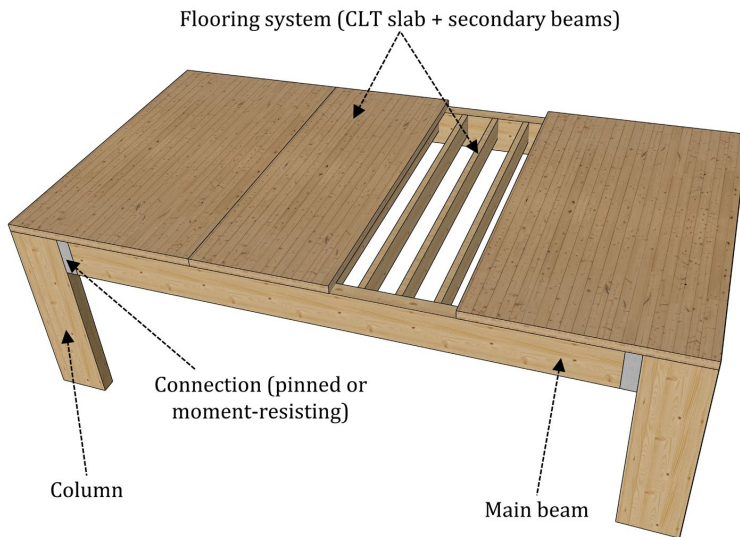


Figure I.4 Components of post and beam structure

d) Lateral load-resisting system (LLRS)

The LLRS transfers the lateral loads (earthquake and wind) through the structure to the foundation. Four methods can be used to provide the lateral stability for post and beam structures, see Figure I.5. Among the four methods shown in Figure I.5, diagonal bracing is more common in multistorey timber buildings.

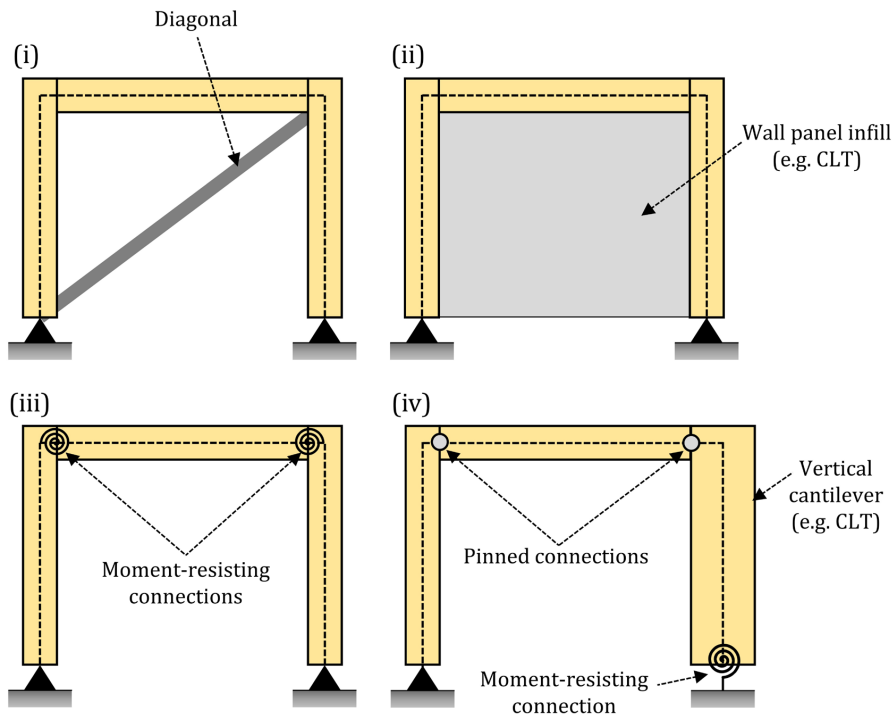


Figure I.5 Lateral stability of post and beam structures using (i) diagonal bracing, (ii) wall panel infill, (iii) moment-resisting connections, and (iv) vertical cantilever

i. Diagonal bracing

Diagonal bracing is often the most material-efficient method to provide the lateral stability for post and beam structures. The bracing elements are placed at the plane of the frame and can be arranged in various layouts, including diagonal bracing shown in Figure I.5 (i), chevron bracing, and X-bracing. The use of diagonal bracing, although effective, requires large bracing elements running along the height of the building, which may compromise the aesthetics and pose architectural limitations. Examples of timber buildings employing diagonal bracing are Mjøstårnet [15] and Treet [11] in Norway, see Figure I.6.

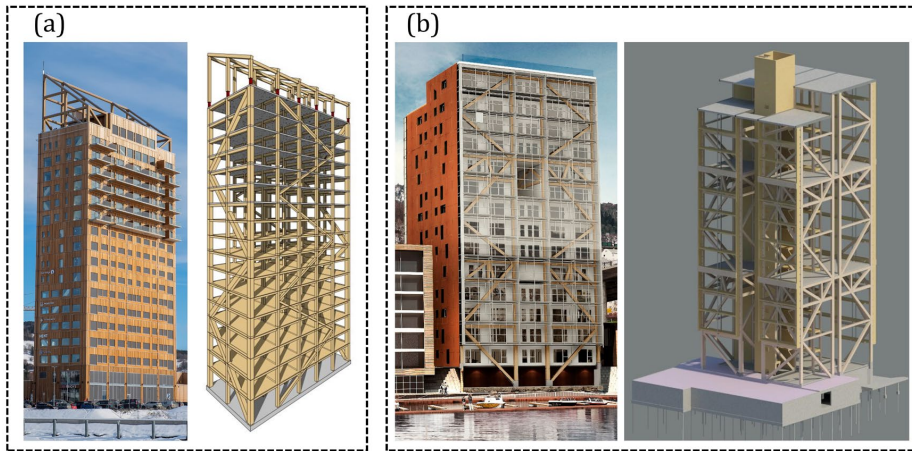


Figure I.6 (a) Mjøstårnet [15] and (b) Treet [11]

ii. Wall panel infill:

Due to their high in-plane stiffness, CLT panels may replace the diagonal bracing and be used as infilled walls to provide the lateral stability for post and beam structures, see Figure I.5 (ii). Experimental work on this type have shown good performance, see e.g. [46]. Other wood-based panels may also be used as infill, see e.g. [47]. While the use of wall panels as infill introduces additional architectural constraints compared to diagonal bracing, they provide a more even distribution of forces between the wall and the main structure along the perimeter. As a result, smaller connections may be required. Nevertheless, the practical application of this system in multistorey timber buildings is still limited.

iii. Moment-resisting connections (MRCs):

MRCs are commonly used in portal frames. Several example projects and variations of MRCs for timber portal frames can be found in [48]. However, the use of MRCs (i.e. MRTFs) is less common in multistorey timber buildings, mainly due to their low stiffness. Therefore, the development of stiffer connections can result in more practical applications of MRTFs. An example building that utilizes MRTFs is Beatrice Tinsley building in New Zealand. The building utilizes MRTFs in one direction, and lateral bracing with diagonals in the other direction, see Figure I.7.



Figure I.7 Beatrice Tinsley building (source: pres-lam.com)

iv. Vertical cantilever:

Vertical cantilevers can be used to provide the necessary lateral stability for post and beam structures. The stability is provided by use of MRCs between the wall and the foundation, confer Figure I.5 (iv). In this system, the walls are usually contained in the core of the building, surrounding the staircase or the elevator. Buildings that utilize CLT cantilever walls (i.e. CLT shear walls) as LLRS include the Arbora building complex (two 8-storey buildings, one 9-storey building) and the 13-storey Origine building in Canada, see Figure I.8. In these buildings, the GLRS consists of CLT floor panels supported by a glulam post-and-beam structure. More details on these buildings can be found in [49].

(a)



(b)



Figure I.8 (a) Arbora building complex [49] and (b) Origine building [50]

2.3 3D modular construction

3D modular construction comprises prefabricated room-sized or apartment-sized volumetric building modules. The modules are usually prefabricated off-site in controlled conditions, leading to improved quality and accuracy of construction and faster installation on-site. The prefabrication process can also include the windows, doors, finishes, and other mechanical and electrical installations. Modular buildings offer the potential for disassembly and reuse, therefore can maintain their asset value, and reduce the environmental impact of construction. An example building with prefabricated 3D modulus is shown in Figure I.9.



Figure I.9 Rigot Collective Dwelling Centre (source: Marcel Kultscher) (a) during construction and (b) completed construction

Despite the advantages of 3D modular construction, there are several challenges associated with the use of this construction type. These challenges include:

1. Establishing a load path for lateral loads can be challenging.
2. Modular construction, in the current form, is commonly used in cellular-type buildings such as hotels, student residences, military accommodation, and social housing, due to manufacturers' limitations. As a result, the use of modular construction for buildings with irregular geometry or those requiring creative solutions may be deemed unfeasible.
3. Transportation of the modules is subject to local transportation regulations.
4. Increased material usage occurs due to the duplication of walls and floors between adjacent modules.

3 Serviceability of dual frame-wall structural system: challenges and mitigation techniques

Timber buildings are characterized by their lightweight and moderate stiffness. As a result, they are usually prone to serviceability performance issues, such as large lateral displacements and accelerations under service-level wind loading [7-13]. In this chapter, the serviceability performance of MRTFs combined with CLT walls (i.e. dual frame-wall) under service-level wind loading is discussed. A benchmark 2D dual frame-wall system was considered and used as a basis for discussion. Although the focus of this chapter is on SLS, some ULS considerations are also discussed.

3.1 Structural system, materials, and finite element analysis

A 10-storey, 3-bay dual frame-wall was considered as a benchmark system in this chapter, see Figure I.10. The dual system consists of two external continuous glulam columns, two internal continuous CLT walls, and glulam beams. The columns, walls, and beams were assumed of double cross-sections. The cross-sectional dimensions are shown in Figure I.10.

OpenSeesPy [51] Python library was used to perform linear elastic 2D FEA. All structural elements were modelled using Timoshenko beam elements (1D elements). The beam elements representing the CLT walls were verified against layered shell elements under in-plane loading. The verification included both stresses and deformations. The difference between the beam elements and the layered shell elements was found to be approximately 5%. Based on this small difference, beam elements were deemed to provide sufficient accuracy for the intended analysis.

The connections of the columns and the walls to the foundation were modelled using rotational springs with stiffness $K_{\theta,c}=5000$ kNm/rad and $K_{\theta,w}=75000$ kNm/rad, respectively, confer Figure I.10. The connections between the beams and the columns/walls were modelled using rotational springs with stiffness $K_{\theta,b}=7500$ kNm/rad. The values of $K_{\theta,c}$, $K_{\theta,w}$, and $K_{\theta,b}$ are given here for a single cross-section, hence the values for a double cross-section are double these values. The use of

translational springs with reasonable stiffness has shown very small differences compared to the analysis with connections assumed to be rigid in translation [8]. Therefore, all connections were considered rigid with respect to translation.

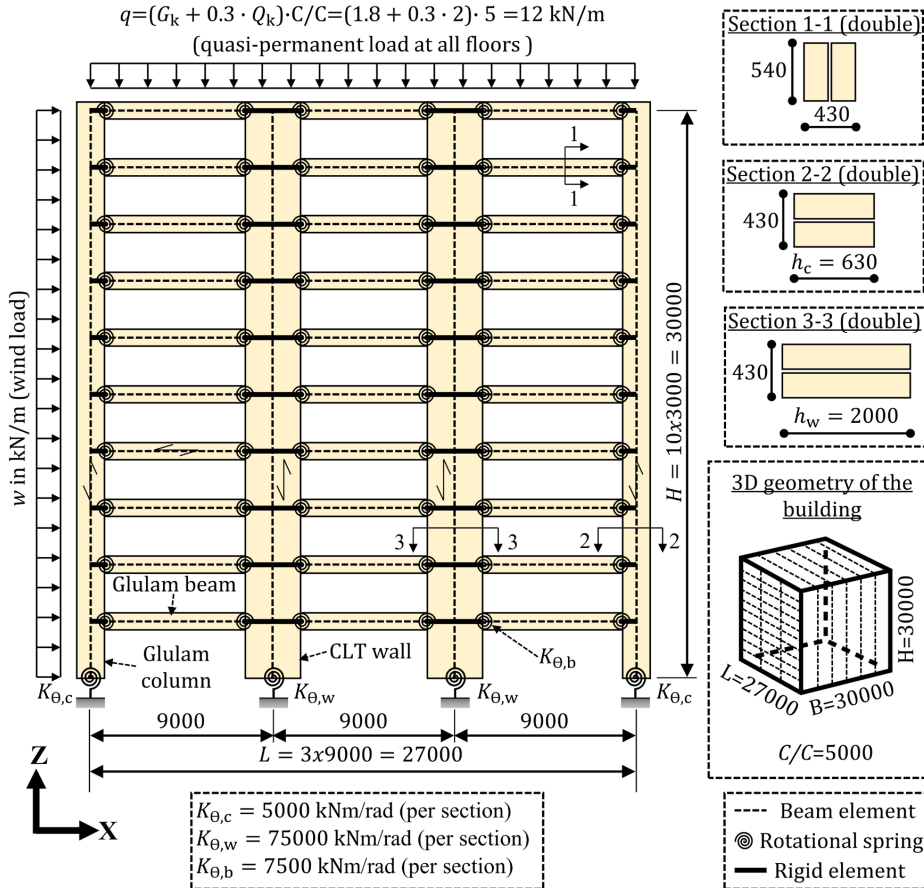


Figure I.10 The considered benchmark dual frame-wall system (dimensions in mm)

To account for the increased span length of beams caused by modelling columns and walls as 1D elements (beam elements), rigid elements with high shear and bending stiffness were used at both ends of all beams, see Figure I.10. The length of these rigid elements corresponds to half the column/wall height (h_c and h_w in Figure I.10).

The glulam beams and columns were assumed of strength class GL30c according to EN 14080 [52], with mean elastic modulus ($E_{0,mean}$) of 13000 N/mm² and mean shear modulus (G_{mean}) of 650 N/mm².

The lamellae constituting the CLT walls were assumed of strength class C24 according to EN 338 [53]. It was assumed that two-thirds ($2/3$) of the lamellae are parallel to the longitudinal (main) direction of the CLT walls (vertical). The remaining one-third ($1/3$) of the lamellae were assumed to be orthogonal to the main direction. The CLT walls were simplified by assuming a homogeneous cross-section with equivalent material properties, calculated using the method described in [54]. This simplified approach was considered reasonably accurate for CLT walls subjected to in-plane loading [55]. Based on the aforementioned assumptions, the equivalent elastic modulus ($E_{eq,0,mean}$) and shear modulus ($G_{eq,mean}$) used in this study are 8000 N/mm^2 and 518 N/mm^2 , respectively.

In this chapter, only 2D FEA was performed. To verify the validity of the 2D FEA, an 8-storey timber building with the dual frame-wall system (in one direction) was analysed in both 2D and 3D, and the results were compared. The comparison showed that 2D FEA provides a reasonable level of accuracy compared to 3D FEA. Details of this example can be found in [7] (Paper III in this thesis).

3.2 Calculation of wind-induced acceleration and lateral displacements

3.2.1 Wind-induced acceleration

Several methods are available in building design codes for estimating wind-induced acceleration, a comparison of different methods can be found in [56, 57]. In this thesis, the method described in EN 1991-1-4 (Annex B) [28] was used to calculate the peak wind-induced acceleration. The procedure is based on gust factor approach. Table I.1 summarizes key parameters used for the calculation. The damping ratio in Table I.1 ($\xi=0.02$) was reasonably assumed based on the results presented in [17, 58].

Additional to the parameters in Table I.1, the mode shape and the fundamental frequency are required for the calculation of acceleration. OpenSeesPy [51] was used for modal analysis to obtain the frequency and mode shape, with modal mass calculated using the quasi-permanent load shown in Figure I.10 ($q = 12 \text{ kN/m}$). The

quasi-permanent load ($q = (G_k + 0.3 \cdot Q_k) \cdot C/C$) was calculated assuming a dead load (G_k) of 1.8 kN/m² and a live load (Q_k) of 2 kN/m² (residential buildings as defined by EN 1991-1-1 [59]). The C/C distance (see Figure I.1) was assumed to be 5.0 m. Alternatively, the used q could also correspond to G_k of 1.5 kN/m² (lighter floors) and Q_k of 3 kN/m² (office buildings as defined by EN 1991-1-1 [59]).

Table I.1 Assumed parameters for calculation of wind-induced acceleration

Parameter	Value
Directional factor (C_{dir})	1.0
Seasonal factor (C_{season})	1.00
Probability factor (C_{prob}) ^a	0.73
Orography factor ($C_{0(z)}$)	1.00
Turbulence factor (k_1)	1.00
Terrain category	Urban environment (IV)
Reference height (Z_t)	200 (m)
Reference length (L_t)	300 (m)
L, B, H (see Figure I.1)	27, 30, 30 (m)
Damping ratio (ξ)	0.02

^a Corresponds to 50% probability of exceedance in half a year

3.2.2 Lateral displacements

As shown in Figure I.10, the dual frame-wall system is subjected to a uniform lateral wind load (w). The wind load (w) is calculated assuming urban environment (IV) as defined by EN 1991-1-4 [28]. The out-of-plane spacing between adjacent frames was assumed 5 m (C/C distance in Figure I.1), and the width of the building (B) (perpendicular to the wind) was assumed 30 m, confer Figure I.10.

OpenSeesPy [51] was used for 2D linear elastic FEA to calculate lateral displacements. The second-order effects due to non-linear geometry were not included. The inclusion of the second-order effects results in approximately 5%-10% increase in lateral displacements, confer Paper IV in this thesis and [8].

3.3 Acceptance criteria

3.3.1 Wind-induced acceleration

Human perception of acceleration is highly subjective. An acceleration level that causes discomfort to one individual may go unnoticed by another. Furthermore, the acceleration level that can cause discomfort to a person sitting at home may differ for the same person when walking in a busy shopping area. Acceleration acceptance criteria aim to address this subjectivity by specifying different levels of acceptance for various situations. A review of different studies addressing human perception of acceleration and comfort criteria can be found in [60].

In this chapter, and throughout the thesis, the acceptance criterion of ISO 10137 [61] for wind-induced acceleration is used. Figure I.11 depicts ISO 10137 [61] acceptance criterion for peak wind-induced acceleration. The criterion covers buildings with fundamental frequency ranging from 0.063 Hz to 5 Hz, subjected to maximum wind velocity with 1 year return period. As shown in Figure I.11, the criterion is more stringent for residential buildings compared to office buildings.

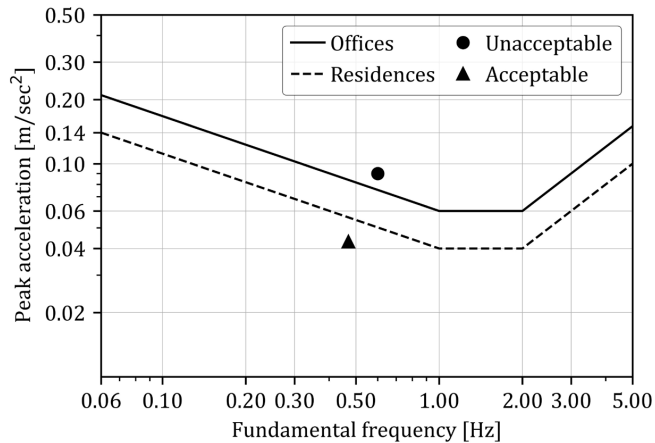


Figure I.11 Evaluation curves for wind-induced acceleration according to ISO 10137 [61] for a one-year return period

3.3.2 Lateral displacements

EN 1995-1-1 [62] provides recommendations for deflection limits for beams. However, no limits for the maximum horizontal displacements are given. The

following limits were reasonably assumed for top-floor displacement (Δ) and maximum inter-storey drift (δ_{max}):

$$\Delta \leq \frac{H}{300} \quad , \quad \delta_{max} \leq \frac{h}{300} \quad (I.1)$$

where H is the total height of the building and h is the storey height, confer Figure I.12.

Substituting in Eq. (I.1) with $H=30000$ and $h=3000$ (confer Figure I.10):

$$\Delta \leq 100 \text{ mm} \quad , \quad \delta_{max} \leq 10 \text{ mm} \quad (I.2)$$

It should be noted that the limits in Eq. (I.1) are indicative, and different limits may be considered based on individual projects. For instance, the presence of brittle partition walls may require more stringent limits. However, for the purpose of this study, the limits specified in Eq. (I.1) are assumed to be reasonable.

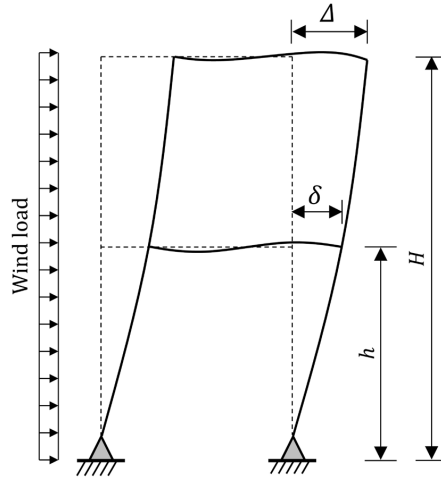


Figure I.12 Top-floor displacement (Δ) and inter-storey drift (δ)

3.4 Performance of the dual frame-wall structural system

The serviceability performance of the benchmark dual frame-wall shown in Figure I.10 is evaluated in terms of peak wind-induced acceleration, maximum inter-storey drift (abbr. IDR), and top-floor displacement. The peak wind-induced acceleration is calculated at the top storey. In addition to the dual frame-wall shown in Figure I.10,

a MRTF was also solved, where the internal CLT walls are replaced with glulam columns with the same dimensions as the external columns. The performance was evaluated assuming a basic wind velocity (v_b) ranging from 20 m/sec to 30 m/sec.

Figure I.13 shows the top-storey peak wind-induced acceleration for the benchmark dual frame-wall system and the MRTF. The dual system shows 36% higher frequency and approximately 24% lower acceleration compared to the MRTF.

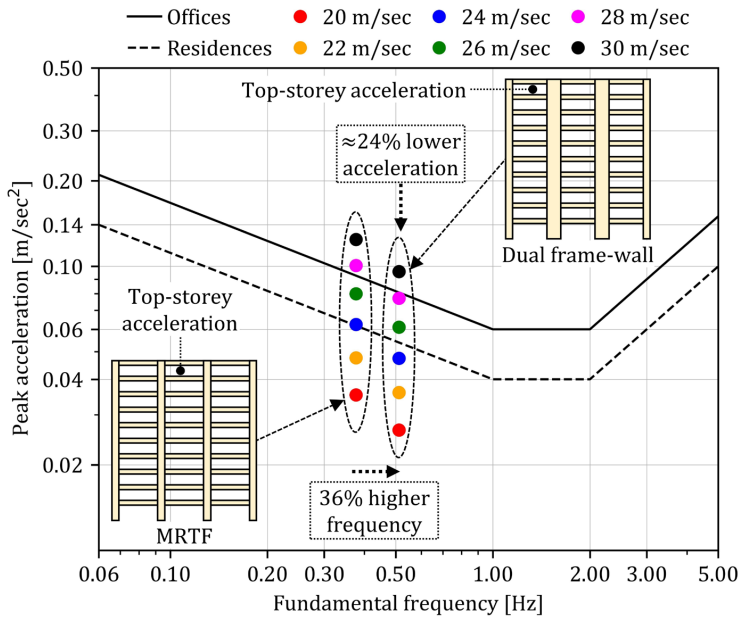


Figure I.13 Top-storey peak wind-induced acceleration for the benchmark dual frame-wall and the MRTF against ISO 10137 criterion [61]

As shown in Figure I.13, the dual system can be used for wind velocities up to 24 m/sec and 28 m/sec while meeting the acceleration requirements for residential buildings and offices, respectively. The MRTF can be used for wind velocities up to 22 m/sec and 26 m/sec while meeting the requirements for residential buildings and offices, respectively. The use of mitigation techniques can further improve the performance, more details are given in section 3.5.

Figure I.14 shows the lateral displacements and inter-storey drift for the benchmark dual system and the MRTF. The dual system shows 42% and 59% lower top-floor displacement and inter-storey drift compared to the MRTF, respectively.

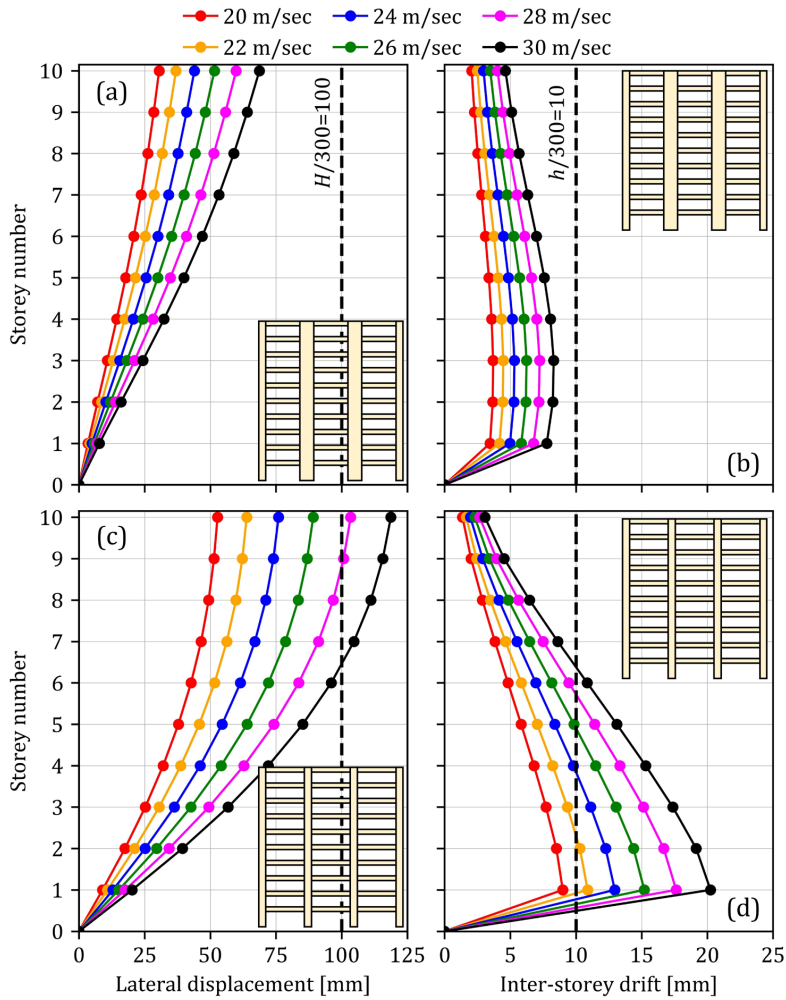


Figure I.14 Lateral displacement and inter-storey drift (a)-(b) for the benchmark dual frame-wall and (c)-(d) for the MRTF

As shown in Figure I.14, the dual system meets the limits for top-floor displacement and inter-storey drift defined in Eq. (I.2) for all wind velocities. The MRTF meets the requirement for top-floor displacement for wind velocities ≤ 26 m/sec, and meets the requirements for inter-storey drift for wind velocities ≤ 20 m/sec.

Figure I.14 shows that the maximum inter-storey drift occurs at lower storeys, notably for the MRTF. This is due to the fact that, under lateral loading, the MRTF exhibits a shear-dominant deformed shape, with larger deformations in the lower

storeys. Under lateral loading, the CLT walls exhibit a bending-dominant deformed shape (as a cantilever), with larger deformations in the upper storeys. The use of CLT walls with MRTF (dual system) results in a significant reduction in inter-storey drift and top-floor displacement. In the dual frame-wall system, compatibility of lateral displacements generates interaction between the MRTF and the CLT walls. This interaction results in an enhanced stiffness, the CLT walls restrain the MRTF at the lower storeys and the MRTF restrains the CLT walls at the upper storeys.

For the MRTF, inter-storey drift is the governing SLS criterion. On the other hand, wind-induced acceleration is the governing SLS criterion for the dual frame-wall system, confer Figure I.13 and Figure I.14.

Based on the results shown in Figure I.13 and Figure I.14, and the preceding discussion, it is apparent that the use of CLT walls, in combination with MRTFs, can provide an improved performance with respect to lateral displacements and accelerations, and allow for the fulfilment of SLS requirements.

3.5 Mitigation techniques

In this section, various mitigation techniques to further improve the serviceability performance of the dual system are discussed and their efficiency is compared. The mitigation techniques are evaluated in terms of wind-induced acceleration only because it was found to be the governing SLS criterion, see section 3.4.

Mitigation techniques, which can be used to reduce wind-induced accelerations, can be categorized into three categories:

1. Increasing the stiffness: the use of stiffer connections and/or larger cross-sections results in an increased stiffness, hence lower acceleration.
2. Increasing the mass: the use of heavier floors (e.g. with concrete topping) can reduce the acceleration.
3. Increasing the damping: in timber buildings, damping is typically limited under service-level loads. The use of dampers is possible, but may result in considerable costs and regular maintenance.

Figure I.15 illustrates the influence of increasing stiffness, mass, and damping on wind-induced accelerations.

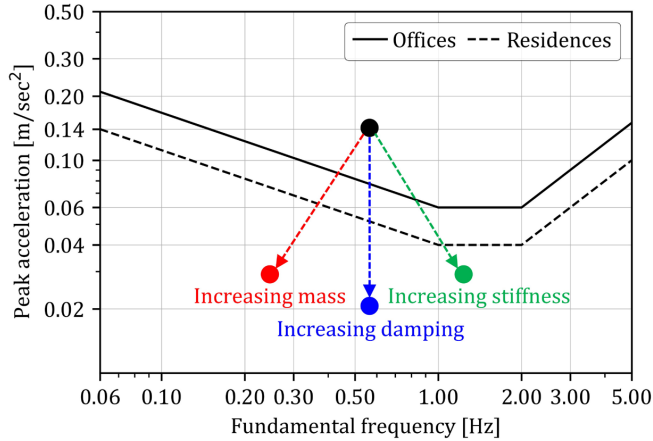


Figure I.15 Influence of increasing stiffness, mass and damping on wind-induced acceleration (illustrative)

Based on the three categories depicted in Figure I.15, a total of six mitigation techniques are explored in this section:

1. Increasing the beam-to-column/wall connection stiffness ($K_{\theta,b}$).
2. Increasing the CLT wall-to-foundation connection stiffness ($K_{\theta,w}$).
3. Increasing the CLT wall height (h_w).
4. Using an outrigger (abbr. OR) at the 5th storey, see Figure I.16. An effective axial stiffness ($K_{ax,ef}$) of 125 kN/mm (including the flexibility of connections) is assumed for the diagonal elements. The placement of the OR at the 5th storey is optimal for reducing wind-induced acceleration, confer Paper V. Placing the OR elsewhere to meet the architectural requirements may result in lower efficiency.
5. Increasing the quasi-permanent mass (i.e. q).
6. Increasing the damping ratio (ξ).

To evaluate the efficiency of each mitigation technique (e.g. increasing $K_{\theta,b}$), one parameter was varied at a time ($K_{\theta,b}$) while keeping all other parameters the same as in Figure I.10 (the benchmark dual system). The six mitigation techniques were

evaluated under a basic wind velocity (v_b) ranging from 20 m/sec to 30 m/sec. Figure I.17 shows the influence of each of the six techniques on the acceleration.

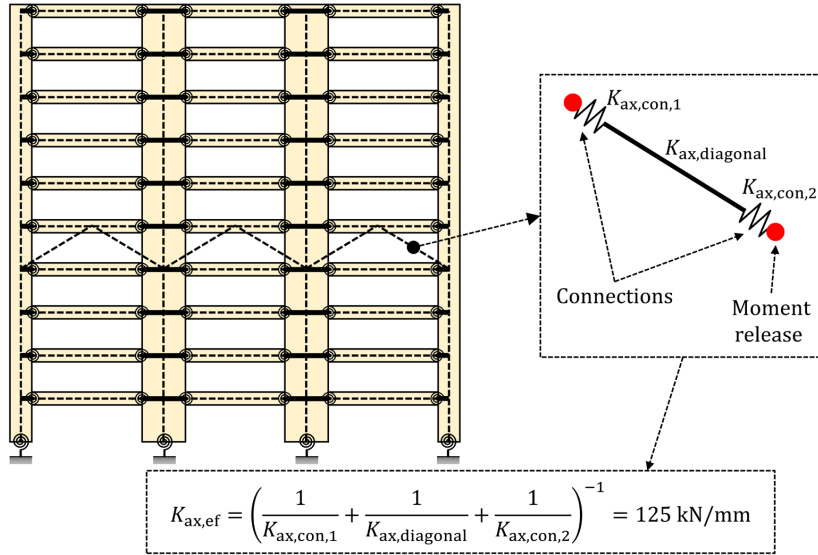


Figure I.16 An outrigger at the 5th storey of the dual frame-wall system

Based on Figure I.17, several observations can be drawn (averaging results for $v_b = 20 \rightarrow 30$ m/sec):

1. Increasing $K_{\theta,b}$ from 5000 kNm/rad to 15000 kNm/rad (per section) results in 29% reduction in the acceleration.
2. Increasing $K_{\theta,w}$ from 0 kNm/rad to 150000 kNm/rad (per section) results in 17% reduction in the acceleration.
3. Increasing h_w from 1000 mm to 3500 mm results in 28% reduction in the acceleration.
4. The use of an outrigger at the 5th storey results in 34% reduction in the acceleration.
5. Increasing q (represents mass) from 8 kN/m to 16 kN/m results in 25% reduction in the acceleration.
6. Increasing ξ from 0.01 to 0.03 results in 40% reduction in the acceleration.

The efficiency of each technique, along with remarks regarding practicality and drawbacks, are summarized in Table I.2. Mitigation techniques involving the increase of $K_{\theta,b}$, $K_{\theta,w}$, h_w , or the use of an outrigger result in increased stiffness. Combining these solutions will result in a higher reduction in acceleration.

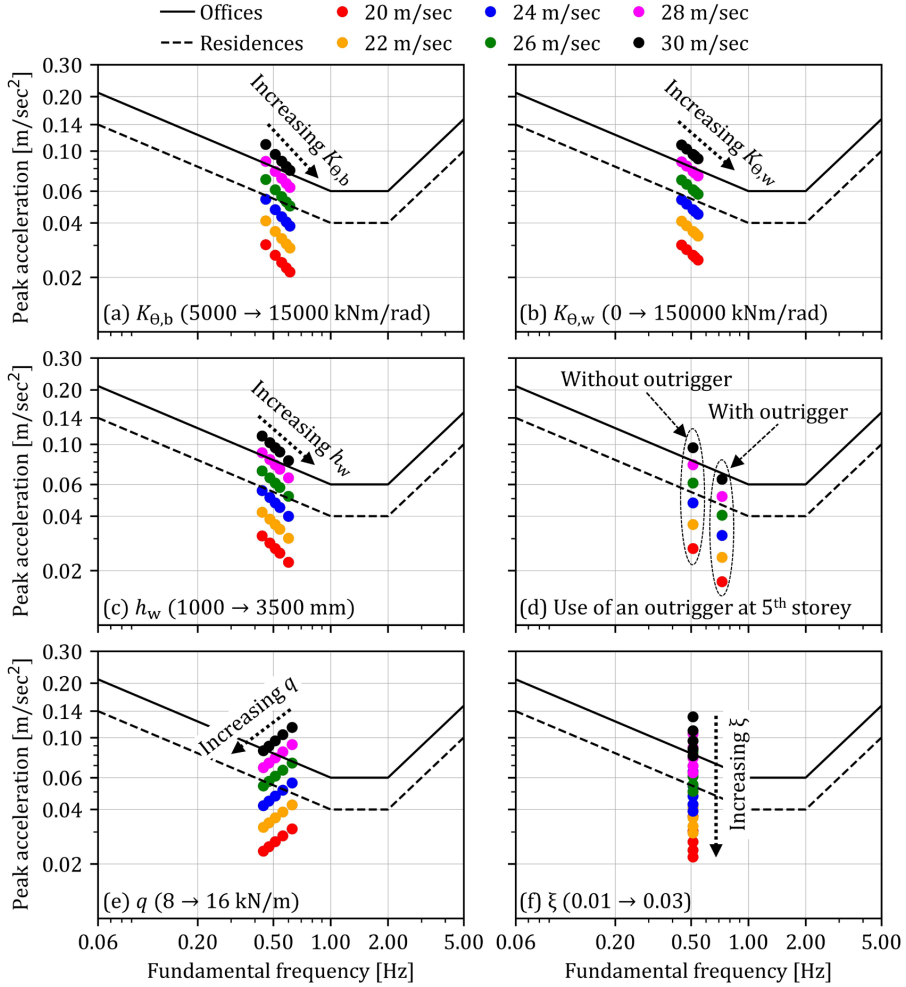


Figure I.17 The influence of the six mitigation techniques on top-storey wind-induced acceleration of the benchmark dual frame-wall system

Table I.2 Summary and remarks on the six mitigation techniques used to reduce wind-induced acceleration for the benchmark dual frame-wall system

Mitigation technique	Remarks
Increasing $K_{\theta,b}$ (Figure I.17 (a))	<ul style="list-style-type: none"> • Up to 29% reduction in acceleration. • Allows for open space. • Improved floor performance against human-induced vibrations [7, 18]. • Difficult to achieve timber connections with high stiffness ($K_{\theta,b}$) using the currently available solutions in practice.
Increasing $K_{\theta,w}$ (Figure I.17 (b))	<ul style="list-style-type: none"> • Up to 17% reduction in acceleration. • May require large foundation.
Increasing h_w (Figure I.17 (c))	<ul style="list-style-type: none"> • Up to 28% reduction in acceleration. • Large CLT walls can be used around elevator/staircase. • Less open space when large walls are used (away from elevator/staircase shaft).
Use of OR (Figure I.17 (d))	<ul style="list-style-type: none"> • Up to 34% reduction in acceleration. • Architectural restrictions at the floor where the OR is located (should be coordinated with the architect).
Increasing q (Figure I.17 (e))	<ul style="list-style-type: none"> • Up to 25% reduction in acceleration. • Increased seismic demands (for seismic areas). • Larger cross-sections and foundation.
Increasing ξ (Figure I.17 (f))	<ul style="list-style-type: none"> • Up to 40% reduction in acceleration. • Damping is a property of the building, which should be estimated experimentally. Currently, there is a lack of knowledge on damping of multistorey timber buildings and research is needed. • The use of dampers may result in considerable costs and regular maintenance.

3.6 Ultimate limited state considerations

In this section, the ULS design is performed for the benchmark dual system shown in Figure I.10. The structural design was performed for beams, columns, and walls assuming no seismic actions. A basic wind velocity ranging from 20 m/sec to 30 m/sec was used for the calculation of the wind loads, assuming urban environment (IV). For the calculation of forces and moments used in the design, the fundamental ULS combination defined in EN 1990 [63] with wind being the leading variable action was used:

$$E_d = \gamma_G \cdot G_k + \gamma_Q \cdot w_k + \gamma_Q \cdot \psi_0 \cdot Q_k \quad (1.3)$$

where $\gamma_G = 1.20$, $\gamma_Q = 1.50$, $\psi_0 = 0.70$, G_k is the dead load, w_k is the wind load, and Q_k is the live load.

The dead load (G_k) and the live load (Q_k) were kept the same as in Figure I.10 ($G_k = 1.8 \text{ kN/m}^2$ and $Q_k = 2 \text{ kN/m}^2$). The C/C distance was also kept the same as in Figure I.10 (5.0 m).

The structural design for the glulam beams and columns was performed in accordance with EN 1995-1-1 [62]. Since no design guidelines for CLT elements are included in the current EN 1995-1-1 [62], the design checks of the CLT walls were performed according to [64].

To calculate the instability factors ($k_{c,y}$ and $k_{c,z}$ in EN 1995-1-1 [62]) used in the design of walls and columns, the buckling length (l_k) is required. The out-of-plane buckling length of walls and columns is equal to the floor height ($h = 3000 \text{ mm}$). The in-plane buckling length was estimated using linearized buckling analysis:

$$l_k \approx \sqrt{\frac{\pi^2 \cdot E_{0.05} \cdot I}{N_{cr}}} \quad (1.4)$$

where l_k is the buckling length, $E_{0.05}$ is the characteristic elastic modulus, I is the moment of inertia of the cross-sectional area, and N_{cr} is the critical axial load that can cause buckling.

The critical axial load N_{cr} can be calculated as:

$$N_{cr} = N_{max} \cdot \beta \quad (I.5)$$

where N_{max} is the maximum compression force in the wall/column, calculated using FEA with the load combination in Eq. (I.3), and β is the buckling factor. The buckling factor was calculated using FEA by performing linear buckling analysis (with the load combination in Eq. (I.3)).

The utilization ratios for the beams, columns, and walls are shown in Figure I.18 for basic wind velocities 20-30 m/sec. The dual system shown Figure I.10 comprises 30 beams, two columns, and two CLT walls. The utilization ratios shown in Figure I.18 are for the most critical beam, column, and wall. The design of the connections is not included.

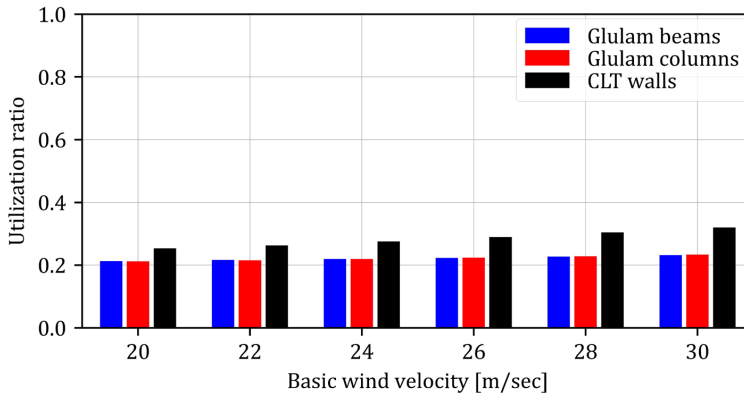


Figure I.18 Utilization ratios for beams, columns, and CLT walls

As shown in Figure I.18, the utilization ratios are well below the unity, indicating that for the dual system, ULS design is unlikely to govern the design. Instead, it is more likely that the design of the dual system is governed by the SLS requirements as presented in section 3.4. However, this conclusion may not hold true if seismic actions were included.

To estimate bending moment demands at the connections of the beams, the bending moment is calculated at all connections (60 connections for the 30 beams) and the maximum absolute value is selected. The results (for a single cross-section) are

shown in Figure I.19 for wind velocities in the range of 20-30 m/sec. As shown in the figure, the bending moments are in the range of 35-50 kNm.

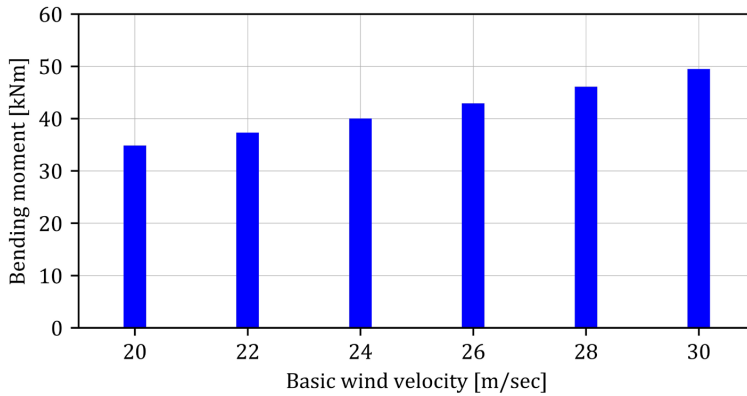


Figure I.19 Maximum moment at beam-to column/wall connections (values for a single cross-section)

An experimental work performed on MRCs based on threaded rods [20] reported moment capacity up to 133 kNm with glulam beams and columns of cross-sectional dimensions 140·450 mm². The use of larger beams (as in Figure I.10) will result in higher moment capacity. Based on the calculated bending moments (Figure I.19), and the results in [20], the connections of the beams seem to be feasible. However, the tests in [20] were performed using glulam beams and columns. Furthermore, the limited number of experiments performed does not allow the estimation of characteristic capacity. Experimental work on MRCs with threaded rods and CLT is lacking in the literature.

3.7 Stiffness variability

The dual system shown in Figure I.10 is highly indeterminate and the magnitude and distribution of internal forces and moments depend on the stiffness of the connections. Due to the inherent variability in the properties of timber connections, variability in internal forces and moments arises [65]. To explore the influence of connection stiffness variability, a normal distribution with 20% Coefficient of Variation (abbr. CoV) was assumed for $K_{\theta,b}$, $K_{\theta,c}$, and $K_{\theta,w}$, confer Figure I.20. The 20% CoV was reasonably assumed based on previous experimental work on timber MRCs with threaded rods [66].

A total of 3000 FEA simulations were performed, considering a basic wind velocity (v_b) of 26 m/sec. For each simulation, random stiffness values drawn from the normal distributions are assigned to all the connections of beams, columns, and walls.

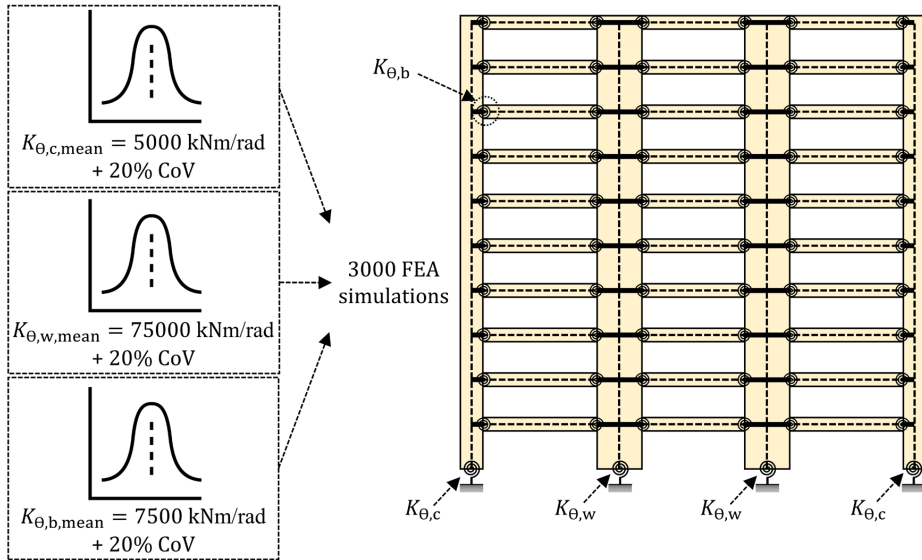


Figure I.20 Variability of connection stiffness (stiffness values are for a single cross-section)

3.7.1 SLS response parameters

Figure I.21 shows the variability in four SLS response parameters, namely: frequency, top-storey wind-induced acceleration, top-floor displacement, and inter-storey drift. The figure demonstrates that the stiffness variability leads to variability in all the response parameters compared to the reference case (obtained using the mean stiffness). However, compared to the reference case, the change (increase/decrease) in all response parameters is small, and hence unlikely to cause serviceability issues and may be neglected.

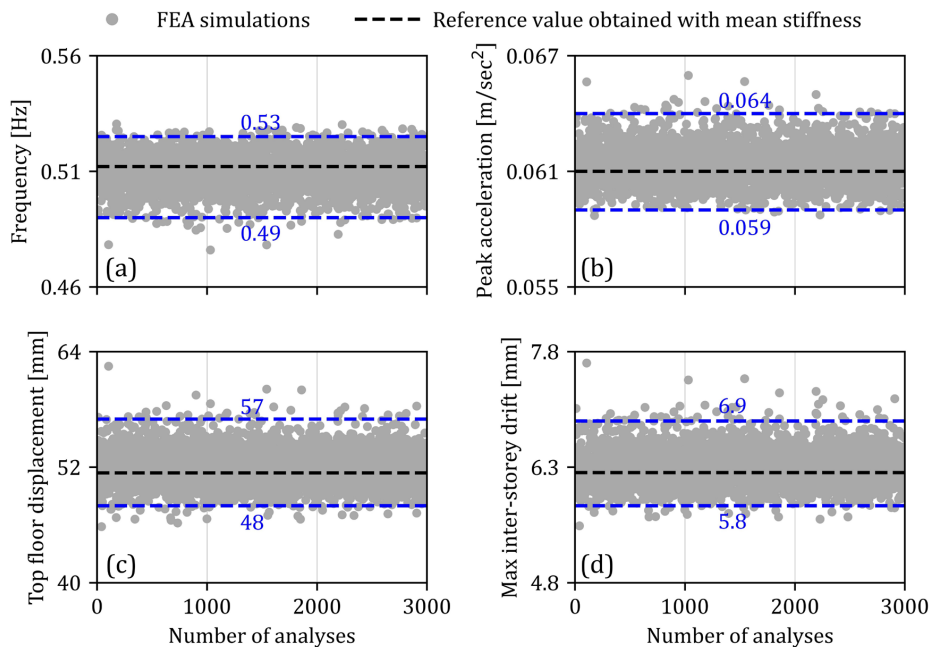


Figure I.21 Variability in (a) frequency, (b) top-storey wind-induced acceleration, (c) top-floor displacement, and (d) inter-storey drift, due to stiffness variability

3.7.2 ULS response parameters

The following ULS response parameters were considered:

1. Maximum bending moment and shear at the connections of the beams.
2. Maximum bending moment and shear at the connections of the columns to the foundation.
3. Maximum bending moment and shear at the connections of the CLT walls to the foundation.

The dual system shown Figure I.10 comprises 30 beams, two columns, and two CLT walls. The response parameters are only reported for the most critical (with the highest bending moment) beam, column, and wall.

The variability in the ULS response parameters is depicted in Figure I.22 (for a single cross-section). The ratios of the 95th and 98th percentiles to the reference case are summarized in Table I.3. Apart from the shear at the beam connections, all response parameters are highly sensitive to stiffness variability. For the connection of the

column, the ratios of the 95th and 98th percentiles to the reference case are high. However, due to the presence of CLT walls (with high lateral stiffness), the shear force and bending moment at the connection of the column are relatively small.

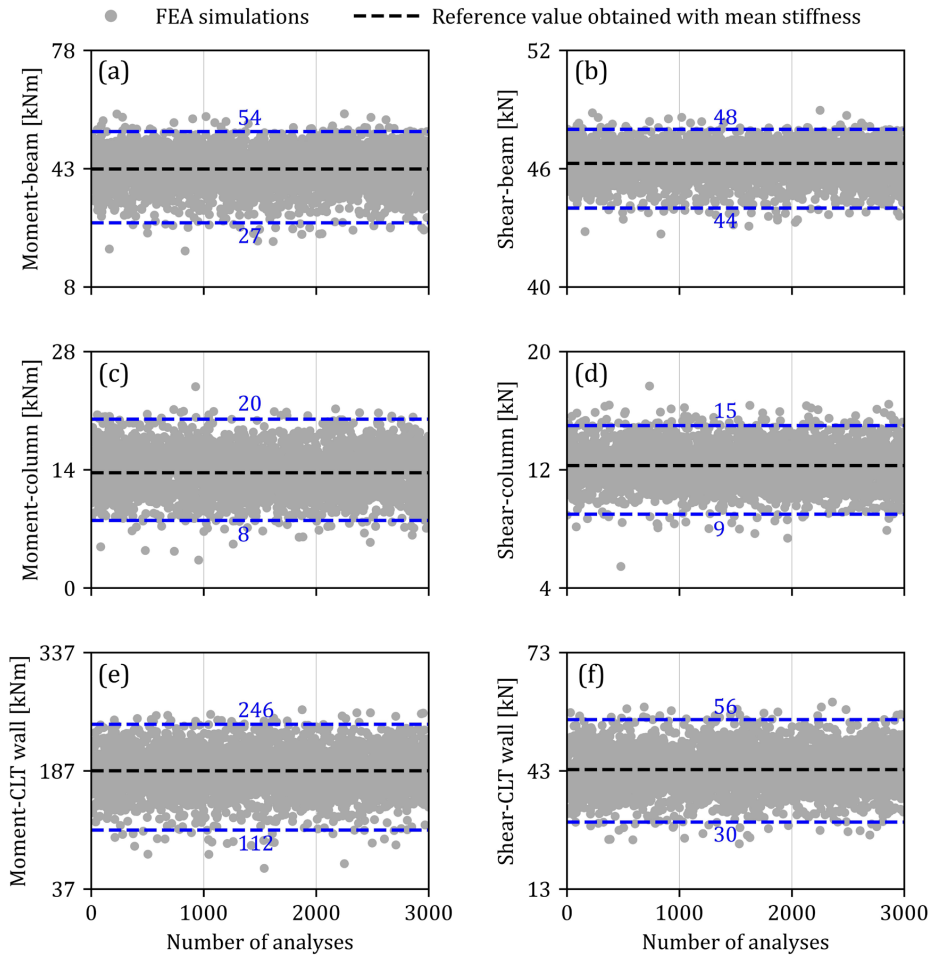


Figure 1.22 Variability in bending moment and shear in the connections of (a)-(b) beam, (c)-(d) column, and (e)-(f) CLT wall

The 95th and 98th percentiles of the bending moments and the shear forces are approximately 18%-40% higher than the reference values obtained by FEA with the mean stiffness values. Such increase should be considered in the design for ULS. However, the use of capacity-designed, ductile connections allows for stress redistribution and can help mitigate these higher forces and moments.

Table I.3 Ratios of 95th and 98th percentiles to the reference case for ULS response parameters

ULS response parameter	$\frac{95^{\text{th}} \text{ percentile}}{\text{Reference case}}$ (%)	$\frac{98^{\text{th}} \text{ percentile}}{\text{Reference case}}$ (%)
Moment-beam connections	119.6%	124.3%
Shear-beam connections	103.5%	103.5%
Moment-column connection	131.6%	140.6%
Shear-column connection	118.2%	123.1%
Moment-CLT wall connection	123.3%	128.2%
Shear-CLT wall connection	120.2%	125.5%

4 Moment-resisting connections for multistorey timber buildings

Moment-resisting timber connections may be categorized into two main categories, namely: connections with laterally-loaded (dowel-type) fasteners and connections with axially-loaded fasteners. Both are discussed in two separate sections.

4.1 Connections with laterally-loaded fasteners

Connections with laterally-loaded fasteners are a type of connection where the fasteners predominantly act in shear under applied loads. Common types of fasteners include bolts, dowels, nails, and screws. If connections with laterally-loaded fasteners meet the requirements for ductile behaviour, which involves embedment and yielding of the fasteners, they can be designed based on the European Yield Model (abbr. EYM) [67]. EYM is based on the work of Johansen [68] and Meyer [69], and is currently implemented in EN 1995-1-1 [62].

Connections can be either timber-to-timber or steel-to-steel connections. Steel-to-timber connections are more common in practice, and feature twice the stiffness of the timber-to-timber connections as suggested by EN 1995-1-1 [62]. Figure I.23 shows examples of MRCs with laterally-loaded fasteners.

A connection with adequate end and edge distances, adequate thickness of timber elements (with respect to the diameter of the steel fasteners), and reinforced with self-tapping screws (abbr. STS), can exhibit good ductility [70]. Experimental work on moment-resisting connections with laterally-loaded fasteners has shown that the use of STS as reinforcement, see Figure I.23 (c), can prevent brittle splitting failure, provide higher ductility, and higher capacity, see e.g. [71, 72].

Despite their ductility, MRCs with laterally-loaded fasteners usually exhibit low stiffness and considerable pinching under cyclic loading, see e.g. [72-75]. Furthermore, connections with laterally-loaded fasteners are generally characterized by low initial stiffness caused by assembly tolerances and imperfections in the contact zones [67, 76].

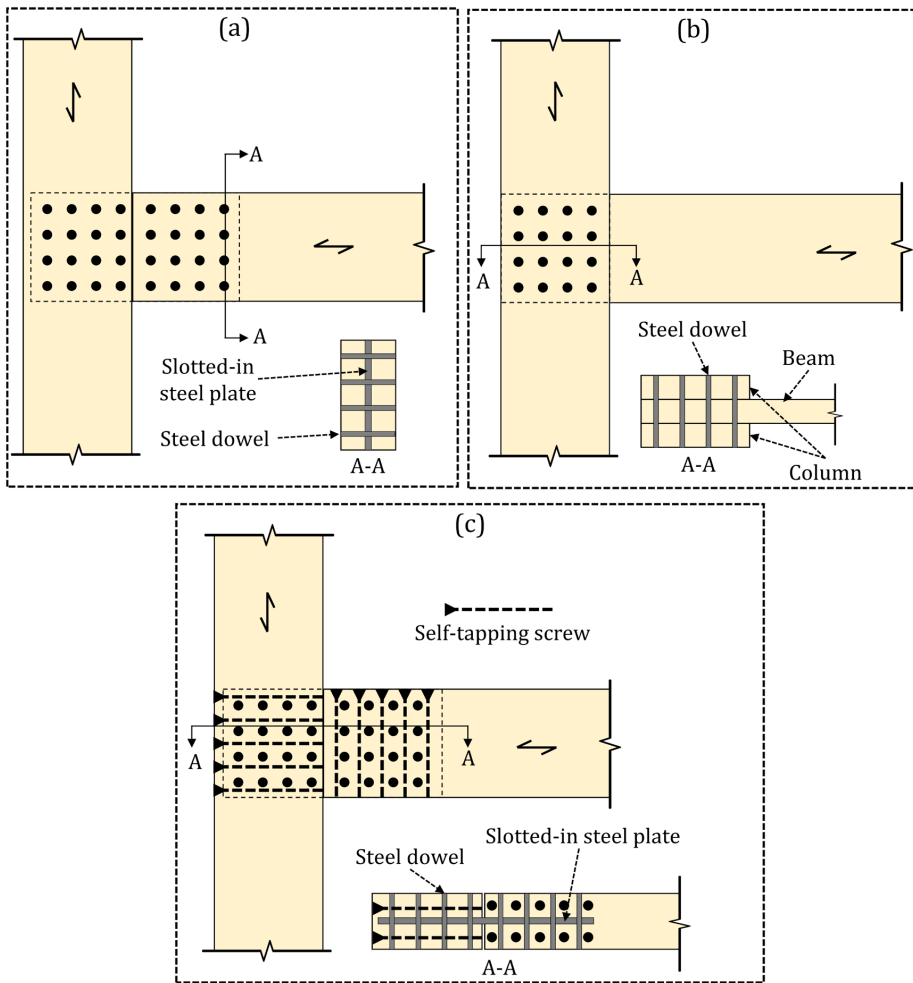


Figure 1.23 Moment-resisting connections with laterally-loaded dowels (a) steel-to-timber, (b) timber-to-timber, and (c) steel-to-timber reinforced with STS

4.2 Connections with axially-loaded fasteners

Moment-resisting timber connections can also be realized using axially-loaded fasteners such as threaded rods [19, 20], STS [77-79], or Glued-in Rods (abbr. GiRs) [80-86]. These connections are generally characterized by a higher stiffness and a lower pinching compared to connections with laterally-loaded fasteners, and allow immediate load take-up without initial slip [18].

GiRs have gained popularity as fasteners in timber connections due to their high strength and stiffness. Connections based on GiRs consist of rods (typically steel) inserted into predrilled holes filled with an adhesive. Commonly used adhesives include epoxy, and polyurethane, but other adhesives may also be used [89]. The manufacturing process of GiRs should be done in a controlled environment with good quality control. Defects and insufficient quality can adversely influence the capacity of GiRs [90]. GiRs can be used for various types of timber connections, including beam-to column and wall-to-foundation MRCs. A review on various applications of GiRs in timber connections can be found in [91].

Figure I.25 shows three variations of beam-to-column, MRCs utilizing GiRs. The first variation shown in Figure I.25 (a) consists of steel bars glued into the beam and the column. This variation may require gluing on-site, which is undesirable and may lead to quality problems. Other variations with steel profiles are shown in Figure I.25. In these variations, the use of steel profiles allows for all gluing to be done in a controlled environment (e.g. factory), and only bolted connections are done on-site. Moreover, these steel profiles can be capacity-designed to allow for a ductile behaviour [85]. It is important that the additional steel profiles are properly protected against fire.

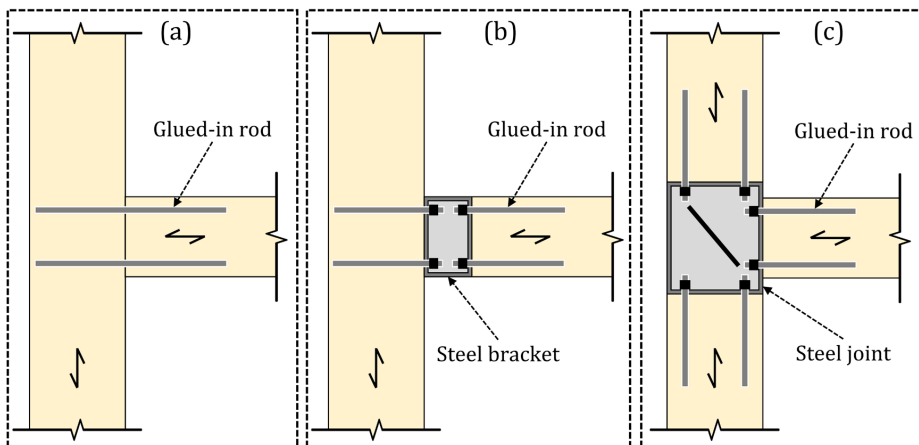


Figure I.25 Moment-resisting connections with GiRs adopted from [85] (a) with GiRs only, (b) with steel bracket, and (c) with steel joint

Threaded rods feature wood thread and are screwed into predrilled holes with a diameter approximately equal to their core diameter. Experimental work on the withdrawal behaviour of axially-loaded threaded rods screwed into glulam [92-94] has shown that they feature high withdrawal stiffness and capacity. Compared to GiRs, systems of screwed-in rods exhibit better fire resistance due to absence of glue, are less brittle, and are less susceptible to quality control problems. Moreover, threaded rods enable a high degree of pre-fabrication since the drilling of holes and installation of rods can be done off-site, thereby reducing the work on-site. The good withdrawal properties of threaded rods, together with the aforementioned advantages, make them suitable for use as fasteners in stiff MRCs.

Several beam-to-column MRCs have been developed at the Norwegian University of Science and Technology, using threaded rods inserted into glulam elements [18-20, 66, 95, 96]. Two notable variations are shown in Figure I.26, where steel coupling parts have been used to connect the rods at the beam side to those at the column side. In these two variations, the threaded rods are predominantly axially loaded. This is because their axial stiffness is much higher than their lateral stiffness. Other variations without any steel coupling parts have also been developed and tested [18], but those lack practicality due to their difficult assembly.

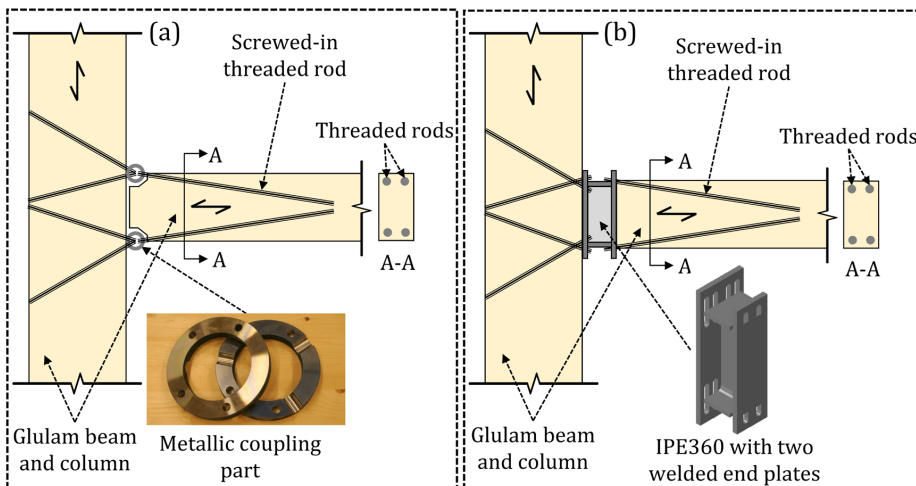


Figure I.26 Moment-resisting connections with threaded rods (a) adopted from [20] and (b) adopted from [66]

The observed failure mode for the connections shown in Figure I.26 is brittle splitting, either in the beam or the column, see Figure I.27. This failure mode is typically caused by high shear stresses and tensile stresses perpendicular to the grain. CLT consists of timber boards arranged in two orthogonal directions, which can potentially prevent the splitting cracks observed in these connections, hence achieve higher capacity and ductility. Additionally, both connections shown in Figure I.26 are challenging to assemble on-site, and do not allow the possibility for increased tolerances. On this basis, one of the primary motivations for this Ph.D. thesis is to develop a timber MRC that addresses these drawbacks. The concept of the developed connection is presented in section 4.3.

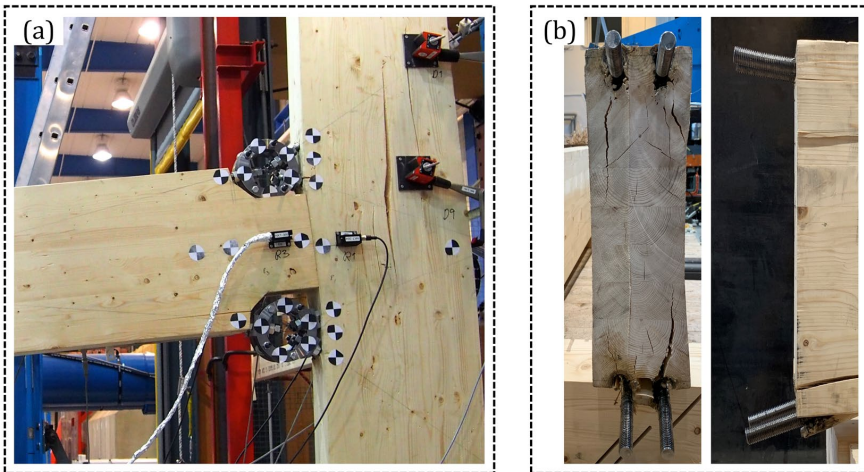


Figure I.27 Splitting (a) in the column [96] and (b) in the beam [66]

4.3 Slip-friction moment connection using threaded rods and CLT

In this Ph.D. thesis, a beam-to-column, MRC with CLT and screwed-in threaded rods was developed and experimentally tested through full-scale testing. In CLT, the transverse layers work as a reinforcement for the main layers. This reinforcement effect has the potential to prevent the splitting cracks that have been observed in connections made with threaded rods and glulam. Furthermore, the connection employs the concept of slip-friction, which has been successfully used in several steel structures, and allows for damage-free ductility through friction slip. The

developed connection features ease of assembly and disassembly with large construction tolerances, resulting in fast construction and the possibility for reuse, further enhancing the sustainability of timber buildings.

Since the concept of slip-friction is a main ingredient of the developed connection, the subsequent subsection (4.3.1) is devoted to an introduction to this type of connections.

4.3.1 Slip-friction connections: background and general concept

Timber exhibits nearly linear elastic behaviour with brittle failure in bending, shear, and tension [21]. However, the incorporation of ductile and dissipative connections can enhance the ductility and enable greater energy dissipation [21]. By utilizing ductile connections, along with capacity-designed timber elements, post-elastic deformations and damage predominantly occur at the connections, leading to an overall ductile behaviour of the structure [21].

Ductile behaviour is particularly important in regions prone to earthquakes as it allows structures to absorb and dissipate seismic energy without collapsing. Ductile behaviour also enhances the robustness of the structure [21], and allows stress redistribution in indeterminate structures, resulting in a higher capacity compared to the capacity obtained from elastic analysis [21]. Furthermore, the increase in bending moments and shear forces due to stiffness variability, as presented in subsection 3.7.2, can be mitigated by use of capacity-designed ductile connections, as they enable stress redistribution.

Ideally, timber connections should exhibit stiff behaviour under wind loads and moderate earthquakes. This is essential to ensure the fulfilment of SLS requirements. Furthermore, these connections should possess adequate ductility to allow for sufficient energy dissipation under design-level earthquakes.

A conventional approach to dissipate energy in timber connections is through embedment and yielding of the fasteners [22]. However, this energy dissipation mechanism leads to irreversible damage, necessitating the rehabilitation of structural elements and connections following a seismic event. The incorporation of

damage-free energy dissipation mechanism can greatly reduce post-earthquake damage. Slip-friction connections have demonstrated the potential for damage-free energy dissipation through friction slip.

The typical components of slip-friction connections are depicted in Figure I.28 (a). These connections consist of multiple elements (three elements, marked 1-3 in Figure I.28 (a)) clamped together using high strength bolt(s). One of the clamped elements incorporates an oversized hole to accommodate movements after slip. The clamping force exerted by the bolt(s) creates friction forces between the contact surfaces, holding the elements of the connection together, confer Figure I.28 (b)

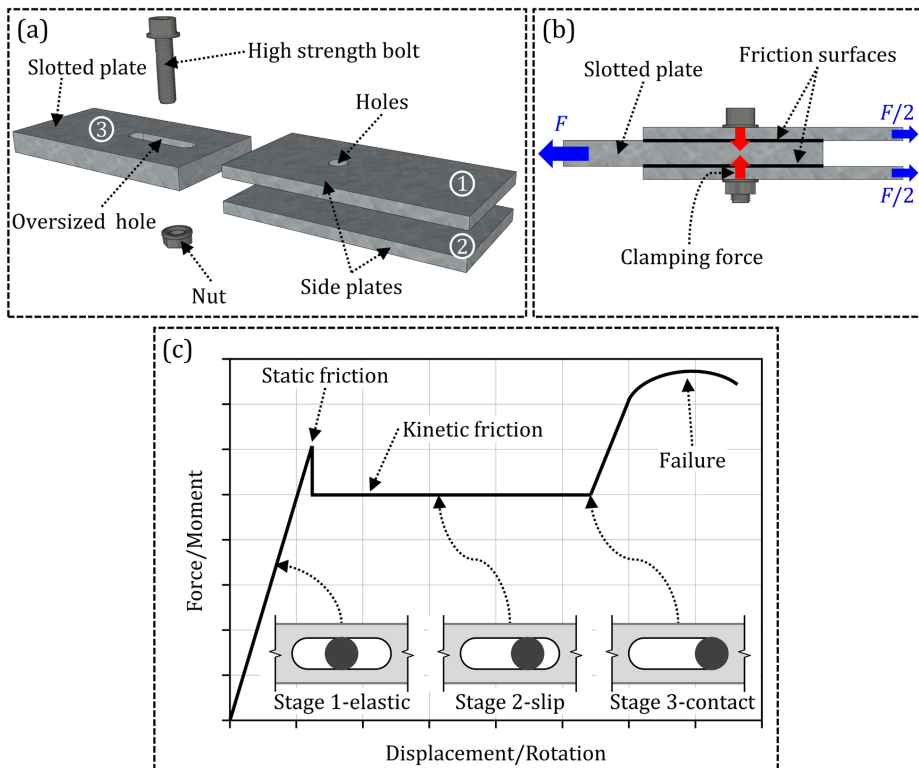


Figure I.28 Friction connection (a) components, (b) assembly, and (c) illustrative force-displacement (or moment-rotation) curve under monotonic loading

At low levels (service-level loads), the connection behaves elastic without slip, confer Stage 1 in Figure I.28 (c). Further increase of the load results in slip, confer Stage 2 in Figure I.28 (c). Upon the first slip, a drop in the load occurs due to the

transition from static to kinetic friction. Depending on the size of the oversized hole, the bolt can come into contact with the edge of the hole, resulting in an increase in the force until failure, confer Stage 3 in Figure I.28 (c).

Slip-friction connections are commonly categorized into two types: Symmetric Friction Connections (abbr. SFCs) and Asymmetric Friction Connections (abbr. AFCs), confer Figure I.29. Research has been conducted on both SFCs [97] and AFCs [98], demonstrating that both types can exhibit significant energy dissipation. However, an experimental study by Hatami et al. [99] has shown that SFCs exhibit better hysteresis behaviour with simultaneous slip activation at the two friction surfaces, higher slip force, and less prestressing loss in the bolt.

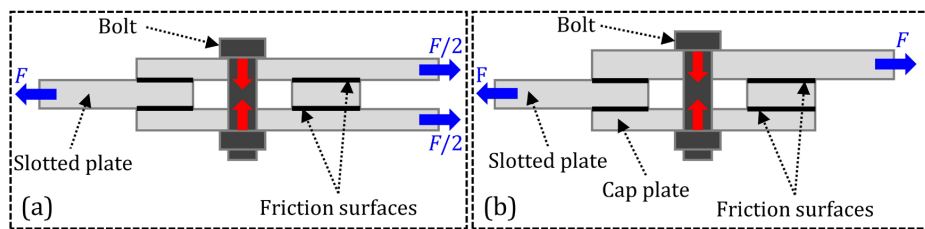


Figure I.29 (a) SFC and (b) AFC

Slip-friction connections have been investigated and implemented in steel structures, see e.g. [24-27]. Nevertheless, there has been limited research on their use in timber structures. Leimcke et al. [100] proposed a slip-friction timber MRC using GiRs and steel profiles. The results in [100] showed that energy dissipation can be achieved without damage in the timber elements. Leo et al. [101] conducted quasi-static cyclic tests on timber shear walls employing SFCs as hold-downs. The results in [101] demonstrated that the use of SCFs resulted in a ductile behaviour. Hashemi et al. [102] performed full-scale testing on a rocking CLT wall utilizing SFCs as hold-downs and incorporating die springs to introduce self-centring.

Hashemi et al. [88] presented full-scale testing of LVL wall equipped a friction connection with integrated self-centring. The connection includes tooth-shaped metallic plates and disc springs, which provide both friction resistance and self-centring capability. This connection is referred to as *Resilient Slip Friction Joint* (abbr. RSFJ). Figure I.30 shows the main components of the RSFJ. The RSFJ has been

used in practice in buildings made of concrete, steel, and timber, mainly in shear walls and bracing elements. Example projects with RSFJ are shown in Figure I.31.

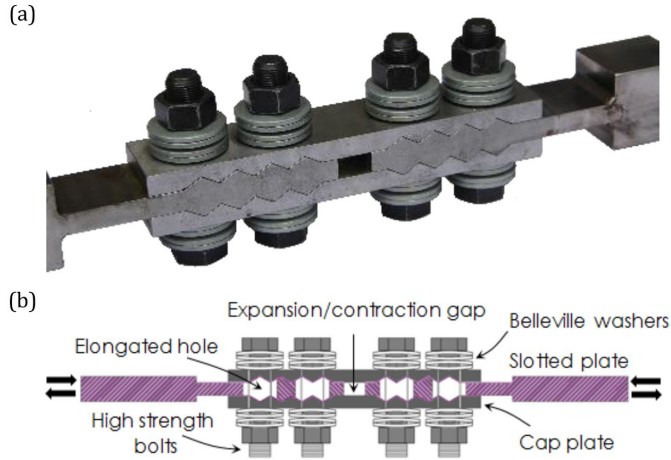


Figure I.30 RSFJ [103] (a) assembly and (b) components

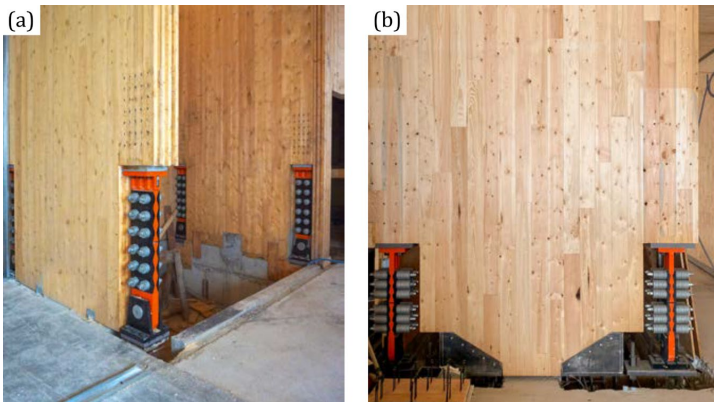


Figure I.31 Projects with RSFJ [104] (a) Fast+Epp head office and (b) oN5 office building

4.3.2 The developed connection: components and assembly

Figure I.32 shows the main components of the developed connection, in addition to the CLT beams and columns. As shown in the figure, the connection consists of purpose-made threaded rods and steel connectors, a steel plate with circular holes, and High Strength Bolts (abbr. HSBs). The used threaded rods have wood thread at one end, and a metric thread at the other end, see Figure I.32 (a). The wood thread

3. Step 3: the steel plate with holes (of 40 mm diameter) is inserted between the two planes of rods, confer Figure I.33 (c).
4. Step 4: the connection is clamped using M30 HSBs (diameter of 30 mm) with predefined torque level (i.e. prestressing level), confer Figure I.33 (d). The M30 HSB goes through the 33 mm hole in the purpose-made connector (see Figure I.32 (b)), and the 40 mm hole in the steel plate.

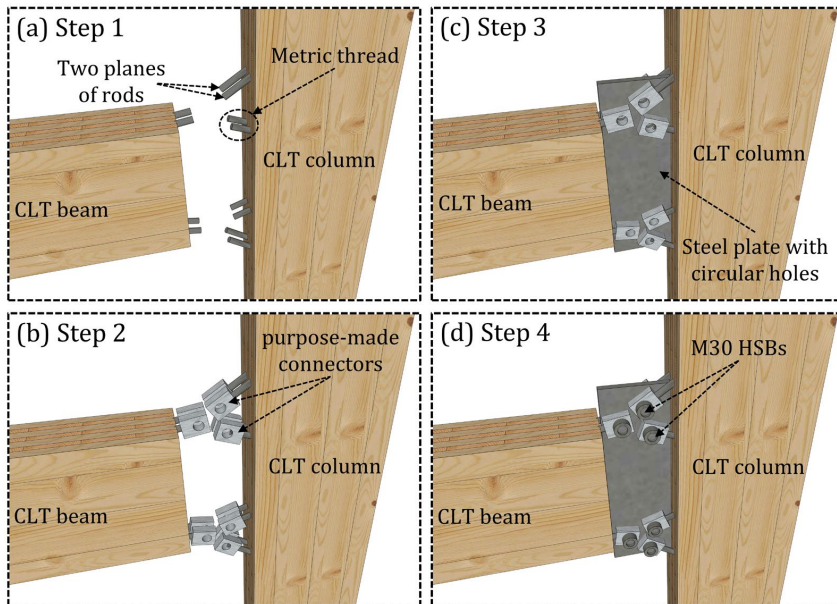


Figure I.33 Main assembly steps of the developed connection

The difference in diameter between the HSB and the hole in purpose-made connector ($33 - 30 = 3$ mm) is made to provide assembly tolerance. The difference between the diameter of the HSBs and the holes in the steel plate ($40 - 30 = 10$ mm) is made to allow slip of the connector at threshold force level. The force level at which slip occurs depends on the clamping force in the HSBs and the friction coefficient between the connector and the steel plate. Allowing slip provides ductility without damaging the timber, i.e. the slip protects the connection by capping the moment acting on it.

4.3.3 Experimental work

The connection presented in subsection 4.3.2 has been tested on a full scale. CLT layup, rods angle to grain, and clamping force (i.e. torque applied to the M30 HSBs) were varied during testing. A total of four full-scale tests have been conducted, where each test specimen has been first tested under non-destructive, service-level, cyclic loading, then tested under destructive cyclic loading. Testing under service-level loading was performed to estimate stiffness and energy dissipation properties of the connection. The destructive testing was performed to evaluate the hysteresis behaviour, ductility, capacity, and failure mode.

The CLT layups used for testing are shown in Figure I.34. The grain direction of the outer layers (main direction) was vertical for the columns and horizontal for the beams. For all tests, two planes of rods have been used, confer Figure I.33 (a). The distance between the two planes of rods was chosen to achieve a minimum thickness of the steel plate while also maintaining a reasonable spacing between rods, and to ensure that the rods are screwed into the desired lamellae. The in-plane dimensions of the steel plate and the location of holes were the same for all specimens, only the thickness of the steel plate (t) was varied. The test specimens are summarized in Table I.4 and depicted in Figure I.35.

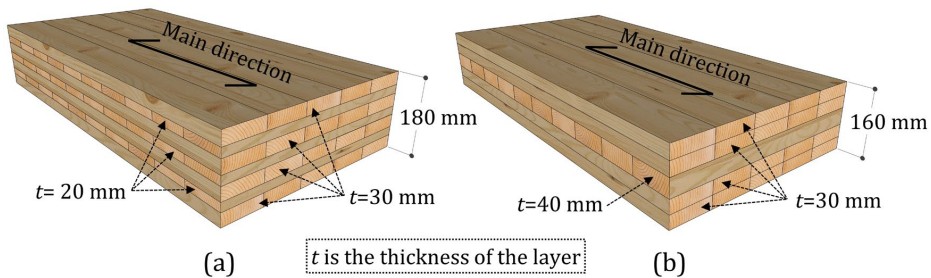


Figure I.34 CLT layups (a) 7 layers and (b) 5 layers

The torque was applied to the HSBs using a hydraulic torque wrench. The prestressing force resulting from the input torque was estimated using the short-form torque–preload equation [105]:

$$M_T = K \cdot D \cdot F_p \quad (1.6)$$

where M_T is the input torque in N.m, K is the nut factor (dimensionless), D is the diameter of the HSB in m, and F_p is the prestressing force in N.

While the nut factor (K) should, ideally, be estimated experimentally, reasonable estimates based on previous testing can be made. For the estimation of the prestressing force (F_p) shown in Table I.4, a nut factor of 0.20 was assumed, a value that is typically used for steel fasteners used in bolted connections [105].

Table I.4 Test specimens

Test no.	CLT layup	HSB torque (N.m)	Layout of the rods	Beam/column (mm ²)	Plate (mm)
1	7 layers	2100 (350 kN) ^a	Figure I.35 (a)	180 · 450	$t = 20$
2	7 layers	2100 (350 kN) ^a	Figure I.35 (b)	180 · 450	$t = 20$
3	5 layers	2100 (350 kN) ^a	Figure I.35 (c)	160 · 450	$t = 30$
4	7 layers	2400 (400 kN) ^a	Figure I.35 (a)	180 · 450	$t = 20$ ^b

^a F_p , estimated with $K = 0.20$, ^b The plate from test 1 was sandblasted and reused

Figure I.36 (a) shows the experimental setup used for testing, a photo of test 2 is shown in Figure I.36 (b). Each specimen was instrumented with a total of 14 Linear Variable Differential Transducers (abbr. LVDTs), confer Figure I.37. The LVDTs were used in pairs to allow for measuring the rotation angle (θ) using the following formula:

$$\theta = \arctan\left(\frac{\delta_i - \delta_j}{d_{i-j}}\right) \quad (I.7)$$

where δ_i and δ_j are the displacements of a pair of LVDTs, and d_{i-j} is the distance between them.

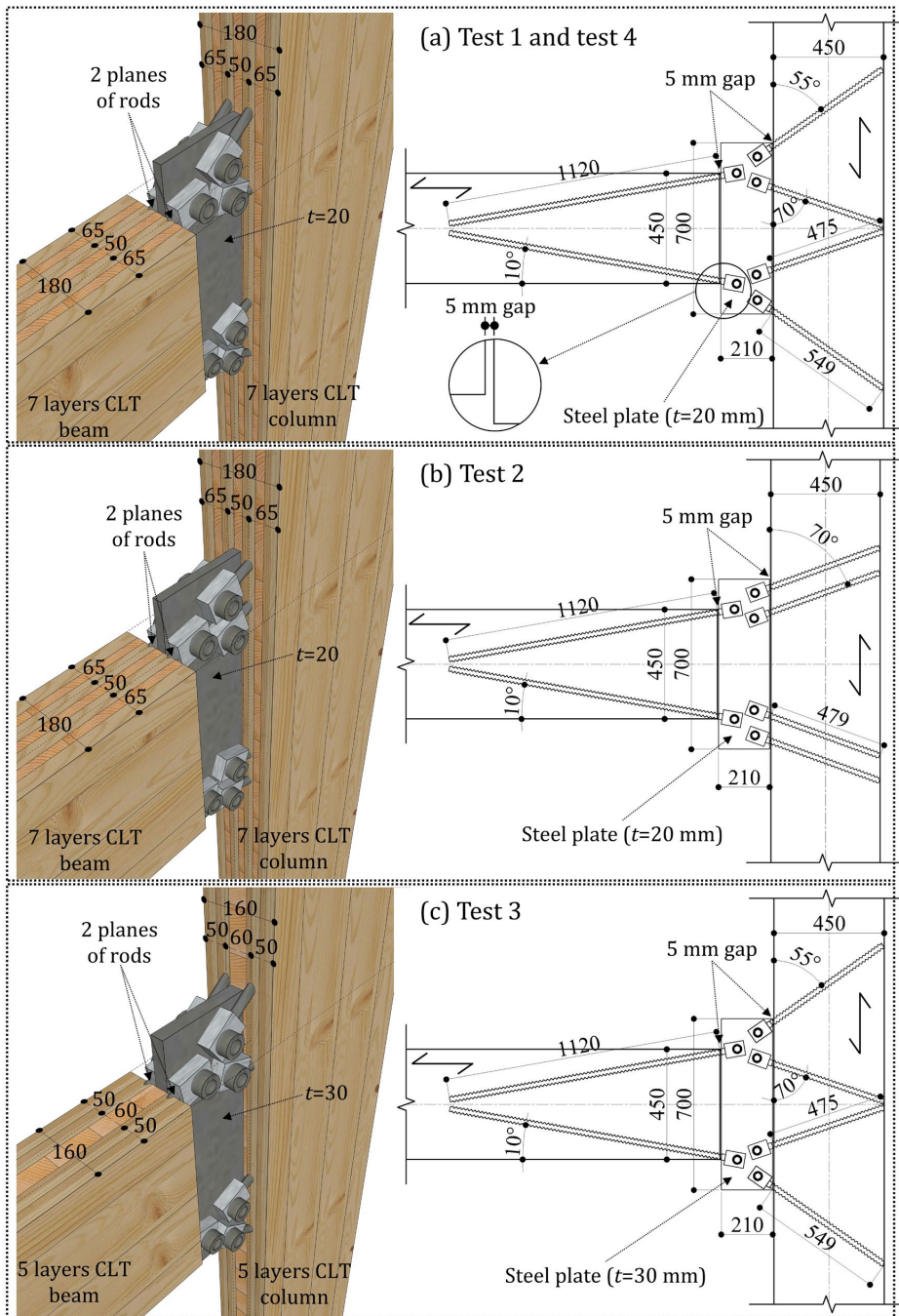


Figure 1.35 Layouts of threaded rods (dimensions in mm) for (a) tests 1 & 4, (b) test 2, and (c) test 3

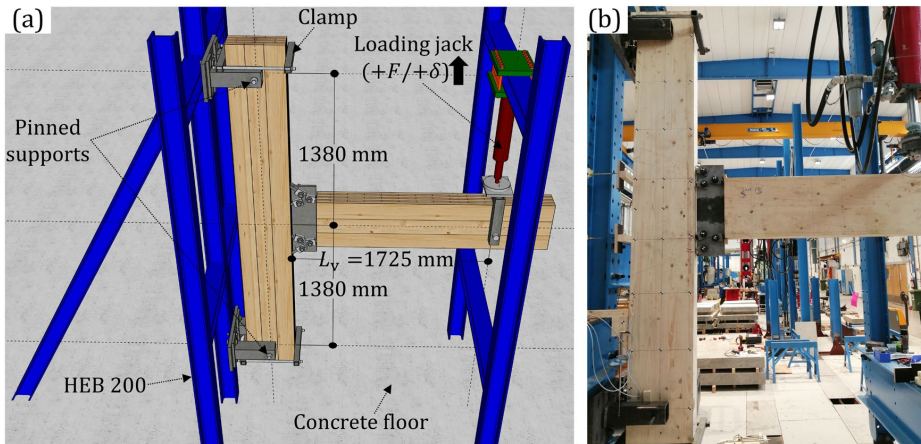


Figure I.36 (a) experimental setup and (b) photo of test 2

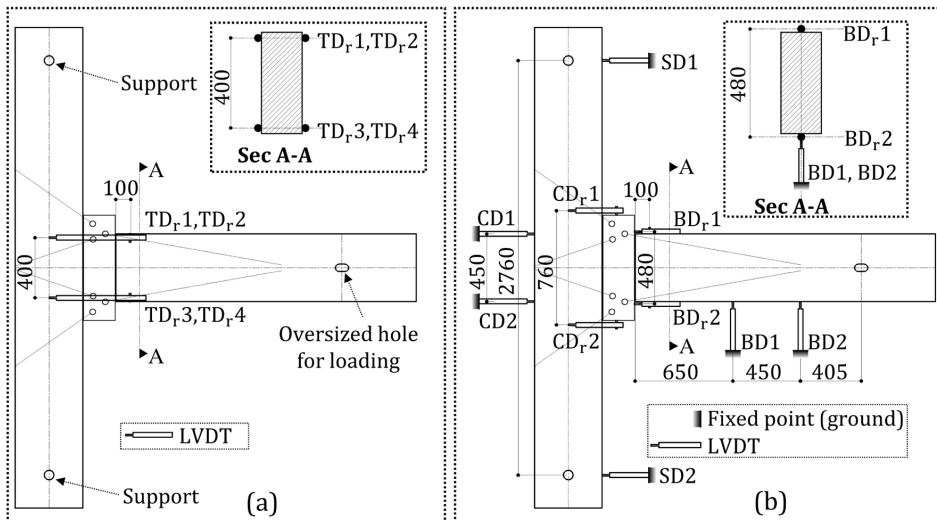


Figure I.37 LVDTs (dimensions in mm) for (a) left & right sides and (b) middle plane

In total, three non-destructive, service-level, force-controlled, cyclic loading protocols were applied to each test specimen, namely: fully reversed moment, negative moment (downwards jack force), and positive moment (upwards jack force), confer Figure I.38. A lever arm (L_v) of 1725 mm was considered for moment calculation, confer Figure I.36 (a). The service-level loading was limited to approximately 40% of the estimated load that results in slip of the purpose-made connectors to ensure linear elastic behaviour.

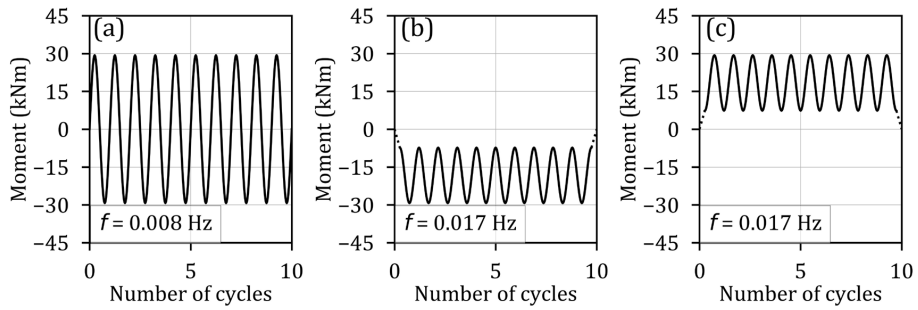


Figure I.38 Non-destructive, service-level, cyclic loading (lever arm of 1725 mm) (a) fully reversed moment, (b) negative moment, and (c) positive moment

Following the testing under service-level loading, the test specimens were tested to failure under a quasi-static, displacement-controlled, sinusoidal loading with increasing amplitude, confer Figure I.39. Prior to testing, the jack displacement (δ_s) corresponding to the onset of slip was estimated. The displacement amplitudes were set as multiples of δ_s , confer Figure I.39. Beyond displacement of δ_s , the displacement amplitude was increased at a step of δ_s until failure. The frequencies of loading cycles were selected to achieve a reasonable test duration of 2-3 hours.

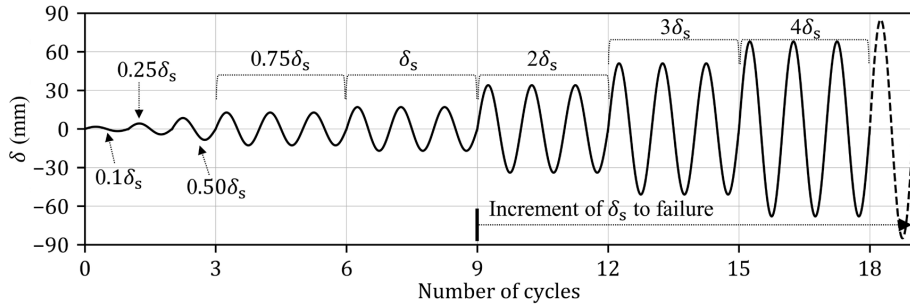


Figure I.39 Displacement regime for destructive loading

Under service-level loading, the connection exhibited high stiffness and immediate load take-up. Under destructive loading, the connection exhibited damage-free energy dissipation via friction slip, demonstrated by large hysteresis loops. The failure in all tests was associated with plastic hinging in the threaded rods inserted at the beam. Detailed experimental results and discussions can be found in Paper II in this thesis. The main findings of the experimental work can be summarized as follows:

1. In general, the connection exhibited very little pinching and immediate load take-up without initial soft behaviour.
2. Under service-level cyclic loading, the connection exhibited high stiffness in the range of 10000-20000 kNm/rad, and approximately 4% equivalent viscous damping ratio.
3. Under destructive loading, and after the onset of slip, the connection exhibited large energy dissipation, demonstrated by large hysteresis loops, without damage in the timber.
4. The slip occurred between the connectors attached to the beam and the steel plate, with the exception of test 1 where slip also occurred at the connectors attached to the column. This is due to the fact that twice the number of rods were used at the column (8 rods in the column and 4 rods in the beam, see Figure I.33).
5. Immediately after the first slip, large drop in the force due to transition from static to kinetic friction was observed. The connection exhibited hardening behaviour in the subsequent cycles. The use of friction shims between the sliding parts has shown to reduce this drop in the force and provide a more stable friction coefficient. In the context of the developed connection, further testing is needed with friction shims placed between the purpose-made connectors and the steel plate. Experimental testing on five different shim materials has been carried out, description of the experimental work, results, and discussions are given in Appendix C.
6. In all the tests, the failure was associated with plastic hinging in the threaded rods inserted at the beam. The observed ultimate moment capacity is in the range of 164-180 kNm. The knowledge of the ultimate capacity of the connection allows the design of the connection according to capacity-based design approach. However, further research is required to determine the appropriate overstrength factor to be used for this connection. By controlling slip at a moment level \leq connection capacity/overstrength factor, brittle failure modes can be avoided.
7. The connections exhibited ductile behaviour with ductility ratios in the range of 4.0-6.6.

8. In all the tested specimens, the columns remained elastic. On the other hand, in similar connections made with glulam, brittle splitting due to high shear and tensile stresses perpendicular to grain was the dominant failure mode. In CLT, the presence of transverse layers seems to reinforce the splitting perpendicular to grain in the panel zone of the column.

4.3.4 Analytical modelling

Figure I.40 shows the two rods layouts that were used in the experimental testing presented in subsection 4.3.3, referred to as Configuration A and Configuration B. In this subsection, an analytical method to estimate their rotational stiffness is presented.

The connections in Figure I.40 can be considered as systems of springs in series, namely: column side spring with rotational stiffness $K_{\theta,c}$, steel plate spring with rotational stiffness $K_{\theta,plate}$, and beam side spring with rotational stiffness $K_{\theta,b}$. The connection rotational stiffness $K_{\theta,con}$ can be calculated using the following formula:

$$K_{\theta,con} = \left(\frac{1}{K_{\theta,c}} + \frac{1}{K_{\theta,plate}} + \frac{1}{K_{\theta,b}} \right)^{-1} \quad (I.8)$$

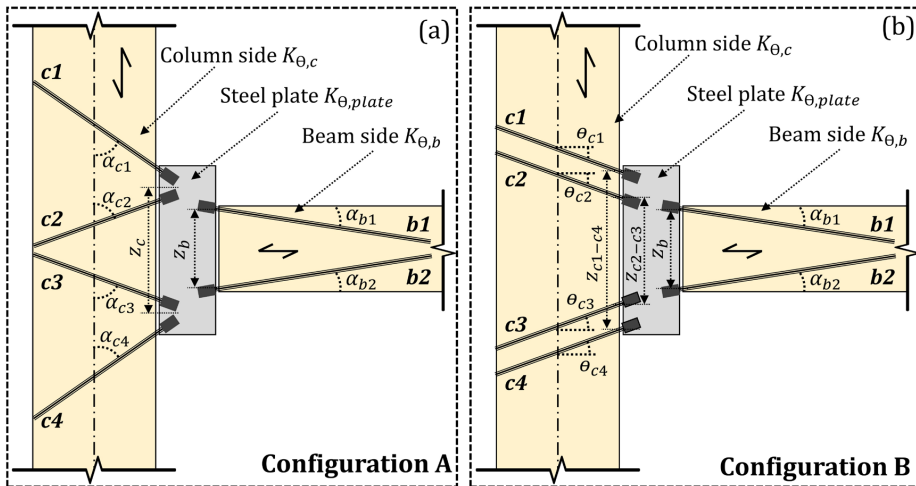


Figure I.40 (a) configuration A and (b) configuration B

The rotational stiffness of the column side ($K_{\theta,c}$) and the beam side ($K_{\theta,b}$) have been derived in [20] by use of the component method and validated by experimental results. The rotational stiffness of the steel plate ($K_{\theta,plate}$) can be estimated by use of FEA. Equations (I.9)-(I.29) apply per plane of rods.

4.3.4.1 Beam side stiffness: configurations A and B

For both configurations in Figure I.40, The stiffness for the beam side ($K_{\theta,b}$) can be calculated using the following formula [20]:

$$K_{\theta,b} = \frac{z_b^2}{(S_{xx,b1} + S_{xx,b2}) + (S_{xy,b2} - S_{xy,b1}) \cdot z_b / (2 \cdot L_v)} \quad (I.9)$$

The compliance terms (S -terms) for the beam side can be calculated as follows [20]:

$$S_{xx,b1} = s_{b1}^2 / K_{v,b1} + c_{b1}^2 / K_{ax,b1} \quad ; \quad S_{xy,b1} = s_{b1} \cdot c_{b1} \cdot (1 / K_{v,b1} - 1 / K_{ax,b1}) \quad (I.10)$$

$$S_{xx,b2} = s_{b2}^2 / K_{v,b2} + c_{b2}^2 / K_{ax,b2} \quad ; \quad S_{xy,b2} = s_{b2} \cdot c_{b2} \cdot (1 / K_{ax,b2} - 1 / K_{v,b2}) \quad (I.11)$$

where L_v is the Moment/Shear ratio, $c_i = \cos\alpha_i$, $s_i = \sin\alpha_i$, $K_{ax,i}$ is the axial stiffness of the threaded rod, and $K_{v,i}$ is the lateral stiffness of the threaded rod.

Prior to structural analysis, L_v is not known and approximations are needed. Neglecting the shear terms in Eq. (I.9) results in the following approximate $K_{\theta,b}$ [65]:

$$K_{\theta,b} \approx \frac{z_b^2}{(S_{xx,b1} + S_{xx,b2})} \quad (I.12)$$

If the rods are inserted at equal angles in the beam ($\alpha_{b1} = \alpha_{b2} = \alpha_b$), and assuming that they approximately have equal axial and lateral stiffness ($K_{ax,b1} = K_{ax,b2} = K_{ax,b}$ and $K_{v,b1} = K_{v,b2} = K_{v,b}$), the following approximation can be obtained [65]:

$$K_{\theta,b} \approx \frac{z_b^2 \cdot K_{ax,b} / 2}{(K_{ax,b} / K_{v,b}) \cdot s_b^2 + c_b^2} \quad (I.13)$$

For the column side stiffness, the formulas are different for the two configurations shown in Figure I.40, therefore, they are presented separately.

4.3.4.2 Column side stiffness: configuration A

For configuration A, the transfer of forces in the column side resembles the transfer of forces in a truss system, where all elements are loaded axially. This is due to the high stiffness of the rods compared to their lateral stiffness. Therefore, the lateral forces in the rods $c1$, $c2$, $c3$ and $c4$ may be neglected.

The stiffness for the column side ($K_{\theta,c}$) can be calculated using the following formula [20]:

$$K_{\theta,c} = \frac{z_c^2}{(S_{xx,c}^{(c1-c2)} + S_{xx,c}^{(c3-c4)}) + (S_{xy,c}^{(c3-c4)} - S_{xy,c}^{(c1-c2)}) \cdot z_c / (2 \cdot L_v)} \quad (I.14)$$

The compliance terms for column side can be calculated as follows:

$$S_{xx,c}^{(c1-c2)} = \frac{c_{c1}^2 / K_{ax,c2} + c_{c2}^2 / K_{ax,c1}}{(c_{c1} \cdot s_{c2} + c_{c2} \cdot s_{c1})^2} \quad ; \quad S_{xy,c}^{(c1-c2)} = \frac{c_{c1} \cdot s_{c1} / K_{ax,c2} - c_{c2} \cdot s_{c2} / K_{ax,c1}}{(c_{c1} \cdot s_{c2} + c_{c2} \cdot s_{c1})^2} \quad (I.15)$$

$$S_{xx,c}^{(c3-c4)} = \frac{c_{c3}^2 / K_{ax,c4} + c_{c4}^2 / K_{ax,c3}}{(c_{c3} \cdot s_{c4} + c_{c4} \cdot s_{c3})^2} \quad ; \quad S_{xy,c}^{(c3-c4)} = \frac{c_{c3} \cdot s_{c3} / K_{ax,c4} - c_{c4} \cdot s_{c4} / K_{ax,c3}}{(c_{c3} \cdot s_{c4} + c_{c4} \cdot s_{c3})^2} \quad (I.16)$$

where L_v is the Moment/Shear ratio, $c_i = \cos\alpha_i$, $s_i = \sin\alpha_i$, and $K_{ax,i}$ is the axial stiffness of the threaded rod.

Neglecting the shear terms in Eq. (I.14) results in the following approximate $K_{\theta,c}$ [65]:

$$K_{\theta,c} \approx \frac{z_c^2}{(S_{xx,c}^{(c1-c2)} + S_{xx,c}^{(c3-c4)})} \quad (I.17)$$

If the rods are inserted at equal angles in the column ($\alpha_{c1} = \alpha_{c2} = \alpha_{c3} = \alpha_{c4} = \alpha_c$), and assuming that they approximately have equal axial stiffness ($K_{ax,c1} = K_{ax,c2} = K_{ax,c3} = K_{ax,c4} = K_{ax,c}$), the following approximation can be obtained [65]:

$$K_{\theta,c} \approx z_c^2 \cdot K_{ax,c} \cdot s_c^2 \quad (I.18)$$

4.3.4.3 Column side stiffness: configuration B

The rods in the column of configuration B are arranged in parallel. Although this results in a higher axial stiffness of rods, the rods are also laterally loaded. The column side stiffness ($K_{\theta,c}$) can be calculated using Eqs. (I.19)-(I.21), and the compliance terms can be calculated using Eqs. (I.22)-(I.25).

$$K_{\theta,c} = K_{\theta}^{(c1-c4)} + K_{\theta}^{(c2-c3)} \quad (I.19)$$

$$K_{\theta}^{(c1-c4)} = \frac{z_{c1-c4}^2}{(S_{xx,c1} + S_{xx,c4}) + (S_{xy,c4} - S_{xy,c1}) \cdot z_{c1-c4} / (2 \cdot L_v)} \quad (I.20)$$

$$K_{\theta}^{(c2-c3)} = \frac{z_{c2-c3}^2}{(S_{xx,c2} + S_{xx,c3}) + (S_{xy,c3} - S_{xy,c2}) \cdot z_{c2-c3} / (2 \cdot L_v)} \quad (I.21)$$

$$S_{xx,c1} = s_{c1}^2 / K_{v,c1} + c_{c1}^2 / K_{ax,c1} \quad ; \quad S_{xy,c1} = s_{c1} \cdot c_{c1} \cdot (1 / K_{v,c1} - 1 / K_{ax,c1}) \quad (I.22)$$

$$S_{xx,c2} = s_{c2}^2 / K_{v,c2} + c_{c2}^2 / K_{ax,c2} \quad ; \quad S_{xy,c2} = s_{c2} \cdot c_{c2} \cdot (1 / K_{v,c2} - 1 / K_{ax,c2}) \quad (I.23)$$

$$S_{xx,c3} = s_{c3}^2 / K_{v,c3} + c_{c3}^2 / K_{ax,c3} \quad ; \quad S_{xy,c3} = s_{c3} \cdot c_{c3} \cdot (1 / K_{ax,c3} - 1 / K_{v,c3}) \quad (I.24)$$

$$S_{xx,c4} = s_{c4}^2 / K_{v,c4} + c_{c4}^2 / K_{ax,c4} \quad ; \quad S_{xy,c4} = s_{c4} \cdot c_{c4} \cdot (1 / K_{ax,c4} - 1 / K_{v,c4}) \quad (I.25)$$

where L_v is the Moment/Shear ratio, $c_i = \cos \theta_i$, $s_i = \sin \theta_i$, $K_{ax,i}$ is the axial stiffness of the threaded rod, and $K_{v,i}$ is the lateral stiffness of the threaded rod.

Neglecting the shear terms in Eqs. (I.20) and (I.21) results in the following approximate $K_{\theta}^{(c1-c4)}$ and $K_{\theta}^{(c2-c3)}$:

$$K_{\theta}^{(c1-c4)} \approx \frac{z_{c1-c4}^2}{(S_{xx,c1} + S_{xx,c4})} \quad (I.26)$$

$$K_{\theta}^{(c2-c3)} \approx \frac{z_{c2-c3}^2}{(S_{xx,c2} + S_{xx,c3})} \quad (I.27)$$

If the rods are inserted at equal angles in the column ($\theta_{c1} = \theta_{c2} = \theta_{c3} = \theta_{c4} = \theta_c$), and assuming that they approximately have equal axial and lateral stiffness ($K_{ax,c1} = K_{ax,c2} = K_{ax,c3} = K_{ax,c4} = K_{ax,c}$ and $K_{v,c1} = K_{v,c2} = K_{v,c3} = K_{v,c4} = K_{v,c}$), the following approximation can be obtained:

$$K_{\theta}^{(c1-c4)} \approx \frac{z_{c1-c4}^2 \cdot K_{ax,c} / 2}{(K_{ax,c} / K_{v,c}) \cdot s_c^2 + c_c^2} \quad (I.28)$$

$$K_{\theta}^{(c2-c3)} \approx \frac{z_{c2-c3}^2 \cdot K_{ax,c} / 2}{(K_{ax,c} / K_{v,c}) \cdot s_c^2 + c_c^2} \quad (I.29)$$

The stiffness of the developed connection was calculated using the analytical expressions presented in this subsection. The stiffness values of the threaded rods estimated from the experimental work which will be presented in subsection 4.4.2 were used. The calculated connection stiffness was compared with the stiffness values estimated from the full-scale testing described in subsection 4.3.3, and the comparison shows good agreement. Detailed calculations are given in Appendix A.

4.4 Screwed-in threaded rods

4.4.1 Background

Threaded rods can be seen as an extension of STS, but with larger length and diameter, resulting in higher stiffness and capacity. They have been originally developed for use as reinforcement in timber elements [106]. Previous research on threaded rods inserted into glulam [92-94] has shown that, when axially loaded, they feature high stiffness and capacity. When used as fasteners in timber MRCs, the arrangement of the rods to ensure they are predominantly axially loaded is important to achieve high stiffness, see e.g. [19, 20]. Arranging the rods to act in shear (laterally-loaded) results in a softer behaviour and hence a softer connection.

Threaded rods can be inserted into wood at different angles to grain. Previous research has shown that they are very robust when inserted perpendicular to grain. Inserting rods parallel to grain, although shows higher stiffness compared to rods inserted perpendicular to grain [93], results in a large variation in their capacity [94]. Example load-displacement curves for rods inserted parallel and perpendicular to grain are shown in Figure I.41. As shown in the figure, the behaviour is more brittle for rods inserted parallel to grain. Furthermore, rods inserted parallel to grain are vulnerable to cracks, a crack along the grain in the same plane as the rod can result in a significant loss of strength. Therefore, it is important that the rods are inserted at an angle to the grain.

Previous research has investigated the strength and stiffness of threaded rods inserted into glulam, see e.g. [92-94, 107]. Several experimental and numerical studies have been conducted on GiRs inserted into CLT, see e.g. [108-115]. However,

to the knowledge of the author, experimental studies of threaded rods inserted into CLT elements are lacking in the literature. Therefore, a series of experiments were conducted on threaded rods inserted parallel and perpendicular to the grain into CLT elements.

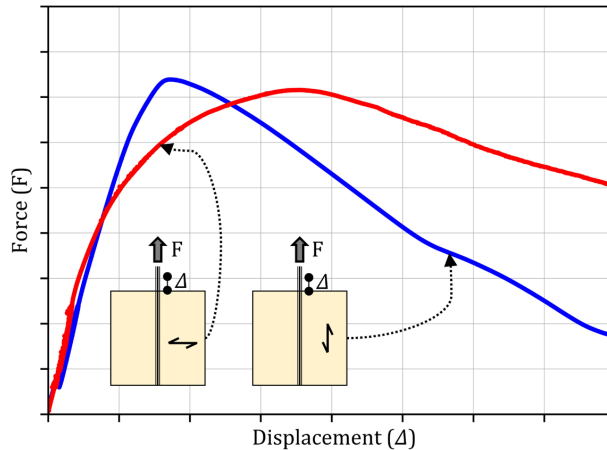


Figure I.41 Typical force-displacement curves for rods inserted parallel and perpendicular to grain, adopted from [116]

4.4.2 Threaded rod inserted into CLT: experimental work

A series of experiments were conducted to investigate the withdrawal behaviour of threaded rods inserted into the narrow face of CLT elements. The experimental investigation included rods inserted parallel and perpendicular to the grain. It should be noted that rods parallel to the grain should be avoided; the experimental work performed here is for characterization purposes. Identical threaded rods to that shown in Figure I.32 (a) were used for the testing. The threaded rods were inserted into the middle layer of three-layer, non-edge glued CLT panels in pre-drilled holes with a diameter equal to their core diameter (16.1 mm), see Figure I.42. Two force levels were considered in the experimental work, namely: non-destructive, service-level loading and destructive loading, confer Figure I.43. The service-level loading consists of three cyclic loading protocols, namely: tension (8 cycles), compression (8 cycles), and fully reversed (8 cycles), confer Figure I.43 (a). In the service-level loading, the load was limited to 40% of the estimated withdrawal

capacity ($F_{ax,est}$) to ensure elastic behaviour. The destructive loading involves applying a monotonic load (tension or compression) until failure as specified by EN 26891 [117], confer Figure I.43 (b).

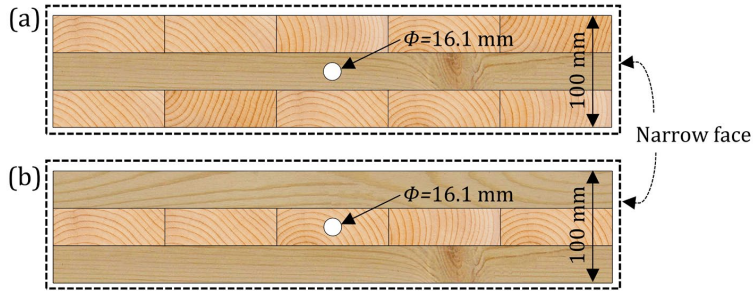


Figure I.42 Rods inserted (a) perpendicular to the grain and (b) parallel to the grain

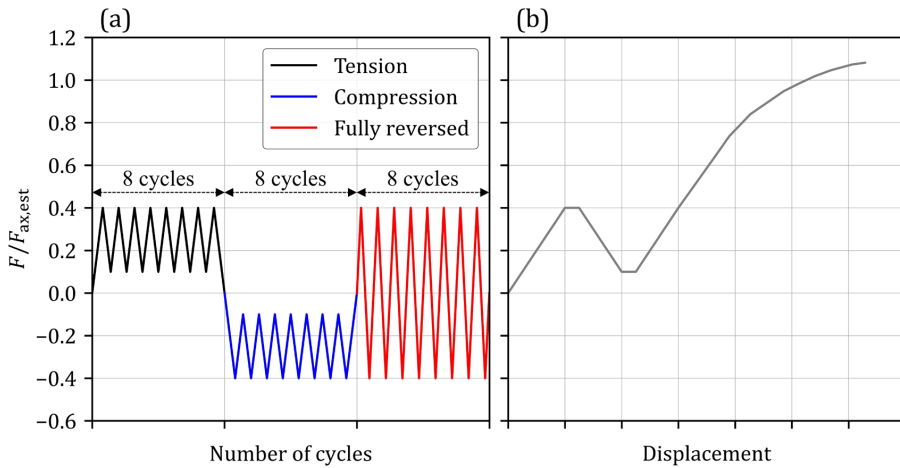


Figure I.43 (a) non-destructive, service-level, cyclic loading and (b) destructive monotonic loading

For the specimens tested under non-destructive, service-level loading, the penetration length was varied from 5 to 20 times the outer thread diameter of the rod ($d = 22 \text{ mm}$) to study the influence of penetration length on the withdrawal stiffness. The threaded rod is first screwed into the specimens at a $5d$ penetration length, and all service-level load testing is performed. The same threaded rod is further screwed into the specimen at a step of $5d$, and the testing is performed again for $10d$, $15d$ and $20d$ penetration lengths, confer Figure I.44. The variation of penetration length results in a total of 12 non-destructive tests per specimen.

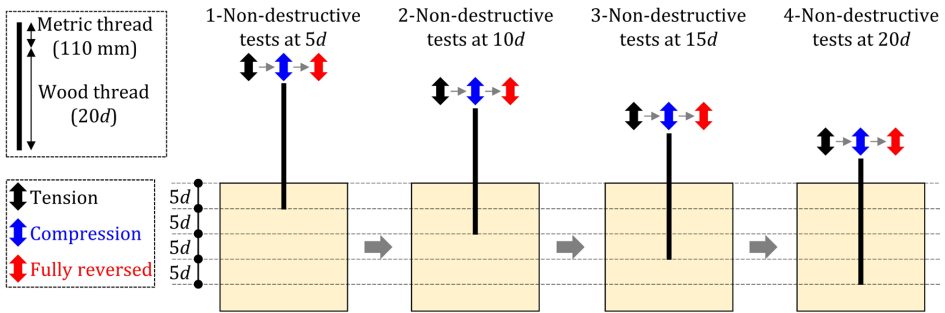


Figure I.44 Variation of rod penetration length during non-destructive, service-level, cyclic loading

Two loading configurations were considered, namely: pull-pull and pull-push, confer Figure I.45. Specimens tested in pull-pull were prepared longer to accommodate the two supporting rods. Specimens tested in pull-push were prepared wider to accommodate the supporting beams. Two LVDTs were placed at both sides of the specimen, confer Figure I.45. The average displacement of the two LVDTs was used as the withdrawal displacement. The experimental results were used to evaluate the stiffness under cyclic and monotonic loading, the damping ratios, the withdrawal capacity, and the failure mode.

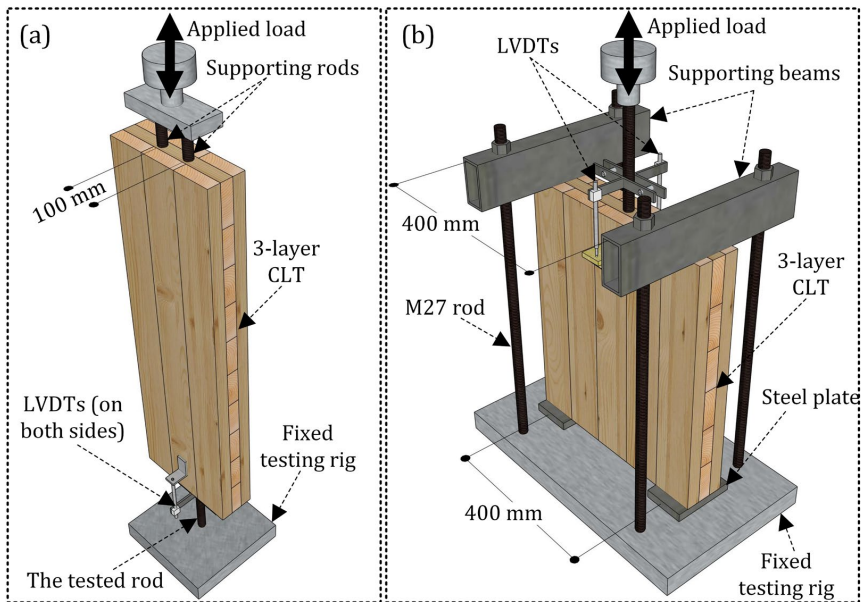


Figure I.45 Loading configurations (a) pull-pull and (b) pull-push

Figure I.46 summarizes all test series. In total, seven test series were conducted:

1. **PL** (the rod was inserted perpendicular to the grain, see Figure I.46 (a)):
Four specimens were tested in pull-pull loading. The specimens were first tested under service-level cyclic loading at four penetration lengths ($5d$, $10d$, $15d$, and $20d$, see Figure I.44), then tested to failure under monotonic tension at $20d$.
2. **PL-R** (the rod was inserted perpendicular to the grain, see Figure I.46 (b)):
Four specimens were tested in pull-pull loading. The specimens had an identical geometry to PL, but were reinforced with eight STS. The specimens were first tested under service-level cyclic loading at four penetration lengths ($5d$, $10d$, $15d$, and $20d$, see Figure I.44), then tested to failure under monotonic tension at $20d$.
3. **PS** (the rod was inserted perpendicular to the grain, see Figure I.46 (c)):
Six specimens were tested in pull-push loading. The specimens were first tested under service-level cyclic loading at four penetration lengths ($5d$, $10d$, $15d$, and $20d$, see Figure I.44), then tested to failure under monotonic tension at $20d$.
4. **PS-T** (the rod was inserted perpendicular to the grain, Figure I.46 (d)):
Five specimens were tested in pull-push loading. The specimens were tested to failure under monotonic tension at $20d$ penetration length. In this series, no non-destructive testing was performed at $5d$, $10d$, $15d$ and $20d$.
5. **PS-C** (the rod was inserted perpendicular to the grain, Figure I.46 (e)):
Four specimens were tested in pull-push loading. The specimens were tested to failure under monotonic compression at $20d$ penetration length. In this series, no non-destructive testing was performed at $5d$, $10d$, $15d$ and $20d$.
6. **PS-0** (the rod was inserted parallel to the grain, Figure I.46 (f)):
Seven specimens were tested in pull-push loading. The specimens were first tested under service-level cyclic load at four penetration lengths ($5d$, $10d$, $15d$, and $20d$, see Figure I.44), then tested to failure under monotonic tension at $20d$.
7. **PS-0-T** (the rod was inserted parallel to the grain, Figure I.46 (g)):
Seven specimens were tested in pull-push loading. The specimens were tested to failure under monotonic tension at $20d$ penetration length. In this series, no non-destructive testing was performed at $5d$, $10d$, $15d$ and $20d$.

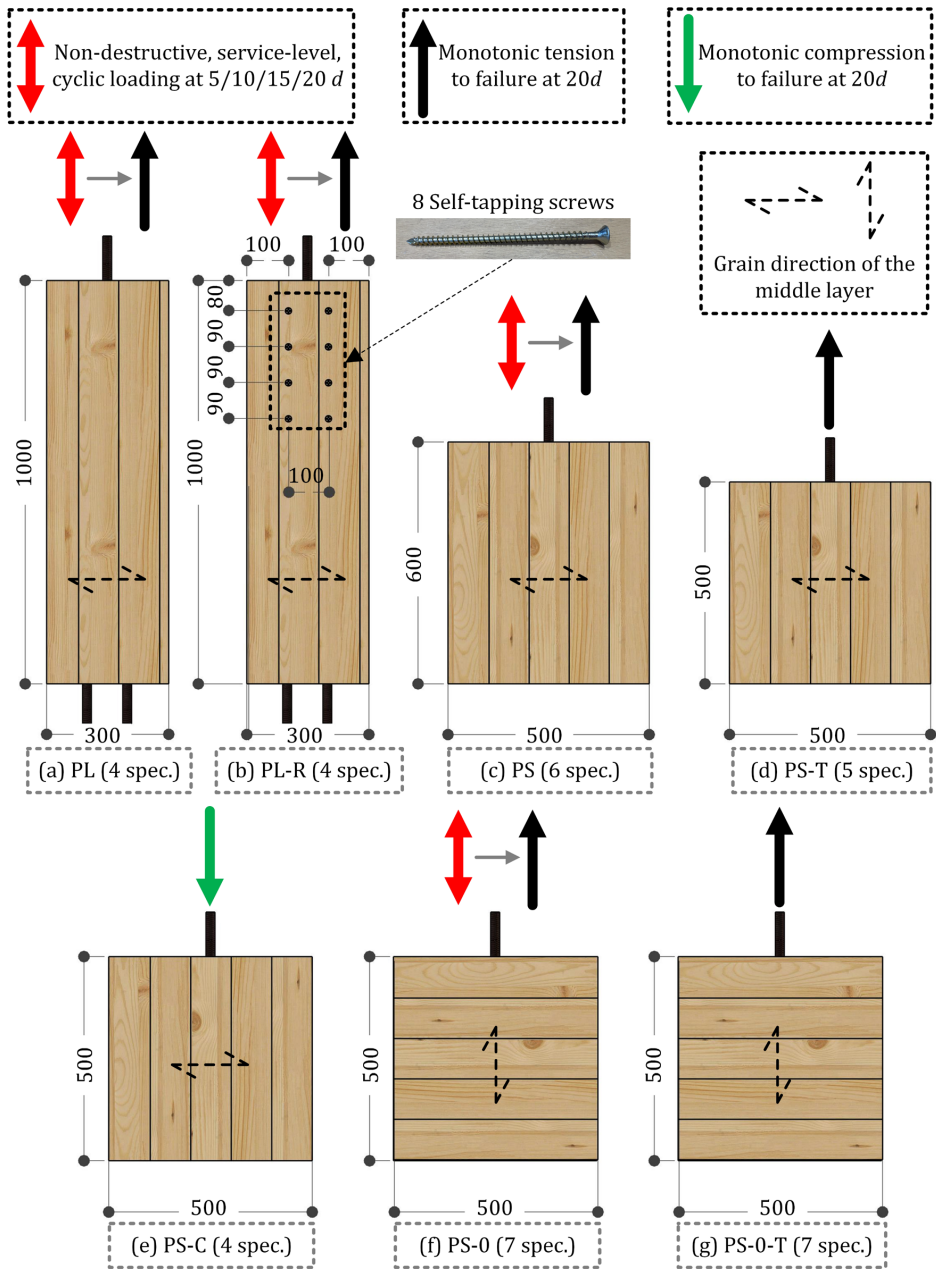


Figure I.46 Test series with rods inserted (a)-(e) perpendicular to the grain and (f)-(g) parallel to the grain, (dimensions in mm)

For test series PL, PL-R, PS, PS-T, and PS-C shown in Figure I.46 (i.e. rods inserted perpendicular to the grain), detailed experimental results and discussions are in Paper I in this thesis. Experimental results and discussions for test series PS-0 and PS-0-T (i.e. rods inserted parallel to the grain) are in Appendix B. The main findings drawn from the experimental work (including all test series) can be summarized as follows:

1. Threaded rods inserted perpendicular to the grain exhibited high withdrawal stiffness. When inserted at a penetration length of $20d$ (440 mm), the mean withdrawal stiffness ranges from 100 to 250 kN/mm. On average, the measured stiffness is 18% higher than the stiffness reported in [118] for identical rods inserted perpendicular to the grain into glulam. This higher stiffness can be attributed to the fact that while the rods were inserted perpendicular to the grain into the middle layer, the outer layers are parallel to the applied load (higher material stiffness along the grain). The variation in the measured stiffness is possibly due to the different loading types (tension, compression, and fully reversed) and the loading configurations (pull-pull and pull-push). Furthermore, the stiffness exhibits a non-linear relationship with the penetration length, showing noticeable convergence beyond $15d$ (330 mm).
2. The mean withdrawal stiffness for the rods inserted parallel to the grain ranges from 125 to 210 kN/mm for $20d$ penetration length. The measured stiffness is comparable to the stiffness reported in [118] for identical rods inserted parallel to the grain into glulam. The stiffness for rods inserted parallel to the grain shows faster convergence with penetration length compared to the rods inserted perpendicular to the grain.
3. The stiffness of rods inserted parallel to the grain is generally higher than the stiffness of rods inserted perpendicular to the grain, particularly for short penetration lengths ($5d$ - $10d$). For penetration lengths of $5d$ and $10d$, the stiffness of rods inserted parallel to the grain is nearly double the stiffness of rods inserted perpendicular to the grain. For penetration lengths of $15d$ and $20d$, the stiffness of rods inserted parallel to the grain is 30% higher than the stiffness of

rods inserted perpendicular to the grain. These ratios are based on test series PS and PS-0 with the same loading configuration (pull-push).

4. Threaded rods inserted perpendicular to the grain exhibited high withdrawal capacity. When inserted at a penetration length of $20d$, the mean withdrawal capacity ranges from 137 to 163 kN. The measured capacities are comparable to those of identical threaded rods inserted perpendicular to the grain into glulam [118]. The capacity seems to be not very sensitive to the loading type and loading configuration. For rods inserted at a penetration length of $20d$ and tested under destructive monotonic load, reinforcement with self-tapping screws can provide a more ductile load-displacement curve without noticeable increase in the withdrawal capacity.
5. All threaded rods (parallel and perpendicular to the grain) with a penetration length of $20d$ failed in withdrawal failure mode. Only for the PL series (pull-pull without reinforcement), the withdrawal failure was combined with splitting.
6. For the rods inserted perpendicular to the grain, the withdrawal capacity seems to be not sensitive to the loading history (screwing-in and loading at different penetration lengths prior to the destructive loading).
7. For the rods inserted parallel to the grain, a withdrawal capacity in the range of 66-123 kN and 103-148 kN was observed for PS-0 series (with loading history) and PS-0-T series (without loading history), respectively. The lower withdrawal capacity observed in PS-0 series may be attributed to the loading history. However, while the specimens of the PS-0-T series were prepared and tested within days, the specimens of the PS-0 series were tested under destructive loading after seven months from the time the rods were screwed into the specimens. Therefore, cracks may have developed and contributed to the lower capacity observed in PS-0 series. This requires more in-depth investigation.
8. The withdrawal capacity of rods inserted perpendicular to the grain shows small variation, ranging from 137 to 163 kN. On the other hand, significant variation was observed in the withdrawal capacity of rods inserted parallel to the grain, ranging from 66 to 148 kN.

5 Summary of the appended papers

This Ph.D. thesis is paper-based, the papers published or submitted to international peer-reviewed journals and conferences are summarized in this chapter. The full papers are included in Paper II of this thesis.

5.1 Paper I

Experimental investigation on axially-loaded threaded rods inserted perpendicular to grain into cross laminated timber

This paper presents an experimental study on the withdrawal behaviour of threaded rods inserted perpendicular to the grain into the narrow face of CLT elements. Threaded rods with outer thread diameter (d) of 22 mm and core diameter (d_1) of 16.1 mm were used. The rods were inserted into the narrow face of 3-layer, non-edge glued CLT elements. Two load levels were considered in this study, namely: non-destructive service-level cyclic loading, and monotonic to failure loading. Throughout the experimental work, the following parameters were varied:

1. Penetration length: the rods were inserted into the CLT elements at four penetration lengths, namely: $5d$, $10d$, $15d$, and $20d$.
2. Loading type: the specimens were tested under tension, compression, and fully reversed cyclic loading.
3. Loading configuration: the specimens were tested under two different loading configurations, namely: pull-pull and pull-push.
4. Use of reinforcement: self-tapping screws (STS) were used in one of the test series to study their influence on the withdrawal behaviour.

The experimental work comprised five test series (with a total of 23 test specimens) as follows:

1. **PL** (four specimens): the specimens were tested in pull-pull loading configuration under non-destructive, service-level, cyclic loading (tension, compression, and fully reversed) at four penetration lengths ($5d$, $10d$, $15d$, and $20d$). Following the service-level loading tests, the specimens were tested to failure under a monotonic tension load.

2. **PL-R** (four specimens): identical to PL series with the exception of using STS as reinforcement.
3. **PS** (six specimens): the specimens were tested in pull-push loading configuration under service-level loading at four penetration lengths. Following the service-level loading tests, the specimens were tested to failure under a monotonic tension load.
4. **PS-T** (five specimens): identical to PS series, but the specimens were only tested to failure under a monotonic tension load at $20d$ penetration length. In this series, no non-destructive testing was performed at $5d$, $10d$, $15d$ and $20d$.
5. **PS-C** (four specimens): identical to PS series, but the specimens were only tested to failure under a monotonic compression load at $20d$ penetration length. In this series, no non-destructive testing was performed at $5d$, $10d$, $15d$ and $20d$.

The experimental results were used to evaluate stiffness under cyclic and monotonic loading, damping ratios, withdrawal capacity, and failure mode. In view of the experimental results, the following main conclusions can be drawn:

1. Threaded rods inserted perpendicular to grain into the narrow face of CLT elements exhibited high withdrawal stiffness and capacity. When inserted at a $20d$ penetration length, the mean withdrawal stiffness ranges from 100 to 250 kN/mm and the mean withdrawal capacity ranges from 137 to 163 kN.
2. For rods with $20d$ penetration length, the use of STS can provide a more ductile load-displacement curve, without noticeable increase in the capacity.
3. All threaded rods inserted at a $20d$ failed in withdrawal failure mode. The only exception was for rods tested in pull-pull loading configuration without reinforcement where the withdrawal failure was combined with splitting.
4. Stiffness exhibits a non-linear relationship with the penetration length, showing noticeable convergence beyond $15d$ (330 mm).
5. Stiffness under cyclic loading is generally higher than the stiffness under monotonic loading.
6. Under service-level loading, the equivalent viscous damping ratio ranges from 3 to 12%.

5.2 Paper II

An innovative slip-friction moment-resisting connection using screwed-in threaded rods in cross laminated timber and steel coupling parts: An experimental study

This paper presents a novel slip-friction, beam-to-column, moment-resisting connection with threaded rods screwed into CLT. The connection employs the concept of slip-friction, which has been successfully used in several steel structures and allows for damage-free energy dissipation through friction slip. In total, four full-scale tests have been conducted, where each specimen has been subjected to a series of non-destructive, service-level, cyclic loading tests, followed by a destructive cyclic loading.

The connection consists of purpose-made threaded rods and steel connectors, a steel plate, high strength bolts (HSBs), and CLT beam and column. The components and assembly of the connection are presented in detail in subsection 4.3.2. Throughout the experimental work, the following parameters were varied:

1. Threaded rods layout: two different layouts have been tested, see Figure I.35.
2. CLT layup: two different CLT layups (7 layers and 5 layers) have been used, see Figure I.34.
3. Prestressing of the high strength bolts: two different prestressing levels have been used (torque of 2100 and 2400 Nm applied to the HSBs).

Based on the experimental results, the following key conclusions can be drawn:

1. Under service-level loading, the connection exhibited high stiffness in the range of 10000-20000 kNm/rad.
2. Following the onset of slip, the connection exhibited large energy dissipation demonstrated by large hysteresis loops. The energy was dissipated through friction slip, without damage in the timber.
3. The connection demonstrated high capacity in the range of 164-180 kNm. The failure was associated with plastic hinging in the threaded rods.
4. The connection exhibited ductile behaviour with ductility ratios in the range of 4.0-6.6.

5.3 Paper III

Serviceability performance of timber dual frame-wall structural system under wind loading

In this paper, the feasibility of moment-resisting timber frames combined with CLT walls (i.e. dual system) was investigated. A parametric study using 2D linear elastic finite element analysis (FEA) was performed to explore the feasibility of the dual system in regions with moderate to high wind velocities, considering serviceability requirements (lateral displacements and wind-induced acceleration). Floor vibration under human excitation was also investigated and discussed. A 3D FEA model was used to verify the results of the 2D FEA model.

Although the emphasis of the paper was on addressing serviceability requirements, some Ultimate Limit State considerations were also discussed. It has been shown that, for non-seismic design, the serviceability requirements, specifically wind-induced accelerations, are likely to govern the design of the dual frame-wall system. The results of this study demonstrate the feasibility of using the dual system for multistorey timber buildings up to 12 storeys and 5 m out-of-plane spacing between adjacent frames in regions with basic wind velocities up to 26 m/sec.

5.4 Paper IV

Parametric analysis of moment-resisting timber frames combined with cross laminated timber walls and prediction models using nonlinear regression and artificial neural networks

In this paper, prediction models were developed for the dual system discussed in Paper III. An extensive 2D finite element analysis (FEA) database was built using OpenSeesPy [51] Python library. The FEA database was used to derive simplified analytical expressions for fundamental frequency, mode shape, top-floor displacement, maximum inter-storey drift, and top-floor wind-induced acceleration. The database was also used to train artificial neural networks (ANNs) to predict the aforementioned parameters with an improved accuracy.

Some simplified analytical expressions for frequency and mode shape are available in building design codes. However, these expressions cannot be used for multistorey timber buildings and may lead to significant deviations compared to FEA results. On the other hand, the developed analytical expressions and ANNs have shown the capability to predict frequency, mode shape, top-floor displacement, maximum inter-storey drift, and top-floor wind-induced acceleration with high accuracy.

Although the derived analytical expressions and the ANNs are designed for 2D analysis, analytical expressions were derived to allow for extrapolation to a 3D building. A 3D building was solved using FEA and the results were compared with those obtained using the derived analytical expressions and the ANNs. The comparison shows good agreement, indicating the possibility of using the analytical expressions or the ANNs for preliminary assessment of multistorey timber buildings employing MRTFs, with and without CLT walls, specifically addressing serviceability requirements.

5.5 Paper V

Feasibility of outrigger structural system for tall timber buildings: A numerical study

The performance of the dual system presented in Paper III can be further enhanced by employing an outrigger. This paper aims to address the following:

1. Optimize the location of one and two outriggers considering different serviceability requirements as optimization criteria.
2. Evaluate and compare the efficiency of different outrigger layouts.
3. Identify the stiffness requirements of the outrigger.
4. Investigate the feasibility of the dual system (presented in Paper III) combined with one or two outriggers for up to 20 storeys and considering wind velocities up to 30 m/sec. Although the feasibility was assessed primarily with respect to serviceability requirements, some ultimate limit state considerations were also discussed.
5. Investigate the influence of connection stiffness variability on the overall performance of the dual system combined with an outrigger.

The results of the feasibility study show that building up to 16 storeys is feasible with a basic wind velocity of 26-30 m/sec. Building 20 storeys is, however, challenging and can be limited to lower basic wind velocities. It has been observed that the variability of connection stiffness has negligible influence on lateral displacements and wind-induced acceleration. On the other hand, the variability in connection stiffness has caused approximately 10% increase in the forces on the outrigger elements compared to the reference value obtained by FEA with the mean stiffness values.

5.6 Paper VI

Analysis and design aspects of moment-resisting, beam-to-column, timber connections with inclined threaded rods: from fastener level to construction level

This paper provides an overview of analysis and design aspects of moment-resisting connections with inclined threaded rods. Since MRTFs are highly indeterminate structures, the variability in the stiffness of their connections influences their response. In common engineering practice, the mean stiffness values are used for FEA. On this basis, this paper consists of two parts:

1. Part 1: this part includes analytical expressions that can be used to estimate the connection stiffness and the forces in the threaded rods used in timber MRCs. The provided expressions are for configuration A shown in Figure I.40 (a).
2. Part 2: in this part, a parametric study was performed to evaluate the influence of connection stiffness variability on the response of MRTFs. It has been shown that this variability has insignificant influence on the serviceability performance (displacements and accelerations) and may be neglected. However, the variability in stiffness results in a noticeable variability in the internal forces and moments. The results demonstrate that the end moments of the beams are particularly sensitive to such variability, with 98th percentile of the order of 20%-40% higher than the reference values obtained by analysis with mean stiffness values.

6 Suggestions for future work

In view of the state-of-the-art knowledge and based on the results from the experimental and theoretical work performed in this thesis, suggestions for further research are presented here.

1. Withdrawal tests on threaded rods:

- a. Only short-term loading was considered in the withdrawal testing of rods; therefore, future testing of rods should consider long-term loading, moisture dependency, and fatigue loading.
- b. The conducted testing was limited to threaded rods inserted parallel and perpendicular to grain. Therefore, rods inserted at various angles to grain should be considered in future testing.
- c. The destructive testing was limited to a penetration length of 20 times the outer thread diameter of the used threaded rod. Destructive testing with shorter and longer penetration lengths should be considered.
- d. The conducted testing has been limited to a single rod of 22 mm outer thread diameter, inserted into 3-layer CLT panels. In future testing, multiple rods, different rod diameters, and different CLT layups should be considered.

2. Performance of the developed moment-resisting connection (MRC):

- a. The developed MRC was tested under short-term loading only. Future testing considering long-term loading, moisture dependency, and fatigue loading is recommended.
- b. Fire testing of an early prototype of a MRC with threaded rods (without coupling parts, i.e. no exposed steel parts) has been conducted [119]. The results show that the connection can withstand the expected fire duration determined by the charring rate of wood, in that case more than 60 minutes (R60). However, the developed MRC has exposed steel parts. The performance of the connection with respect to fire requires further research.

- c. The use of friction shims can enhance the behaviour of the developed MRC by reducing the difference between the static and kinetic friction, ensuring a reliable slip-force level, and mitigating the hardening behaviour observed under cyclic loading. Preliminary tests have been conducted on various materials intended for use as friction shims, see Appendix C. Full-scale testing of the connection with the use of friction shims is deemed necessary.
- d. Finite element modelling of the developed MRC would enable better understanding of the behaviour and allow for further optimization of the connection. The results obtained from the experimental work in this Ph.D. thesis can be used for calibration of such models.
- e. The developed MRC lacks the self-centring capability. This could potentially limit its application in high-seismic regions. The introduction of self-centring to the connection requires further research and development.

3. Performance of moment-resisting timber frames:

- a. Buildings are typically subjected to permanent loads, such as their own weight and finishes. The presence of these permanent loads, along with the variation in moisture content, results in creep deformations. Indeed, this is the case for the connections of MRTFs. In structures with structural components with different time-dependent properties, redistribution of forces and moments takes place over time. Future studies should consider the performance of the dual frame-wall system, as well as the MRTFs, with respect to SLS and ULS, considering long-term loading and moisture content variations.
- b. The performance of the dual frame-wall system has been evaluated mainly with respect to serviceability requirements. The performance of the dual system (as well as the MRTFs) considering seismic actions should be considered in future studies.

4. **Threaded rods as fasteners in CLT shear walls:** the withdrawal testing of threaded rods inserted into CLT elements has shown that they exhibit high stiffness and capacity. This makes them suitable for use as fasteners in the connections of CLT shear walls. Testing of CLT walls with threaded rods used as hold-downs is recommended.
5. **Threaded rods as fasteners in bracing elements:** given their high stiffness and capacity, threaded rods can be used in the connections of bracing elements made with CLT. Testing of such axially-loaded connections is recommended.

References

- [1] N. Kisku, H. Joshi, M. Ansari, S.K. Panda, S. Nayak, S.C. Dutta, A critical review and assessment for usage of recycled aggregate as sustainable construction material, *Construction and Building Materials* 131 (2017) 721-740.
- [2] Summary for Policymakers, in: C. Intergovernmental Panel on Climate (Ed.), *Global Warming of 1.5°C: IPCC Special Report on Impacts of Global Warming of 1.5°C above Pre-industrial Levels in Context of Strengthening Response to Climate Change, Sustainable Development, and Efforts to Eradicate Poverty*, Cambridge University Press, Cambridge, 2022, pp. 1-24.
- [3] A. Eliassen, S. Faanes, R. Bohne, Comparative LCA of a concrete and steel apartment building and a cross laminated timber apartment building, *IOP Conference Series: Earth and Environmental Science*, IOP Publishing, 2019, p. 012017.
- [4] J.L. Skullestad, R.A. Bohne, J. Lohne, High-rise timber buildings as a climate change mitigation measure—A comparative LCA of structural system alternatives, *Energy Procedia* 96 (2016) 112-123.
- [5] P. Börjesson, L. Gustavsson, Greenhouse gas balances in building construction: wood versus concrete from life-cycle and forest land-use perspectives, *Energy Policy* 28(9) (2000) 575-588.
- [6] Statistics Norway: Waste accounts. <https://www.ssb.no/en/natur-og-miljo/avfall/statistikk/avfallsregnskapet>. (Accessed 9 December 2023).
- [7] O.A. Hegeir, H. Stamatopoulos, K.A. Malo, Serviceability performance of timber dual frame-wall structural system under wind loading, *World Conference on Timber Engineering (WCTE 2023)*, Oslo, Norway (2023).
- [8] A. Vilguts, H. Stamatopoulos, K.A. Malo, Parametric analyses and feasibility study of moment-resisting timber frames under service load, *Engineering Structures* 228 (2021).
- [9] H. Stamatopoulos, K. Malo, Wood frame solutions for free space design in urban buildings (WOODSOL), *Proceedings of the 7th Forum Wood Building Nordic*, Växjö, Sweden, 2018, pp. 27-28.
- [10] A.S. Cao, H. Stamatopoulos, A theoretical study of the dynamic response of planar timber frames with semi-rigid moment-resisting connections subjected to wind loads, *Engineering Structures* 240 (2021).
- [11] K.A. Malo, R.B. Abrahamsen, M.A. Bjertnæs, Some structural design issues of the 14-storey timber framed building “Treet” in Norway, *European Journal of Wood and Wood Products* 74(3) (2016) 407-424.
- [12] A. Aloisio, D.P. Pasca, Y. De Santis, T. Hillberger, P.F. Giordano, M.M. Rosso, R. Tomasi, M.P. Limongelli, C. Bedon, Vibration issues in timber structures: A state-of-the-art review, *Journal of Building Engineering* (2023) 107098.
- [13] M. Johansson, A. Linderholt, K. Jarnerö, P. Landel, Tall timber buildings: a preliminary study of wind-induced vibrations of a 22-storey building, *World Conference on Timber Engineering (WCTE 2016)*, August 22-25, 2016, Vienna, Austria, Vienna University of Technology, 2016.
- [14] S. Chapain, A.M. Aly, Vibration Attenuation in a High-Rise Hybrid-Timber Building: A Comparative Study, *Applied Sciences* 13(4) (2023) 2230.

- [15] R. Abrahamsen, Mjøstårnet-Construction of an 81 m tall timber building, Internationales Holzbau-Forum IHF, Garmisch-Partenkirchen, Germany, 2017.
- [16] M. Wells, Stadthaus, London: raising the bar for timber buildings, Proceedings of the Institution of Civil Engineers-Civil Engineering, Thomas Telford Ltd, 2011, pp. 122-128.
- [17] S. Tulebekova, K.A. Malo, A. Rønnquist, Dynamic identification and model calibration of connection stiffness in multi-storey cross-laminated timber buildings, Journal of Building Engineering 72 (2023) 106607.
- [18] K.A. Malo, H. Stamatopoulos, Connections with threaded rods in moment resisting frames, World Conference on Timber Engineering (WCTE2016), Vienna, Austria, 2016.
- [19] A. Vilguts, S.Ø. Nesheim, H. Stamatopoulos, K.A. Malo, A study on beam-to-column moment-resisting timber connections under service load, comparing full-scale connection testing and mock-up frame assembly, European Journal of Wood and Wood Products 80(4) (2022) 753-770.
- [20] H. Stamatopoulos, K.A. Malo, A. Vilguts, Moment-resisting beam-to-column timber connections with inclined threaded rods: Structural concept and analysis by use of the component method, Construction and Building Materials 322 (2022) 126481.
- [21] A. Jorissen, M. Fragiaco, General notes on ductility in timber structures, Engineering structures 33(11) (2011) 2987-2997.
- [22] A.S. Rebouças, Z. Mehdipour, J.M. Branco, P.B. Lourenço, Ductile moment-resisting timber connections: A review, Buildings 12(2) (2022) 240.
- [23] A. Hashemi, P. Zarnani, A. Valadbeigi, R. Masoudnia, P. Quenneville, Seismic Resistant Timber Walls with New Resilient Slip Friction Damping Devices, Proceedings of the International Network on Timber Engineering Research (2016).
- [24] E.P. Popov, C.E. Grigorian, T.-S. Yang, Developments in seismic structural analysis and design, Engineering structures 17(3) (1995) 187-197.
- [25] R. Tremblay, Seismic behavior and design of friction concentrically braced frames for steel buildings, University of British Columbia, 1993.
- [26] G.A. MacRae, G.C. Clifton, H. Mackinven, N. Mago, J. Butterworth, S. Pampanin, The sliding hinge joint moment connection, Bulletin of the New Zealand Society for Earthquake Engineering 43(3) (2010) 202-212.
- [27] S. Shabankareh, P. Zarnani, A. Hashemi, P. Quenneville, A novel connection system for seismic damage avoidance design of moment resisting frames, Proc., Pacific Conf. on Earthquake Engineering (PCEE) and New Zealand Society for Earthquake Engineering (NZSEE). Wellington, New Zealand: New Zealand Society for Earthquake Engineering, 2019.
- [28] CEN, NS-EN 1991-1-4:2005+NA:2009: Actions on Structures-Part 1-4: General Actions-Wind Actions European Committee for Standardization: Brussels, Belgium (2009).
- [29] H. Svatoš-Ražnjević, L. Orozco, A. Menges, Advanced Timber Construction Industry: A Review of 350 Multi-Storey Timber Projects from 2000-2021, Buildings 12(4) (2022) 404.

- [30] E. Hurmekoski, R. Jonsson, T. Nord, Context, drivers, and future potential for wood-frame multi-story construction in Europe, *Technological Forecasting and Social Change* 99 (2015) 181-196.
- [31] V. Salvadori, Worldwide Structural Survey of 197 Multi-Storey Timber-Based Buildings From 5 to 24 Storeys, *World Conference on Timber Engineering (WCTE 2020)*, 2021.
- [32] M. Premrov, V. Žegarac Leskovar, Innovative Structural Systems for Timber Buildings: A Comprehensive Review of Contemporary Solutions, *Buildings* 13(7) (2023) 1820.
- [33] I. Gavric, M. Fragiacomio, A. Ceccotti, Cyclic Behavior of CLT Wall Systems: Experimental Tests and Analytical Prediction Models, *Journal of Structural Engineering* 141(11) (2015).
- [34] M. Izzi, D. Casagrande, S. Bezzi, D. Pasca, M. Follesa, R. Tomasi, Seismic behaviour of Cross-Laminated Timber structures: A state-of-the-art review, *Engineering structures* 170 (2018) 42-52.
- [35] O. Hansen, M. Fjeld Olsen, Measuring Vibrations and assessing Dynamic Properties of tall Timber Buildings-Måling av vibrasjoner og kartlegging av dynamiske egenskaper i høye trehus, NTNU, 2016.
- [36] I. Gavric, M. Fragiacomio, A. Ceccotti, Cyclic behaviour of typical metal connectors for cross-laminated (CLT) structures, *Materials and structures* 48 (2015) 1841-1857.
- [37] I. Gavric, M. Fragiacomio, A. Ceccotti, Cyclic behavior of typical screwed connections for cross-laminated (CLT) structures, *European Journal of Wood and Wood Products* 73 (2015) 179-191.
- [38] J. Schneider, Y. Shen, S. Stiemer, S. Tesfamariam, Assessment and comparison of experimental and numerical model studies of cross-laminated timber mechanical connections under cyclic loading, *Construction and Building Materials* 77 (2015) 197-212.
- [39] A. Ceccotti, C. Sandhaas, M. Okabe, M. Yasumura, C. Minowa, N. Kawai, SOFIE project-3D shaking table test on a seven-storey full-scale cross-laminated timber building, *Earthquake Engineering & Structural Dynamics* 42(13) (2013) 2003-2021.
- [40] M. Shahnewaz, T. Tannert, M.S. Alam, M. Popovski, Seismic Performance of Cross Laminated Timber (CLT) Platform Building by Incremental Dynamic Analysis, *IABSE Symposium Report, International Association for Bridge and Structural Engineering*, 2017, pp. 422-428.
- [41] CSA O86 Engineering design in wood, Canadian standards association (2016).
- [42] S. Nesheim, K.A. Malo, N. Labonnote, Effects of interconnections between timber floor elements: dynamic and static evaluations of structural scale tests, *European Journal of Wood and Wood Products* 79(5) (2021) 1163-1182.
- [43] J. Bjerve, E. Sagerud, H. Stamatopoulos, K. Malo, A. Rønquist, Dynamic tests on a long-span, stressed-skin, timber floor, *Wood Material Science & Engineering* (2023) 1-10.
- [44] S. Cuerrier-Auclair, Design guide for timber-concrete composite floors in Canada, *FPInnovations, Montréal* (2020).
- [45] B.S. Smith, I. Salim, Formulae for optimum drift resistance of outrigger braced tall building structures, *Computers & Structures* 17(1) (1983) 45-50.

- [46] G. Ren, J. Xue, Y. Ding, Effect of infilled CLT shear walls on the lateral performance of glued-laminated timber frames: Experimental and numerical analysis, *Structures* 50 (2023) 80-96.
- [47] J. Xue, G. Ren, L. Qi, X. Zhang, Lateral behavior of glued-laminated timber frame infilled with light-wooden-frame wall hybrid system: Experimental and numerical analysis, *Structures* 30 (2021) 352-367.
- [48] D. King, A.V. Houtte, NZ Wood Design Guides-Portal Knee Connections, NZ Journal of Forestry (2020).
- [49] M. Oberholzer, Building complex Arbora (434 residential units) in Montreal and Origine (13 storeys) in Quebec City, Internationales Holzbau-Forum IHF, 2016.
- [50] E. Karacabeyli, C. Lum, Technical Guide for the Design and Construction of Tall Wood Buildings in Canada, Second Edition ed., FPInnovations, 2022.
- [51] M. Zhu, F. McKenna, M.H. Scott, OpenSeesPy: Python library for the OpenSees finite element framework, *SoftwareX* 7 (2018) 6-11.
- [52] CEN, NS-EN 14080: Timber structures-Glued laminated timber and glued solid timber-Requirements, European Committee for Standardization: Brussels, Belgium (2013).
- [53] CEN, NS-EN 338: Structural timber-Strength classes, European Committee for Standardization: Brussels, Belgium (2016).
- [54] H.J. Blass, P. Fellmoser, Design of solid wood panels with cross layers, 8th world conference on timber engineering, 2004.
- [55] M. Follesa, I. Christovasilis, D. Vassallo, M. Fragiacomio, A. Ceccotti, Seismic design of multi-storey CLT buildings according to Eurocode 8. *Ingegneria Sismica, International Journal of Earthquake Engineering, Special Issue on Timber Structures* 30(4) (2013) 27-53.
- [56] R. Steenbergen, A. Vrouwenvelder, C. Geurts, The use of Eurocode EN 1991-1-4 procedures 1 and 2 for building dynamics, a comparative study, *Journal of wind engineering and industrial aerodynamics* 107 (2012) 299-306.
- [57] P. Landel, M. Johansson, A. Linderholt, Comparative study of wind-induced accelerations in tall timber buildings according to four methods, WCTE 2021, World Conference on Timber Engineering, Santiago, Chile, 9-12 August, World Conference on Timber Engineering, WCTE, 2021.
- [58] A. Feldmann, H. Huang, W. Chang, R. Harris, P. Dietsch, M. Gräfe, C. Hein, Dynamic properties of tall timber structures under wind-induced vibration, World Conference on Timber Engineering (WCTE 2016), 2016.
- [59] CEN, NS-EN 1991-1-1: 2002+ NA: 2019: Actions on Structures-Part 1-1: General Actions-Densities, self-weight, imposed loads for buildings, European Committee for Standardization: Brussels, Belgium (2019).
- [60] K.C. Kwok, P.A. Hitchcock, M.D. Burton, Perception of vibration and occupant comfort in wind-excited tall buildings, *Journal of Wind Engineering and Industrial Aerodynamics* 97(7-8) (2009) 368-380.
- [61] ISO, ISO 10137: Bases for design of Structures - Serviceability of Buildings and Walkways against Vibrations, International Organization for standardization (2007).

- [62] CEN, NS-EN 1995-1-1:2004+A1:2008+NA:2010: Design of timber structures–Part 1-1: General–Common rules and rules for buildings, European Committee for Standardization: Brussels, Belgium (2010).
- [63] CEN, NS-EN 1990:2002+A1:2005+NA:2016: Basis of structural design, European Committee for Standardization: Brussels, Belgium (2016).
- [64] A. Gustafsson, *The CLT Handbook: CLT structures-facts and planning*, First ed., Swedish Wood 2019.
- [65] H. Stamatopoulos, O.A. Hegeir, K.A. Malo, Analysis and Design Aspects of Moment-Resisting, Beam-to-Column, Timber Connections with Inclined Threaded Rods: From Fastener Level to Construction Level, *World Conference on Timber Engineering (WCTE 2023)*, 2023, pp. 1206-1215.
- [66] A. Vilguts, *Moment-resisting timber frames with semi-rigid connections*, Department of Structural Engineering, Norwegian University of Science and Technology, 2021.
- [67] R. Jockwer, D. Caprio, A. Jorissen, Evaluation of parameters influencing the load-deformation behaviour of connections with laterally loaded dowel-type fasteners, *Wood Material Science & Engineering* 17(1) (2022) 6-19.
- [68] K.W. Johansen, *Theory of timber connections*, International Assoc. of Bridge and Structural Engineering Publication 9 (1949) 249-262.
- [69] A. Meyer, Die tragfähigkeit von nagelverbindungen bei statischer belastung, *HOLZ als Roh-und Werkstoff* 15(2) (1957) 96-109.
- [70] H.J. Blaß, P. Schädle, Ductility aspects of reinforced and non-reinforced timber joints, *Engineering Structures* 33(11) (2011) 3018-3026.
- [71] C. Zhang, H. Guo, K. Jung, R. Harris, W.-S. Chang, Using self-tapping screw to reinforce dowel-type connection in a timber portal frame, *Engineering Structures* 178 (2019) 656-664.
- [72] M.-j. He, H.-f. Liu, Comparison of glulam post-to-beam connections reinforced by two different dowel-type fasteners, *Construction and Building Materials* 99 (2015) 99-108.
- [73] F. Lam, M. Gehloff, M. Closen, Moment-resisting bolted timber connections, *Proceedings of the Institution of Civil Engineers-Structures and Buildings* 163(4) (2010) 267-274.
- [74] W. Dong, M. Li, M. He, Z. Li, Experimental testing and analytical modeling of glulam moment connections with self-drilling dowels, *Journal of Structural Engineering* 147(5) (2021) 04021047.
- [75] J. Zhang, J. Yi, Y. Xu, M. Zhang, Cyclic response of moment-resisting glulam hybrid joints with bolts and side steel plates, *Journal of Building Engineering* 51 (2022) 104310.
- [76] M. Dorn, *Investigations on the serviceability limit state of dowel-type timber connections*, 2012.
- [77] L. Fang, L. Wang, W. Qu, S. Zhang, Mechanical performance of glulam beam-column moment-resisting connections with self-tapping screws as fasteners, *Journal of Building Engineering* 54 (2022) 104586.
- [78] K. Komatsu, Q. Teng, Z. Li, X. Zhang, Z. Que, Experimental and analytical investigation on the nonlinear behaviors of glulam moment-resisting joints

composed of inclined self-tapping screws with steel side plates, *Advances in Structural Engineering* 22(15) (2019) 3190-3206.

[79] R. Gohlich, J. Erochko, J.E. Woods, Experimental testing and numerical modelling of a heavy timber moment-resisting frame with ductile steel links, *Earthquake Engineering & Structural Dynamics* 47(6) (2018) 1460-1477.

[80] M. Fragiaco, M. Batchelar, Timber frame moment joints with glued-in steel rods. II: Experimental investigation of long-term performance, *Journal of Structural Engineering* 138(6) (2012) 802-811.

[81] M. Fragiaco, M. Batchelar, Timber frame moment joints with glued-in steel rods. I: Design, *Journal of Structural Engineering* 138(6) (2012) 789-801.

[82] N. Gattesco, A. Gubana, M. Buttazzi, M. Melotto, Experimental investigation on the behavior of glued-in rod joints in timber beams subjected to monotonic and cyclic loading, *Engineering Structures* 147 (2017) 372-384.

[83] É. Gauthier-Turcotte, S. Ménard, M. Fiset, Strength and Behavior of Spruce Pine Glulam Timber Moment Connections Using Glued-In Steel Rods, *Journal of Structural Engineering* 148(12) (2022) 04022192.

[84] H. Yang, W. Liu, X. Ren, A component method for moment-resistant glulam beam-column connections with glued-in steel rods, *Engineering Structures* 115 (2016) 42-54.

[85] A. Buchanan, R. Fairweather, Seismic design of glulam structures, *Bulletin of the New Zealand Society for Earthquake Engineering* 26(4) (1993) 415-436.

[86] S. Navaratnam, J. Thamboo, T. Ponnampalam, S. Venkatesan, K.B. Chong, Mechanical performance of glued-in rod glulam beam to column moment connection: An experimental study, *Journal of Building Engineering* 50 (2022) 104131.

[87] M. Andreolli, M. Piazza, R. Tomasi, R. Zandonini, Ductile moment-resistant steel-timber connections, *Proceedings of the Institution of Civil Engineers-Structures and Buildings* 164(2) (2011) 65-78.

[88] A. Hashemi, H. Bagheri, S.M.M. Yousef-Beik, F.M. Darani, A. Valadbeigi, P. Zarnani, P. Quenneville, Enhanced seismic performance of timber structures using resilient connections: Full-scale testing and design procedure, *Journal of structural engineering* 146(9) (2020) 04020180.

[89] M. Kemmsies, Comparison of pull-out strengths of 12 adhesives for glued-in rods for timber structures, 1999.

[90] D. Kohl, N. Ratsch, S. Böhm, M. Voß, M. Kaufmann, T. Vallée, Influence of manufacturing methods and imperfections on the load capacity of glued-in rods, *The Journal of Adhesion* 96(8) (2018) 738-759.

[91] H. Zhang, H. Li, A. Dauletbek, R. Lorenzo, I. Corbi, O. Corbi, Research status of glued-in rods connections in wood structures, *Journal of Building Engineering* (2022) 105782.

[92] H. Stamatopoulos, K.A. Malo, On strength and stiffness of screwed-in threaded rods embedded in softwood, *Construction and Building Materials* 261 (2020).

[93] H. Stamatopoulos, K.A. Malo, Withdrawal stiffness of threaded rods embedded in timber elements, *Construction and Building Materials* 116 (2016) 263-272.

[94] H. Stamatopoulos, K.A. Malo, Withdrawal capacity of threaded rods embedded in timber elements, *Construction and Building Materials* 94 (2015) 387-397.

- [95] A. Vilguts, K.A. Malo, H. Stamatopoulos, Moment resisting frames and connections using threaded rods in beam-to-column timber joints, World Conference on Timber Engineering (WCTE2018), Seoul, Republic of Korea, 2018.
- [96] K. Nordal, K. Lied, A conceptual study of glulam connections using threaded rods and connecting circular steel profiles, NTNU Norwegian University of Science and Technology: Trondheim, Norway., 2016.
- [97] J.C.C. Golondrino, G.A. MacRae, J.G. Chase, G.W. Rodgers, G.C. Clifton, Seismic behaviour of symmetric friction connections for steel buildings, *Engineering Structures* 224 (2020) 111200.
- [98] J.C.C. Golondrino, G.A. MacRae, J.G. Chase, G.W. Rodgers, G.C. Clifton, Asymmetric friction connection (AFC) design for seismic energy dissipation, *Journal of Constructional Steel Research* 157 (2019) 70-81.
- [99] M. Hatami, G. MacRae, G. Rodgers, G. Clifton, Numerical and experimental study on friction connections performance-asymmetric and symmetric (AFC/SFC), The 11th Pacific Conference on Earthquake Engineering. Auckland, New Zealand, 2019.
- [100] J. Leimcke, N. R  ther, P. Guindos, M. Brunnermeier, Moment connection with frictional damping for timber post and beam construction in earthquake-prone areas. 22, Internationales Holzbau-Forum IHF, 2016.
- [101] W.Y. Loo, C. Kun, P. Quenneville, N. Chouw, Experimental testing of a rocking timber shear wall with slip-friction connectors, *Earthquake engineering & structural dynamics* 43(11) (2014) 1621-1639.
- [102] A. Hashemi, P. Quenneville, Large-scale testing of low damage rocking Cross Laminated Timber (CLT) wall panels with friction dampers, *Engineering Structures* 206 (2020) 110166.
- [103] P. Zarnani, A. Valadbeigi, A. Hashemi, F.M. Darani, S.M.M. Yousef-Beik, H. Bagheri, P. Quenneville, Rotational performance of resilient slip friction joint (RSFJ) as a new damage free seismic connection, 2018 World Conference on Timber Engineering (WCTE2018), 2018.
- [104] <https://www.tectonus.com/projects>. (Accessed 19 November 2023).
- [105] J.H. Bickford, M. Oliver, Introduction to the design and behavior of bolted joints: non-gasketed joints, CRC press 2022.
- [106] P. Dietsch, R. Brandner, Self-tapping screws and threaded rods as reinforcement for structural timber elements – A state-of-the-art report, *Construction and Building Materials* 97 (2015) 78-89.
- [107] H.J. Bla  , O. Kr  ger, Schubverst  rkung von Holz mit Holzschrauben und Gewindestangen, KIT Scientific Publishing, Karlsruhe, 2010.
- [108] M. Sofi, E. Lumantarna, R. Hault, M. Mooney, N. Mason, J. Lu, Bond strength of GiR in cross-laminated timber: A preliminary study, *Construction and Building Materials* 301 (2021) 123864.
- [109] Y. Shirmohammadli, A. Hashemi, R. Masoudnia, P. Quenneville, Experimental and numerical investigation of cross-laminated timber joints with multiple glued-in rods, World Conference on Timber Engineering (WCTE 2023), Oslo, Norway (2023).
- [110] B. Azinovi  , E. Serrano, M. Kramar, T. Pazlar, Experimental investigation of the axial strength of glued-in rods in cross laminated timber, *Materials and Structures* 51(6) (2018).

- [111] G.S. Ayansola, T. Tannert, T. Vallee, Experimental investigations of glued-in rod connections in CLT, *Construction and Building Materials* 324 (2022).
- [112] G.S. Ayansola, T. Tannert, T. Vallee, Glued-in multiple steel rod connections in cross-laminated timber, *The Journal of Adhesion* 98(6) (2022) 810-826.
- [113] B. Azinović, V. Sebera, M. Kržan, A. Pondelak, J. Gašper, A.K. Pečnik, Glued-in rod CLT connections with flexible polymer adhesive, *World Conference on Timber Engineering (WCTE 2023)*, Oslo, Norway (2023).
- [114] B. Azinović, H. Danielsson, E. Serrano, M. Kramar, Glued-in rods in cross laminated timber – Numerical simulations and parametric studies, *Construction and Building Materials* 212 (2019) 431-441.
- [115] Y. Shirmohammadli, A. Hashemi, R. Masoudnia, P. Quenneville, Numerical modeling investigation of cross-laminated timber connections consisting of multiple glued-in rods, *Structures* 53 (2023) 491-500.
- [116] O.A. Hegeir, H. Stamatopoulos, Experimental investigation on axially-loaded threaded rods inserted perpendicular to grain into cross laminated timber, *Construction and Building Materials* 408 (2023) 133740.
- [117] CEN, EN 26891:1991 (ISO 6891:1983): Timber structures-Joints Made with Mechanical Fasteners- General Principles for the Determination of Strength and Deformation Characteristics, (1991).
- [118] A. Resch, An experimental investigation of the mechanical properties of axially loaded threaded rods embedded in glued-laminated timber elements, NTNU, 2022.
- [119] N. Westerheim, Konseptstudie av knutepunkt i limtre og lange aksialbærende treskruer utsatt for brannbelastning, Institutt for konstruksjonsteknikk, 2013.

Part II

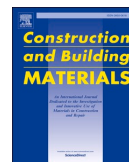
Appended papers

Paper I

Experimental investigation on axially-loaded threaded rods inserted perpendicular to grain into cross laminated timber

Osama Abdelfattah Hegeir, Haris Stamatopoulos

Published at ***Construction and Building Materials*** journal



Experimental investigation on axially-loaded threaded rods inserted perpendicular to grain into cross laminated timber

Osama Abdelfattah Hegeir^{*}, Haris Stamatopoulos

Department of Structural Engineering, Norwegian University of Science and Technology (NTNU), Rich. Barcelonese 1A, 7491 Trondheim, Norway

ARTICLE INFO

Keywords:

Cross laminated timber (CLT)
Threaded rod
Self-tapping screws
Cyclic stiffness
Monotonic stiffness
Withdrawal stiffness
Withdrawal capacity
Pull-push loading configuration
Pull-pull loading configuration
Damping

ABSTRACT

This paper presents an experimental work on axially-loaded threaded rods inserted perpendicular to grain into the narrow face of cross laminated timber (CLT). Penetration length, loading type (tension, compression, fully reversed), and loading configuration (pull-pull and pull-push) were varied. The use of self-tapping screws as reinforcement was also explored. Stiffness under cyclic and monotonic loading, damping ratio, withdrawal capacity, failure mode, reinforcement effect, and influence of loading history were investigated. The experimental results highlight the high withdrawal stiffness and capacity of threaded rods embedded into CLT elements, and hence their effectiveness as fasteners for stiff timber connections.

1. Introduction

1.1. Background

The light weight and moderate stiffness of timber buildings limit the possibility for taller timber buildings. This is mainly due to increased wind-induced accelerations and lateral deformations under service-level loading [1–4]. The structural performance of timber structures relies heavily on their connections' properties [1–4]. Stiff connections can therefore be used to allow for taller timber buildings [4].

Connections with threaded rods (i.e. rods with wood screw threads and greater diameters than self-tapping screws, typically 16–22 mm) generally feature high withdrawal strength and stiffness [5–7]. Threaded rods can be used in timber structures as fasteners in moment resisting connections [8], axially loaded connections, or can be used as reinforcements [9]. Compared to glued-in rods (abbr. GiR), threaded rods are less prone to construction quality problems. Experimental work on GiR has shown that the presence of defects or sawdust in the pre-drilled holes can influence their behavior [10,11]. Compared to GiR, systems of rods screwed into wood exhibit better fire resistance [12], and they are less brittle [5,13]. Threaded rods can also be pre-installed allowing a high degree of pre-fabrication [8], reducing the work onsite. Moreover, threaded rods can be designed following capacity design

principles to allow for ductile behavior (e.g. yielding in the steel rods) [5,7].

Using cross laminated timber (abbr. CLT) elements as lateral load resisting system is becoming popular [14–19] due to their high in-plane strength and stiffness and their availability in larger dimensions than standard glued laminated timber (abbr. glulam). CLT panels consist of sawn timber boards, glued together in alternating directions resulting in panels with high in-plane strength and stiffness and better dimensional stability [20]. Due to their high in-plane strength and stiffness, the performance of CLT panels depends highly on their connections [20].

The advantage of utilizing the high withdrawal strength of inclined self-tapping screws (abbr. STS) was first presented by Bejtka and Blaß [21]. A predictive model based on the results of 387 withdrawal tests for STS inserted into the wide and narrow face of CLT was developed by Uibel and Blaß [22]. Equations for the calculation of withdrawal capacity and strength of STS in softwood based on 1850 withdrawal tests were proposed by Frese and Blaß [23]. Pirnbacher et al. [24] investigated the influence of several parameters on withdrawal strength of STS and proposed a calculation equation for the withdrawal strength. Subsequently, numerous studies have investigated the behavior of STS. This includes research on their withdrawal capacity [25–32], their stiffness properties [25,33], their use as reinforcement [9], their use in timber-to-timber joints [34] and in steel-to-timber joints [35], and force

^{*} Corresponding author.

E-mail addresses: osama.a.s.a.hegeir@ntnu.no (O.A. Hegeir), haris.stamatopoulos@ntnu.no (H. Stamatopoulos).

distribution along screws [36].

The behavior of GiR in glulam and CLT has also been investigated by several studies, addressing their withdrawal capacity [37–44], stiffness [37,39,44], behavior as a group [45,46], failure modes [38], durability [47], use for strengthening existing timber structures [48], behavior in beam-to-beam [49,50] and beam-to-column [51,52] moment connections, and the impact of construction methods and defects on their capacity [10,11,53].

On the contrary, little research has investigated the properties of threaded rods embedded in timber. The withdrawal capacity and stiffness of threaded rods were studied by Stamatopoulos and Malo [5–7] and Blaß and Krüger [54]. However, these studies were only conducted on glulam. An experimental study was conducted by Yang et al. [55] to investigate the pull-out behavior of threaded rods in CLT elements using a wall-type loading setup. In their study [55], the penetration length, number of threaded rods, and the effect of using reinforcement were investigated. Only monotonic tension load was applied to the rods, and therefore, properties such as cyclic stiffness, energy dissipation, and equivalent viscous damping were not reported in [55]. Besides – and to the knowledge of the authors – experimental studies of threaded rods embedded in CLT, subjected to pure axial loading conditions are lacking in the literature.

1.2. Objective and scope

In the research presented, an experimental work was performed to investigate the behavior of steel threaded rods screwed into CLT elements. Five test series were carried out with a total of 23 test specimens. Out of the five series, three series were first tested under service-level cyclic loading followed by a monotonic tension load to failure, one series was tested only under monotonic tension load to failure, and the last series was tested only under monotonic compression load to failure.

The experimental work aimed to investigate the withdrawal capacity, stiffness under monotonic and cyclic loading, energy dissipation, failure modes, and the influence of STS as reinforcement. The penetration length, the loading type (tension, compression, fully reversed), and the loading configuration (pull–push, pull–pull) were varied. The scope of this paper is limited to threaded rods inserted perpendicular to grain into the narrow face of CLT elements made of softwood with a reference moisture content of approximately 12%. Moreover, only short-term loading is considered, and therefore, issues such as long-term loading, moisture dependency, and fatigue are out of the scope of this work.

2. Materials and test methods

2.1. Materials

Fig. 1 depicts the CLT panel used in this study. Non-edge glued, three-layer CLT panels made of Norwegian spruce were used. The board



Fig. 1. CLT panel.

Table 1
Material properties of lamellae [57].

Strength class	$f_{m,k}$	$f_{t,0,k}$	$f_{c,0,k}$	$E_{0,mean}$	$E_{90,mean}$	ρ_k	ρ_{mean}
	N/mm ²					kg/m ³	
T15	22.0	15	21	11,500	380	360	430
T22	30.5	22	26	13,000	430	390	470

thickness and width were 33 mm and 100 mm, respectively, and the total thickness was 100 mm, see Fig. 1. The outer layers and the inner layer were strength class T22 and T15, respectively (strength classes as defined by EN338 [56]). The CLT panels were stored in a climate room with controlled temperature and relative humidity of 20 °C and 65%, respectively. Prior to testing, the moisture content of each specimen was measured using an electric moisture meter and verified to be in the range of 10–12%. The material properties of the used CLT panels are summarized in Table 1.

Fig. 2(a) shows the geometry of the threaded rod used in this study. The rod is of class 8.8 and consists of 110 mm metric thread and 440 mm wood thread. The metric thread is used for attaching the rod to the loading jack. The wood thread has a core diameter (d_1) of 16.1 mm, an outer thread diameter (d) of 22 mm, and a thread pitch of 8 mm. The rods were screwed into the narrow face of the CLT panels in pre-drilled holes with diameter equal to their core diameter (d_1), confer Fig. 2(b). The holes are drilled all the way through the test specimen.

In one of the test series, STS was used as reinforcement. STS with 100 mm length (equal to the thickness of the CLT elements) were not available at the time of testing. Instead, 160 mm-long screws were used, 60 mm longer than the thickness of the CLT. Since the actual embedded length of the screws is limited to the CLT panel thickness, the use of 160 mm-long is equivalent to the use of 100 mm-long screws. The screws have an outer thread diameter of 8 mm, an inner thread diameter of 5 mm, and a characteristic yield strength of 1000 N/mm² [58].

2.2. Loading and variation of penetration length

In this paper, two force levels were considered: service-level load and destructive load. The service-level load is taken to be 40% of the capacity, as recommended by EN 12512 [59] to ensure elastic behavior. Prior to testing, the withdrawal capacity is unknown and therefore was estimated ($F_{ax,est}$) by use of a simplified equation proposed by Stamatopoulos and Malo [7]:

$$F_{ax,est} \approx 15 \cdot d \cdot l \cdot \left(\frac{\rho_{mean}}{470} \right) \quad (1)$$

where $F_{ax,est}$ is the estimated withdrawal capacity in N, d is the outer thread diameter of the rod in mm, l is the penetration length in mm, and ρ_{mean} is the mean density in kg/m³.

To study the effect of the penetration length on the withdrawal stiffness, four penetration lengths were investigated: 5, 10, 15 and 20 times the outer thread diameter ($5d$, $10d$, $15d$, $20d$), confer Fig. 3. The threaded rod is first screwed into the specimens at a $5d$ penetration length, and the service-level load testing is then performed. The same threaded rod is further screwed into the specimen at a step of $5d$, and testing is performed again for $10d$, $15d$ and $20d$ penetration lengths. At penetration lengths of $5d$, $10d$, $15d$, and $20d$, the rod fully penetrated one, two, three and four lamellae, respectively.

Monotonic loading does not represent various real-case loading scenarios such as wind or human excitation. To investigate stiffness and energy dissipation under such scenarios, cyclic load testing is more representative. Therefore, in this paper, two loading protocols were considered:

1. Service-level: Cyclic loading was applied for each penetration length shown in Fig. 3.
2. Destructive: Monotonic load is applied to failure, only at a $20d$ penetration length.

The loading protocols for service-level and destructive loading are shown in Fig. 4. Three test series were tested under service-level loading followed by destructive loading (in tension). Two test series were tested only under destructive loading, with one series tested in tension and the other in compression.

A simplified cyclic loading with constant amplitude was used in this paper, confer Fig. 4(a). Three types of cyclic loading were applied: cyclic

tension (abbr. T), cyclic compression (abbr. C), and cyclic fully reversed (abbr. FR). The load limits for tension and compression cyclic loading were set to $0.10 \cdot F_{ax,est} \leftrightarrow 0.40 \cdot F_{ax,est}$ (the forces are negative for compression and positive for tension). The load limits for fully reversed cyclic loading were set to $-0.40 \cdot F_{ax,est} \leftrightarrow +0.40 \cdot F_{ax,est}$. For each type of cyclic loading (T, C, FR), eight cycles were applied. The load was applied with force control and a quasi-static loading rate of one minute per cycle for tension and compression and two minutes per cycle for fully reversed. The loading rate was chosen to achieve a reasonable test duration, while also maintaining quasi-static loading within the range of approximately 0.02 mm/sec - 0.20 mm/sec [59]. The number of cycles was determined to allow for the examination of cyclic stiffness variation, if present, while still achieving a reasonable test duration.

Monotonic loading was applied until failure of the specimen to investigate the withdrawal capacity. Since the monotonic loading was applied after the cyclic loading tests were performed, only a penetration length of $20d$ could be tested. Hence, the influence of varying the penetration length on the withdrawal capacity was not investigated. The monotonic loading specified by EN 26891 [60] was adopted, see Fig. 4 (b).

2.3. Experimental setup

Two loading configurations were considered in this study, pull-push loading, and pull-pull loading, confer Figs. 5 and 6, respectively. In the pull-push loading (Fig. 5), the specimen was supported on two steel plates at the bottom and clamped using two steel rectangular hollow

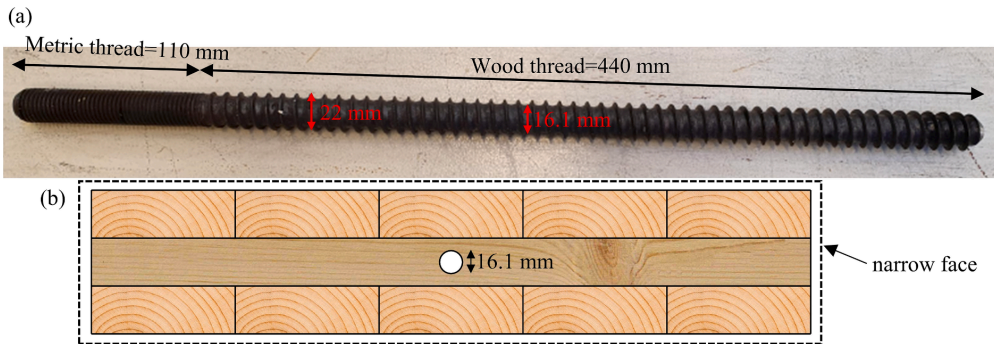


Fig. 2. (a) threaded rod, (b) predrilled hole at the narrow face of the CLT panel.

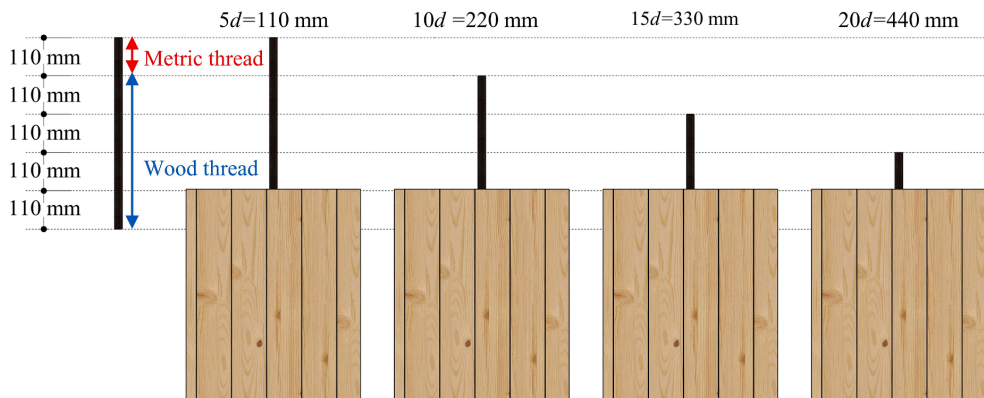


Fig. 3. Variation of penetration length.

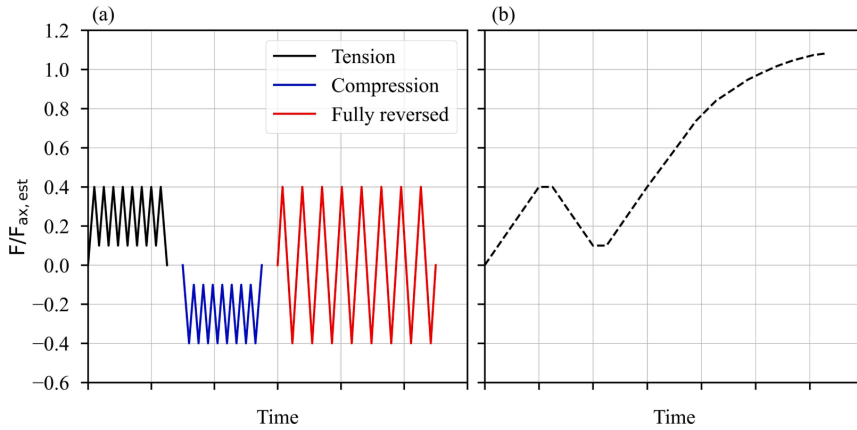


Fig. 4. Loading protocols (a) service level cyclic loading, (b) monotonic to failure loading.

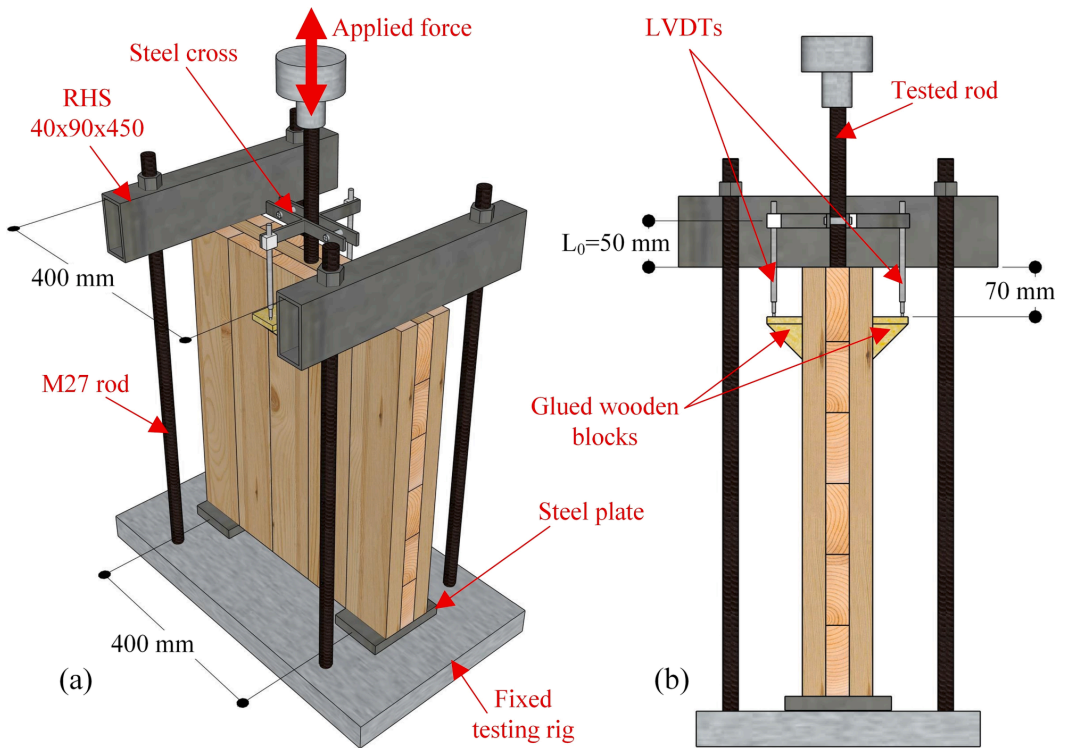


Fig. 5. Pull-push loading (a) 3D view, (b) side view.

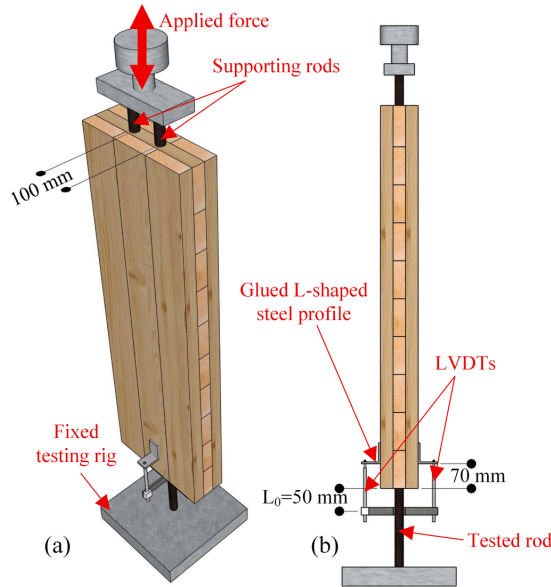


Fig. 6. Pull-pull loading (a) 3D view, (b) side view.

sections (abbr. RHS) at the top. In the pull-pull loading (Fig. 6), one rod (the tested rod) was inserted at one end of the specimen, and two rods were inserted at the other end. The use of two rods ensures the failure of the tested rod. For both loading configurations, linear variable differential transformers (abbr. LVDTs) were used to measure the displacements of the threaded rod relative to the test specimen, see in detail Figs. 5 and 6. Two wooden blocks or L-shaped steel profiles were glued at each side of the specimen to allow for measuring the relative

displacement between the rod and the CLT specimen, confer Figs. 5 and 6. The average displacement of the two LVDTs was used as the withdrawal displacement. The LVDTs were attached to the rod using a purpose-made steel cross. The load was applied by attaching the metric part of the threaded rod to a loading jack. To facilitate the testing in pull-pull loading configuration, the specimens were rotated upside down (the tested rod is at the bottom) as shown in Fig. 6. To apply the load, the two rods at the top were connected to a rigid steel attachment and then

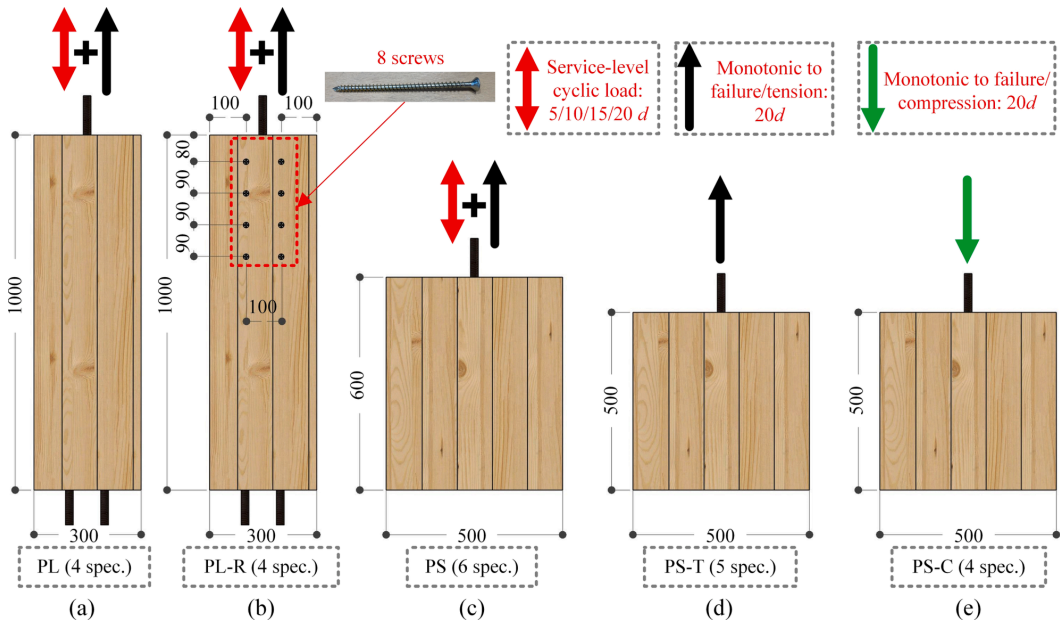


Fig. 7. Overview of test series (dimensions in mm).

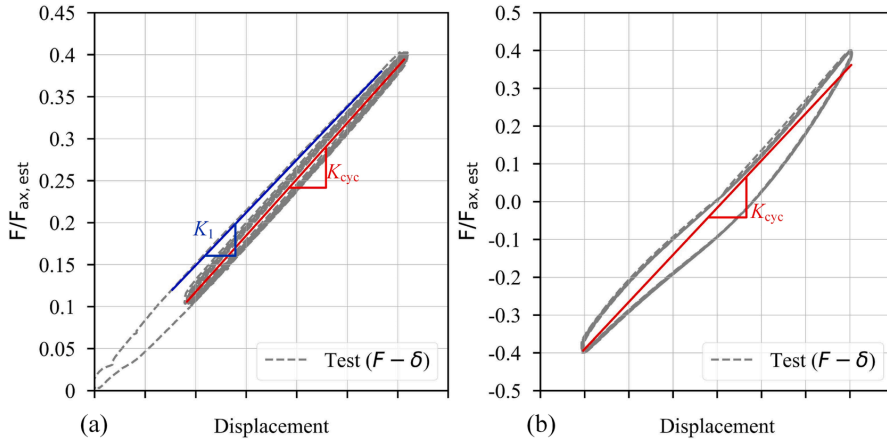


Fig. 8. Axial cyclic and monotonic stiffness (a) tension loading, (b) fully reversed loading.

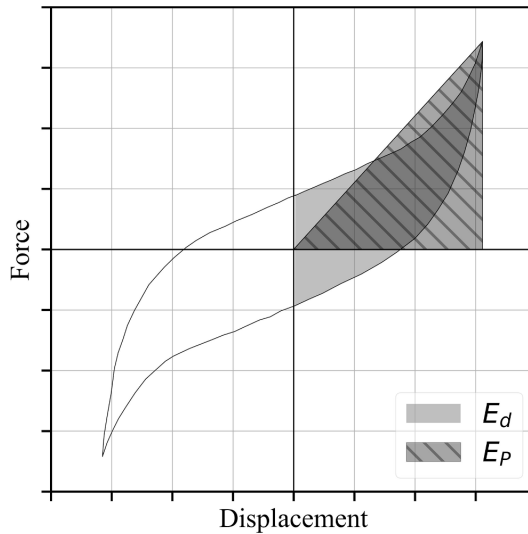


Fig. 9. Definition of dissipated and potential energy.

connected to a loading jack.

2.4. Test series

Fig. 7 illustrates all test series. In total, five experimental test series were conducted as follows:

1. PL (Fig. 7 (a)): Four specimens were tested in pull-pull loading (Fig. 6). The specimens were first subjected to service-level cyclic load at different penetration lengths, then tested to failure under monotonic tension at 20d penetration length.
2. PL-R (Fig. 7 (b)): Four specimens were tested in pull-pull loading (Fig. 6). The specimens had an identical geometry to PL, but were reinforced using eight STS. The specimens were first subjected to service-level cyclic load at different penetration lengths, then tested to failure under monotonic tension at 20d penetration length.

3. PS (Fig. 7 (c)): Six specimens were tested in pull-push loading (Fig. 5). The specimens were first subjected to service-level cyclic load at different penetration lengths, then tested to failure under monotonic tension at 20d penetration length.
4. PS-T (Fig. 7 (d)): Five specimens were tested in pull-push loading (Fig. 5). The specimens were tested to failure under monotonic tension at 20d penetration length.
5. PS-C (Fig. 7 (e)): Four specimens were tested in pull-push loading (Fig. 5). The specimens were tested to failure under monotonic compression at 20d penetration length.

Specimens tested in pull-push loading were prepared wider to allow for placing the supporting RHS beams on the top (Fig. 5). Specimens tested in pull-pull loading were prepared higher to accommodate the two supporting rods (Fig. 6). For both loading configurations, the number of vertical lamellae that were free to deform was approximately the same (three), confer Figs. 5-7.

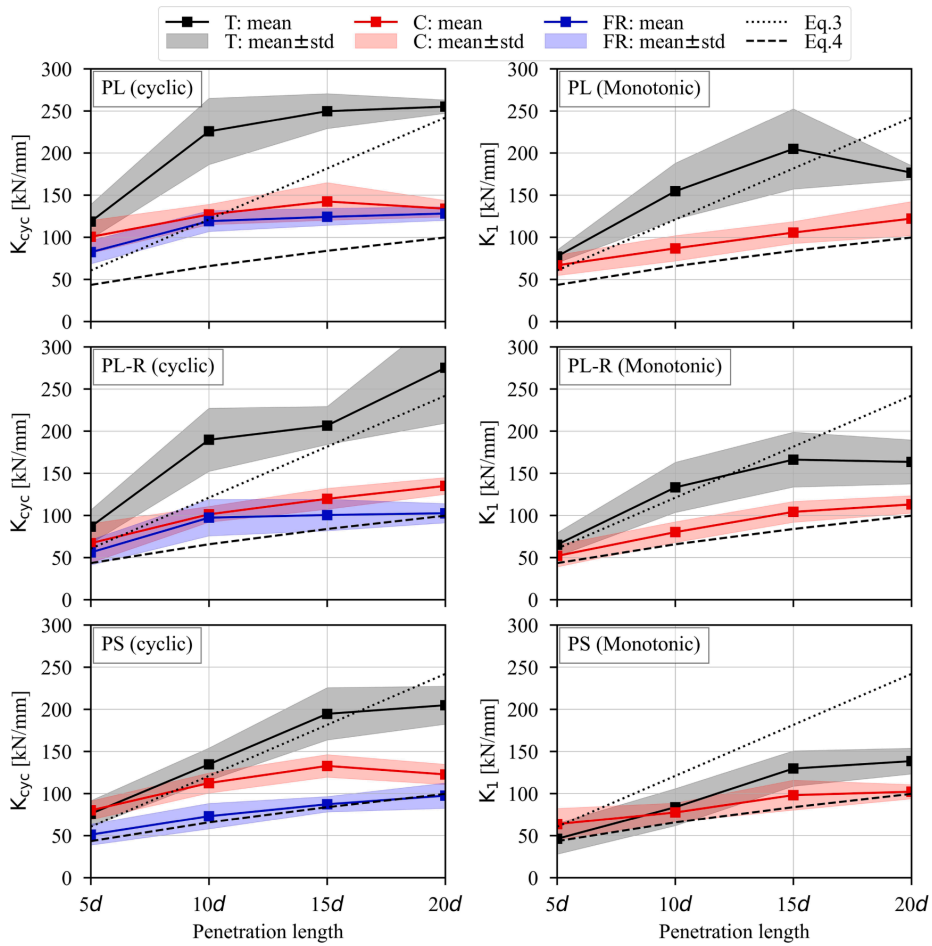


Fig. 10. Mean and standard deviation of cyclic and monotonic stiffness under cyclic loading.

Table 2
Mean and coefficient of variation (COV) of cyclic and monotonic stiffness under cyclic loading.

Test series	Loading type	Penetration length	Cyclic stiffness K_{cyc}^{**}		Monotonic stiffness K_1^{**}	
			Mean (kN/mm)	COV (%)	Mean (kN/mm)	COV (%)
PL	Cyclic tension	5d	118.4	17.2	77.2	9.8
		10d	225.5	17.5	154.5	21.5
		15d	249.7	8.3	204.7	23.3
		20d	255.1	3.1	176.5	4.7
	Cyclic compression	5d	100.4	19.5	66.6	18.2
		10d	126.9	9.5	86.8	17.3
		15d	142.4	15.7	105.5	12.3
		20d	133.8	7.3	122.1	16.6
	Cyclic fully reversed	5d	82.2	16.9	–	–
		10d	119.1	10.4	–	–
		15d	124.1	8.1	–	–
		20d	128.1	6.4	–	–
PL-R	Cyclic tension	5d	86.5	23.0	65.3	21.4
		10d	189.7	19.8	133.2	22.3
		15d	206.6	10.9	166.1	19.6
		20d	275.1	23.9	163.4	16.0
	Cyclic compression	5d	67.0	34.7	51.9	25.2
		10d	101.3	9.2	80.1	15.3
		15d	119.6	10.4	104.2	11.9
		20d	134.9	7.3	113.0	9.2
	Cyclic fully reversed	5d	56.0	26.7	–	–
		10d	97.3	22.2	–	–
		15d	100.4	18.7	–	–
		20d	102.6	11.1	–	–
PS*	Cyclic tension	5d	76.0	20.3	46.2	39.7
		10d	134.7	14.3	83.8	26.3
		15d	194.6	15.9	129.7	16.2
		20d	204.8	11.0	138.5	11.0
	Cyclic compression	5d	80.0	13.9	63.7	29.2
		10d	112.5	10.6	77.5	14.4
		15d	132.8	10.1	98.1	18.1
		20d	122.7	9.8	102.2	8.2
	Cyclic fully reversed	5d	51.1	24.3	–	–
		10d	73.1	20.8	–	–
		15d	87.3	10.5	–	–
		20d	97.5	15.4	–	–

*Result from one test specimen was considered as an outlier and was not included in the calculation, ** The reported values refer to the stiffness at the entrance point; the effect of the free length ($L_0 = 50$ mm) is removed considering the embedded part and the free length of the rod as springs in series.

2.5. Stiffness estimation

In the current version of Eurocode 5 [61], no formula is provided to calculate the axial stiffness of threaded rods in glulam or CLT. Under service-level cyclic loading (Fig. 4 (a)), two types of stiffness were estimated, the cyclic stiffness (K_{cyc}) and the monotonic stiffness (K_1), i.e. the stiffness at the first loading, confer Fig. 8.

The cyclic stiffness (K_{cyc}) was estimated by fitting a straight line (using the method of least squares) through each hysteresis loop of the cyclic test. The stiffness for each cycle was calculated individually, then the average value for all cycles was calculated and used as cyclic stiffness (K_{cyc}). The stiffness was calculated for all penetration lengths (5d, 10d, 15d, 20d), for cyclic tension, compression, and fully reversed loading ($K_{cyc,T}$, $K_{cyc,C}$, and $K_{cyc,FR}$).

The monotonic stiffness (K_1) was also estimated for all penetration lengths, for both cyclic tension and compression loading ($K_{1,T}$, $K_{1,C}$). According to EN 26891 [60], the stiffness is estimated from the monotonic loading protocol shown in Fig. 4 (b). The initial half cycle of the cyclic loading (from 0 to 40 % of $F_{ax,est}$) resembles the first loading ramp in the monotonic loading (from 0 to 40 % of $F_{ax,est}$). Therefore, the monotonic stiffness was estimated by fitting a line to the initial half cycle of the cyclic loading, see Fig. 8 (a). The stiffness under the monotonic loading shown in Fig. 4 (b) was also estimated by fitting a line to the first loading ramp from 10 % to 40 % of $F_{ax,est}$.

2.6. Equivalent viscous damping ratio

Under cyclic loading, several mechanisms contribute to energy dissipation. It is nearly impossible to describe such mechanisms mathematically [62]. It is therefore widely accepted to sum all energy dissipation mechanisms in an equivalent viscous damper [62]. The equivalent viscous damping ratio (ξ_{eq}) can be calculated as per EN 12512 [59]:

$$\xi_{eq} = \frac{1}{2\pi} \frac{E_d}{E_p} \quad (2)$$

where E_d is the energy dissipated per half cycle and E_p is the available potential energy, confer Fig. 9. The damping ratio for each cycle was calculated individually, then the average value across all cycles was calculated and used as the equivalent viscous damping ratio (ξ_{eq}). The equivalent viscous damping ratio (ξ_{eq}) is a non-dimensional parameter that represents the hysteresis damping of a joint. The damping ratio can be used for modeling the energy dissipation of members and connections under service-level cyclic loading using finite element analysis, see e.g. [8].

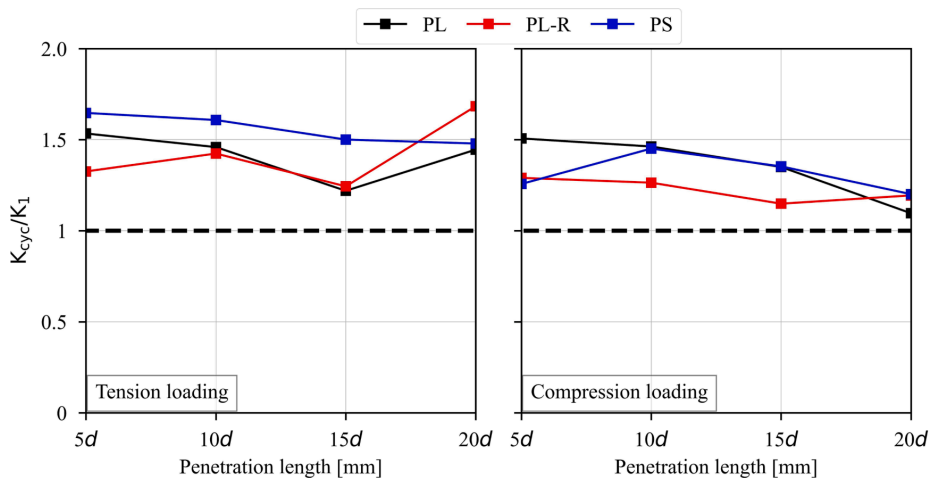


Fig. 11. Ratio of mean cyclic stiffness to mean monotonic stiffness.

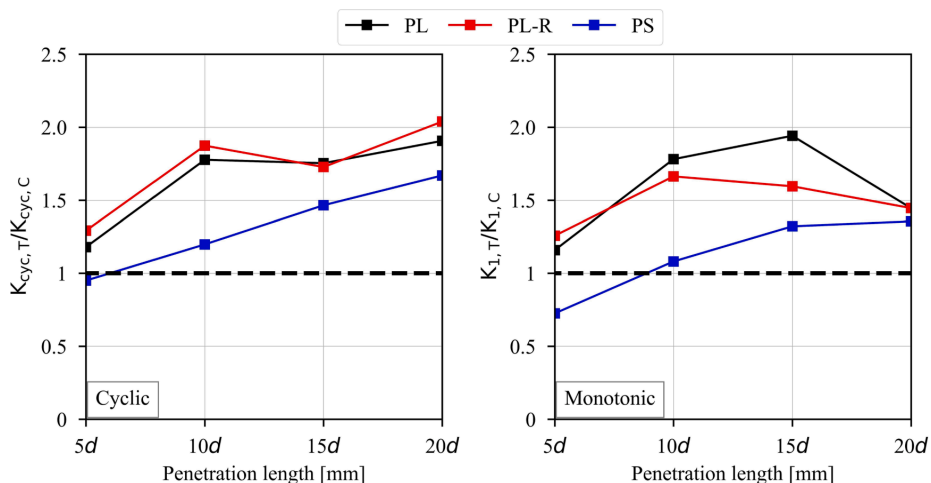


Fig. 12. Ratio of mean stiffness for tension to compression loading.

3. Experimental results and discussion

3.1. Service-level cyclic loading

3.1.1. Cyclic and monotonic stiffness

Fig. 8 (a) shows a representative force–displacement curve in tension at service-level cyclic loading, similar curves were observed for compression. Fig. 8 (b), shows a representative force–displacement curve under fully reversed service-level cyclic loading. As shown in this figure, little pinching (i.e. low stiffness around zero force) and immediate load-take up without initial slip was observed. As a result of the different stiffness in tension and compression (confer section 3.1.3), and the small pinching effect, the fitting of a line to the force–displacement curve under fully reversed loading has small deviation, confer Fig. 8 (b). However, it provides a fairly good fit to the experimental results. As shown in Fig. 8, the $F-\delta$ curves of all cycles coincide, and the stiffness estimated from all cycles was found to be nearly identical. Therefore, using the mean stiffness of all cycles provides an accurate

approximation. Given the low load level and the observed identical $F-\delta$ curves for all cycles, it is likely that further loading cycles would exhibit a similar behavior.

Fig. 10 shows the cyclic and monotonic withdrawal stiffness of PL, PL-R, and PS test series, obtained from the cyclic load tests as function of penetration length. The results are also summarized in Table 2. The mean value is indicated by a solid line and the standard deviation (abbr. std) is indicated by a shaded area around the mean, confer Fig. 10. As shown in the figure, in general, both cyclic and monotonic stiffness (K_{cyc} and K_1) are higher for tension loading than for compression loading. This difference may be attributed to the different boundary conditions and different load paths under tension and compression loading. Claus et al. [36] performed withdrawal testing using innovative screws with internal fiber Bragg gratings to measure the forces along screws embedded in wood. The results in [36] show significant differences in the force distribution along the screw length under different boundary conditions. Experimental work by Ringhofer and Schickhofer [63] has shown that testing boundary conditions have no major influence on the

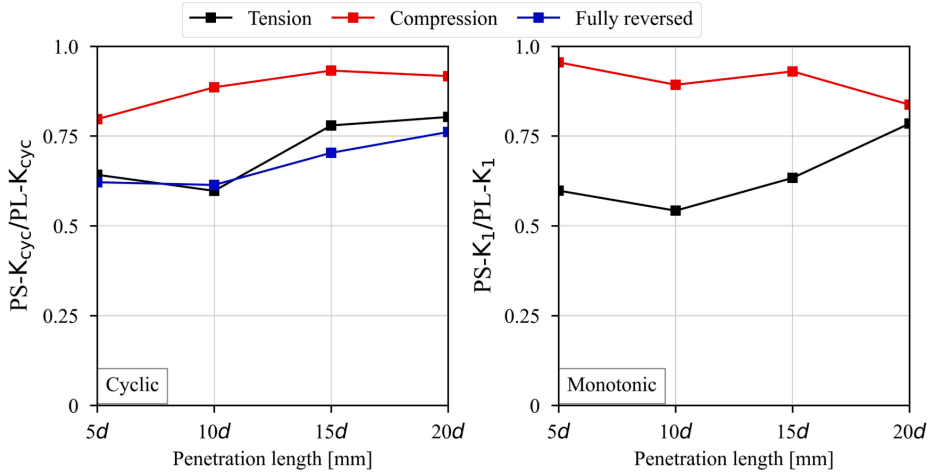


Fig. 13. Ratio of mean stiffness for pull-pull to pull-push loading.

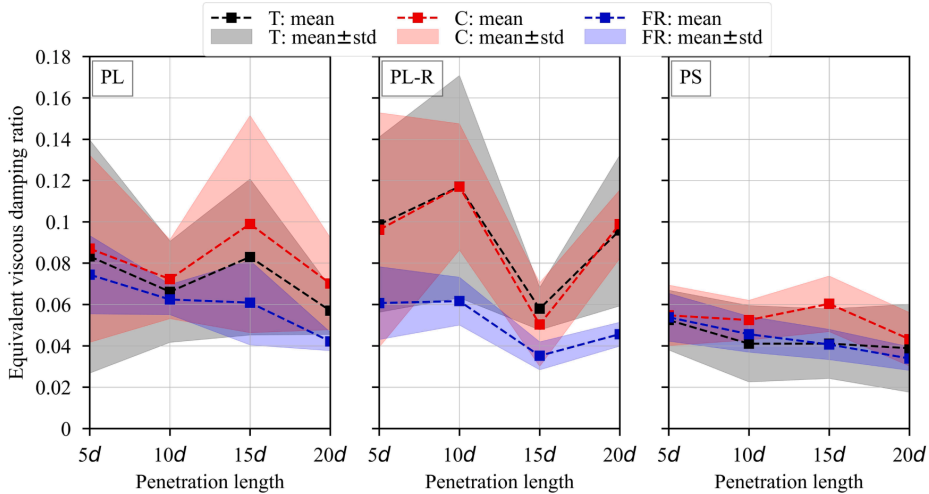


Fig. 14. Mean and standard deviation of equivalent viscous damping ratio.

withdrawal capacity of STS. However, studies on the influence of testing boundary conditions on the withdrawal stiffness of STS and threaded rods are lacking in literature.

As a result of small pinching effects, the fully reversed loading shows lowest stiffness compared to tension and compression loading. Both cyclic and monotonic stiffness exhibit a non-linear relationship with penetration length, showing noticeable convergence beyond 15d (330 mm) penetration length.

Several models for calculating the withdrawal stiffness $K_{SLS,ax}$ of STS and threaded rods are available in literature. Eq. (3) is commonly reported in several technical approvals. Despite the lack of guidelines for the estimation of the withdrawal stiffness of axially loaded fasteners in the current version of Eurocode 5 [61], the current draft for the next generation of Eurocode 5 [64] provides Eq. (4) for withdrawal stiffness of axially loaded screws and threaded rods.

$$K_{SLS,ax} = 25 \cdot d \cdot l \tag{3}$$

$$K_{SLS,ax} = 160 \cdot \left(\frac{\rho_{mean}}{420}\right)^{0.85} \cdot d^{0.9} \cdot l^{0.6} \tag{4}$$

In Eq. (3) and Eq. (4), $K_{SLS,ax}$ is in N/mm, d and l are in mm, and ρ_{mean} is in kg/m^3 .

As shown in Fig. 10, Eq. (4) represents a lower bound for the cyclic and monotonic stiffness under tension, compression, and fully reversed loading. A better stiffness estimation can be obtained by use of Eq. (3). However, a limit on the penetration length should be set for Eq. (3) as the stiffness shows a noticeable convergence beyond 15d (330 mm) penetration length.

To evaluate the difference in displacements between the outer layers (measured by the LVDTs shown in Figs. 5 and 6) and the middle layer, two additional LVDTs were placed at the top of the test specimens of series PS. The stiffness estimated from these additional LVDTs at the top was found to be, on average, 5 % different from the stiffness estimated from the LVDTs placed at the sides, showing that deformations occur predominantly in the middle layer.



Fig. 15. Failure modes of all test series.



Fig. 16. Representative cut-open specimens.

3.1.2. Cyclic vs monotonic stiffness

Fig. 11 shows the ratio of the mean cyclic stiffness to the mean monotonic stiffness (K_{cyc}/K_1) under cyclic tension and compression. The cyclic stiffness is 10–68 % higher than the monotonic stiffness. On average, cyclic stiffness is 45 % and 30 % higher than monotonic stiffness for tension and compression loading, respectively.

3.1.3. Tension vs compression

The ratio of the mean cyclic stiffness under tension and compression loading ($K_{cyc,T}/K_{cyc,C}$) and the ratio of mean monotonic stiffness ($K_{1,T}/K_{1,C}$) are shown in Fig. 12. Apart from the PS series with 5d penetration length, stiffness values are higher for tension loading than compression loading.

3.1.4. Pull-pull vs pull-push

The mean cyclic and monotonic stiffness for PL series (pull-pull) and PS series (pull-push) were compared. Fig. 13 shows the ratio of mean cyclic stiffness ($PS-K_{cyc}/PL-K_{cyc}$) and mean monotonic stiffness ($PS-K_1/PL-K_1$). Mean stiffness of the pull-push series (PS) is lower compared to the pull-pull series (PL).

3.1.5. Equivalent viscous damping ratio

Fig. 14 shows the mean and standard deviation of the equivalent viscous damping ratio ξ_{eq} calculated according to Eq. (2). The mean damping ratio for all test series ranges from 0.03 to 0.12. In general, pull-pull loading (PL and PL-R) shows higher mean values and higher variability than pull-push loading (PS).

3.2. Monotonic to failure loading

The failure modes were visually inspected after each test. Fig. 15 shows the failure modes of representative specimens from the five test series. For PL series, the four specimens failed in a combined withdrawal and splitting failure, confer Fig. 15 (a). The PL-R, however, did not show splitting failure and only withdrawal failure was observed for all specimens, confer Fig. 15 (b). This suggests that the use of reinforcement can prevent splitting failure. For PS and PS-T series, all specimens failed in withdrawal failure mode, confer Fig. 15 (c) and (d). For PS-C series,

under compression loading, the threaded rod pushed through the CLT specimen, and the thickness of the specimen increased around the location of the rod (*bulging*), confer Fig. 15 (e).

Representative specimens from test series PS-T and PS-C were cut open to examine their internal surface, confer Fig. 16. As shown in Fig. 16, the failure is accompanied by rolling shear failure and splitting perpendicular to grain in the middle layer. Despite this failure mode, high withdrawal capacity was attained in all tests. Failure accompanied by rolling shear failure has been reported for GiR [46] and screwed-in threaded rods [55] inserted perpendicular to grain into the narrow face of CLT elements.

Fig. 17 shows the monotonic load–displacement curves for all test series. The mean load–displacement ($F-\delta$) curves were calculated by fitting a higher degree polynomial to the test results. To ease the comparison between different test series, both tension and compression forces and the corresponding displacements are plotted positive.

Fig. 18 shows the mean load–displacement ($F-\delta$) curves for all test series. Comparing the PL (pull-pull, unreinforced) with the PL-R (pull-pull, reinforced), both have similar mean withdrawal capacity. However, the PL-R has better post failure load carrying capacity and shows more gradual drop in the load beyond failure. This suggests that using STS as reinforcement can enhance the post failure behavior without noticeable increase in withdrawal capacity. However, since only the rods at 20d penetration length were tested to failure, the effect of reinforcement using STS at different penetration lengths was not investigated. Experimental results of threaded rods embedded in CLT [55] shows that the effect of STS varies depending on the embedment length, with greater effect observed for shorter lengths.

Comparing the load–displacement curves (confer Figs. 17 and 18) of test series PS (with loading history) and PS-T (without loading history), small difference can be observed with PS-T showing lower stiffness and withdrawal capacity. However, the difference is small and therefore difficult to conclude whether this difference is attributed to loading history or natural variability of the tested material. The observed failure mode for all specimens of PS and PS-T series was withdrawal (confer Fig. 15 (c) and (d)), suggesting no influence of loading history on the failure mode. Among all test series tested in pull–push (PS, PS-T, and PS-C), the PS-C series shows the highest withdrawal capacity and lowest

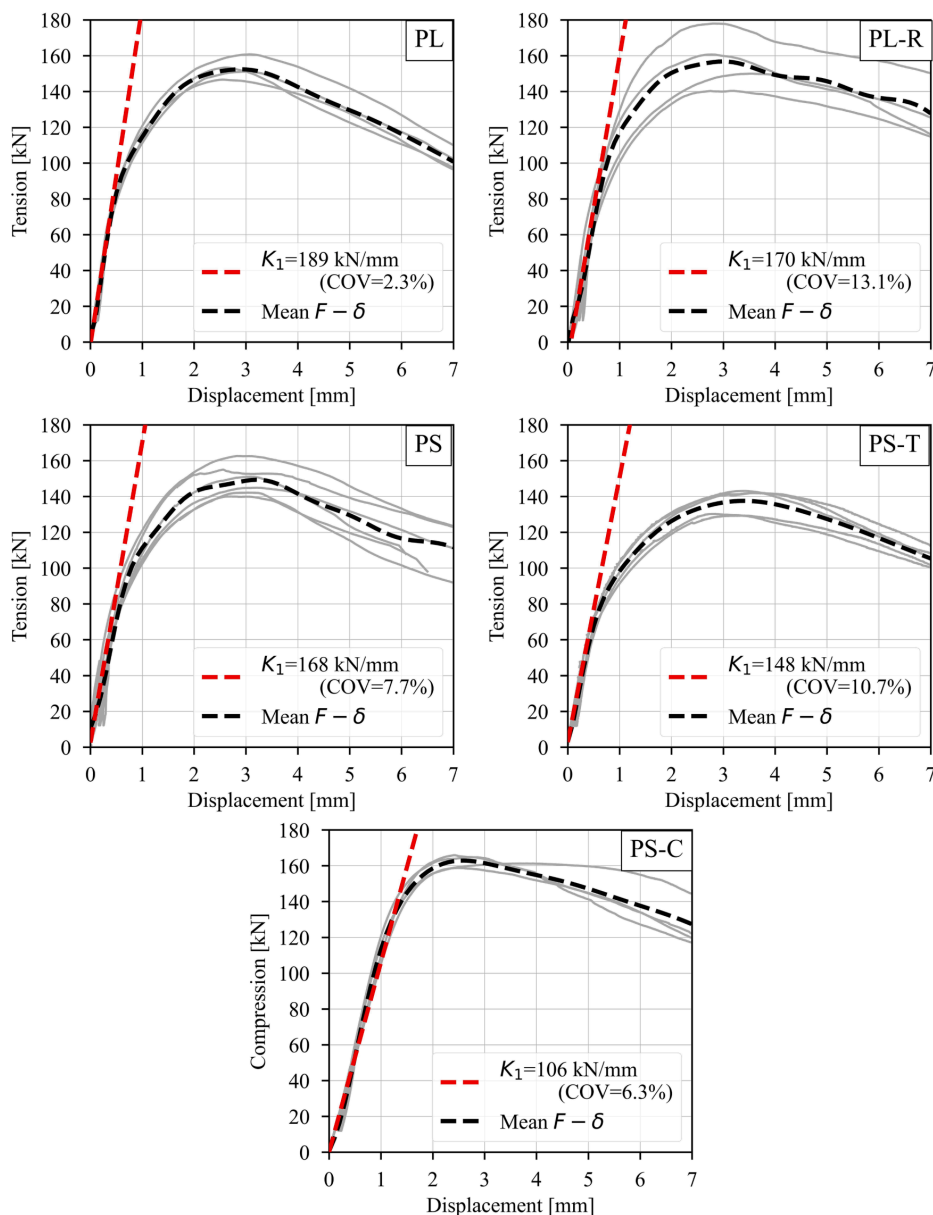


Fig. 17. Monotonic load–displacement curves.

monotonic stiffness, confer Figs. 17 and 18.

The mean withdrawal capacity ($F_{ax,mean}$) and mean withdrawal strength ($f_{ax,mean} = F_{ax,mean}/\pi dl$) at failure were calculated, see Table 3. The mean withdrawal capacity of all test series is comparable, with a difference of less than 20 % between different series. The characteristic withdrawal capacity $F_{ax,k}$ and the characteristic withdrawal strength ($f_{ax,k}$) were calculated according to EN 14358 [65] assuming lognormal distribution, see Table 3. Although test series PL-R shows higher mean withdrawal strength compared to PL, it has higher variability resulting in lower estimation for the characteristic withdrawal capacity.

Stamatopoulos and Malo [7] estimated mean withdrawal strength in the range of 4.46–5.12 N/mm² for threaded rods inserted perpendicular to grain in glulam. Blaß and Krüger [54] reported mean withdrawal strength in the range of 3.72–4.68 N/mm² for similar rods inserted perpendicular to grain in softwood. Yang et al. [55] observed mean withdrawal strength in the range of 2.98–7.86 N/mm² for threaded rods inserted perpendicular to grain into the narrow face of CLT. Li et al. [30] reported mean withdrawal strength in the range of 4.76–8.10 N/mm² for STS inserted perpendicular to grain into the narrow face of CLT. The results shown in Table 3 agrees best with the values reported by

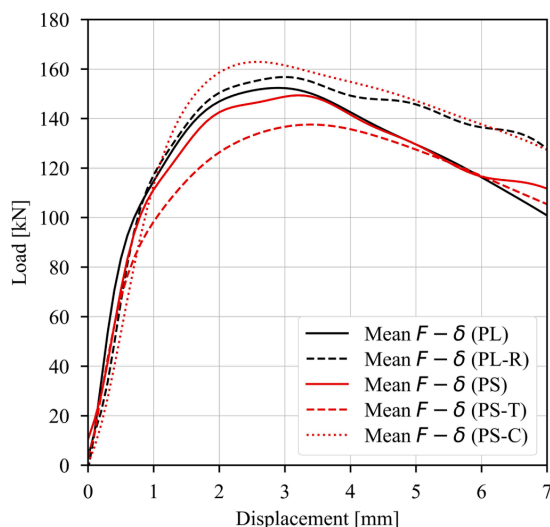


Fig. 18. Mean monotonic load–displacement curves.

Table 3
Mean and characteristic capacity and withdrawal stress.

Series	$F_{ax,mean}$ (kN)	$f_{ax,mean}$ (N/mm ²)	$F_{ax,k}$ (kN)*	$f_{ax,k}$ (N/mm ²)*
PL	152.9 (COV = 3.8 %)	5.03	133.5	4.39
PL-R	157.2 (COV = 10.2 %)	5.17	119.0	3.91
PS	149.3 (COV = 5.8 %)	4.91	130.5	4.29
PS-T	137.3 (COV = 5.0 %)	4.52	120.9	3.98
PS-C	162.7 (COV = 2.0 %)	5.35	142.0	4.67

*Considering a minimum of 5% variability as specified by EN14358 [65].

Stamatopoulos and Malo [7] where threaded rods with similar diameter and wood of the same species were used.

4. Conclusions

This paper investigates the pullout behavior of threaded rods inserted perpendicular to grain into the narrow face of CLT elements. Threaded rods with outer thread diameter (d) of 22 mm were used in this study. Five test series were carried out, with three series tested under service-level cyclic loading followed by destructive monotonic loading, and two test series were tested under monotonic loading only. The influence of the penetration length, the loading type (tension, compression, fully reversed), the loading configuration (pull–pull, pull–push), and the effect of using self-tapping screws as reinforcement were investigated. The following main conclusions are drawn:

- Threaded rods inserted perpendicular to grain into the narrow face of CLT elements exhibit high withdrawal stiffness. When inserted at a penetration length of $20d$, the mean withdrawal stiffness ranges from 100 to 250 kN/mm. The variation in the stiffness is possibly due to the different loading types and loading configurations.
- The mean withdrawal stiffness under cyclic loading is generally higher than the stiffness under monotonic loading.
- Under service-level loading, the equivalent viscous damping ratio ranges from 3 to 12 %.
- Stiffness exhibits a non-linear relationship with the penetration length, showing noticeable convergence beyond $15d$ (330 mm).

- Threaded rods inserted perpendicular to grain into the narrow face of CLT elements exhibit high withdrawal capacity. When inserted at a penetration length of $20d$, the mean withdrawal capacity ranges from 137 to 163 kN. The capacity seems not sensitive to the loading type and loading configuration.
- Reinforcement with self-tapping screws can provide more ductile load–displacement curve without noticeable increase in the withdrawal capacity. However, the effect of reinforcement at rod penetration lengths other than $20d$ was not investigated.
- All threaded rods with a penetration length of $20d$ failed in withdrawal failure mode. The only exception was for rods tested in pull–pull loading configuration without reinforcement where the withdrawal failure was combined with splitting failure. However, the influence of varying the penetration length on the failure mode was not investigated.

CRedit authorship contribution statement

Osama Abdelfattah Hegeir: Conceptualization, Methodology, Software, Validation, Formal analysis, Investigation, Data curation, Writing – original draft, Visualization, Project administration.

Declaration of Competing Interest

The authors declare that they have no known competing financial interests or personal relationships that could have appeared to influence the work reported in this paper.

Data availability

Data will be made available on request.

Acknowledgment

The authors acknowledge the contribution of Master Students Elisabeth Frette, Amund Hegheim, Thomas Munkeby, Haakon Flaten, Ulrik Sæther Langvik, and Simen Kåre Bokalrud in the preparation and execution of the experiments.

References

- [1] A.S. Cao, H. Stamatopoulos, A theoretical study of the dynamic response of planar timber frames with semi-rigid moment-resisting connections subjected to wind loads, *Eng. Struct.* 240 (2021), <https://doi.org/10.1016/j.engstruct.2021.112367>.
- [2] K.A. Malo, R.B. Abrahamsen, M.A. Bjertnes, Some structural design issues of the 14-storey timber framed building “Tree” in Norway, *Eur. J. Wood Wood Prod.* 74 (3) (2016) 407–424, <https://doi.org/10.1007/s00107-016-1022-5>.
- [3] A. Vilguts, H. Stamatopoulos, K.A. Malo, Parametric analyses and feasibility study of moment-resisting timber frames under service load, *Eng. Struct.* 228 (2021), <https://doi.org/10.1016/j.engstruct.2020.111583>.
- [4] O. A. Hegeir, H. Stamatopoulos, and K.A. Malo, “Serviceability performance of timber dual frame-wall structural system under wind loading,” *World Conference on Timber Engineering (WCTE 2023)*, Oslo, Norway, 2023, doi: 10.52202/069179-0384.
- [5] H. Stamatopoulos, K.A. Malo, Withdrawal capacity of threaded rods embedded in timber elements, *Constr. Build. Mater.* 94 (2015) 387–397, <https://doi.org/10.1016/j.conbuildmat.2015.07.067>.
- [6] H. Stamatopoulos, K.A. Malo, Withdrawal stiffness of threaded rods embedded in timber elements, *Constr. Build. Mater.* 116 (2016) 263–272, <https://doi.org/10.1016/j.conbuildmat.2016.04.144>.
- [7] H. Stamatopoulos, K.A. Malo, On strength and stiffness of screwed-in threaded rods embedded in softwood, *Constr. Build. Mater.* 261 (2020), <https://doi.org/10.1016/j.conbuildmat.2020.119999>.
- [8] A. Vilguts, S.Ø. Nesheim, H. Stamatopoulos, K.A. Malo, A study on beam-to-column moment-resisting timber connections under service load, comparing full-scale connection testing and mock-up frame assembly, *Eur. J. Wood Wood Prod.* 80 (4) (2022) 753–770, <https://doi.org/10.1007/s00107-021-01783-2>.
- [9] P. Dietsch, R. Brandner, Self-tapping screws and threaded rods as reinforcement for structural timber elements – a state-of-the-art report, *Constr. Build. Mater.* 97 (2015) 78–89, <https://doi.org/10.1016/j.conbuildmat.2015.04.028>.
- [10] N. Ratsch, S. Böhm, M. Voß, M. Kaufmann, T. Vallée, Influence of imperfections on the load capacity and stiffness of glued-in rod connections, *Constr. Build. Mater.* 226 (2019) 200–211, <https://doi.org/10.1016/j.conbuildmat.2019.07.278>.

- [11] D. Kohl, N. Ratsch, S. Böhm, M. Voß, M. Kaufmann, T. Vallée, Influence of manufacturing methods and imperfections on the load capacity of glued-in rods, *J. Adhes.* 96 (8) (2018) 738–759, <https://doi.org/10.1080/00218464.2018.1508351>.
- [12] V. Di Maria, L. D'Andria, G. Muciaccia, A. Ianakiev, Influence of elevated temperature on glued-in steel rods for timber elements, *Constr. Build. Mater.* 147 (2017) 457–465.
- [13] G. Thustochowicz, E. Serrano, R. Steiger, State-of-the-art review on timber connections with glued-in steel rods, *Mater. Struct.* 44 (5) (2010) 997–1020, <https://doi.org/10.1617/s11527-010-9682-9>.
- [14] M. Wells, "Stadthaus, London: raising the bar for timber buildings," in Proceedings of the Institution of Civil Engineers-Civil Engineering, 2011, vol. 164, no. 3: Thomas Telford Ltd, pp. 122–128.
- [15] I. Gunawan et al., "Verification of seismic resistant performance of developed original cross-laminated timber core structure method by shaking table experiment," in IOP Conference Series: Materials Science and Engineering, 2020, vol. 935, no. 1: IOP Publishing, p. 012065.
- [16] Z. Chen, M. Popovski, A. Iqbal, Structural performance of post-tensioned CLT shear walls with energy dissipators, *J. Struct. Eng.* 146 (4) (2020), 04020035.
- [17] M. Shahnewaz, C. Dickof, T. Tannert, Seismic behavior of balloon frame CLT shear walls with different ledgers, *J. Struct. Eng.* 147 (9) (2021), 04021137.
- [18] X. Sun, M. He, Z. Li, F. Lam, Seismic performance assessment of conventional CLT shear wall structures and post-tensioned CLT shear wall structures, *Eng. Struct.* 196 (2019), 109285.
- [19] I. Gavric, M. Fragiaco, A. Ceccotti, Cyclic behavior of CLT wall systems: experimental tests and analytical prediction models, *J. Struct. Eng.* 141 (11) (2015) pp. [https://doi.org/10.1061/\(asce\)st.1943-541x.0001246](https://doi.org/10.1061/(asce)st.1943-541x.0001246).
- [20] R. Brandner, G. Flatscher, A. Ringhofer, G. Schickhofer, A. Thiel, Cross laminated timber (CLT): overview and development, *Eur. J. Wood Wood Prod.* 74 (3) (2016) 331–351, <https://doi.org/10.1007/s00107-015-0999-5>.
- [21] H. Blass, "Joints with inclined screws," CIB-W18, 2002, 9, 2002.
- [22] T. Uibel and H. J. Blaß, "Edge joints with dowel type fasteners in cross laminated timber," in Proceedings. CIB-W18 Meeting, 2007.
- [23] M. Frese and H. J. Blaß, "Models for the calculation of the withdrawal capacity of self-tapping screws," presented at the Proceedings of the 42nd CIB-W18 meeting Dübendorf, Switzerland, 2009.
- [24] G. Pirnbacher, "Base parameters of self-tapping screws," in International Council for Research and Innovation in Building and Construction, Working Commission W18-Timber Structures, Meeting, 2009, pp. 42-7-1/1-42-7-1/16.
- [25] R. Tomasi, A. Crosatti, M. Piazza, Theoretical and experimental analysis of timber-to-timber joints connected with inclined screws, *Constr. Build. Mater.* 24 (9) (2010) 1560–1571, <https://doi.org/10.1016/j.conbuildmat.2010.03.007>.
- [26] J. Xu, S. Zhang, G. Wu, Y. Gong, H. Ren, Withdrawal properties of self-tapping screws in Japanese larch (*Larix kaempferi* (Lamb.) Carr.) Cross Laminated Timber, *Forests* 12 (5) (2021) pp. <https://doi.org/10.3390/f12050524>.
- [27] S. Maleki, S. Kazemi Najafi, G. Ebrahimi, M. Ghofrani, Withdrawal resistance of screws in structural composite lumber made of poplar (*Populus deltoides*), *Constr. Build. Mater.* 142 (2017) 499–505, <https://doi.org/10.1016/j.conbuildmat.2017.03.039>.
- [28] A. Ringhofer, R. Brandner, G. Schickhofer, Withdrawal resistance of self-tapping screws in unidirectional and orthogonal layered timber products, *Mater. Struct.* 48 (5) (2013) 1435–1447, <https://doi.org/10.1617/s11527-013-0244-9>.
- [29] M.P. Gutknecht, C. MacDougall, Withdrawal resistance of structural self-tapping screws parallel-to-grain in common Canadian timber species, *Can. J. Civ. Eng.* 46 (10) (2019) 952–962, <https://doi.org/10.1139/cjce-2018-0374>.
- [30] X. Li, M. Ashraf, M. Subhani, K. Ghabraie, H. Li, and P. Kremer, "Withdrawal resistance of self-tapping screws inserted on the narrow face of cross laminated timber made from Radiata Pine," in Structures, 2021, vol. 31: Elsevier, pp. 1130–1140.
- [31] J. Brown, M. Li, B. Karalus, and S. Stanton, "Withdrawal behaviour of self-tapping screws in New Zealand cross-laminated timber," 2020.
- [32] A. Ringhofer, "Axially loaded self-tapping screws in solid timber and laminated timber products," 2017.
- [33] N. Jacquier, U.A. Girhammar, Tests on glulam-CLT shear connections with double-sided punched metal plate fasteners and inclined screws, *Constr. Build. Mater.* 72 (2014) 444–457, <https://doi.org/10.1016/j.conbuildmat.2014.08.095>.
- [34] C. Bedon, M. Fragiaco, Numerical analysis of timber-to-timber joints and composite beams with inclined self-tapping screws, *Compos. Struct.* 207 (2019) 13–28.
- [35] H. Krenn and G. Schickhofer, "Joints with inclined screws and steel plates as outer members," in International Council for Research and Innovation in Building and Construction, Working Commission W18-Timber Structures, Meeting, 2009, pp. 42-7-2, 1-42-7-2, 12.
- [36] T. Claus, W. Seim, J. Küllmer, Force distribution in self-tapping screws: experimental investigations with fibre Bragg grating measurement screws, *Eur. J. Wood Wood Prod.* 80 (1) (2021) 183–197, <https://doi.org/10.1007/s00107-021-01740-z>.
- [37] B. Azinović, E. Serrano, M. Kramar, and T. Pazlar, "Experimental investigation of the axial strength of glued-in rods in cross laminated timber," *Materials and Structures*, vol. 51, no. 6, 2018, doi: 10.1617/s11527-018-1268-y.
- [38] G.S. Ayansola, T. Tannert, T. Vallee, Experimental investigations of glued-in rod connections in CLT, *Constr. Build. Mater.* 324 (2022), <https://doi.org/10.1016/j.conbuildmat.2022.126680>.
- [39] B. Azinović, H. Danielsson, E. Serrano, M. Kramar, Glued-in rods in cross laminated timber – numerical simulations and parametric studies, *Constr. Build. Mater.* 212 (2019) 431–441, <https://doi.org/10.1016/j.conbuildmat.2019.03.331>.
- [40] R. Steiger, E. Gehri, R. Widmann, Pull-out strength of axially loaded steel rods bonded in glulam parallel to the grain, *Mater. Struct.* 40 (1) (2006) 69–78, <https://doi.org/10.1617/s11527-006-9111-2>.
- [41] R. Widmann, R. Steiger, E. Gehri, Pull-out strength of axially loaded steel rods bonded in glulam perpendicular to the grain, *Mater. Struct.* 40 (8) (2007) 827–838, <https://doi.org/10.1617/s11527-006-9214-9>.
- [42] D. Otero Chans, J. Estévez Cimadevila, E. Martín Gutiérrez, Withdrawal strength of threaded steel rods glued with epoxy in wood, *Int. J. Adhes. Adhes.* 44 (2013) 115–121, <https://doi.org/10.1016/j.ijadhadh.2013.02.008>.
- [43] C. Grunwald, et al., Rods glued in engineered hardwood products part II: Numerical modelling and capacity prediction, *Int. J. Adhes. Adhes.* 90 (2019) 182–198, <https://doi.org/10.1016/j.ijadhadh.2019.05.004>.
- [44] B.-H. Xu, D.-F. Li, Y.-H. Zhao, A. Bouchaïr, Load-carrying capacity of timber joints with multiple glued-in steel rods loaded parallel to grain, *Eng. Struct.* 225 (2020), 111302.
- [45] E. Gonzales, C. Avez, T. Tannert, Timber joints with multiple glued-in steel rods, *J. Adhes.* 92 (7–9) (2015) 635–651, <https://doi.org/10.1080/00218464.2015.1099098>.
- [46] Y. Shirmohammadi, A. Hashemi, R. Masoudnia, P. Quenneville, Numerical modeling investigation of cross-laminated timber connections consisting of multiple glued-in rods, *Structures* 53 (2023) 491–500.
- [47] E. Martín-Gutiérrez, J. Estévez-Cimadevila, D. Otero-Chans, Durability of joints made with threaded steel rods glued in chestnut timber – An experimental approach, *Compos. B Eng.* 108 (2017) 413–419, <https://doi.org/10.1016/j.compositesb.2016.10.010>.
- [48] R. Steiger, et al., Strengthening of timber structures with glued-in rods, *Constr. Build. Mater.* 97 (2015) 90–105, <https://doi.org/10.1016/j.conbuildmat.2015.03.097>.
- [49] N. Gattesco, A. Gubana, M. Buttazzi, M. Melotto, Experimental investigation on the behavior of glued-in rod joints in timber beams subjected to monotonic and cyclic loading, *Eng. Struct.* 147 (2017) 372–384.
- [50] B.-H. Xu, A. Bouchaïr, P. Racher, Analytical study and finite element modelling of timber connections with glued-in rods in bending, *Constr. Build. Mater.* 34 (2012) 337–345.
- [51] S. Navaratnam, J. Thamboo, T. Ponnampalam, S. Venkatesan, K.B. Chong, Mechanical performance of glued-in rod glulam beam to column moment connection: An experimental study, *J. Build. Eng.* 50 (2022), 104131.
- [52] É. Gauthier-Turcotte, S. Ménard, M. Fiset, Strength and behavior of spruce pine glulam timber moment connections using glued-in steel rods, *J. Struct. Eng.* 148 (12) (2022), 04022192.
- [53] E. Gonzales, T. Tannert, T. Vallee, The impact of defects on the capacity of timber joints with glued-in rods, *Int. J. Adhes. Adhes.* 65 (2016) 33–40, <https://doi.org/10.1016/j.ijadhadh.2015.11.002>.
- [54] H.J. Blaß, O. Krüger, Schubverstärkung von Holz mit Holzschrauben und Gewindestangen, KIT Scientific Publishing, Karlsruhe, 2010.
- [55] H. Yang, J. Ji, H. Tao, B. Shi, J. Hu, B. Wen, Pull-out behaviour of axially loaded screwed-in threaded rods embedded in CLT elements: experimental study, *J. Renewable Mater.* 10 (1) (2022) 105–117, <https://doi.org/10.32604/jrm.2021.016118>.
- [56] CEN, "NS-EN 338: Structural timber-Strength classes," *European Committee for Standardization: Brussels, Belgium*, 2016.
- [57] SINTEF Certification-TG 20712 Splitkon krysslimt tre, 2022.
- [58] ETA-Danmark A/S, European Technical Assessment ETA-12/0114, SPAX self-tapping screws, 2017.
- [59] CEN, "EN 12512: Timber structures-Test methods-Cyclic testing of joints made with mechanical fasteners," *European Committee for Standardization: Brussels, Belgium*, 2001.
- [60] CEN, "EN 26891:1991 (ISO 6891:1983): Timber structures-Joints Made with Mechanical Fasteners- General Principles for the Determination of Strength and Deformation Characteristics," 1991.
- [61] CEN, "NS-EN 1995-1-1:2004+A1:2008+NA:2010: Design of timber structures-Part 1-1: General-Common rules and rules for buildings," *European Committee for Standardization: Brussels, Belgium*, 2010.
- [62] A.K. Chopra, *Dynamics of Structures*, fifth ed., Pearson Education Limited, London, United Kingdom, 2020.
- [63] A. Ringhofer and G. Schickhofer, "Influencing parameters on the experimental determination of the withdrawal capacity of self-tapping screws," in Proceedings of the 13th World Conference on Timber Engineering, Canada, World Conference on Timber Engineering, 2014, vol. 2014, pp. 906–915.
- [64] CEN/TC250/SC5N1650, "prEN 1995-1-1: Design of timber structures-Part 1-1: General rules and rules for buildings," *European Committee for Standardization: Brussels, Belgium*, 2022.
- [65] CEN, "EN 14358:2016: Timber Structures: Calculation and verification of characteristic values," *European Committee for Standardization: Brussels, Belgium*, 2016.

Paper II

An innovative slip-friction moment-resisting connection using screwed-in threaded rods in cross laminated timber and steel coupling parts: An experimental study

Osama Abdelfattah Hegeir, Kjell Arne Malo, Haris Stamatopoulos

Submitted to an international peer-reviewed journal

This paper is awaiting publication and is not included in NTNU Open

Paper III

Serviceability performance of timber dual frame-wall structural system under wind loading

Osama Abdelfattah Hegeir, Haris Stamatopoulos, Kjell Arne Malo

In proceedings of the ***World Conference on Timber Engineering*** (WCTE 2023),

Oslo, 2023

SERVICEABILITY PERFORMANCE OF TIMBER DUAL FRAME-WALL STRUCTURAL SYSTEM UNDER WIND LOADING

Osama Abdelfattah Hegeir¹, Haris Stamatopoulos², Kjell Arne Malo³

ABSTRACT: Due to the moderate stiffness and low mass of timber multi-storey buildings, wind-induced accelerations and displacements usually govern the design. Moment-resisting timber frames (MRTFs) are structural systems that can provide open space and architectural flexibility. However, in regions with moderate to high wind velocities, MRTFs can be used for up to 8 storeys with small out-of-plane spacing between frames (C/C distance of the order of 2-3 m). In this paper, a dual frame-wall structural system is investigated. A parametric study using 2D linear elastic Finite Element Analysis (FEA) is performed to explore the feasibility of the system in regions with moderate wind velocities, considering serviceability requirements (lateral displacements and wind-induced accelerations). Floor vibrations are also taken into account. A 3D FEA model is used to verify the results of the 2D FEA model. Although the focus of the paper is devoted to serviceability requirements, some ultimate limit state considerations are discussed. The results highlight the possibility of using the dual system for multi-storey buildings, with up to 12 storeys and 5 m C/C distance in regions with basic wind velocities up to 26 m/sec.

KEYWORDS: Moment-resisting frames, serviceability, deflections, CLT, glulam, wind-induced accelerations, human-induced vibrations

1 INTRODUCTION

Timber has a very good strength/weight ratio due to its light weight compared to other building materials such as concrete and steel. Moreover, timber can be considered a more environment-friendly construction material than concrete and steel in terms of greenhouse gas emissions [1, 2]. Due to the lightweight nature and moderate stiffness of wood, timber structures are prone to serviceability problems such as excessive accelerations and displacements [3, 4]. Excessive accelerations can cause discomfort to the occupants, and excessive displacements can cause damage and therefore should be kept within acceptable limits.

There exist several structural systems that can provide lateral stiffness to a building. A common structural system used for tall timber buildings is diagonal bracing, such as Treet [4] and Mjøstårnet [5] in Norway. However, these buildings require huge bracing elements running along the height of the structure, which may compromise the architecture flexibility. Cross laminated timber (abbr. CLT) can also be used as a Lateral Load Resisting System (abbr. LLRS). An example of timber building with CLT walls is Stadthaus in London [6]. However, such structures are material-intensive, cellular, and can impose space limitations.

Open and flexible architectural design of buildings is a desirable property, which can be achieved by use of Moment-Resisting Timber Frames (abbr. MRTFs) as a LLRS. In MRTFs, the lateral stiffness relies largely on the

stiffness of beam-to-column connections. A feasibility study of glulam MRTFs has been carried out by Vilguts et al. [3], showing that in high-wind regions, glulam MRTFs can hardly be used for more than 8 storeys. The study [3] assumes a prefabricated floor with a small 2.40 m out-of-plane spacing between adjacent frames (abbr. C/C). These limitations are due to wind-induced accelerations and lateral displacements [3].

To overcome the limitations on the number of storeys and achieve larger C/C distance, it is necessary to use larger columns and beams compared to standard glulam dimensions. CLT panels are currently produced with standard dimensions up to 3.5x16.0 m, and therefore can be used to achieve these larger dimensions.

In this paper, the feasibility of using dual frame-wall structural system to build up 12 storeys with C/C distance of 5 m considering a basic wind velocity of 26 m/sec is explored. The system consists of CLT walls, glulam columns and beams, and semi-rigid connections between beams and columns/walls. The feasibility of the system is evaluated, mainly, in terms of Serviceability Limit State (abbr. SLS). However, some Ultimate Limit State (abbr. ULS) considerations are also presented.

2 STRUCTURAL SYSTEM

In this section, the dual frame-wall structural system is explained. Both the LLRS and floor system are described in two different subsections.

¹ Osama Abdelfattah Hegeir osama.a.s.a.hegeir@ntnu.no

² Haris Stamatopoulos haris.stamatopoulos@ntnu.no

³ Kjell Arne Malo kjell.malo@ntnu.no

Department of Structural Engineering, Norwegian University of Science and Technology (NTNU)

2.1 LATERAL LOAD RESISTING SYSTEM

An example of the structural system is shown in Figure 1 (a). In this paper, the focus is given to the structural system in X direction (marked with dotted red box in Figure 1 (a)) where the dual system is used. It consists of continuous CLT walls, continuous glulam columns, and glulam beams. Semi-rigid connections using threaded rods are assumed between beams and walls/columns (see Figure 1 (b)). More details on the connections using threaded rods can be found in [7]. In Y direction, the building may be stabilized by use of diagonal bracing. The LLRS is discussed in more detail in section 4.

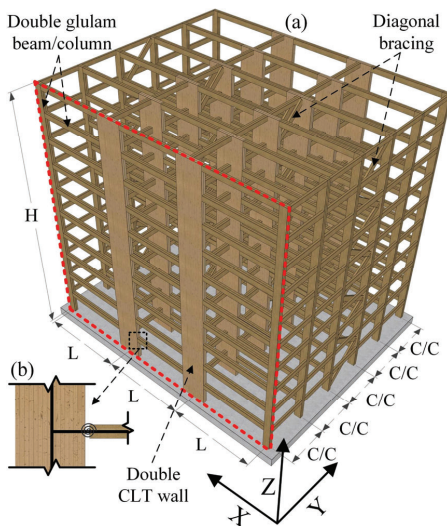


Figure 1: (a) 3D view of the structural system, (b) semi-rigid moment connection

2.2 FLOOR SYSTEM

In this paper, a ribbed slab floor system is assumed, see Figure 2. The system consists of CLT panels resting on simply supported secondary beams (glulam). The secondary beams are supported on the main LLRS working in X direction. The floor system is one way with load bearing parallel to Y axis. For better acoustic performance, double beams, columns, and walls are considered. Analysis of floors is discussed in section 3.

3 ANALYSIS OF FLOORS

Human-induced vibrations can be decisive in the design of timber floors [8, 9]. This section explores the serviceability performance of the floor system shown in Figure 2, which includes satisfying deflection limits and human-induced vibrations. However, the vibrations were found to be more critical than deflections. Therefore, the performance was only evaluated with respect to human-induced vibrations.

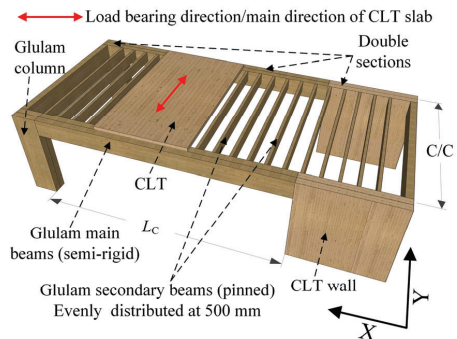


Figure 2: Floor system

Linear elastic Finite Element Analysis (abbr. FEA) was used to calculate the fundamental frequency and the deflection of the floor under unit load. The clear span L_C (confer Figure 2) and the stiffness of main beams' connections (confer Figure 2) were varied. The vibration performance of the floor was evaluated using the simplified Hu and Chui criterion [8].

3.1 MATERIALS

The glulam beams used in the floor is assumed of strength class GL30c as defined by EN 14080 [10]. The boards constituting the CLT panels are assumed of strength class C24 as defined by EN 338 [11]. In this paper, it was assumed that (2/3) of the boards are parallel to the main direction of CLT panels (confer Figure 2). The remaining (1/3) are orthogonal to the main direction. Table 1 summarizes mean stiffness properties for GL30c and C24, and the corresponding material axes are illustrated in Figure 3.

Table 1: Mean stiffness properties for floor elements

	GL30c	C24	Unit
E_1	13000	11000	N/mm ²
E_2	300	370	N/mm ²
E_3	300	370	N/mm ²
G_{12}	650	690	N/mm ²
G_{13}	650	690	N/mm ²
G_{23}	65	69	N/mm ²

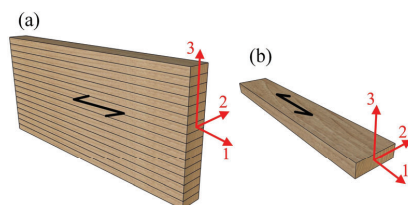


Figure 3: Material axes for (a) glulam GL30c, (b) C24 boards

3.2 FINITE ELEMENT MODELLING

CSI SAP2000 [12] was used for FEA. The software can be automated using Open Application Programming Interface (abbr. OAPI). The FEA model of the floor is shown in Figure 4. The main beams (glulam) are modelled using linear beam elements. The ends of the main beams are partially released with respect to bending moment to consider the semi-rigid connections. The secondary beams (glulam) are modelled using shell elements (shown in blue in Figure 4). The CLT slabs are modelled using layered shell elements (shown in red in Figure 4). The connections between the CLT slab and secondary beams, and the connections between the secondary beams and the main beams are modelled using link elements with only axial and shear stiffness (no rotational stiffness).

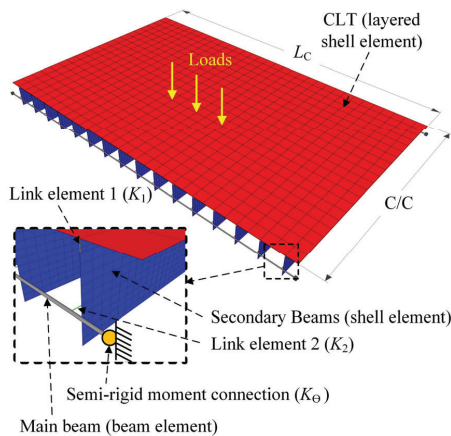


Figure 4: FEA model of the floor

3.3 ACCEPTANCE CRITERIA

Several design criteria exist for assessing floor vibrations caused by human activity (e.g. [8, 13]), each taking into account different factors and making different assumptions. In this paper, the simplified criterion proposed by Hu and Chui [8] is used:

$$\frac{(f_{n,1}/18.7)^{2.27}}{w_{1 \text{ kN}}} \geq 1.0 \quad (1)$$

Where $f_{n,1}$ and $w_{1 \text{ kN}}$ are the fundamental frequency and the static deflection due to 1.0 kN.

The criterion [8] was developed based on testing of more than one hundred timber floors. Although this criterion [8] was developed in Canada, it is based on physical and subjective evaluations of floors with damping properties comparable to wooden floors found in Norway [14].

3.4 PARAMETRIC STUDY

A parametric study was performed to evaluate the performance of the floor. The parameters varied are summarized in Table 2. Two load scenarios are investigated, namely: heavy load, and light load, see

Table 3. The heavy floors represent a case where additional mass is added to improve the performance of the building with respect to wind-induced accelerations (discussed in section 4).

The fundamental frequency $f_{n,1}$ used in evaluating human-induced vibration (see equation (1)) is calculated assuming only the dead load is applied to the CLT slab.

The connections between the CLT slab and the secondary beams, as well as the connections between the secondary beams and the main beams are assumed of equal translational stiffness K_1 and K_2 respectively, confer Figure 4 and Table 2. The main beams connection stiffness K_0 is reasonably assumed based on the experimental work performed by Vilguts et al. [7] and the analytical work done by Stamatopoulos et al. [15]. Two sets of beams cross-sections and CLT layups are used depending on the load scenario, see Table 4. In total, 60 3D linear elastic analyses were performed.

Table 2: Parameters used in the parametric study of the floors

	Value(s)	Unit
Clear span L_c	7–9	m
C/C	5	m
K_0	0–15,000	kN·m/rad
K_1^*	10	kN/mm
K_2	20	kN/mm
Damping ratio (ζ)	2	%

* Evenly distributed at 250 mm

Table 3: Load scenarios

	Heavy load	Light load	Unit
Dead load G_k^*	2.0	1.0	kN/m ²
Live load Q_k	3.0**	2.0***	kN/m ²

* Including the own weight of beams and slabs

** Office buildings as defined by EN 1991-1-1 [16]

*** Residential buildings as defined by EN 1991-1-1 [16]

Table 4: Beams cross-sections and CLT layups used in the parametric study of the floors

	Load scenario	Cross-section/layup	Unit
Main beam	Heavy/light	215 · 585	mm ²
Sec. beam	Heavy	115 · 450	mm ²
CLT slab		30/30/30	mm
Sec. beam	Light	90 · 450	mm ²
CLT slab		40/40/40	mm

Figure 5 shows the performance of the floor according to Hu and Chui [8] as function of the clear span L_c . As shown in Figure 5, for $K_0 = 15,000$ kN·m/rad, light floors with clear span up to 8.5 m and heavy floors with clear span up to 7.5 meet the acceptance limit. For $K_0 = 0$ (pinned), only light floors with clear span of 7.0 m meet the limit.

According to EN 1995-1-1 [17], special investigation is needed for residential timber floors with fundamental frequency less than 8 Hz. Modal analysis is used to calculate the fundamental frequency assuming only dead

load is applied to the CLT slab. The frequencies of light and heavy floors are shown in Figure 6. For floors with $K_{\theta} = 15,000$, the frequencies of all light floors meet the acceptance limit (8 Hz), while only heavy floors with clear span ≤ 7.5 m meet the limit. For floors with $K_{\theta} = 0$, only light floors with clear span ≤ 8.5 m meet the frequency limit.

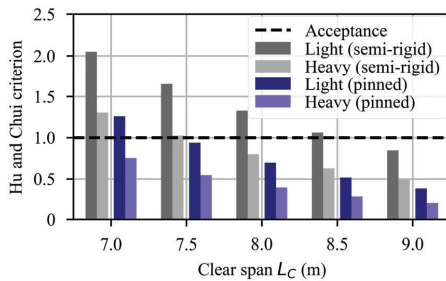


Figure 5: Hu and Chui [8] criterion for human-induced vibrations (pinned: $K_{\theta}=0$, and semi-rigid: $K_{\theta}=15,000$ kN-m/rad)

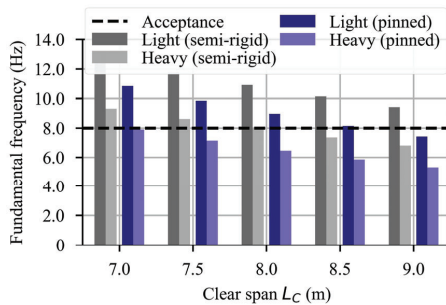


Figure 6: Fundamental frequencies of floors (pinned: $K_{\theta}=0$, semi rigid: $K_{\theta}=15,000$ kN-m/rad, and only the dead load is considered)

According to Hu and Chui criterion [8], and in compliance with EN 1995-1-1 [17] requirement of a minimum frequency of 8 Hz, some conclusions can be drawn from the parametric study (see Table 2):

- Light floors with clear span ≤ 8.5 m satisfy the requirements given that $K_{\theta} \geq 15,000$ kN-m/rad.
- Heavy floors with clear span ≤ 7.5 m satisfy the requirements given that $K_{\theta} \geq 15,000$ kN-m/rad.
- If pinned connections are used ($K_{\theta} = 0$), only light floors with clear span ≤ 7 m meet the requirements.

The influence of main beam connection stiffness (K_{θ}) on frequency and vibration performance is shown in Figure 7, where the rotational stiffness (K_{θ}) is varied from 0 (pinned) to 15,000 kN-m/rad for a light floor with a clear span of 8 m. As depicted in Figure 7, an increase in K_{θ} results in a higher floor frequency and improved vibration performance, owing to the increased floor stiffness.

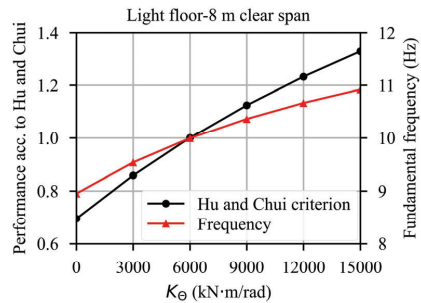


Figure 7: Influence of main beams connections' stiffness on frequency and vibration performance as per Hu and Chui [8]

4 ANALYSIS OF LATERAL LOAD RESISTING SYSTEM

Figure 1 shows a 3D structural system with X and Y directions perpendicular to each other. In this section, a small parametric study is performed to evaluate the feasibility of the dual frame-wall LLRS (in X direction) using 2D linear elastic FEA. Although the feasibility is evaluated primarily with respect to SLS, some ULS considerations are discussed. To validate the conclusions drawn from the 2D FEA, a 3D linear elastic FEA model was prepared, and the results were compared with those of the 2D FEA model.

Intuitively, higher connections' stiffness is required at lower storeys. The possibility of using lower connections' stiffness at the higher storeys is also explored.

4.1 MATERIALS

The LLRS in X direction consists of glulam beams, glulam columns, and CLT walls. The stiffness properties of glulam are the same as the floor (see Table 1).

A simplified modelling approach of CLT is to model CLT using equivalent stiffness properties assuming homogeneous cross-section with grain direction of all layers parallel to stress direction as proposed by [18]. This simplified modelling of CLT has shown good accuracy for CLT loaded in-plane [19]. Similar to the floors, 2/3 of the boards are assumed parallel to the main direction of CLT panels and the remaining 1/3 are orthogonal to the main direction. Equivalent stiffness properties of CLT walls are summarized in Table 5. The corresponding material axes are shown in Figure 8. Since linear elements were used to model the CLT walls (explained in 4.2 in this paper), only E_1 and G_{12} are relevant (confer Figure 8). E_1 affects the vertical axial stiffness and the bending stiffness of the CLT walls, and G_{12} affects their in-plane shear stiffness.

Table 5: Equivalent stiffness properties of CLT walls

	Equivalent stiffness	Unit
E_1	7457	N/mm ²
G_{12}	518	N/mm ²

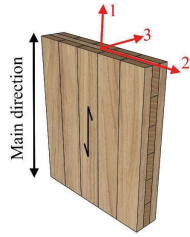


Figure 8: Material axes for CLT walls

4.2 FINITE ELEMENT MODELLING

Figure 9 shows the FEA model of the dual frame-wall system (X direction). CSI SAP2000 [12] was used to perform 2D linear elastic FEA. Glulam columns and beams were modelled using linear beam elements with the stiffness properties in Table 1. The CLT walls were also modelled using linear beam elements with the equivalent properties in Table 5. The linear beam elements representing the CLT walls were verified against the layered shell elements available in CSI SAP2000 [12] under in-plane loading. The verification was done on both stresses and displacements and the difference was less than 5%. Hence, linear beam elements were deemed to have sufficient accuracy for the purpose of this study.

All connections (beam-column/wall, wall-foundation, and column-foundation) were modelled using moment partial release available in CSI SAP2000 [12], and were considered semi-rigid with respect to moment and rigid with respect to translation.

Columns and walls have finite heights (in-plane dimension of the cross-section), therefore, when modelled using linear elements, beams' spans are increased. To account for this increase, end-length offset available in CSI SAP2000 [12] is used, see Figure 9. At each end of the beam, a length equal to half the column/wall height is assumed rigid for bending and shear deformations.

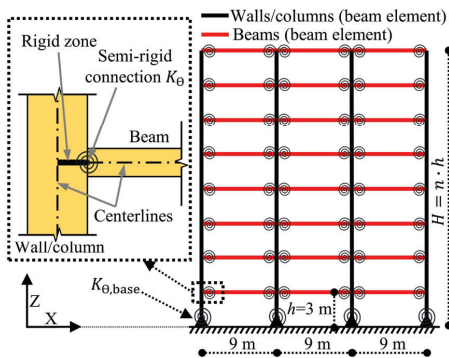


Figure 9: 2D FEA model of LLRS in X direction

4.3 PARAMETRIC STUDY

In this parametric study, two variations of the LLRS in X direction shown in Figure 9 are considered, namely:

exterior CLT walls, and interior CLT walls, see Figure 10. Both heavy and light loading scenarios are considered (see Table 3). The dead load in Table 3 includes the weight of the floor, while the own weight of LLRS is automatically calculated by CSI SAP2000 [12]. The parameters of the parametric study are summarized in Table 6 (total of 520 analyses).

The cross-sections of walls and columns, and the stiffness of their connections to the foundation were varied according to the number of storeys n , see Table 7. All beams, columns, and walls are double sections, confer Figure 2. The cross-sections and stiffness values in Table 6 and Table 7 are for single cross-section.

Table 6: Parameters of the parametric study of the LLRS

Parameter	Value(s)
Number of storeys (n)	4/6/8/10/12
Number of bays (n_b)	3
Gravity loads	Light/heavy
Variation	Interior/exterior CLT
C/C (Figure 1)	5 m
Basic wind velocity	26 m/sec
Beams	215 · 585 mm ²
Beam-column/wall connection stiffness (K_θ)	2,500-15,000 kN·m/rad

Table 7: Cross-section of columns and walls and the stiffness of their connection to foundation (n : number of storeys)

	n	Cross-sec. (mm ²)	$K_{\theta,base}$ (kN·m/rad)
Glulam columns	12	215 · 720	5,000
	10	215 · 630	3,750
	8	215 · 540	2,500
	6	215 · 450	1,250
	4	215 · 450	1,250
CLT walls	12	215 · 3500	200,000
	10	215 · 3000	150,000
	8	215 · 2500	100,000
	6	215 · 2000	60,000
	4	215 · 1500	30,000

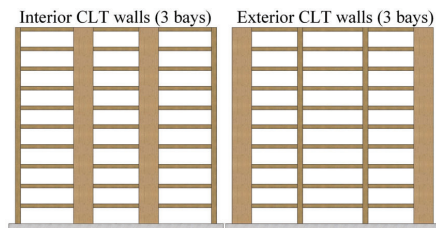


Figure 10: Two variations of LLRS in X direction

4.3.1 Serviceability performance

The serviceability performance of LLRS is evaluated in terms of wind-induced accelerations, top floor displacement (abbr. Disp.), and inter-storey drift (abbr. IDR). For the calculation of lateral displacements (Disp. and IDR) due to wind loading (W_k), the characteristic load

combination as defined in EN 1990 [20] with wind as a leading variable was used:

$$E_d = G_k + W_k + \psi_0 \cdot Q_k \quad (2)$$

The combination factor ψ_0 was set to 0.70 according to EN 1990 [20].

Some recommendations of deflections limits are provided by EN 1995-1-1 [17]. According to these recommendations, deflections in simple beams under characteristic load combination defined in EN 1990 [20] should be limited to $1/300 - 1/500$ of the span. No recommendations are given on structure level. As an approximation, the limits for simple beams are used for both lateral displacement at the top of the building (Δ) and relative displacement between two successive storeys (δ):

$$\Delta \leq H/300, \delta \leq h/300 \quad (3)$$

Where h is the height of a storey and H is the total height of the building.

For the calculations of wind-induced accelerations, procedure 1 in Annex B of EN 1991-1-4 [21] was used. The procedure is based on gust factor approach. For the calculation of wind-induced accelerations according to EN 1991-1-4 [21], the mode shape, and the fundamental frequency are required. To obtain both the mode shape and the fundamental frequency, modal analysis using CSI SAP2000 [12] was performed. In the modal analysis, the mass is calculated using the quasi-permanent load combination defined in EN 1990 [20]:

$$E_d = G_k + 0.3 \cdot Q_k \quad (4)$$

Damping is an important input to the wind-induced acceleration calculation. Little research has been done on damping of timber structures, see e.g. [22]. In this paper, 2% damping ratio (ζ) was assumed based on [22]. Basic wind velocity of 26 m/sec and urban environment (IV) as defined by EN 1991-1-4 [21] were assumed for the calculation of wind loads and wind-induced accelerations. Relevant parameters used in the calculation of wind-induced accelerations are summarized in Table 8.

Table 8: Relevant parameters for calculation of wind loads and wind-induced accelerations

Parameter	Value
Directional factor C_{dir}	1.0
Seasonal factor C_{season}	1.00
Probability factor C_{prob}	0.73
Orography factor $C_{0(z)}$	1.00
Turbulence factor k_1	1.00
Terrain category	IV
Reference height Z_t	200
Reference length L_t	300
Structural damping ξ	2%
Width of the building ($C/C \cdot 5$)	25 m

In this paper, the wind-induced acceleration acceptance criterion of ISO 10137 [13] is used. The criterion covers the range from a fundamental frequency of 0.063 to 5 Hz for a maximum wind velocity with a return period of one year, for both residential and office buildings.

Figure 11 shows the wind-induced accelerations against ISO 10137 criterion [13] for all frames (see Table 6). Figure 12 shows the maximum and minimum lateral displacements and IDR for all frames (see Table 6), where maximum and minimum correspond to a set of frames with common parameters and $K_\theta = 2,500$ kN·m/rad and 15,000 kN·m/rad respectively. Light and heavy frames have the same lateral displacements since gravity loads have no influence on lateral displacements.

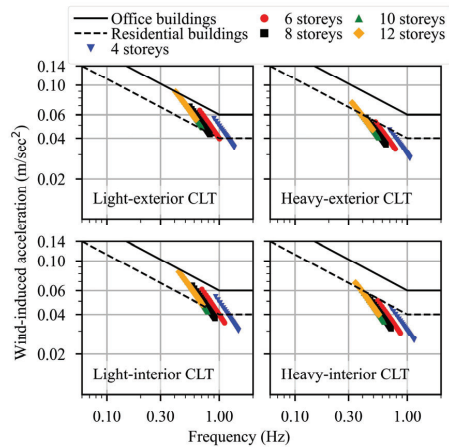


Figure 11: Wind-induced accelerations against ISO 10137 [13] criterion

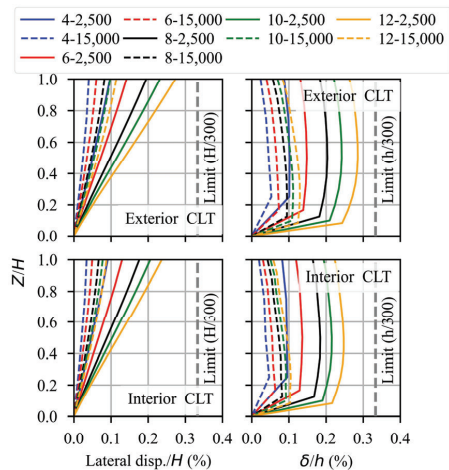


Figure 12: Lateral displacements and inter-storey drift (Legend: number of storeys- K_θ , and Z : height above ground)

As shown in Figure 11 and 12, the variation with interior CLT walls is slightly outperforming the variation with exterior CLT walls. The variation with interior CLT walls has 5-10% lower wind-induced accelerations and 5-15%

lower lateral displacements. Frames with heavy loads have 20% lower wind-induced accelerations. Observing Figure 11 and Figure 12, some conclusions can be made:

- All frames satisfy the requirements of top floor displacement and IDR by a good margin.
- Heavy frames up to 12 storeys meet the requirement of residential buildings provided that $K_{\theta} \geq 2 \cdot 5,500$ kN-m/rad (5,500 for single cross-section).
- Light frames up to 10 storeys meet the requirement of residential buildings provided that $K_{\theta} \geq 2 \cdot 11,500$ kN-m/rad (11,500 for single cross-section).
- Light frames of 12 storeys do not meet the requirement of residential buildings.
- Light and heavy frames up to 12 storeys meet the requirement of office buildings provided that $K_{\theta} \geq 2 \cdot 2,500$ kN-m/rad (2,500 for single cross-section).

4.3.2 Stiffness reduction in higher storeys

Connections with high stiffness are intuitively required at lower storeys, and connections with lower stiffness may be used in upper storeys. To verify such hypothesis, a 10-storey frame, with interior CLT walls and light gravity loads, is selected as a benchmark. All other parameters remain the same (see Tables 5-7).

A rotational stiffness (K_{θ}) of 5,000 kN-m/rad is assigned to all beam-to-column/wall connections, this is referred to as the reference case. High stiffness of (K_{θ}) 15,000 kN-m/rad is then assigned to all connections of one floor at each step starting from the bottom up (total of 10 steps). At the final step, all connections have a stiffness (K_{θ}) of 15,000 kN-m/rad. The case of all connections being rotationally rigid is also shown. In total, 12 analyses were performed. Figure 13 shows the top floor displacement, maximum IDR, and wind-induced acceleration, all normalized to the reference case ($K_{\theta} = 5,000$ kN-m/rad). In Figure 13, a value of 0 at the horizontal axis represents all connections with stiffness of 5,000 kN-m/rad (reference case), while a value of 10 represents all connections with a stiffness of 15,000 kN-m/rad.

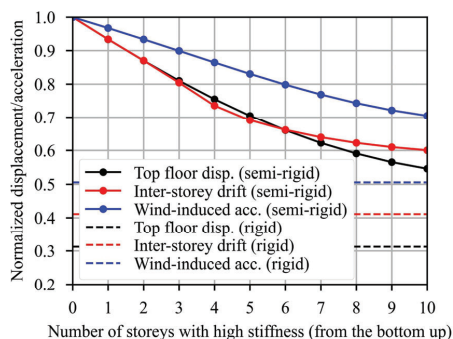


Figure 13: Top floor displacement, maximum IDR, and wind-induced acceleration with variable K_{θ} (higher at lower storeys) normalized to the reference case ($K_{\theta} = 5,000$ kN-m/rad).

As shown in Figure 13, IDR shows the fastest convergence, followed by top floor displacement and wind-induced acceleration. Using high stiffness ($K_{\theta} = 15,000$ kN-m/rad) for the bottom 5-6 storeys results in 70-90% of the reduction in lateral displacements (top floor displacement and IDR) compared to the case with all connections of high stiffness (10 at the horizontal axis of Figure 13). Using high stiffness for the bottom 5-6 storeys results in 60-70% of the reduction in wind-induced acceleration compared to the case with all connections of high stiffness.

4.3.3 Ultimate limit state considerations

The results of the parametric study (520 analyses) are used to perform design checks for beams, columns, and CLT walls. For the calculation of forces used in the design, the fundamental ULS combination defined in EN 1990 [20] with wind as leading variable action was used:

$$E_d = \gamma_G \cdot G_k + \gamma_Q \cdot W_k + \gamma_Q \cdot \psi_0 \cdot Q_k \quad (5)$$

Where $\gamma_G = 1.20$, $\gamma_Q = 1.50$, $\psi_0 = 0.70$.

The structural design was performed in accordance with EN 1995-1-1 [17]. Since no CLT design checks are included in EN 1995-1-1 [17], the design checks of CLT walls were performed according to [23]. The buckling length was evaluated using linearized buckling analysis. The utilization ratios for beams, columns, and CLT walls are shown in Figure 14 for a total of 520 analyses. As shown in Figure 14, all utilization ratios of beams, columns, and walls are well below unity.

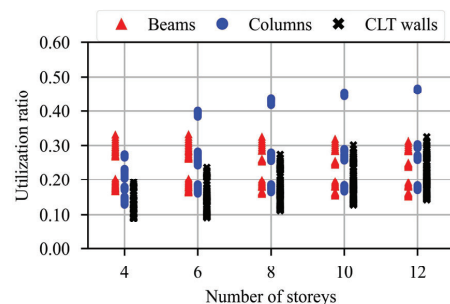


Figure 14: Utilization ratio for beams, columns, and CLT walls

Another important consideration is the beam-column/wall connection capacity. For each analysis case (out of the 520), bending moments are calculated at all connections in the frame, the maximum absolute value is then selected, the results are shown in Figure 15.

As shown in Figure 15, all moments are below 70 kN-m. An experimental work performed on moment resisting connections based on threaded rods [24] reported capacity up to 130 kN-m with glulam beams and columns of dimensions ($140 \cdot 450$ mm²). Based on the calculated bending moments (see Figure 15), and the results in [24], the connections in the dual frame-wall system seem feasible. However, the reported testes in [24] were performed on glulam beam-column connections. Moreover, the limited number of experiments performed

on such connections does not allow the estimation of characteristic capacity. Therefore, further experimental work on moment resisting connections using threaded rods and CLT is needed.

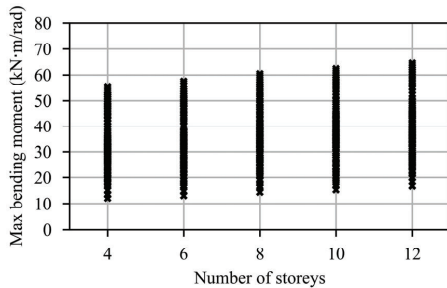


Figure 15: Maximum absolute bending moment at all beam-to-column/wall connections

4.4 3D STRUCTURE

To verify the results of the 2D FEA analysis performed in the parametric study, the dual frame-wall system is analysed in 3D. A 3D FEA model of an 8-storey building is analysed using CSI SAP2000 [12].

In X direction, the building is stabilized using the dual frame-wall system with interior CLT walls (confer Figure 1 and Figure 9). The beam-to-column/wall connection stiffness (K_{θ}) is set to $2 \cdot 12,500$ kN·m/rad (double cross-section), see Figure 9.

In Y direction, the building is stabilized using diagonal bracing (confer Figure 1 and Figure 16). The diagonals are modelled using link elements with axial stiffness only. The axial stiffness of each link element representing a diagonal is assumed to be 100 kN/mm (see Figure 16). This value takes into account the axial stiffness of both the diagonal member and the connections at each end of the member. The secondary beams (parallel to Y direction) are modelled using pinned beam elements. Similar to the FEA model of the floor, the CLT slab is modelled using layered shell elements.

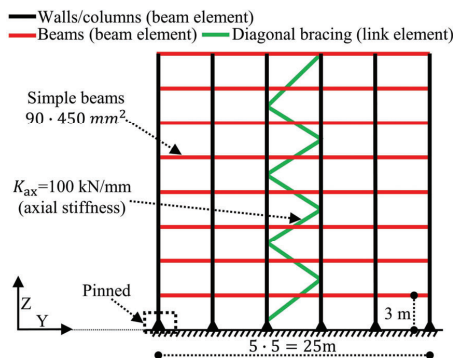


Figure 16: 2D FEA model of LLRS in Y direction

Figure 17 shows the FEA model of the 3D structure (combining the structural systems in both X and Y). Light loads are applied to the CLT slab (Table 3). Wind loads, load combinations, parameters used for wind-induced accelerations, and cross-sections are the same as the parametric study (section 4.3, Tables 6-8).

Modal analysis of the 3D FEA model showed that the first 2 mode shapes are translational (no torsional modes). Wind-induced acceleration is calculated in X and Y directions. Figure 18 shows the accelerations against the ISO10137 [13] criterion based on 2D and 3D analyses. Wind-induced acceleration in X and Y directions meet the requirement for residential buildings.

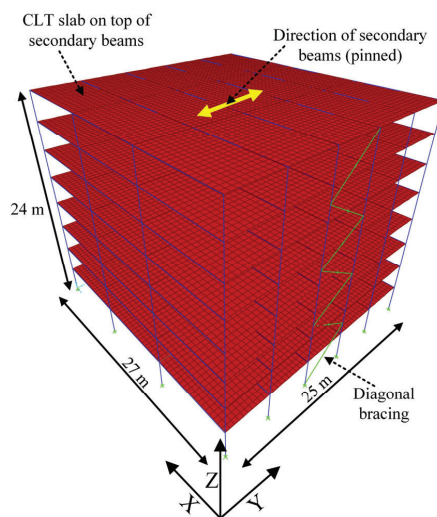


Figure 17: 3D FEA model

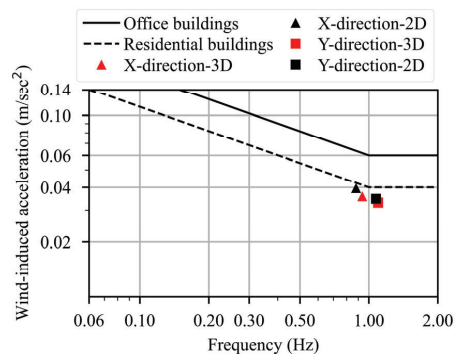


Figure 18: Wind induced accelerations in X and Y directions of the 3D and the 2D FEA models against ISO 10137 [13] criterion

The fundamental frequency, top floor displacement, inter-storey drift, and wind-induced accelerations of the 3D

model are summarized in Table 9 (both in X and Y direction). The results of the 2D counterpart model in X direction (results from section 4.3 in this paper) and Y direction are also summarized in Table 9 for comparison. The results of both 3D model and the 2D counterparts show that 2D analysis provides reasonable accuracy with the 3D model being slightly stiffer.

Table 9: Frequency, lateral displacements, and wind-induced accelerations for the 3D FEA model and the 2D counterpart

Direction	Property	2D	3D
X	Frequency (Hz)	0.88	0.94
	Top floor disp. (mm)	17.67	14.98
	IDR (mm)	2.61	2.18
	Acceleration (m/sec ²)	0.040	0.036
Y	Frequency (Hz)	1.07	1.10
	Top floor disp. (mm)	13.14	11.81
	IDR (mm)	2.39	2.29
	Acceleration (m/sec ²)	0.035	0.033

5 CONCLUSIONS

In this paper, a dual frame-wall structural system used as a lateral load resisting system in multi-storey timber buildings is studied. Parametric study using 2D linear elastic FEA was performed to evaluate the feasibility of the lateral load resisting system. The vibration performance of floors with respect to human-induced vibration is also discussed using linear elastic FEA. Although the main focus of the paper is on serviceability limit state, some ultimate limit state considerations are presented. To validate the results obtained from the 2D FEA model, a 3D FEA model was also prepared, and the results of both models were compared. The following conclusions are drawn (assuming wind speed of 26 m/sec and urban environment):

- Wind-induced acceleration is more critical than lateral displacements.
- Ultimate limit state is less critical than serviceability limit state. The utilization ratios of all structural elements are well below unity.
- Construction of multi-storey buildings up to 10 storeys with an out-of-plane spacing of 5 m and light flooring system is feasible if the stiffness of the beam-to-column connections is $\geq 2 \cdot 11,500$ kN·m/rad (11,500 for single cross-section).
- Construction of multi-storey buildings up to 12 storeys with an out-of-plane spacing of 5 m and heavy flooring system is feasible if the stiffness of the beam-to-column connections is $\geq 2 \cdot 5,500$ kN·m/rad (5,500 for single cross-section).
- The use of stiff connections can be optimized in such a way that stiffer connections are used in the lower storeys.
- Stiff beam-to-column connections improve the performance of the lateral load resisting system. Moreover, they also improve the performance of the floors with respect to human-induced vibration.

- The use of simplified 2D FEA modelling approach seems to give reasonable accuracy compared to 3D FEA modelling.

REFERENCES

- [1] J. L. Skullestad, R. A. Bohne, and J. Lohne, "High-rise timber buildings as a climate change mitigation measure—A comparative LCA of structural system alternatives," *Energy Procedia*, vol. 96, pp. 112-123, 2016.
- [2] O. A. Hegeir, T. Kvande, H. Stamatopoulos, and R. A. Bohne, "Comparative Life Cycle Analysis of Timber, Steel and Reinforced Concrete Portal Frames: A Theoretical Study on a Norwegian Industrial Building," *Buildings*, vol. 12, no. 5, p. 573, 2022. [Online]. Available: <https://www.mdpi.com/2075-5309/12/5/573>.
- [3] A. Vilguts, H. Stamatopoulos, and K. A. Malo, "Parametric analyses and feasibility study of moment-resisting timber frames under service load," *Engineering Structures*, vol. 228, 2021, doi: 10.1016/j.engstruct.2020.111583.
- [4] K. A. Malo, R. B. Abrahamsen, and M. A. Bjertnæs, "Some structural design issues of the 14-storey timber framed building "Tree" in Norway," *European Journal of Wood and Wood Products*, vol. 74, no. 3, pp. 407-424, 2016, doi: 10.1007/s00107-016-1022-5.
- [5] R. Abrahamsen, "Mjøstårnet—Construction of an 81 m tall timber building," in *Internationales Holzbau-Forum IHF*, Garmisch-Partenkirchen, Germany, 2017, vol. 2017.
- [6] M. Wells, "Stadthaus, London: raising the bar for timber buildings," in *Proceedings of the Institution of Civil Engineers-Civil Engineering*, 2011, vol. 164, no. 3: Thomas Telford Ltd, pp. 122-128.
- [7] A. Vilguts, S. Ø. Nesheim, H. Stamatopoulos, and K. A. Malo, "A study on beam-to-column moment-resisting timber connections under service load, comparing full-scale connection testing and mock-up frame assembly," *European Journal of Wood and Wood Products*, vol. 80, no. 4, pp. 753-770, 2022, doi: 10.1007/s00107-021-01783-2.
- [8] L. J. Hu and Y. Chui, "Development of a design method to control vibrations induced by normal walking action in wood-based floors," in *World Conference on Timber Engineering (WCTE2004)*, Lahti, Finland, 2004, vol. 2, pp. 217-222.
- [9] P. Hamm, A. Richter, and S. Winter, "Floor vibrations—new results," in *Proceedings of 11th World Conference on Timber Engineering (WCTE2010)*, Riva del Garda, 2010.
- [10] CEN, "NS-EN 14080: Timber structures—Glued laminated timber and glued solid timber—Requirements," *European Committee for Standardization: Brussels, Belgium*, 2013.

- [11] CEN, "NS-EN 338: Structural timber–Strength classes," *European Committee for Standardization: Brussels, Belgium*, 2016.
- [12] *CSI SAP2000 Structural analysis and design*. Computers and Structures. [Online]. Available: <https://www.csiamerica.com/products/sap2000>
- [13] ISO, "ISO10137: Bases for design of Structures - Serviceability of Buildings and Walkways against Vibrations," *International Organization for standardization*, 2007.
- [14] A. Homb and S. T. Kolstad, "Evaluation of floor vibration properties using measurements and calculations," *Engineering Structures*, vol. 175, pp. 168-176, 2018.
- [15] H. Stamatopoulos, K. A. Malo, and A. Vilguts, "Moment-resisting beam-to-column timber connections with inclined threaded rods: Structural concept and analysis by use of the component method," *Construction and Building Materials*, vol. 322, 2022, doi: 10.1016/j.conbuildmat.2022.126481.
- [16] CEN, "NS-EN 1991-1-1: 2002+ NA: 2019: Actions on Structures–Part 1-1: General Actions–Densities, self-weight, imposed loads for buildings," *European Committee for Standardization: Brussels, Belgium*, 2019.
- [17] CEN, "NS-EN 1995-1-1:2004+A1:2008+NA:2010: Design of timber structures–Part 1-1: General–Common rules and rules for buildings," *European Committee for Standardization: Brussels, Belgium*, 2010.
- [18] H. J. Blass and P. Fellmoser, "Design of solid wood panels with cross layers," in *8th world conference on timber engineering*, 2004.
- [19] M. Follesa, I. Christovasilis, D. Vassallo, M. Fragiaco, and A. Ceccotti, "Seismic design of multi-storey CLT buildings according to Eurocode 8. Ingegneria Sismica," *International Journal of Earthquake Engineering, Special Issue on Timber Structures*, vol. 30, no. 4, pp. 27-53, 2013.
- [20] CEN, "NS-EN 1990:2002+A1:2005+NA:2016: Basis of structural design," *European Committee for Standardization: Brussels, Belgium*, 2016.
- [21] CEN, "NS-EN 1991-1-4:2005+NA:2009: Actions on Structures–Part 1-4: General Actions–Wind Actions " *European Committee for Standardization: Brussels, Belgium*, 2009.
- [22] A. Feldmann *et al.*, "Dynamic properties of tall timber structures under wind-induced vibration," in *World Conference on Timber Engineering (WCTE 2016)*, 2016.
- [23] A. Gustafsson, *The CLT Handbook: CLT structures-facts and planning*, First ed. Swedish Wood, 2019.
- [24] H. Stamatopoulos and K. Malo, "Wood frame solutions for free space design in urban buildings (WOODSOL)," in *Proceedings of the 7th Forum Wood Building Nordic, Växjö, Sweden*, 2018, pp. 27-28.

Paper IV

Parametric analysis of moment-resisting timber frames combined with cross laminated timber walls and prediction models using nonlinear regression and artificial neural networks

Osama Abdelfattah Hegeir, Haris Stamatopoulos, Kjell Arne Malo

Submitted to an international peer-reviewed journal

This paper is awaiting publication and is not included in NTNU Open

Paper V

Feasibility of outrigger structural system for tall timber buildings: A numerical study

Osama Abdelfattah Hegeir, Haris Stamatopoulos

Published at ***International Wood Products Journal***

Feasibility of outrigger structural system for tall timber buildings: A numerical study

Osama Abdelfattah Hegeir¹  and Haris Stamatopoulos¹

International Wood Products Journal
1–19
© Institute of Materials, Minerals and
Mining 2023
Article reuse guidelines:
sagepub.com/journals-permissions
DOI: 10.1177/20426445231216013
journals.sagepub.com/home/iwp



Abstract

Tall timber buildings are prone to serviceability problems (e.g. lateral displacements and wind-induced accelerations). This article investigates the feasibility of timber outrigger system to build up to 20 storeys using linear elastic finite element analysis and relevant European and international standards such as EN 1990, EN 1991-1-1, EN 1991-1-4, EN 1995-1-1 and ISO 10137. The location of up to two outriggers was optimised based on different serviceability criteria. Various outrigger layouts were investigated, and their stiffness demands were discussed. The efficiency of outrigger structures in reducing lateral displacements and wind-induced accelerations is highlighted. A feasibility study considering serviceability requirements was performed using different basic wind velocities, number of storeys and gravity loads. Although the focus of the article is on serviceability requirements, some ultimate limit state considerations (forces and stresses) were briefly discussed. The results demonstrate the feasibility of building up to 16 storeys under medium to high wind velocities.

Keywords

outriggers, tall timber buildings, wind-induced acceleration, serviceability of timber buildings, wind load

Received: 26 June 2023; accepted: 2 October 2023

Introduction

The increase in world population results in higher urbanisation. On the other hand, the construction industry is a major contributor to greenhouse gas emissions worldwide.¹ The increased urbanisation can further increase greenhouse gas emissions which have unfavourable impacts on the environment. Therefore, the use of sustainable building materials is of great importance. Timber is a renewable material that can serve as an alternative to concrete and steel to reduce the environmental impact of construction. Eliassen et al.² performed a comparative study using life cycle analysis (LCA) and concluded that using timber can reduce greenhouse gas emissions by more than 13% compared to reinforced concrete and steel. Another LCA study by Skullestad et al.³ on buildings up to 21 storeys showed that timber buildings have 34% to 84% lower climate change impact than reinforced concrete buildings with similar load-carrying capacity.

Timber buildings, due to their lightweight and moderate stiffness, are often susceptible to excessive accelerations and lateral deformations under wind loads.^{4–13} Excessive accelerations can cause occupants discomfort, and excessive lateral deformations can cause damage and may influence the functionality of the building. The acceleration due to wind can be reduced by increasing the building's mass,¹⁰ damping,¹⁴ lateral stiffness,¹³ or a combination.

Several structural systems can be used for multi-storey timber buildings. Cross-laminated timber (CLT) is commonly used for multi-storey timber buildings, for example the 9-storey residential building Stadthaus in London.¹⁵ However, such structures are usually cellular and may not be architecturally spacious. Braced structures are also prevalent in tall timber buildings. Global diagonal bracing was successfully employed in Treet (14 stories)¹⁶ and Mjøstarnet (18 stories)⁵ in Norway. The use of such structures requires large diagonal elements running along the full height of the building, affecting aesthetics and architecture flexibility. Moment resisting timber frames (MRTFs)¹⁷ provide good architectural flexibility. MRTFs achieve lateral stiffness by means of semi-rigid beam-to-column connections. Vilguts et al.⁴ performed a parametric analysis on MRTFs and suggested that such systems can be used up to 8 storeys with 2.4 m spacing between adjacent frames.

¹Department of Structural Engineering, Norwegian University of Science and Technology (NTNU), Trondheim, Norway

Corresponding author:

Osama Abdelfattah Hegeir, Department of Structural Engineering, Norwegian University of Science and Technology (NTNU), Rich. Barcelonese 1A, 7491 Trondheim, Norway.
Email: osama.a.s.a.hegeir@ntnu.no

Outrigger (OR) structural system has been used in many concrete, steel, and composite tall buildings around the world.^{18,19} High-rise buildings usually incorporate a central elevator core(s) together with walls and columns. Outriggers are stiff horizontal structural elements that connect the building's core/wall to the exterior columns.^{20,21} The use of outriggers couples the core, walls and columns, resulting in a higher lateral stiffness and thus increases the possibility of building taller buildings.^{20,21} The structural behaviour of outrigger structures is illustrated in Figure 1. When the central core/wall deflects laterally under lateral loads, a tension-compression couple is generated in the exterior columns, resulting in a restoring moment at the outrigger level. The restoring moment at the outrigger level reduces the lateral displacement and the bending moment at the central core/wall.

The location of outriggers is important and greatly influences the structural behaviour.²² Typically, the location is coordinated with the architect, considering that the presence of an outrigger imposes architectural constraints on the respective floor. Several studies have investigated the optimum location of outriggers.^{22–28} In these studies,^{22–28} the optimum location was selected mainly to achieve smallest lateral displacements. The optimum location of the outrigger depends on the structural characteristics of the building,²² the type of loading,²⁶ and the optimisation criterion.²⁹ However, as a first estimate, the location of outriggers can be reasonably assumed as suggested by Taranath,^{20,21} see Figure 2.

Employing outriggers can enhance the structural robustness in the event of a sudden loss of a local structural element or a connection.^{20,29} This is achieved by providing alternative load paths that can prevent progressive collapse and redistribute the forces upon any local failure.²⁰ In timber structures, and due to the brittle nature of wood under tension and shear, addressing this issue is of great importance.^{30,31}

Several studies have been conducted on the use of outriggers in concrete, steel and composite structures, but little research has been done on timber structures. A study

by Bollards³² showed that timber structures up to 20 storeys are possible using outriggers together with a large central CLT core (9 m · 9 m). Tesfamariam et al.³³ investigated the use of outriggers in timber structures to mitigate earthquake-induced vibrations using shape memory alloy dampers. In previous studies, the lateral displacements (top floor displacement and inter-storey drift) were chosen as the optimisation criteria. However, in timber structures, wind-induced accelerations are very decisive in the design and dimensioning of the structural elements.^{4–11,13} The feasibility of using outriggers in timber buildings and their advantages are not extensively investigated, especially with respect to wind-induced acceleration requirements.

The aim of this article is to investigate the feasibility, advantages and limitations of using outriggers in multi-storey timber buildings. To achieve this, parametric analysis using finite element method (FEM) was performed in conjunction with the respective Eurocodes and standards. The optimum location of one and two outriggers was investigated considering lateral displacements and wind-induced accelerations as optimisation criteria. Several outrigger layouts were investigated, and their efficiency is compared. The effects of several parameters such as outrigger stiffness, number of storeys and wind velocity were also investigated.

Timber structures, due to their lightweight and moderate stiffness, are typically governed by the serviceability limit state (SLS).^{4–11} Therefore, this article focuses on the SLS. However, since the introduction of an outrigger may cause force concentration in structural members and connections at the outrigger level, ultimate limit state (ULS) should be considered as well. In this article, some ULS considerations are briefly discussed to validate the feasibility of such structural system in timber buildings.

Materials and methods

The structural system

Figure 3 shows a 3D view of an example multi-storey timber building. The lateral load resisting system (LLRS)

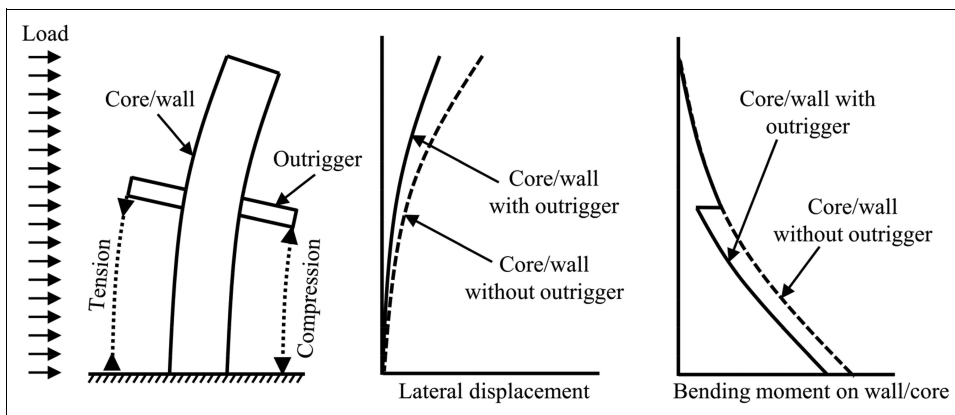


Figure 1. Structural behaviour of outrigger structural system.²²

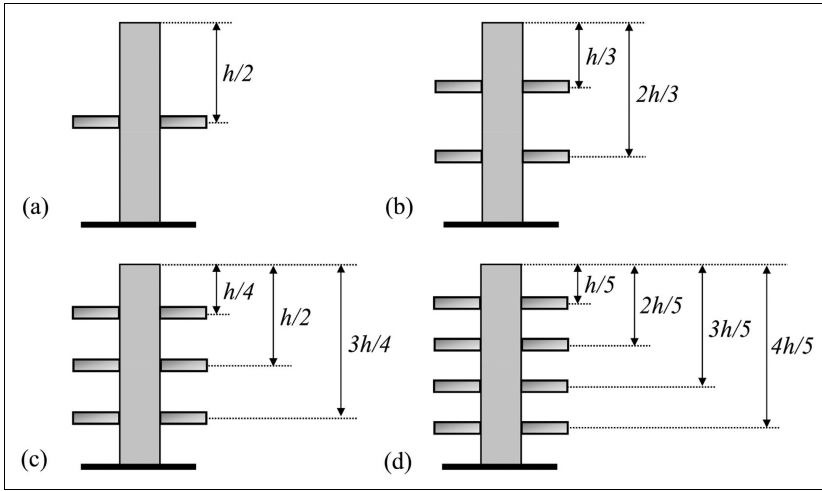


Figure 2. Optimum location of outrigger(s) according to Ref.²⁰

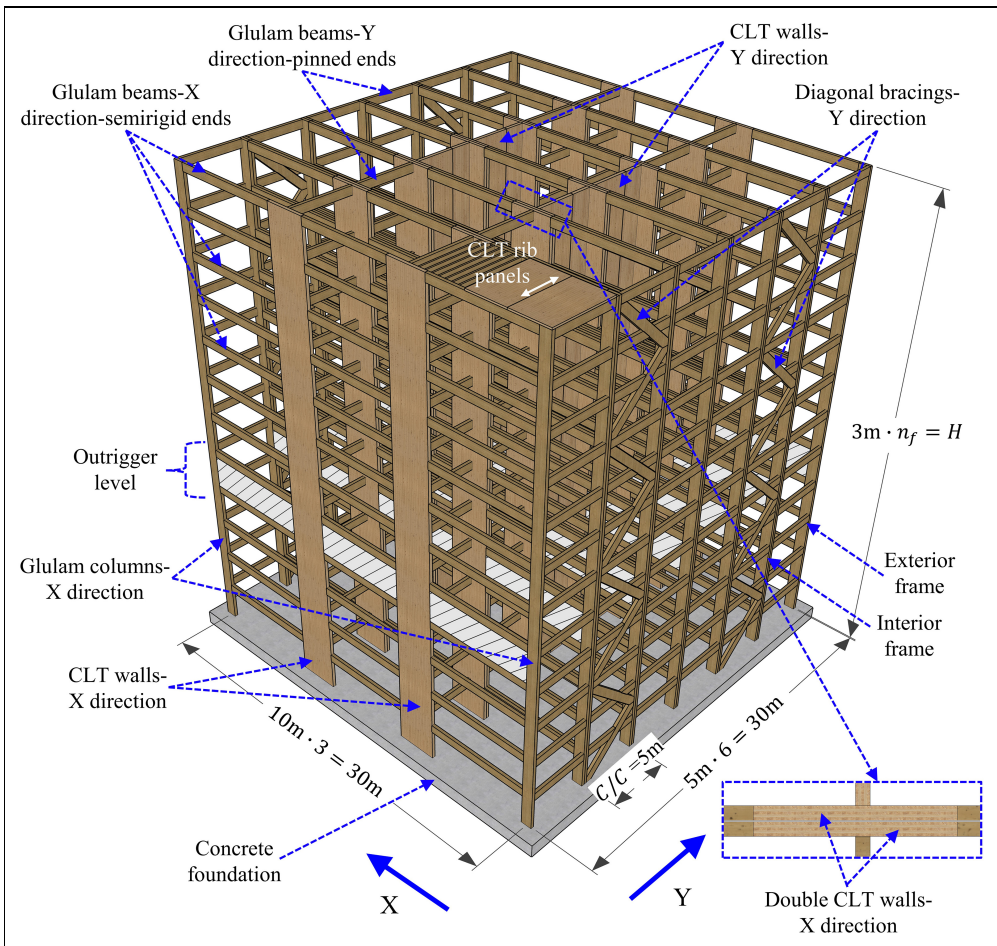


Figure 3. 3D view of an example multi-storey timber building.

in X direction consists of two continuous interior CLT walls, two continuous exterior glued laminated timber (glulam) columns, glulam beams with semi-rigid moment connections and an outrigger. The LLRS in Y direction consists of global diagonal bracings and CLT walls. This article focuses on the structural system in X direction (interior frame with $C/C = 5$ m, see Figure 3). The connections details of the LLRS in X direction are explained in more details in section 'Finite element method and analytical model'.

In this article, six variations of outrigger layouts were analysed (see Figure 4), and their performance is compared. The variations shown in Figure 4(a)–(e) combine MRTFs with outriggers. The first four variations (Figure 4(a)–(d))

employ a glulam truss as outrigger. One variation (Figure 4(e)) employs a CLT panel as outrigger. In the last variation, each of the interior CLT walls was replaced with diagonal truss bracing (consisting of two glulam columns and glulam global diagonal bracing); see Figure 4(f). The span length between each pair of glulam columns replacing an interior CLT wall is equal to the CLT wall width. In this variation (Figure 4(f)), all connections were assumed pinned. The purpose is to compare the variation shown in Figure 4(f) with the variations shown in Figure 4(a)–(e), which relies on moment connections. For all variations shown in Figure 4, the number of storeys was varied from 12 to 20 storeys. Hereafter, the different variations are referred to as variations (a)–(f).

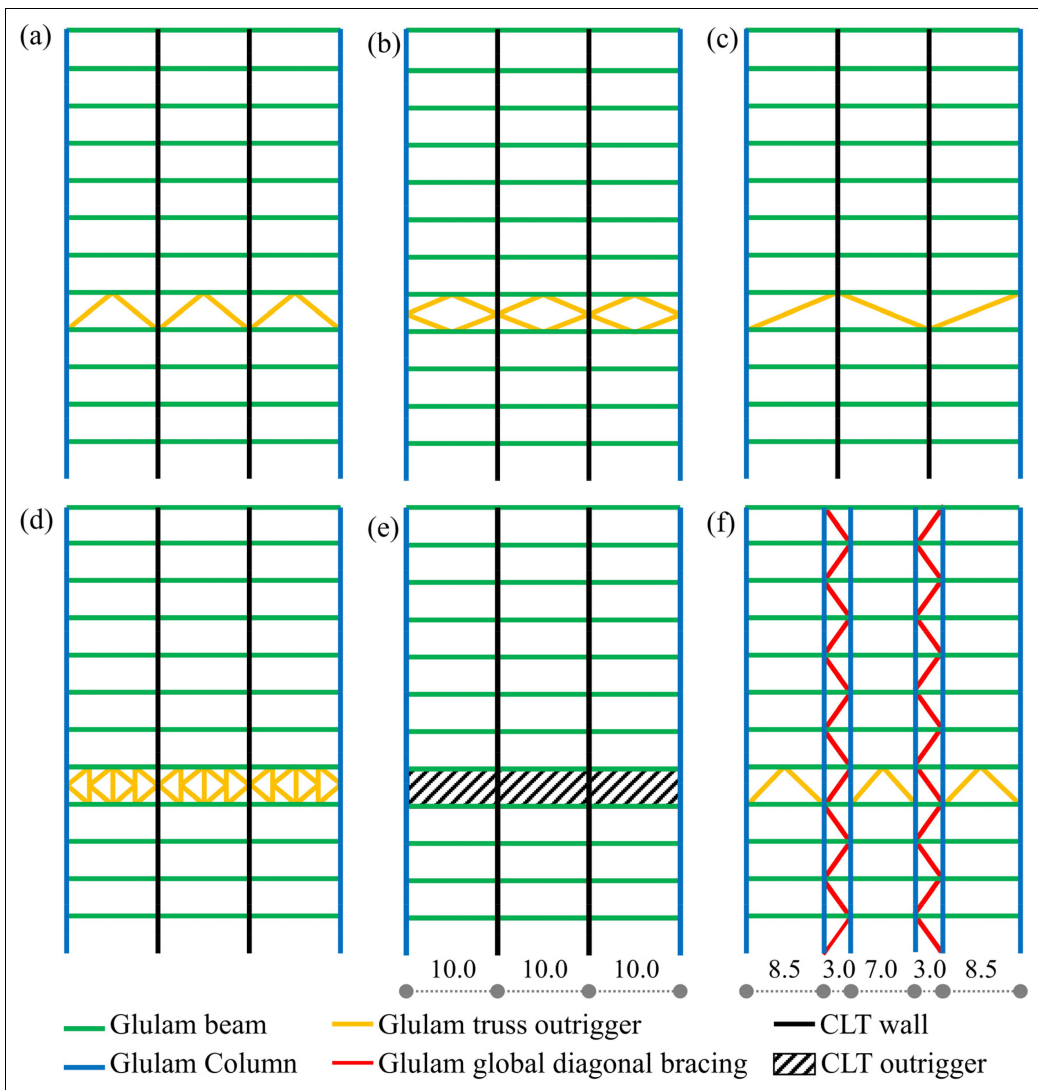


Figure 4. Variations of outrigger layouts (a) variation a, (b) variation b, (c) variation c, (d) variation d, (e) variation e and (f) variation f.

Material properties and cross-sections

Wood is an anisotropic material with different properties in different directions.³⁴ The material can be modelled as orthotropic with three orthogonal symmetry planes.³⁴ Further practical simplification is to model wood with equal properties across the grain. In this study, the glulam was assumed of strength class GL30c as defined by EN 14080.³⁵

In this study and to simplify the modelling using FEM, equivalent material properties of CLT were calculated using the method proposed by.³⁶ A uniform cross-section with a thickness equal to the actual thickness of the CLT and equivalent material properties was used, that is the cross-lamination is considered indirectly. It was assumed that (2/3) of the layers are along the longitudinal (main) direction and the remaining (1/3) are along the orthogonal direction, confer Figure 5(c). This simplified modelling approach is shown to properly capture the in-plane behaviour of CLT.³⁷ The lamellae constituting the CLT panels were assumed of strength class C24 as defined by EN 338.³⁸

The elastic constants of the glulam, the C24 lamellae, and the equivalent CLT are summarised in Table 1. The corresponding material axes are shown in Figure 5.

Walls, columns, beams, outriggers and global diagonal bracing were assumed of double cross-section, see Figure 3. Dimensions of walls, columns, beams, were reasonably assumed and summarised in Table 2. Dimensions of outriggers were varied, and the global diagonal bracing were modelled in terms of their axial stiffness as will be explained in section 'Finite element method and analytical model'.

Finite element method and analytical model

CSI SAP2000³⁹ was used to perform 2D linear elastic FEM. The open application programming interface was used to

drive the software externally. Figure 6 shows the analytical model of variation (b), with example connections details based on Refs.^{6,16,40,41} Glulam columns and beams were modelled using linear elements (considering both bending and shear deformations) with material properties and cross-sections in Tables 1 and 2. The CLT walls were modelled using linear elements with equivalent properties and cross-sections in Tables 1 and 2. The linear elements representing the CLT walls were verified against the layered shell elements available in CSI SAP2000³⁹ under in-plane loading. The verification was done on both stresses and deformations and the difference was less than 5%. Hence, linear elements were deemed to have sufficient accuracy for the purpose of this study.

The CLT panels used as an outrigger in variation (e) were modelled using shell elements with the equivalent properties in Table 1. The shell elements are connected to the main structural system using link elements as shown in Figure 6(d). The link elements represent the connections (e.g. self-taping screws) between the CLT outrigger and the main structural system. The link elements have only axial and shear stiffness (no rotational stiffness).

The beam-to-wall/column connections were assumed semi-rigid with finite rotational stiffness. The stiffness was reasonably assumed based on the experimental work done by Vilguts et al.⁴² and the analytical method proposed by Stamatopoulos et al.⁴³ The stiffness values of the connections are summarised in Table 3.

CLT walls and glulam columns have finite cross-sectional dimensions. Modelling them as linear elements connected at nodes results in larger beam spans, leading to a softer structural system. To account for the fact that the clear spans of beams are shorter than the centreline-to-centreline spans, the end length offset option available in CSI SAP2000³⁹ was used. The concept of the end length offset is illustrated in Figure 6(b). At the beam

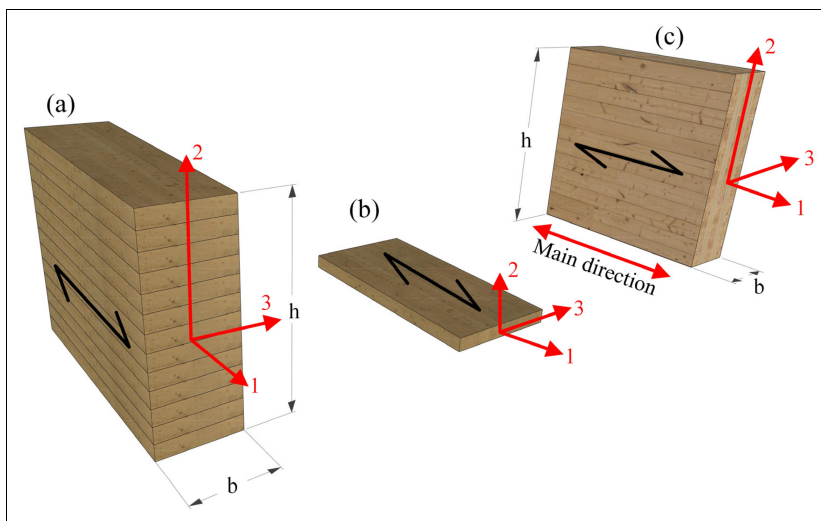


Figure 5. Material axes and cross-sections (a) glulam, (b) C24 lamellae and (c) CLT element.

Table 1. Elastic constants of glulam, C24 lamellae and equivalent CLT.

Property	Glulam	CLT		Unit
	GL30c	Lamellae (C24)	Equivalent	
E_1	13000	11000	7467	N/mm ²
E_2	300	400	3933	N/mm ²
E_3	300	400	400	N/mm ²
G_{12}	650	690	517	N/mm ²
G_{13}	650	690	98	N/mm ²
G_{23}	65	50	54	N/mm ²

Table 2. Cross-sections of walls, columns, beams, outriggers and global bracing.

Structural element	Variation	Cross-section	Unit
CLT walls	a/b/c/d/e	$b \cdot h = 215 \cdot 3000^a$	mm ²
Exterior glulam columns	all	$b \cdot h = 215 \cdot 810^a$	mm ²
Glulam beams	all	$b \cdot h = 215 \cdot 585^a$	mm ²
Truss outrigger	a/b/c/d/f	EA = variable ^b	kN
CLT outrigger	e	Thickness = variable	mm
Interior glulam columns	f	$b \cdot h = 215 \cdot 810^a$	mm ²
Global diagonal bracing	f	EA/L = 200 ^b	kN/mm

^aDouble cross-sections.

^bFurther explanation is provided in section 'Finite element method and analytical model'.

ends, a length equal to half the wall/column width is assumed rigid for bending and shear deformations.

The truss outrigger and the global diagonal bracing elements (confer Figure 4) were modelled using linear elements with pinned ends. The presence of connections at the ends implies the need to use two link elements representing the connections, see Figure 6(c). This situation resembles three springs in series, which can be replaced by one spring with an effective stiffness:

$$\frac{1}{K_{\text{effective}}} = \frac{1}{K_{\text{connection},1}} + \frac{1}{K_{\text{diagonal}}} + \frac{1}{K_{\text{connection},2}} \quad (1)$$

where $K_{\text{effective}}$ is the effective axial stiffness of the equivalent spring, $K_{\text{connection},1}$ and $K_{\text{connection},2}$ are the axial stiffness of the connections at both ends of the element and K_{diagonal} is the axial stiffness of the diagonal, see Figure 6(c).

The diagonal can then be modelled using only one linear element with axial stiffness $K_{\text{effective}}$. The effective axial stiffness of the elements used in the truss outrigger was varied. The effective axial stiffness of the global diagonal bracing (confer Figure 4(f), red lines) was set to 200 kN/mm. In CSI SAP2000,³⁹ this was achieved by using a linear element with pinned ends and an effective

area $A_{\text{effective}}$ to consider the presence of connections:

$$K_{\text{effective}} = \frac{E_1 \cdot A_{\text{effective}}}{L} \quad (2)$$

where L is the length of the element and E_1 is young modulus from Table 1.

Loads and limit states

In this study, three different types of loads were considered, namely: dead load G_k , live load Q_k and wind load W_k . Two load scenarios were assumed, namely: light frames and heavy frames. Both scenarios are summarised in Table 4. Wind load was calculated according to EN 1991-1-4⁴⁴ assuming urban environment (IV). Gravity loads (dead and live loads) were applied as uniform line load to the beams, and wind loads were applied as uniform line load to the exterior columns.

For the calculation of lateral displacements due to wind, the characteristic load combination as defined in EN 1990⁴⁶ with wind as a leading variable was used:

$$E_d = G_k + W_k + \psi_0 \cdot Q_k \quad (3)$$

The combinational factor ψ_0 was set to 0.70 according to the Norwegian National Annex of EN 1990.⁴⁶

EN 1995-1-1⁴⁷ recommends a deflection limit of span/300 – span/500 for simple beams under the characteristic load combination defined in EN 1990.⁴⁶ Based on this, the following limits for the top floor displacement (Δ) and inter-story drift (δ) were considered:

$$\delta \leq \frac{h}{300} \quad \Delta \leq \frac{H}{300} \quad (4)$$

Where h is the storey height and H is the total height of the building.

EN 1991-1-4⁴⁴ provides two equivalent procedures to estimate the wind-induced acceleration. Both procedures are based on gust factor approach but use different simplifications.⁴⁸ In this article, the wind-induced acceleration was calculated using procedure 1 available in Annex B of EN 1991-1-4.⁴⁴

For the calculation of acceleration according to EN 1991-1-4,⁴⁴ the mode shape and the fundamental frequency are required. To obtain the mode shape and the fundamental frequency, modal analysis was performed using CSI SAP2000.³⁹ In modal analysis, the mass corresponding to quasi-permanent load combination defined in EN 1990⁴⁶ was used:

$$E_d = G_k + 0.3 \cdot Q_k \quad (5)$$

Damping ratio is an important parameter for acceleration calculation. There are few studies available with respect to damping ratios of timber buildings. In this article, 2% damping ratio (ξ) was assumed based on available results, see Refs.^{16,49} In this study, 50% probability of exceedance in half a year was assumed, which corresponds to $c_{\text{prob}} = 0.73$. The basic wind velocity was varied from 22 m/sec to 30 m/sec. Relevant parameters used in the acceleration calculation are summarised in Table 5.

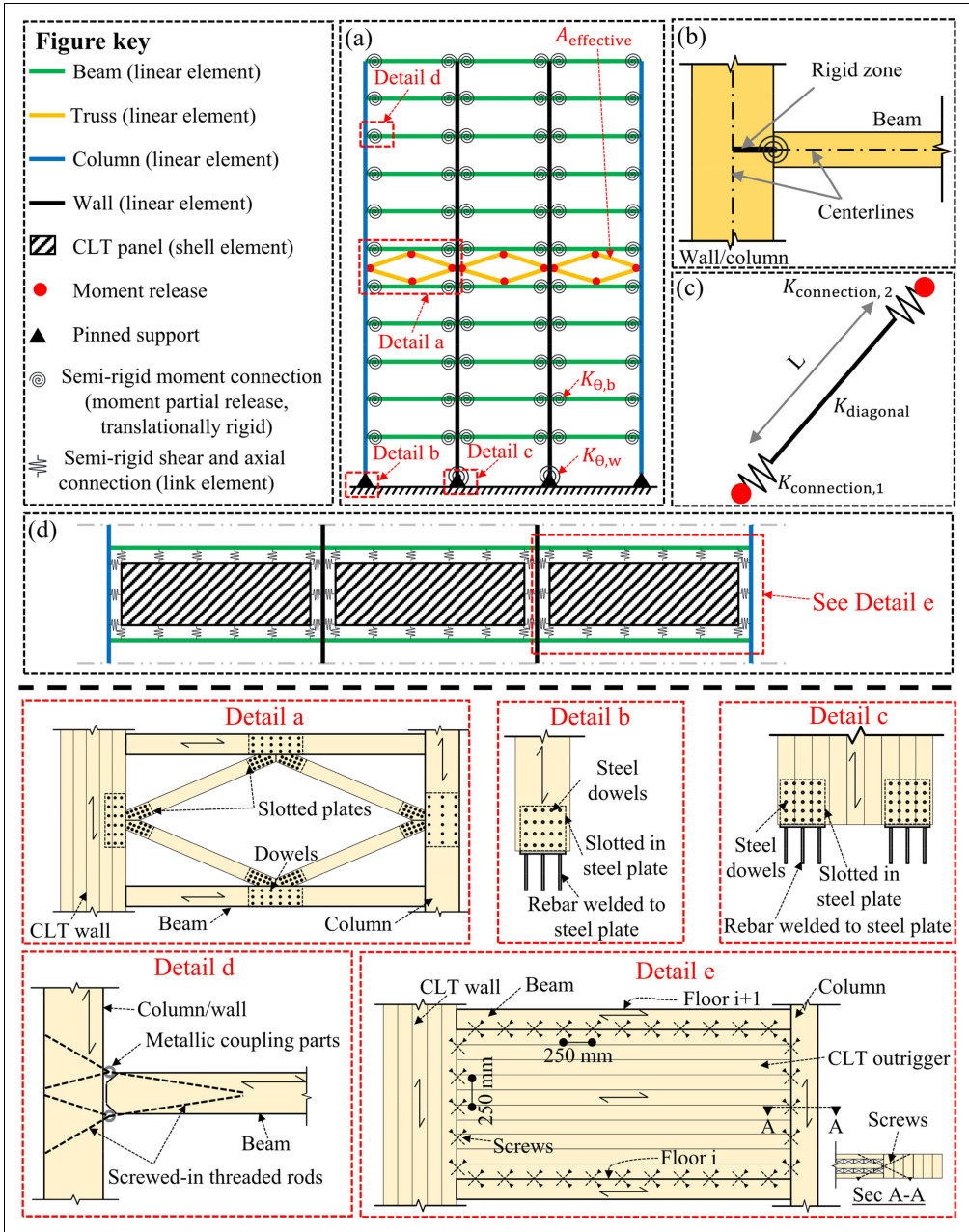


Figure 6. Analytical model with example connections details, (a) 2D frame with truss outrigger, (b) rigid zone in beam-to-wall/column connections, (c) diagonal/truss element and (d) CLT outrigger.

Human perception of acceleration is subjective, and therefore there exist several comfort criteria that can be used to assess the performance of a building under wind load.⁵⁰ In this article, the criterion provided by ISO10137⁵¹ was used. ISO10137⁵¹ covers the range from

a fundamental frequency of 0.063 to 5 Hz for a maximum wind velocity with a return period of one year. The criterion is depicted in Figure 7.

For the calculation of forces and stresses used for discussing the ULS, the fundamental ULS combination

Table 3. Rotational stiffness of the connections.

Variation	Connection	Rotational stiffness (kN.m/rad)
a–e	CLT wall-to-foundation ($K_{\theta,w}$)	300, 000
a–e	Glulam column-to-foundation	0.0 (pinned)
a–e	Beam-to-column/wall ($K_{\theta,b}$)	20, 000
F	All connections	0.0 (pinned)

Table 4. Gravity loads.

Load scenario	Dead load G_k (kN/m ²)	Live load Q_k (kN/m ²)
Light frames	1.0 ^a	2.0 (residential areas ^b)
Heavy frames	2.0 ^a	3.0 (office areas ^b)

^aIncluding the weight of floors and finishings, excluding the own weight of beams, columns, walls and diagonals.

^bAccording to EN 1991-1-1.⁴⁵

defined in EN 1990⁴⁶ with either wind or live load as leading variable action:

$$E_d = \gamma_G \cdot G_k + \gamma_Q \cdot W_k + \gamma_Q \cdot \psi_{0,Q} \cdot Q_k \quad (6)$$

Where $\gamma_G = 1.20$, $\gamma_Q = 1.50$, $\psi_{0,Q} = 0.70$ according to the Norwegian National Annex of EN 1990.⁴⁶

$$E_d = \gamma_G \cdot G_k + \gamma_Q \cdot \psi_{0,w} \cdot W_k + \gamma_Q \cdot Q_k \quad (7)$$

Where $\gamma_G = 1.20$, $\gamma_Q = 1.50$, $\psi_{0,w} = 0.60$ according to the Norwegian National Annex of EN 1990.⁴⁶

The forces and stresses were calculated using the envelop of equations (6) and (7).

Results and discussion

In this section, five subsections are outlined to address the optimum location of outriggers, compare the efficiency of the different variations shown in Figure 4, estimate the stiffness requirements of outriggers, show the feasibility of the system with respect to SLS, and highlight some ULS considerations. For this purpose, five parametric studies were performed. Table 6 provides an overview of the performed parametric studies.

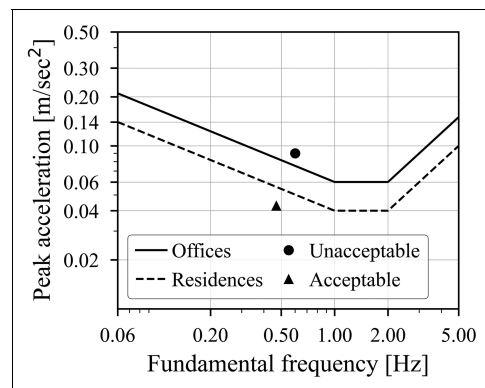
Optimum location of outrigger(s)

To identify the optimum location(s) of OR, three optimisation criteria were considered, namely: top floor displacement, inter-story drift (IDR) and wind-induced acceleration in the top storey. A basic wind velocity of 26 m/s with light gravity loads (see Table 4) was assumed. Three number of storeys were considered, namely: 12, 16 and 20. Exhaustive search algorithm was used to find the optimum location.

The optimum location for one and two outriggers is shown in Figure 8(a) for variations (a)–(e) and in Figure 8(b) for variation (f). The optimal location was

Table 5. The parameters used in the calculation of wind-induced acceleration.

Parameter	Value
Directional factor c_{dir}	1.00
Seasonal factor c_{season}	1.00
Probability factor c_{prob}	0.73
Orography factor $c_{0(z)}$	1.00
Turbulence factor k_1	1.00
Terrain category	IV
Reference height Z_e	200
Reference length L_t	300
Structural damping ξ	2%
Out-of-plane width of the building b	30 m
Basic wind velocity $v_{b,0}$	22/26/30 m/sec

**Figure 7.** Evaluation curves for wind-induced accelerations according to ISO 10137.⁵¹

identical for variations (a)–(e). The location is expressed as a fraction of the total height H . It is worth mentioning that the optimum location for the cases of 12, 16 and 20 storeys differs slightly, approximately 5% of H . Therefore, an average value for the three cases was considered.

Comparing Figure 8(a) and (b), the location of OR(s) is lower (closer to the base) for variations (a)–(e) than variation (f). Assuming no OR is used, the mode shapes for variations (a)–(e) (identical for no OR case) and for variation (f) are plotted in Figure 9. Comparing the mode shapes for variations (a)–(e) and for variation (f), it is obvious that variation (f) exhibits more flexural dominant mode shape than variations (a)–(e). Hence the ORs are closer to the top for variation (f). It is also noticeable that the optimum location for wind-induced acceleration is the highest, followed by top floor displacements and inter-storey drift.

It was observed that when the outriggers are placed at the optimum location for IDR, a reduction of over 94% in top floor displacement is attained. Therefore, it is reasonable to assumed that the optimum location for lateral displacements (considering both IDR and top displacement simultaneously) is the same as for IDR.

Table 6. Overview of the performed parametric studies.

Subsection	Overview
i-Optimum location of OR	<ul style="list-style-type: none"> • Basic wind velocity = 26 m/s and light gravity load (Table 4). • Truss outrigger: $E_1 \cdot A_{\text{effective}} = 13 \times 10^5$ kN. • CLT outrigger: thickness = 120 mm/stiffness = 50 kN/mm/m. • Materials/sections/ stiffness (Tables 1–3). • All possible locations of OR are evaluated (exhaustive search) to find the optimum location considering inter-storey drift/top floor displacement/wind-induced acceleration as optimisation criterion. • Number of storeys: 12/16/20. • Total number of analyses is 2544.
ii-Compare OR variations	<ul style="list-style-type: none"> • The OR is placed in the optimum location obtained from i. • Other relevant parameters are kept the same as i. • The performance of all variations is compared (with respect to lateral displacements and wind-induced accelerations).
iii-OR stiffness requirements	<ul style="list-style-type: none"> • The OR is placed in the optimum location obtained from i. • Stiffness of OR ($E_1 \cdot A_{\text{effective}}$ for truss OR/thickness and connection stiffness for CLT OR) is varied. The influence of OR stiffness on the performance (with respect to displacements and acceleration) is evaluated. • Other relevant parameters are kept the same as i. • Total number of analyses is 1080.
iv-Feasibility study	<ul style="list-style-type: none"> • The OR is placed in the optimum location obtained from i. • Basic wind velocity: 22/26/30 m/s. • Light and heavy gravity load (Table 4). • Other relevant parameters are kept the same as i. • The feasibility of the system is evaluated in terms of lateral displacements and wind induced acceleration. • Total number of analyses is 216.
v-ULS considerations	<ul style="list-style-type: none"> • The OR is placed in the optimum location with respect to wind-induced acceleration (proved to be governing from iv). • Other relevant parameters are kept the same as i. • Forces and stresses in a reference frame are discussed. • Forces in OR connections are calculated and discussed.

Comparison of outrigger variations

To compare the efficiency of the variations shown in Figure 4, the ratios of top floor displacement (Δ), inter-storey drift (δ) and wind-induced acceleration (a) with the use of OR to the case without OR were calculated. The effective area $A_{\text{effective}}$ of the truss elements (confer Figure 6) was set to 0.10 m^2 ($E_1 \cdot A_{\text{effective}} = 13 \times 10^5$ kN). For variation (e), the thickness of the CLT panel used in the outrigger is set to 120 mm, and the connections' shear and axial stiffness is set to 50 kN/mm/m (confer Figure 6(d)). A basic wind velocity of 26 m/s with light gravity loads (see Table 4) was assumed. Three number of storeys were considered, namely: 12, 16 and 20. Both the case of 1 and 2 ORs were considered, and the ORs were placed at the optimum locations shown in Figure 8 for top floor displacement, inter-storey drift and wind-induced acceleration, respectively. Figure 10 shows the ratios of (Δ), (δ) and (a) with the use of OR to the case without OR.

As shown in Figure 10, variation (f) shows the highest efficiency for the case of 16 and 20 storeys. This is expected as the outrigger system is generally less effective when the mode shape is more shear dominant.²⁹ The most effective variation among (a)–(e) variations is variation (d) followed by variation (a). Figure 10 also shows that ORs are less

effective in reducing wind-induced acceleration compared to lateral displacements.

The presence of ORs stiffens the structure and leads to an increased fundamental frequency. The ratio of the frequency with ORs (f_{OR}) to the frequency without OR (f_0) is shown in Figure 11. Since frequency is essential in wind-induced acceleration calculations, the ORs are placed at the optimum location for accelerations. As shown in Figure 11, for all variations except variation (f), the ratio f_{OR}/f_0 decreases with the increase in number of storeys. For variation (f), the ratio f_{OR}/f_0 increases with the increase in number of storeys. For variations (a)–(e), the frequency increase is approximately 20% to 45% using one OR and 35% to 95% using 2 ORs. For variation (f), the frequency increase is approximately 40% to 60% using one OR and 75% to 100% using 2 ORs.

The constructability of each variation is also an important aspect to be compared. For some variations, namely: (a), (c) and (f), the OR connections and the moment connections (beam-wall/column) intersect. This intersection can impose constructability difficulties. In this regard, variations (b), (d) and (e) can provide more practical alternatives. However, variation (d) has more connections than variations (b) and (e), which might be undesired.

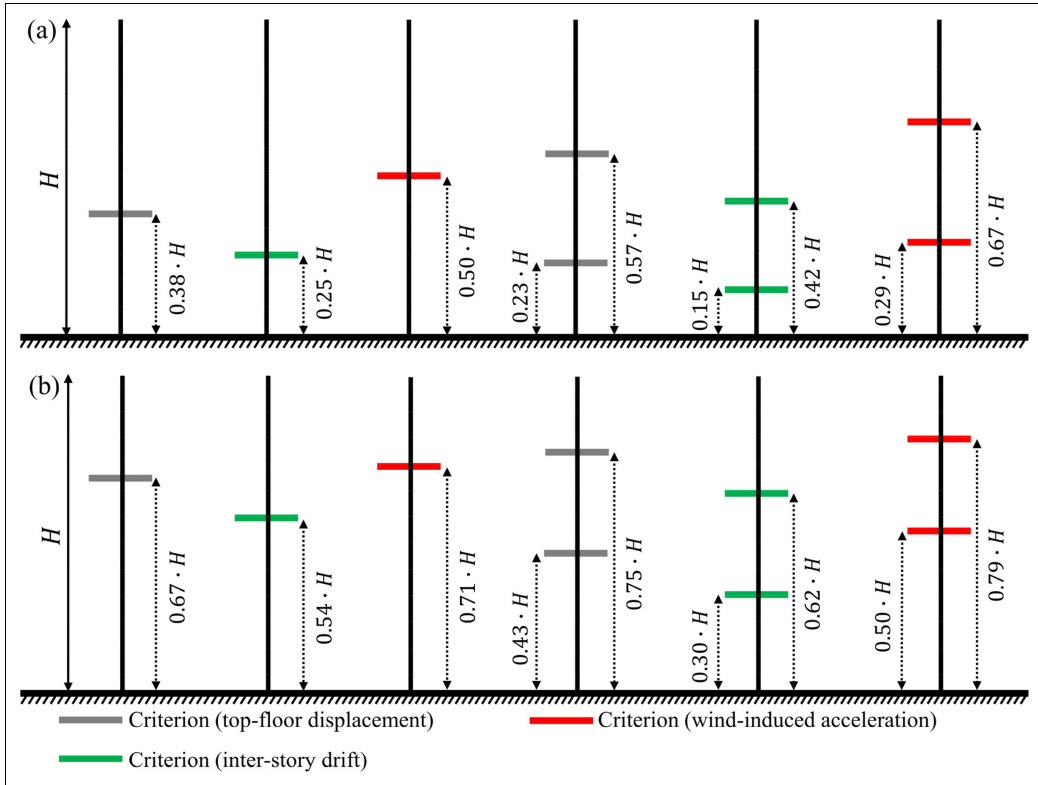


Figure 8. Optimum location of OR based on three criteria for (a) variation a-e; and (b) variation f.

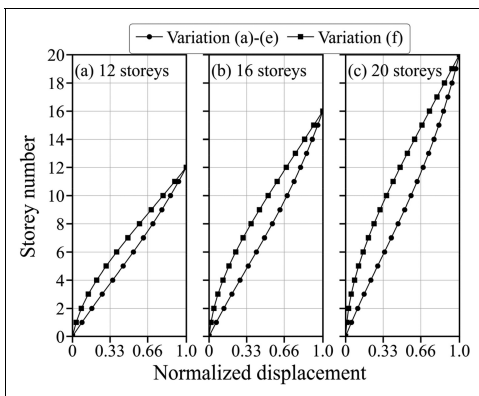


Figure 9. Mode shapes with no outriggers.

Stiffness of outriggers

Since the lengths of the truss elements are not the same for all variations shown in Figure 4, it is best to replace the effective axial stiffness ($K_{\text{effective}}$) of the element with $E_1 \cdot A_{\text{effective}}$. Both are related and can be calculated using equation (2). The effective area of the truss ($A_{\text{effective}}$) was varied from 0 to 0.40 m^2 , where 0 m^2 represents the case

of no outriggers. The ORs were placed at the optimum location(s) shown in Figure 8 for top floor displacement, inter-story drift and wind-induced acceleration, respectively. A basic wind velocity of 26 m/sec was assumed.

Figure 12 shows the lateral displacements (Δ , δ) and wind induced acceleration (a) as function of $E_1 \cdot A_{\text{effective}}$. With an effective area of approximately 0.10 m^2 ($E_1 \cdot A_{\text{effective}}$ of $13 \times 10^5 \text{ kN}$), 80% to 90% of the maximum improvement can be achieved. Increasing $A_{\text{effective}}$ beyond 0.20 m^2 nearly shows no improvement as all response quantities (Δ , δ , a) converge.

For variation (e), the outrigger stiffness was measured in terms of the thickness of the CLT panels used as OR, and the stiffness of the connections connecting the CLT OR to the main structure. It was assumed that these connections have shear and axial stiffness of the same magnitude. Figures 13 and 14 show the lateral displacements and wind induced acceleration as function of CLT thickness and the connections stiffness, respectively. When the CLT thickness was varied, the connections stiffness was set to 100 kN/mm/m . When the connections stiffness was varied, the CLT thickness was set to 300 mm . As shown in Figures 13 and 14, good reductions can be achieved with CLT thickness of around 100 mm and connections stiffness in the range of 25 to 50 kN/mm/m .

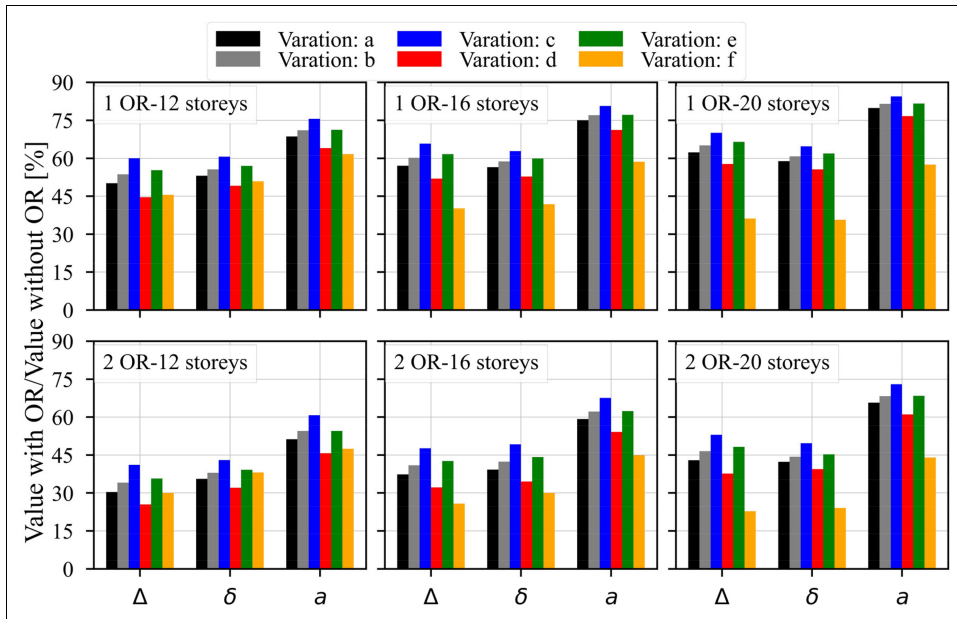


Figure 10. Ratios of top floor displacement (Δ), inter-storey drift (δ) and wind-induced acceleration (a) with the use of OR to the case without OR.

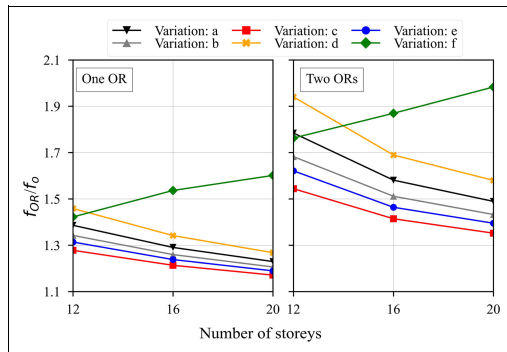


Figure 11. Ratio of the frequency with the use of OR (f_{OR}) to the case without OR (f_0).

Feasibility study

In this section, a parametric study is presented. The parameters used in this study are summarised in Table 7. The feasibility is evaluated in terms of top floor displacement, inter-storey drift and wind induced acceleration.

Figure 15 shows the peak acceleration for the frames in Table 7. For simplicity, variations (a)–(e) were considered one group, and variation (f) was considered the second group. For the frames shown in Table 7, Figures 16 and 17 show lateral displacements and inter-storey drift, respectively. Since linear elastic FEM was performed, gravity loads do not contribute to lateral displacements. Hence, Figures 16 and 17 are shown for the case of light frames.

Table 7. Parameters used in the feasibility study.

Parameter	Value
Variation	a/b/c/d/e/f (with and without ORs)
Basic wind velocity $v_{b,0}$	22/26/30 m/s
Number of storeys	12/16/20
Number of outriggers	1/2
Location of ORs	Optimum location (Figure 8)
Gravity loads	Heavy/Light
Truss outrigger	$A_{effective} = 0.10 \text{ m}^2$
CLT outrigger	CLT thickness = 300 mm, connections stiffness = 50 kN/mm/m

As shown in Figures 16 and 17, using only one OR, variations (a), (d) and (f) meet the requirements for top floor displacement and inter-storey drift for all basic wind velocities and all number of storeys. Based on Figures 15–17, it can be observed that wind-induced acceleration is the governing response parameter compared to lateral displacements. Based on Figures 15–17, several conclusions can be drawn, these are summarised in Table 8.

Ultimate limit state considerations

Some considerations with respect to the feasibility of the OR-system in terms of the ULS are provided in this section. In subsection ‘Stresses in an example frame’, the stress levels of the beams, columns and walls of a benchmark frame are used as a basis for discussion. In subsection ‘Forces in the OR truss members’, the force levels in the truss elements are summarised and

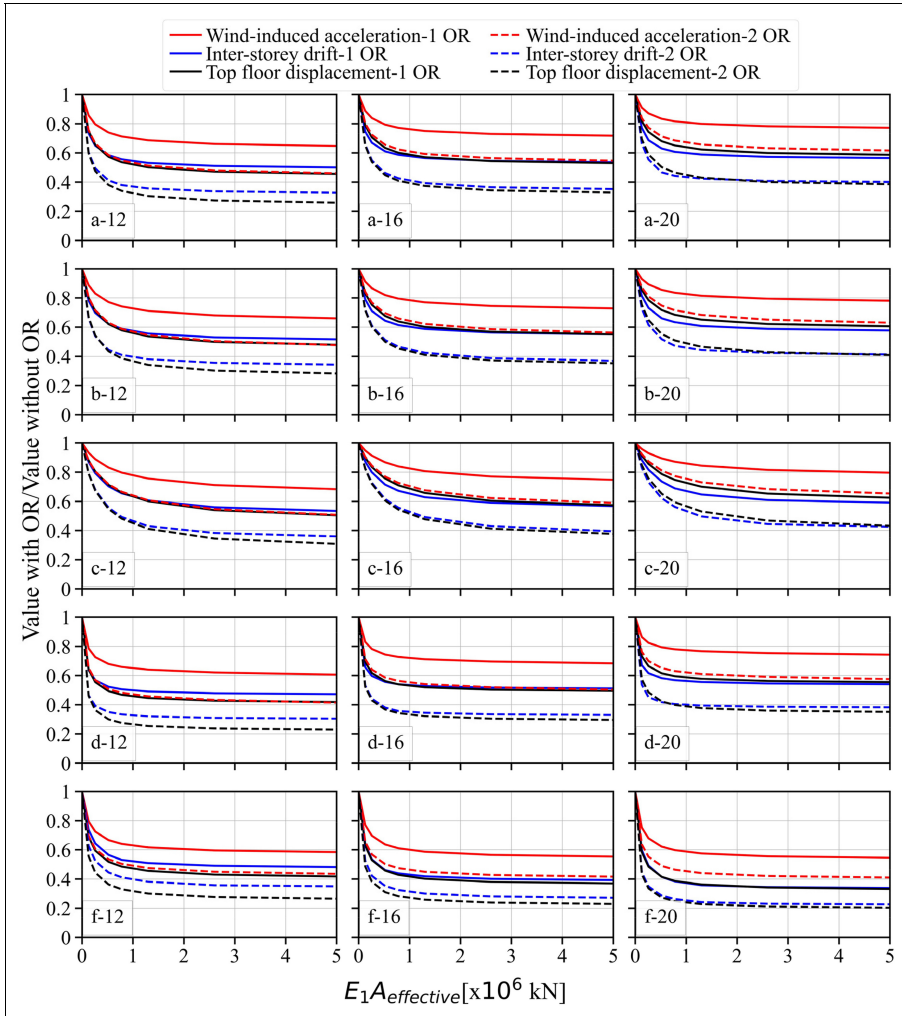


Figure 12. Lateral displacements and acceleration ratios as function of ($E_1 \cdot A_{effective}$) (legend: variation-number of storeys).

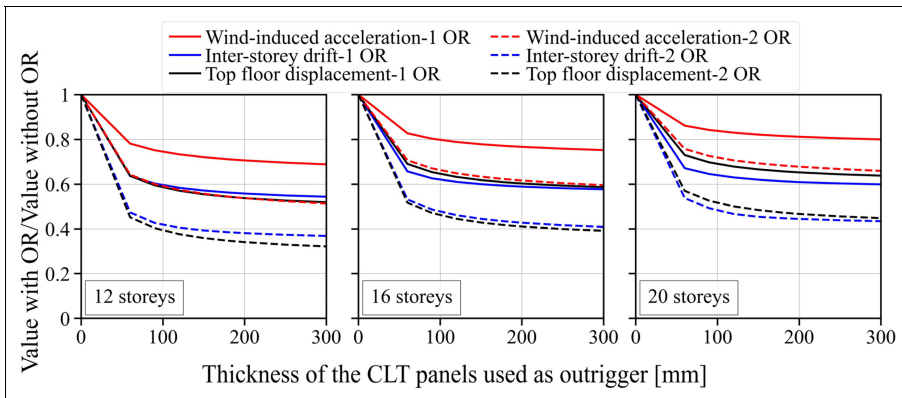


Figure 13. Lateral displacements and acceleration ratios as function of CLT OR thickness for variation (e).

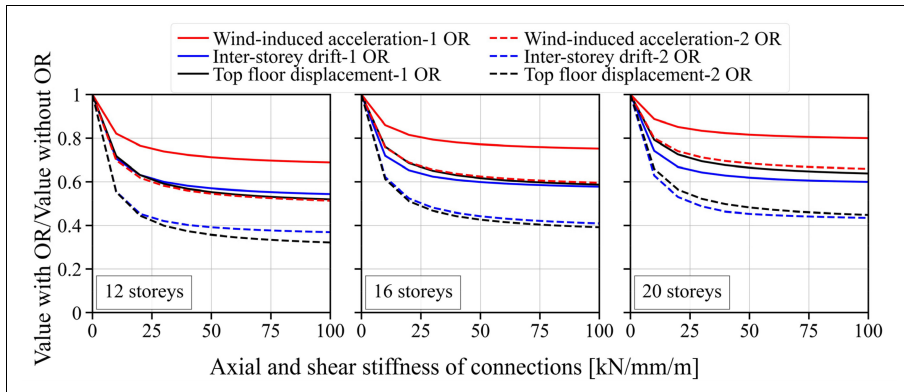


Figure 14. Lateral displacements and acceleration ratios as function of axial and shear stiffness of the connections used in the CLT OR for variation (e).

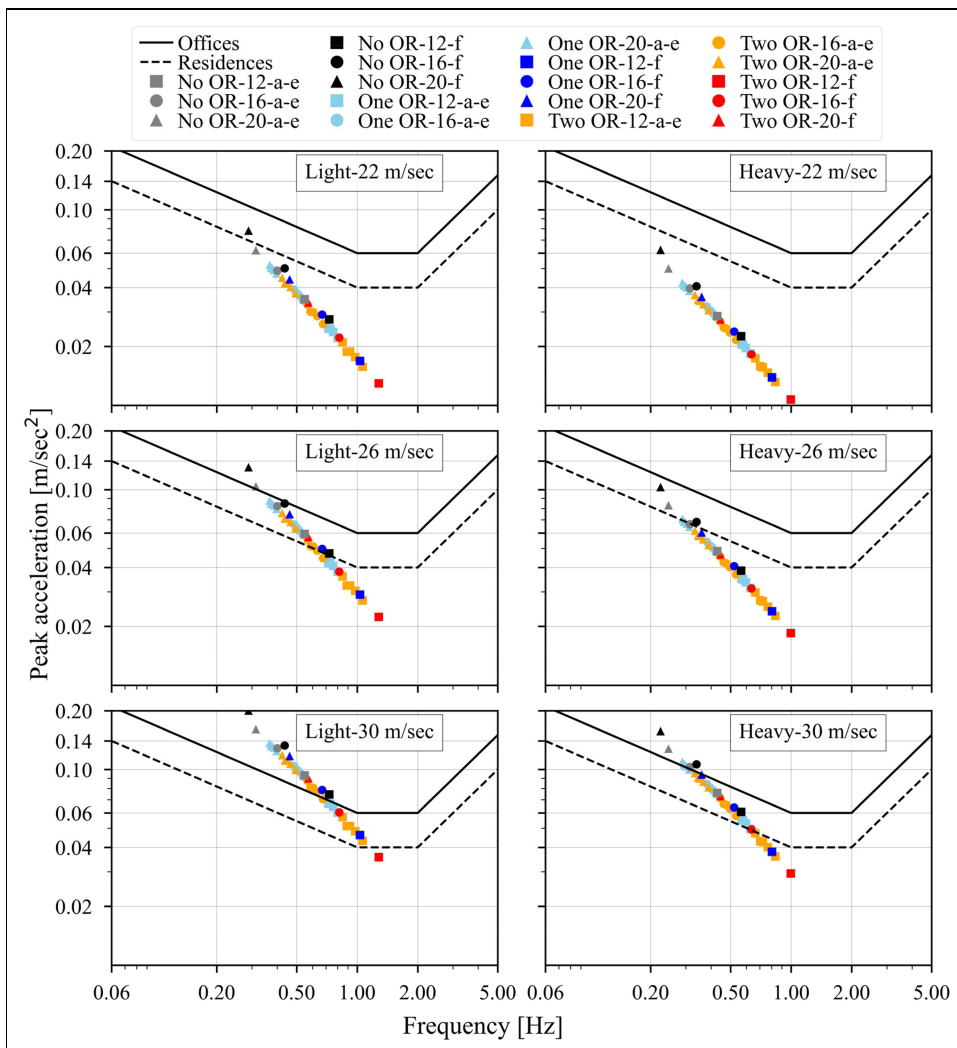


Figure 15. Wind-induced acceleration.

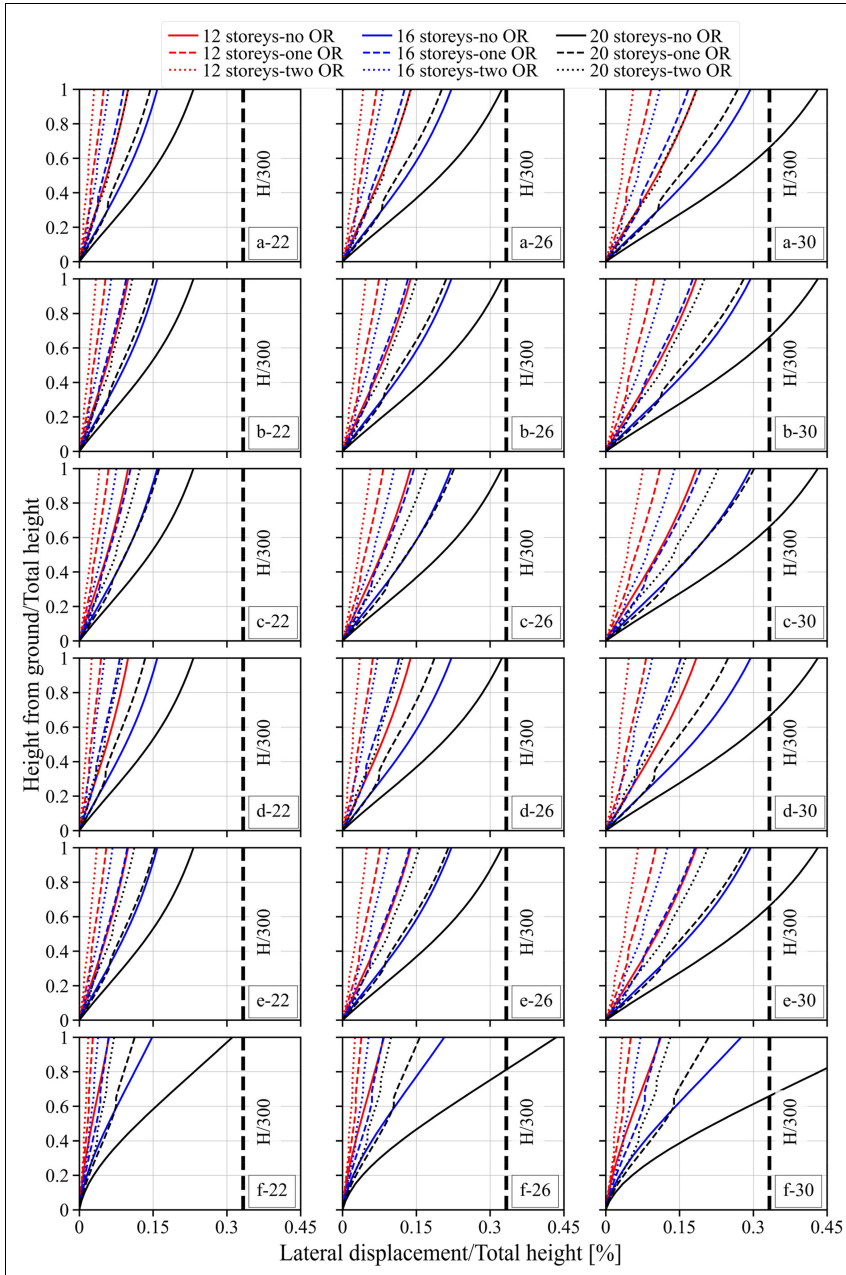


Figure 16. Lateral displacement for all variations (legend: variation-basic wind velocity).

discussed. In both subsections, the results come from the ULS design load combination given by equations (6) and (7).

Stresses in an example frame. An OR frame with the properties shown in Table 9 is used as benchmark to investigate the stress levels in the beams, columns and walls.

Other parameters such as number of bays, bay length, floor height, material properties, connections stiffness and cross-sections were kept the same as in section ‘Materials and methods’ of this article. The OR is placed at the optimal location based on wind-induced acceleration criterion. Stresses in beams, columns and walls are summarised in Table 10. Stresses in the truss

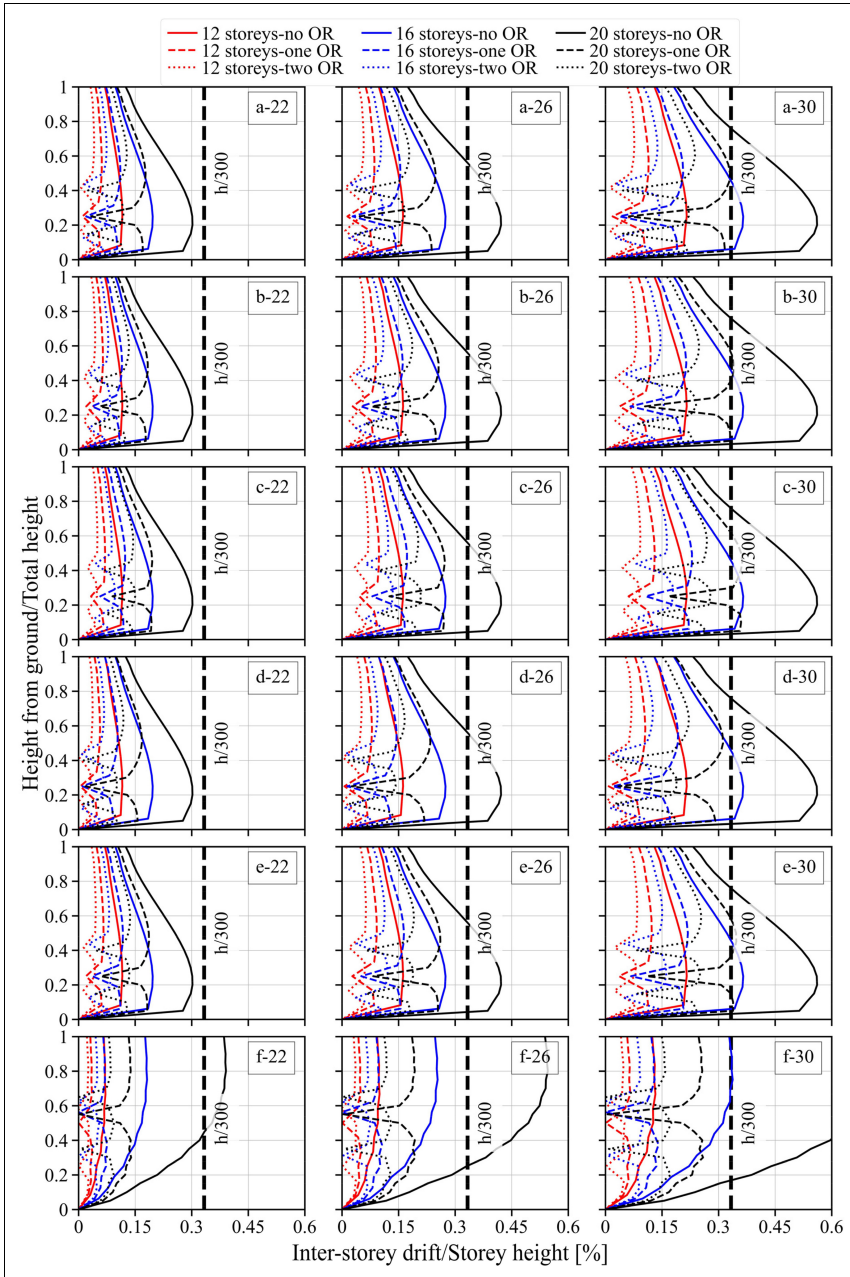


Figure 17. Inter-storey drift for all variations (legend: variation-basic wind velocity).

elements of the OR are not reported here; the ULS of the truss elements are examined in greater detail in subsection ‘Forces in the OR truss members’. As shown in Table 10, the stress-levels are not very high, and these structural elements can be designed such that they satisfy the safety requirements.

Forces in the OR truss members. The maximum forces (tension and compression) in the truss elements of the ORs were calculated for all variations except variation (e). The ORs were placed at the optimal location with respect to wind-induced acceleration. A basic wind velocity of 26 m/s and $E_1 A_{effective}$ of 13×10^5 kN were

Table 8. Conclusions based the feasibility study.

$v_{b,0}$	No. of storeys	Conclusions
22	12	• Variations (a)–(f) (light and heavy) meet the requirements of acceleration (residential) without ORs
	16	• Variations (a)–(f) (light and heavy) meet the requirements of acceleration (residential) without ORs
	20	• Variations (a)–(e) (light and heavy) meet the requirements of acceleration (residential) without ORs • Variation (f) (light) meets the requirements for acceleration (residential) using one OR
26	12	• Variations (a)–(f) (light) without ORs exceed the acceleration limit for residential buildings but meet the requirement for office buildings. • Variations (a)–(f) (heavy) without ORs and variations (a)–(f) (light) with one OR meet the acceleration requirements (residential)
	16	• Variations (a)–(f) (light and heavy) without ORs exceed the limit for residential buildings but meet the requirement for office buildings. • For variations (a)–(f) (light), two ORs are needed to meet the requirements of residential buildings, but only one OR is needed for heavy frames.
30	20	• Variations (a)–(f) (light) can only meet the requirements for office buildings using either one or two ORs. • Variations (a)–(f) (heavy) meet the requirements for residential buildings using one OR.
	12	• For variation (f) (light), two ORs are needed to meet the requirements of residential buildings, but only one OR is needed for heavy frames. • For variations (a)–(f) (light), only office buildings requirements can be met using either one or two OR. But for heavy frames with two OR, residential buildings requirements can be met.
	16	• Variations (a)–(e) (heavy) can only meet the requirements for office buildings using two ORs. • Variation (f) (light) can only meet the requirements for office buildings using two ORs. But the heavy frames can meet the requirements for residential buildings using two ORs.
	20	• Variations (a)–(f) (heavy) can only meet the requirements for office buildings using two ORs.

Table 9. Parameters of the benchmark OR frame used for stresses evaluation.

Property	Value	Unit
Number of storeys	16	-
Number of outriggers	1	-
Location of outrigger	8 th floor	-
Basic wind velocity	26	m/sec
Gravity loads	Light	-
Outrigger variation	b	-
$E_1 A_{\text{effective}}$	$13 \cdot 10^5$	kN

Table 10. Maximum stresses (normal and shear) for the benchmark frame.

Element	Stress type	Stress (N/mm ²)
Beams	Normal stress	5.43
	Shear stress	0.59
Columns	Normal stress	6.61
	Shear stress	0.36
CLT walls	Normal stress	5.80
	Shear stress	0.47

considered. Other relevant parameters were kept the same as in section ‘Materials and methods’ of this article. Figure 18 summarises the maximum axial force-levels in the truss elements. The force levels in Figure 18 correspond to a double cross-section (see Figure 3), so the force levels per member is half the values shown in Figure 18.

As shown in Figure 18, the force levels are quite high for the case of 20 storeys (grey bar), which imposes some challenges on the ULS with respect to cross-sections of the truss elements but mostly with respect to the connections to the main frame. To accommodate such force-level, the connections need to have a sufficient capacity which can be challenging. Among the five variations (a, b, c, d, f), the force-levels in variation (c) tends to be higher. Variation (c) has also the most slender truss elements and buckling may be critical.

For all variations except variation (e), and for the cases of 12 and 16 storeys, the values of the axial forces are in the order of 400 kN (200 kN per cross-section) and therefore these cases are deemed more feasible. Variation (e), on the other hand, can provide uniform distribution of forces between the OR and the main structure along the CLT panels perimeter. Therefore, even though variation (e) is less effective with respect to SLS compared to some other variations (see subsection ‘Comparison of outrigger variations’ in this article), it might be advantageous with respect to ULS to avoid force concentration at the connections.

Variation of connections stiffness and outrigger stiffness

Inherent variability in timber connections can lead to variations in the internal forces and moments of MRTFs.⁵² In this subsection, the same benchmark frame in subsection ‘Stresses in an example frame’ is used to examine the effect of stiffness variability on the internal forces of the outrigger truss elements, lateral displacements and

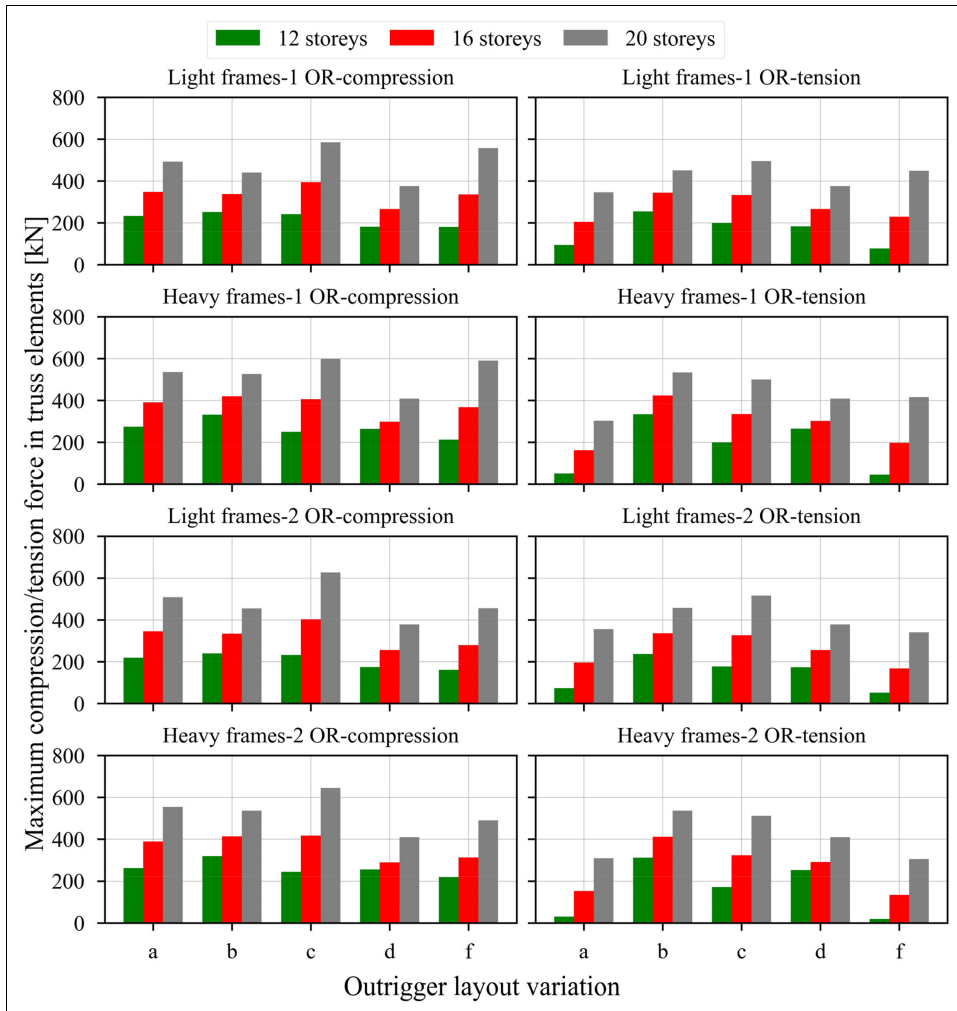


Figure 18. Force levels at the truss elements ($v_{b,0} = 26 \text{ m/s}$, $E_1 A_{\text{effective}} = 13 \times 10^5 \text{ kN}$).

accelerations. A normal distribution with 20% coefficient of variation was assumed for $K_{\theta,w}$, $K_{\theta,b}$ and $A_{\text{effective}}$ (confer Figure 6 and Table 3). A total of 3000 analyses were performed, and the following could be observed:

- The mean value of top floor displacement (obtained from the 3000 analyses) is 1.02% higher than the reference case (which assumes mean $K_{\theta,w}$, $K_{\theta,b}$ and $A_{\text{effective}}$).
- The mean value of IDR is 1.20% higher than the reference case.
- The mean value of peak acceleration is 0.53% higher than the reference case.
- The 95% percentile of the normal force of the outrigger truss elements is 8% higher than the reference case. The use of 98% results in 10% increase in the force.

While mean lateral displacements and accelerations exhibit negligible increase, there is a more noticeable increase in

outrigger forces, which should be considered in the design for the ULS. The variation in connection stiffness of MRTFs has also been shown to have an insignificant influence on lateral displacements and accelerations.⁵²

Conclusions

In this article, the feasibility of using timber outrigger structures to build up to 20 storeys was investigated using linear elastic finite element analysis together with the relevant European and international standards. The feasibility is evaluated assuming wind velocities up to 30 m/s. The optimum location of one and two outriggers was estimated considering three criteria, namely: top floor displacement, inter-storey drift and wind-induced acceleration. Different layouts of outrigger were investigated, and their efficiency was compared. The stiffness of the outriggers was varied to evaluate the stiffness requirements. The influence of

connections' stiffness variability was also investigated. Although the focus of this article was devoted to serviceability requirements, some ULS considerations were briefly discussed. The following main conclusions are drawn:

- Using one outrigger, a reduction of 30% to 65% in lateral displacements (top floor displacement and inter-storey drift) and 15% to 40% in wind-induced acceleration can be achieved.
- Using two outriggers, a reduction of 45% to 75% in lateral displacements and 25% to 55% in wind-induced acceleration can be achieved.
- Considering serviceability requirements, building up to 16 storeys is feasible with basic wind velocity of 26 to 30 m/s. Building 20 storeys is, however, challenging and can be limited to low basic wind velocities.
- Considering ultimate limit state, building up to 16 storeys is feasible. However, for 20 storeys, the forces in the connections can be challenging to design.
- Variability of connections' stiffness has negligible influence on lateral displacements and wind-induced acceleration. On the other hand, an increase on the order of 10% in the force in the outrigger truss elements was observed compared to the reference value obtained using mean stiffness values.

Declaration of conflicting interests

The authors declared no potential conflicts of interest with respect to the research, authorship and/or publication of this article.

Funding

The authors received no financial support for the research, authorship and/or publication of this article.

ORCID iD

Osama Abdelfattah Hegeir  <https://orcid.org/0000-0002-9924-5504>

References

1. 2019 global status report for buildings and construction: Towards a zero-emission, efficient and resilient buildings and construction sector. Global Alliance for Buildings and Construction, International Energy Agency and the United Nations Environment Programme, 2019.
2. Eliassen AR, Faanes S and Bohne RA. Comparative LCA of a concrete and steel apartment building and a cross laminated timber apartment building. *IOP Conf Ser: Earth Environ Sci* 2019; 323: 012017.
3. Skullestad JL, Bohne RA and Lohne J. High-rise timber buildings as a climate change mitigation measure—a comparative LCA of structural system alternatives. *Energy Procedia* 2016; 96: 112–123.
4. Vilguts A, Stamatopoulos H and Malo KA. Parametric analyses and feasibility study of moment-resisting timber frames under service load. *Eng Struct* 2021; 228: 111583.
5. Abrahamsen R. Mjostårmet-Construction of an 81 m tall timber building. In: Internationales Holzbau-Forum IHF, vol. 2017, Garmisch-Partenkirchen, Germany, 2017.
6. Vilguts A, Malo KA and Stamatopoulos H. Moment resisting frames and connections using threaded rods in beam-to-column timber joints. In: World conference on timber engineering (WCTE2018), Seoul, Republic of Korea, 2018.
7. Johansson M, Linderholt A, Järnerö K, et al. Tall timber buildings—a preliminary study of wind-induced vibrations of a 22-storey building. In: World conference on timber engineering (WCTE2016), Vienna, Austria, 2016.
8. Abrahamsen RB. First 14-storey wood building in the world at Bergen in Norway. *5ème Forum Int Bois Constr FBC* 2015; 2015.
9. Edskär I and Lidelöw H. Wind-induced vibrations in timber buildings—parameter study of cross-laminated timber residential structures. *Struct Eng Int* 2017; 27: 205–216.
10. Cao AS and Stamatopoulos H. A theoretical study of the dynamic response of planar timber frames with semi-rigid moment-resisting connections subjected to wind loads. *Eng Struct* 2021; 240: 112367.
11. Stamatopoulos H and Malo KA. Wood frame solutions for free space design in urban buildings (WOODSOL). In: 7th forum wood building nordic, Växjö, Sweden, 2018, pp.27–28.
12. Aloisio A, et al. Vibration issues in timber structures: a state-of-the-art review. *J Build Eng* 2023; 76: 107098.
13. Hegeir OA, Stamatopoulos H and Malo KA. Service ability performance of timber dual frame-wall structural system under wind loading. In: World conference on timber engineering (WCTE 2023), Oslo, Norway, 2023. doi: 10.52202/069179-0384.
14. Chapain S and Aly AM. Vibration attenuation in a high-rise hybrid-timber building: a comparative study. *Appl Sci* 2023; 13: 2230.
15. Wells M. Stadthaus, London: raising the bar for timber buildings. *Proc Inst Civ Eng-Civ Eng* 2011; 164: 122–128.
16. Malo KA, Abrahamsen RB and Bjertnæs MA. Some structural design issues of the 14-storey timber framed building “Treet” in Norway. *Eur J Wood Wood Prod* 2016; 74: 407–424.
17. Malo KA and Stamatopoulos H. Connections with threaded rods in moment resisting frames. In: World conference on timber engineering (WCTE2016), Vienna, Austria, 2016.
18. Ali MM and Moon KS. Advances in structural systems for tall buildings: emerging developments for contemporary urban giants. *Buildings* 2018; 8: 104.
19. Council on Tall Buildings and Urban Habitat. *Outrigger design for high-rise buildings: an output of the CTBUH outrigger working group*. New York, NY: Routledge, 2017.
20. Taranath BS. *Structural analysis and design of tall buildings: steel and composite construction*. Boca Raton, FL: CRC Press, 2016.
21. Taranath BS. *Wind and earthquake resistant buildings: structural analysis and design*. Boca Raton, FL: CRC Press, 2004.
22. Smith BS and Salim I. Formulae for optimum drift resistance of outrigger braced tall building structures. *Comput Struct* 1983; 17: 45–50.
23. Lame A. *Optimization of outrigger structures*. Master's Degree, Department of Civil and Environmental Engineering, Massachusetts Institute of Technology (MIT), 2008.
24. Kim H-S, Lim Y-J and Lee H-L. Optimum location of outrigger in tall buildings using finite element analysis and gradient-based optimization method. *J Build Eng* 2020; 31: 101379.

25. Kim H-S, Lee H-L and Lim Y-J. Multi-objective optimization of dual-purpose outriggers in tall buildings to reduce lateral displacement and differential axial shortening. *Eng Struct* 2019; 189: 296–308.
26. Zhou Y, Zhang C and Lu X. An inter-story drift-based parameter analysis of the optimal location of outriggers in tall buildings. *Struct Des Tall Spec Build* 2016; 25: 215–231.
27. Hoenderkamp J. Second outrigger at optimum location on high-rise shear wall. *Struct Des Tall Spec Build* 2008; 17: 619–634.
28. Hoenderkamp J and Bakker M. Analysis of high-rise braced frames with outriggers. *Struct Des Tall Spec Build* 2003; 12: 335–350.
29. Choi HS and Joseph L. Outrigger system design considerations. *Int J High-Rise Build* 2012; 1: 237–246.
30. Cao AS, Palma P and Frangi A. Column removal analyses of timber structures Framework to assess dynamic amplification factors for simplified structural design methods. In: World conference on timber engineering (WCTE2021), Santiago, Chile, 2021.
31. Huber JA, Ekevad M, Girhammar UA, et al. Structural robustness and timber buildings—a review. *Wood Mater Sci Eng* 2019; 14: 107–128.
32. Boellaard B. *Design of an outrigger structure for tall timber buildings*. Master's Degree, Department of Architecture, Building and Planning, Eindhoven University of Technology, 2012.
33. Tesfamariam S and Das S. Resilient tall timber building design: damped-outrigger system. The University of British Columbia, 2021.
34. *Design of timber structures*. 2nd ed. Stockholm: Swedish Forest Industries Federation, 2016.
35. CEN. NS-EN 14080: Timber structures—Glued laminated timber and glued solid timber—Requirements. *European Committee for Standardization: Brussels, Belgium*, 2013.
36. Blass HJ and Fellmoser P. Design of solid wood panels with cross layers. In: 8th world conference on timber engineering, 2004.
37. Follesa M, Christovasilis I, Vassallo D, et al. Seismic design of multi-storey CLT buildings according to Eurocode 8. *Ingegneria Sismica. Int J Earthq Eng Spec Issue Timber Struct* 2013; 30: 27–53.
38. CEN. NS-EN 338: Structural timber—Strength classes. *European Committee for Standardization: Brussels, Belgium*, 2016.
39. *CSI SAP2000 Structural analysis and design*. Computers and Structures, <https://www.csiamerica.com/products/sap2000>.
40. Loss C, Hossain A and Tannert T. Simple cross-laminated timber shear connections with spatially arranged screws. *Eng Struct* 2018; 173: 340–356.
41. Ottenhaus L-M, Li M and Smith T. Structural performance of large-scale dowelled CLT connections under monotonic and cyclic loading. *Eng Struct* 2018; 176: 41–48.
42. Vilguts A, Nesheim SØ, Stamatopoulos H, et al. A study on beam-to-column moment-resisting timber connections under service load, comparing full-scale connection testing and mock-up frame assembly. *Eur J Wood Wood Prod* 2022; 80: 753–770.
43. Stamatopoulos H, Malo KA and Vilguts A. Moment-resisting beam-to-column timber connections with inclined threaded rods: structural concept and analysis by use of the component method. *Constr Build Mater* 2022; 322: 126481.
44. CEN. NS-EN 1991-1-4:2005+NA:2009: Actions on Structures—Part 1-4: General Actions—Wind Actions. *European Committee for Standardization: Brussels, Belgium*, 2009.
45. CEN. NS-EN 1991-1-1: 2002+ NA: 2019: Actions on Structures—Part 1-1: General Actions—Densities, self-weight, imposed loads for buildings. *European Committee for Standardization: Brussels, Belgium*, 2019.
46. CEN. NS-EN 1990:2002+A1:2005+NA:2016: Basis of structural design. *European Committee for Standardization: Brussels, Belgium*, 2016.
47. CEN. NS-EN 1995-1-1:2004+A1:2008+NA:2010: Design of timber structures—Part 1-1: General—Common rules and rules for buildings. *European Committee for Standardization: Brussels, Belgium*, 2010.
48. Steenbergen R, Vrouwenvelder A and Geurts C. The use of Eurocode EN 1991-1-4 procedures 1 and 2 for building dynamics, a comparative study. *J Wind Eng Ind Aerodyn* 2012; 107-108: 299–306.
49. Feldmann A, et al. Dynamic properties of tall timber structures under wind-induced vibration. In: World conference on timber engineering (WCTE 2016), 2016.
50. Kwok KC, Hitchcock PA and Burton MD. Perception of vibration and occupant comfort in wind-excited tall buildings. *J Wind Eng Ind Aerodyn* 2009; 97: 368–380.
51. ISO. ISO10137: Bases for design of Structures - Serviceability of Buildings and Walkways against Vibrations. *International Organization for standardization*, 2007.
52. Stamatopoulos H, Hegeir OA and Malo KA. Analysis and design aspects of moment-resisting, beam-to-column, timber connections with inclined threaded rods: from fastener level to construction level. In: Presented at the world conference on timber engineering (WCTE 2023), 2023.

Paper VI

Analysis and design aspects of moment-resisting, beam-to-column, timber connections with inclined threaded rods: from fastener level to construction level

Haris Stamatopoulos, Osama Abdelfattah Hegeir, Kjell Arne Malo

In proceedings of the ***World Conference on Timber Engineering*** (WCTE 2023),

Oslo, 2023

ANALYSIS AND DESIGN ASPECTS OF MOMENT-RESISTING, BEAM-TO-COLUMN, TIMBER CONNECTIONS WITH INCLINED THREADED RODS: FROM FASTENER LEVEL TO CONSTRUCTION LEVEL

Haris Stamatopoulos¹, Osama Abdelfattah Hegeir², Kjell Arne Malo³

ABSTRACT: Moment-resisting timber frames (MRTFs) can be an alternative load-carrying system for mid-rise buildings, compared to systems based on walls or diagonals. The response of MRTFs depends largely on their connections. This paper provides an overview of analysis and design aspects of connections for MRTFs based on inclined threaded rods. Simplified expressions are provided for the properties of such connections and for the properties of threaded rods. Finally, the effects of connection's stiffness variability are explored. It is shown that this variability can result in increased values of actions compared to the values obtained by use of mean connection stiffness.

KEYWORDS: Moment-resisting connections, Moment-resisting frames, Threaded rods, Stiffness variability

1 INTRODUCTION

Moment-resisting timber frames (MRTFs) can reduce the need for bracing by shear walls or diagonal elements and allow for greater architectural flexibility in mid-rise buildings. The response of MRTFs depends on the properties of their connections, especially with respect to the serviceability aspects, see e.g.[1]. Moreover, MRTFs are statically indeterminate structures and the magnitude and distribution of internal forces and moments at the Ultimate Limit State, depend on the stiffness of their connections. The variability of the connections' stiffness can also significantly influence the internal forces and moments as will be shown in Section 4.

A concept for a moment-resisting connection with inclined threaded rods is presented in Figure 1. The rods are inserted with an inclination in pre-drilled holes in the beam and the column and jointed by use of metallic coupling parts. In the prototype tests for this concept [2], beams and columns were made of glued-laminated timber (glulam) and purpose-made steel rings were used as the coupling parts, see Figure 1. To allow fastening of rods to the steel rings, threaded rods with metric thread at their end are used, as shown in Figure 1. The use of steel brackets or plates and friction bolts can be an alternative to steel rings, see for example [3].

As shown in Figure 1, the coupling parts are connected to the column by use of a pair of inclined threaded rods (rods c1-c2 at the top and rods c3-c4 at the bottom). Due to rod inclination and the presence of shear forces, a load situation consisting of both axial and lateral forces occurs in the rods. However, the rods will mainly experience axial forces since their axial stiffness is much greater than the lateral one. The transfer of forces in this configuration resembles the transfer of forces in a truss system where all

members are axially loaded. Therefore, the lateral forces in the rods c1, c2, c3 and c4 may be neglected.

The rods in the beam are inserted at a small angle. Rods parallel to the grain are vulnerable to cracks since a single crack along the grain might lead to a considerable loss of strength if the crack occurs in the same plane as the rod. Therefore, the beam is connected to the coupling parts by use of threaded rods (b1 and b2) inserted at a small angle to the grain, i.e. 5°-10°, see Figure 1. Greater angle should be avoided as it would also result in high lateral forces in the threaded rods and therefore smaller stiffness.

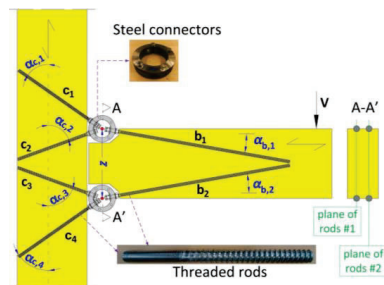


Figure 1: Moment-resisting connection with inclined rods

This paper consists of two parts:

- In the first part (Sections 2 and 3), analytical expressions are provided for the estimation of the properties of a connection as shown in Figure 1 and for the rods, based on recent publications;
- In the second part (Section 4) a **preliminary** study regarding the effects of connection stiffness variability on response of MRTFs is presented.

¹ Haris Stamatopoulos, haris.stamatopoulos@ntnu.no

² Osama Abdelfattah Hegeir, osama.a.s.a.hegeir@ntnu.no

³ Kjell Arne Malo, kjell.malo@ntnu.no

Norwegian University of Science and Technology (NTNU)

2 CONNECTION PROPERTIES

2.1 STIFFNESS

The connection in Figure 1 can be considered as a system of rotational springs in series consisting of: a) the connection of rods c_1 - c_4 to the column with spring constant $K_{\theta,c}$, b) the connection of rods b_1 - b_2 to the beam with spring constant $K_{\theta,b}$ and c) the connectors with spring constant $K_{\theta,con}$. Therefore, the rotational stiffness of the connection can be determined by Eq.(1). The geometry is given in Figure 2. In [4], Eqs.(2)-(3) were derived by use of the component method and validated by

experimental results. The compliance S -terms (Eqs.(4)-(7)) are given as functions of the axial stiffness ($K_{ax,i}$) and lateral stiffness ($K_{v,i}$) of the rods and the rod-to-grain angles (Eq.(8)). In Figure 2 and Eqs.(2)-(3), the lever arm is assumed the same on the beam and the column side ($z_b = z_c = z$). However, Eqs.(2)-(3) can also be applied for different lever arms. Eqs.(2)-(3) depend also on the moment to shear ratio ($L_v = M/V$) which is not known - a priori - in the structural analysis and approximations are needed, see also Eqs.(9)-(12). Eqs.(1)-(8) apply per plane of rods.

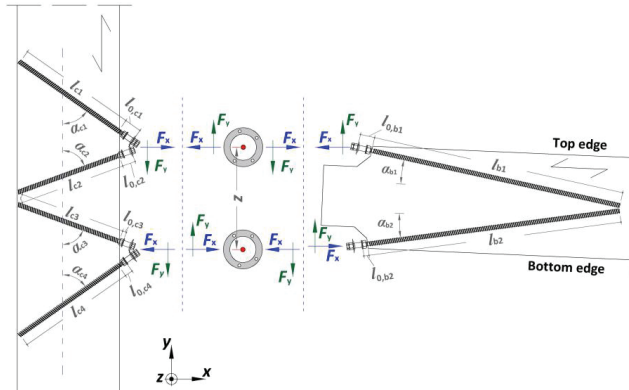


Figure 2: Forces and geometry of a moment resisting connection with inclined threaded rods

$$K_{\theta} = (1/K_{\theta,c} + 1/K_{\theta,b} + 1/K_{\theta,con})^{-1} \quad (1)$$

$$K_{\theta,c} = \frac{z^2}{(S_{xx,c}^{(c1-c2)} + S_{xx,c}^{(c3-c4)}) + (S_{xy,c}^{(c3-c4)} - S_{xy,c}^{(c1-c2)}) \cdot z/(2 \cdot L_v)} \quad (2)$$

$$K_{\theta,b} = \frac{z^2}{(S_{xx,b1} + S_{xx,b2}) + (S_{xy,b2} - S_{xy,b1}) \cdot z/(2 \cdot L_v)} \quad (3)$$

$$S_{xx,c}^{(c1-c2)} = \frac{c_{c1}^2/K_{ax,c2} + c_{c2}^2/K_{ax,c1}}{(c_{c1} \cdot s_{c2} + c_{c2} \cdot s_{c1})^2}; S_{xx,c}^{(c3-c4)} = \frac{c_{c3}^2/K_{ax,c4} + c_{c4}^2/K_{ax,c3}}{(c_{c3} \cdot s_{c4} + c_{c4} \cdot s_{c3})^2} \quad (4)$$

$$S_{xy,c}^{(c1-c2)} = \frac{c_{c1} \cdot s_{c1}/K_{ax,c2} - c_{c2} \cdot s_{c2}/K_{ax,c1}}{(c_{c1} \cdot s_{c2} + c_{c2} \cdot s_{c1})^2}; S_{xy,c}^{(c3-c4)} = \frac{c_{c3} \cdot s_{c3}/K_{ax,c4} - c_{c4} \cdot s_{c4}/K_{ax,c3}}{(c_{c3} \cdot s_{c4} + c_{c4} \cdot s_{c3})^2} \quad (5)$$

$$S_{xx,b1} = s_{b1}^2/K_{v,b1} + c_{b1}^2/K_{ax,b1}; S_{xx,b2} = s_{b2}^2/K_{v,b2} + c_{b2}^2/K_{ax,b2} \quad (6)$$

$$S_{xy,b1} = s_{b1} \cdot c_{b1} \cdot (1/K_{v,b1} - 1/K_{ax,b1}); S_{xy,b2} = s_{b2} \cdot c_{b2} \cdot (1/K_{ax,b2} - 1/K_{v,b2}) \quad (7)$$

$$c_i = \cos \alpha_i; s_i = \sin \alpha_i; L_v = M/V \quad (8)$$

Neglecting the shear term in Eqs.(2)-(3) results in the following crude approximations:

$$K_{\theta,c} \approx z^2 / (S_{xx,c}^{(c1-c2)} + S_{xx,c}^{(c3-c4)}) \quad (9)$$

$$K_{\theta,b} \approx z^2 / (S_{xx,b1} + S_{xx,b2}) \quad (10)$$

Assuming further that the rods are inserted at equal angles in the column ($\alpha_{c1} = \alpha_{c2} = \alpha_{c3} = \alpha_{c4} = \alpha_c$) and the beam ($\alpha_{b1} = \alpha_{b2} = \alpha_b$) and that they approximately have equal stiffness ($K_{ax,c1} = K_{ax,c2} = K_{ax,c3} = K_{ax,c4} = K_{ax,c}$, $K_{ax,b1} = K_{ax,b2} = K_{ax,b}$, $K_{v,b1} = K_{v,b2} = K_{v,b}$), Eqs.(9)-(10) can be further simplified as follows:

$$K_{\theta,c} \approx z^2 \cdot K_{ax,c} \cdot s_c^2 \quad (11)$$

$$K_{\theta,b} \approx \frac{z^2 \cdot K_{ax,b}/2}{(K_{ax,b}/K_{v,b}) \cdot s_b^2 + c_b^2} \quad (12)$$

2.2 FORCES IN THE RODS

The forces in each rod can also be determined by use of the component method [4]. The rods on the column-side are mainly axially loaded and the forces are equal to:

$$\begin{Bmatrix} F_{ax,c1} \\ F_{ax,c2} \end{Bmatrix} = \frac{1}{n} \cdot \begin{Bmatrix} c_{c2} + s_{c2} \cdot z/(2 \cdot L_v) \\ c_{c1} \cdot s_{c2} + c_{c2} \cdot s_{c1} \\ c_{c1} - s_{c1} \cdot z/(2 \cdot L_v) \\ c_{c1} \cdot s_{c2} + c_{c2} \cdot s_{c1} \end{Bmatrix} \cdot \frac{M}{z} \quad (13)$$

$$\begin{Bmatrix} F_{ax,c3} \\ F_{ax,c4} \end{Bmatrix} = -\frac{1}{n} \cdot \begin{Bmatrix} c_{c4} - s_{c4} \cdot z/(2 \cdot L_v) \\ c_{c3} \cdot s_{c4} + c_{c4} \cdot s_{c3} \\ c_{c3} + s_{c3} \cdot z/(2 \cdot L_v) \\ c_{c3} \cdot s_{c4} + c_{c4} \cdot s_{c3} \end{Bmatrix} \cdot \frac{M}{z} \quad (14)$$

On the beam-side, the rods are subjected to combined axial and lateral loading [4]:

$$\begin{Bmatrix} F_{ax,b1} \\ F_{v,b1} \end{Bmatrix} = \frac{1}{n} \cdot \begin{Bmatrix} c_{b1} + s_{b1} \cdot z/(2 \cdot L_v) \\ -s_{b1} + c_{b1} \cdot z/(2 \cdot L_v) \end{Bmatrix} \cdot \frac{M}{z} \quad (15)$$

$$\begin{Bmatrix} F_{ax,b2} \\ F_{v,b2} \end{Bmatrix} = -\frac{1}{n} \cdot \begin{Bmatrix} c_{b2} + s_{b2} \cdot z/(2 \cdot L_v) \\ -s_{b2} + c_{b2} \cdot z/(2 \cdot L_v) \end{Bmatrix} \cdot \frac{M}{z} \quad (16)$$

Eqs.(13)-(16) can be used in the corresponding design checks for the rods, see also Section 3. The parameter n is the number of planes of rods.

2.3 PANEL ZONE

Horizontal forces result in high shear stresses in the panel zone of the column, i.e. the region between rods c1-c2 and c3-c4. Moreover, stresses perpendicular to grain occur around the threaded rods. The combination of tensile stresses perpendicular to grain and shear stresses is unfavourable due to their high degree of interaction [5] and may cause fracture in the panel zone, as shown in Figure 3. Thus, the panel zone must be designed with sufficient strength against combined shear and tension perpendicular to grain. If the rods are long and cross the entire height of the column they act as reinforcements [6], increasing the capacity of the panel zone.

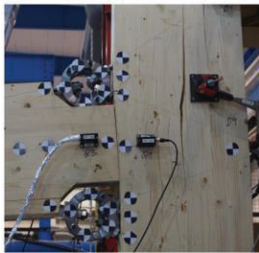


Figure 3: Fracture in the panel zone due to combined shear and tension perpendicular to grain (Photo: [2])

3 FASTENER PROPERTIES

The properties of threaded rods are necessary inputs for the properties of the entire connection. The axial stiffness of a threaded rod is given by:

$$K_{ax} = \frac{K_{ser,ax} \cdot K_{ax,l0}}{K_{ser,ax} + K_{ax,l0}} \quad (17)$$

where $K_{ser,ax}$ is the withdrawal stiffness and $K_{ax,l0}$ is the axial stiffness of the non-embedded part of the rod:

$$K_{ax,l0} = A_{net} \cdot E_s / l_0 \quad (18)$$

where $E_s = 210000$ N/mm² is the modulus of elasticity of steel, A_{net} is the net cross-sectional area and l_0 is the non-embedded length of the rod. Eq.(19) provides an approximation for $K_{ser,ax}$ (in N/mm) as function of the outer-thread diameter d (in mm), the rod-to-grain angle α , the mean density ρ_m (in kg/m³) and the embedment length l (in mm). Eq.(19) was derived in [7] by use of non-linear regression on experimental results for threaded rods with diameters 16-20 mm embedded in softwood, see [8-10].

$$K_{ser,ax} \approx \frac{50000 \cdot \left(\frac{d}{20}\right)^2 \cdot \left(\frac{\rho_m}{470}\right)^2 \cdot k_{length,K}}{0.40 \cdot \cos^{2.3}\alpha + \sin^{2.3}\alpha} \quad (19)$$

$$k_{length,K} = \min\left[\left(l/300\right)^{3/4}, 1\right] \quad (20)$$

The stiffness of a laterally loaded threaded rod can be determined by Eq.(21). Eq.(21) is derived by modelling the rod as a beam on elastic foundation assuming that rotation is restrained at the loading point, see in detail [7]:

$$K_v = \frac{3 \cdot k_v \cdot l_{ch}}{\lambda_0^3 + 3 \cdot \lambda_0^2 + 3 \cdot \lambda_0 + 3} \quad (21)$$

$$\lambda_0 = l_0 / l_{ch} ; l_{ch} = \sqrt[4]{4 \cdot E_s \cdot I_s / k_v} \quad (22)$$

The parameter $I_s \approx \pi \cdot d_1^4 / 64$ is the 2nd moment of area and d_1 is the core diameter of the rod. The parameter k_v is the foundation modulus (i.e. stiffness per unit length) of a laterally loaded rod. According to Eqs.(3),(6),(7) and (12), the lateral stiffness of a rod is an input parameter for the rotational stiffness on the beam-side. There the rods are inserted at small angles to grain and therefore the lateral foundation modulus may be approximately taken as the foundation modulus perpendicular to the grain. Based on an experimental study of laterally loaded rods with $d = 22$ mm embedded in glulam made of pine and spruce [11] an approximate value of $k_v \approx 300$ N/mm² may be used.

A power criterion is often used - as an approximation - to determine the capacity of fasteners subjected to combined axial force (F_{ax}) and lateral force (F_v), i.e.:

$$\left(\frac{F_{ax}}{F_{ax,R}}\right)^q + \left(\frac{F_v}{F_{v,R}}\right)^q \leq 1 \quad (23)$$

In Eq.(23), $F_{ax,R}$ and $F_{v,R}$ are the axial and lateral capacity of a fastener respectively. According to EN 1995-1-1 [12], a quadratic failure criterion applies for screws, i.e. $q = 2$. The quadratic criterion has provided safe-sided predictions for long screws (i.e. with steel failure being

more critical than withdrawal) inserted perpendicular to grain [13] and for glued-in rods parallel to grain [14]. The rods on the beam side are subjected to both lateral and axial forces and therefore their capacity should be checked by use of a criterion that considers the interaction of forces, as the one given by Eq.(23). On the other hand, the rods in the column are mainly axially loaded (i.e. $F_{v,ci} \approx 0$) as explained in Section 1 and therefore in this case Eq.(23) reduces to: $|F_{ax,ci}| \leq F_{ax,R}$.

4 STIFFNESS VARIABILITY EFFECTS

MRTFs are statically indeterminate systems, and the distribution of the internal actions depends on the stiffness of their elements and connections. The internal forces and moments are typically determined by use of mean stiffness values in the structural analysis. However, the inherent variability of the connection stiffness can result in variations of internal forces and moments, compared to the expected values obtained by use of mean stiffness values. In this section, the effects of connection stiffness variability are explored by use of a simple beam model with semi-rigid end restrains (Section 4.1) and by linear-elastic Finite Element simulations of MRTFs with semi-rigid moment connections (Section 4.2).

4.1 BEAM MODEL

A beam with semi-rigid end restrains (Figure 4) subjected to uniformly distributed load q is used here -as a simple example- to study the effects of the connections' stiffness variability. The connections are represented by linear-elastic rotational springs with spring constants $K_{\theta,1}$ and $K_{\theta,2}$ which can be expressed in dimensionless form-by dividing by the beam stiffness-as follows:

$$k_1 = \frac{K_{\theta,1}}{(EI/L)} ; k_2 = \frac{K_{\theta,2}}{(EI/L)} \quad (24)$$

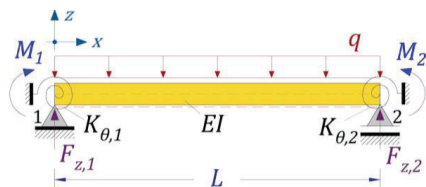


Figure 4: Simply supported beam with semi-rigid end restrains

The moments and the vertical forces at the beam ends can be expressed as functions of k_1 and k_2 as follows:

$$M_1 = -\frac{q \cdot L^2}{12} \cdot \frac{k_1 \cdot (k_2 + 6)}{k_1 \cdot k_2 + 4 \cdot (k_1 + k_2) + 12} \quad (25)$$

$$F_{z,1} = \frac{q \cdot L}{2} \cdot \frac{k_1 \cdot k_2 + 5 \cdot k_1 + 3 \cdot k_2 + 12}{k_1 \cdot k_2 + 4 \cdot (k_1 + k_2) + 12} \quad (26)$$

$$M_2 = -\frac{q \cdot L^2}{12} \cdot \frac{k_2 \cdot (k_1 + 6)}{k_1 \cdot k_2 + 4 \cdot (k_1 + k_2) + 12} \quad (27)$$

$$F_{z,2} = \frac{q \cdot L}{2} \cdot \frac{k_1 \cdot k_2 + 3 \cdot k_1 + 5 \cdot k_2 + 12}{k_1 \cdot k_2 + 4 \cdot (k_1 + k_2) + 12} \quad (28)$$

The maximum span moment can be simply written as function of the forces and moments:

$$M_{span} = M_1 + \frac{F_{z,1}^2}{2 \cdot q} = M_2 + \frac{F_{z,2}^2}{2 \cdot q} \quad (29)$$

By letting $k_1 = k_2 = k_{mean}$, the moments and the reactions at the supports become equal ($M_1 = M_2 = M_{end}$ and $F_{z,1} = F_{z,2} = F_z$):

$$M_{end}(k_1 = k_2 = k_{mean}) = -\frac{q \cdot L^2}{12} \cdot \frac{k_{mean}}{k_{mean} + 2} \quad (30)$$

$$F_z(k_1 = k_2 = k_{mean}) = \frac{q \cdot L}{2} \quad (31)$$

$$M_{span}(k_1 = k_2 = k_{mean}) = \frac{q \cdot L^2}{24} \cdot \frac{k_{mean} + 6}{k_{mean} + 2} \quad (32)$$

For each realization of the connections' stiffness, the ratios between the actual action divided by the corresponding values by use of mean stiffness values were calculated, as specified by Eqs.(33)-(37). These ratios express the deviation between a realization (numerator) and the corresponding value obtained by static analysis by use of mean stiffness (denominator) and they depend only on the normalized stiffness values given by Eq.(24).

$$n_{M,end,1} = \frac{|M_1(k_1, k_2)|}{|M_{end}(k_1 = k_2 = k_{mean})|} \quad (33)$$

$$n_{M,end,2} = \frac{|M_2(k_1, k_2)|}{|M_{end}(k_1 = k_2 = k_{mean})|} \quad (34)$$

$$n_{M,span} = \frac{M_{span}(k_1, k_2)}{M_{span}(k_1 = k_2 = k_{mean})} \quad (35)$$

$$n_{v,end,1} = \frac{F_{z,1}(k_1, k_2)}{F_z(k_1 = k_2 = k_{mean})} \quad (36)$$

$$n_{v,end,2} = \frac{F_{z,2}(k_1, k_2)}{F_z(k_1 = k_2 = k_{mean})} \quad (37)$$

In other words, the ratios by Eqs.(33)-(37) multiplied by the internal forces and moments by use of mean stiffness provide the actual internal forces and moments. Therefore, to get an indication of the unfavourable effect of stiffness variability on the internal forces and moments, it makes sense to consider an upper percentile value of these ratios, e.g. the 95th or 98th percentile. Thus, the variability of the ratios by Eqs.(33)-(37) is important.

To study the effects of stiffness variability, realizations of normalized stiffness values k_1 and k_2 were generated. Note that the variability of parameters k_1 and k_2 results from the variability of the properties of the connection (K_{θ}) and the material (E). Here, for simplicity k_1 and k_2 were assumed as the random variables instead of K_{θ} and E separately. Due to the lack of data with respect to the distribution of the connection stiffness K_{θ} , two different distributions were assumed: namely normal and

lognormal distribution. Figure 6 shows an example of the distribution of the ratio $n_{M,end}$ (Eq.(33) or Eq.(34)) assuming that k_1 and k_2 are either normally or lognormally distributed. The distribution of the output variable $n_{M,end}$ is fairly similar for both assumptions. This observation holds true for relatively small values of k_{mean} and $CoV(k)$ and for the other output variables ($n_{M,span}$ or $n_{V,end}$) with some small deviations.

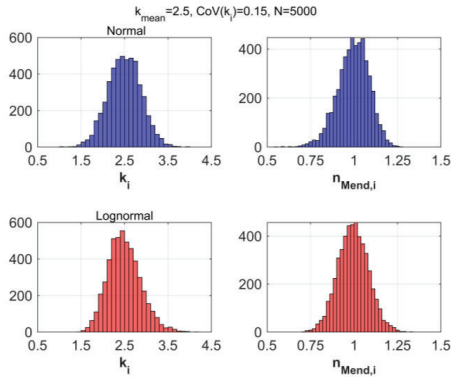


Figure 5: Distribution of $n_{M,end}$ (right) for normal (up-left) and lognormal (bottom-left) distribution of k_1 and k_2 (example here for $k_{mean} = 2.5$ and $CoV(k) = 0.15$)

Given that the distribution of the output variables (Eqs.(33)-(37)) is fairly similar for either normal or lognormal distribution of the input variables k_1 and k_2 , only results assuming normal distribution of k_1 and k_2 are presented further. The mean value is denoted k_{mean} and the coefficient of variation is denoted $CoV(k)$, thus:

$$k_1 = N(k_{mean}, CoV(k)) \quad (38)$$

$$k_2 = N(k_{mean}, CoV(k)) \quad (39)$$

Figure 6 shows the ratio $n_{M,end}$ according to Eq.(33) or Eq.(34) for varying values of k_{mean} based on 5000 realizations per k_{mean} -value. Figure 7 shows the corresponding results for $n_{M,span}$ (Eq.(35)) and Figure 8 for $n_{V,end}$ (Eq.(36) or Eq.(37)). All Figures are plotted for $CoV(k) = 0.15$. Such coefficient of variation has been observed for the rotational stiffness of connections with glulam beams and columns and inclined threaded rods as shown in Figure 1 [15]; however the sample size was small and this number is only used as indicative.

The 95th and the 98th percentiles are also provided in the Figures together with the theoretical estimations that correspond to normal distribution: $X_{95\%} = X_{mean} \cdot (1 + 1.645 \cdot CoV[X])$ and $X_{98\%} = X_{mean} \cdot (1 + 2.054 \cdot CoV[X])$. As shown in the Figures, these estimations are in good agreement with the percentiles of each sample.

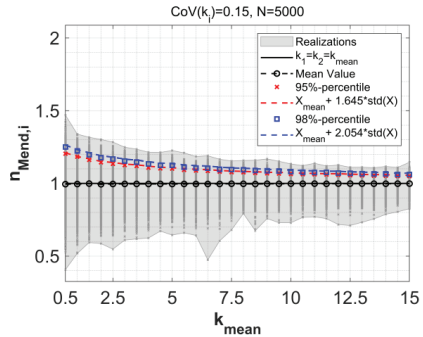


Figure 6: Ratio $n_{M,end}$ for varying k_{mean} and $CoV(k_i) = 0.15$ (5000 realizations per k_{mean} value, assuming that k_1 and k_2 are normally distributed)

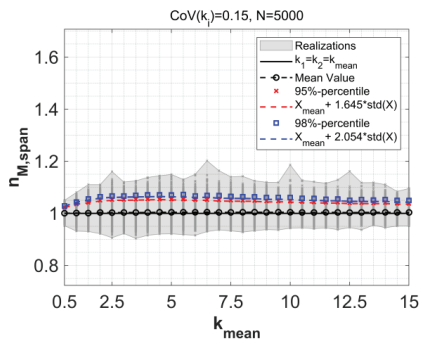


Figure 7: Ratio $n_{M,span}$ for varying k_{mean} and $CoV(k_i) = 0.15$ (5000 realizations per k_{mean} value, assuming that k_1 and k_2 are normally distributed)

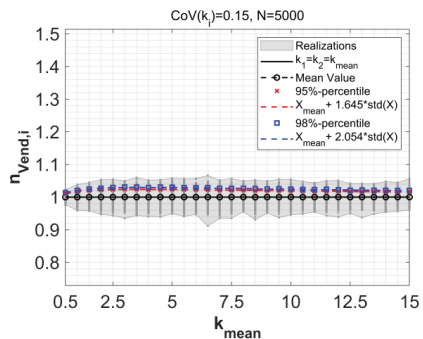


Figure 8: Ratio $n_{V,end}$ for varying k_{mean} and $CoV(k_i) = 0.15$ (5000 realizations per k_{mean} value, assuming that k_1 and k_2 are normally distributed)

As shown in Figure 6, the end moments are significantly influenced by stiffness variability, especially for low k_{mean} -values. Low mean connection stiffness values result in greater variability of the end moments. Timber moment-resisting connections are typically semi-rigid with k_{mean} -values up to maximum 5-6 and thus such

variability of the end moments is to be expected. For increasing k_{mean} -values (i.e. quasi-rigid connections) the variability and the 95th/98th percentiles of the end moments reduce significantly. On the other hand, the variabilities and the 95th/98th percentiles of the span moment (Figure 7) and the shear forces (Figure 8) are fairly small and not sensitive to k_{mean} -values.

Tables 1-3 provide the coefficient of variation and the 95th/98th percentiles of the ratios $n_{M,end}$ (Eq.(33) or Eq.(34)), $n_{M,span}$ (Eq.(35)) and $n_{V,end}$ (Eq.(36) or Eq.(37)) for varying values of k_{mean} and $CoV(k)$ based on 5000 realizations.

Table 1: Coefficient of variation, 95th and 98th percentile of ratio $n_{M,end,i}$ for different mean values and coefficients of variation of the normalized stiffness k (assuming that k is normally distributed, based on 5000 realizations)

CoV($n_{M,end,i}$)					
k_{mean}	CoV(k)				
	0.10	0.15	0.20	0.25	0.30
0.5	0.086	0.130	0.172	0.217	0.261
1	0.076	0.114	0.154	0.194	0.242
1.5	0.069	0.105	0.141	0.184	0.221
2	0.066	0.098	0.131	0.169	0.204
3	0.055	0.086	0.115	0.150	0.183
5	0.044	0.067	0.093	0.120	0.151
10	0.030	0.045	0.065	0.086	0.112
15	0.022	0.036	0.048	0.068	0.091

$n_{M,end,i,95\%}$					
k_{mean}	CoV(k)				
	0.10	0.15	0.20	0.25	0.30
0.5	1.139	1.208	1.268	1.338	1.404
1	1.118	1.178	1.232	1.283	1.348
1.5	1.110	1.162	1.208	1.259	1.305
2	1.101	1.147	1.188	1.232	1.274
3	1.086	1.127	1.166	1.203	1.241
5	1.067	1.098	1.128	1.153	1.184
10	1.044	1.064	1.087	1.105	1.131
15	1.034	1.050	1.066	1.084	1.101

$n_{M,end,i,98\%}$					
k_{mean}	CoV(k)				
	0.10	0.15	0.20	0.25	0.30
0.5	1.173	1.259	1.327	1.412	1.505
1	1.151	1.221	1.284	1.345	1.427
1.5	1.134	1.195	1.257	1.316	1.371
2	1.124	1.176	1.224	1.279	1.327
3	1.106	1.156	1.202	1.250	1.289
5	1.082	1.122	1.154	1.194	1.230
10	1.056	1.080	1.106	1.130	1.160
15	1.042	1.063	1.083	1.106	1.135

The 95th/98th percentiles of $n_{M,end}$ can be approximated by the following expressions:

$$n_{M,end,95\%} \approx 1 + 1.15 \cdot k_{mean}^{-0.35} \cdot CoV(k) \quad (40)$$

$$n_{M,end,98\%} \approx 1 + 1.40 \cdot k_{mean}^{-0.35} \cdot CoV(k) \quad (41)$$

Table 2: Coefficient of variation, 95th and 98th percentile of ratio $n_{M,span}$ for different mean values and coefficients of variation of the normalized stiffness k (assuming that k is normally distributed, based on 5000 realizations)

CoV($n_{M,span}$)					
k_{mean}	CoV(k)				
	0.10	0.15	0.20	0.25	0.30
0.5	0.009	0.013	0.018	0.022	0.026
1	0.013	0.020	0.027	0.034	0.042
1.5	0.016	0.024	0.032	0.042	0.051
2	0.018	0.027	0.036	0.046	0.056
3	0.019	0.029	0.039	0.051	0.062
5	0.018	0.028	0.040	0.052	0.064
10	0.015	0.024	0.033	0.045	0.058
15	0.012	0.019	0.026	0.037	0.052

$n_{M,span,95\%}$					
k_{mean}	CoV(k)				
	0.10	0.15	0.20	0.25	0.30
0.5	1.015	1.022	1.031	1.038	1.045
1	1.024	1.036	1.050	1.061	1.079
1.5	1.028	1.044	1.059	1.080	1.098
2	1.032	1.049	1.068	1.088	1.112
3	1.034	1.053	1.074	1.105	1.130
5	1.033	1.055	1.078	1.109	1.136
10	1.028	1.045	1.067	1.096	1.127
15	1.023	1.038	1.053	1.079	1.109

$n_{M,span,98\%}$					
k_{mean}	CoV(k)				
	0.10	0.15	0.20	0.25	0.30
0.5	1.019	1.028	1.037	1.050	1.058
1	1.029	1.045	1.063	1.078	1.104
1.5	1.035	1.055	1.075	1.107	1.127
2	1.038	1.061	1.086	1.116	1.148
3	1.044	1.069	1.097	1.133	1.172
5	1.040	1.070	1.103	1.145	1.187
10	1.036	1.060	1.092	1.132	1.188
15	1.030	1.049	1.072	1.106	1.165

The 95th/98th percentiles of $n_{M,span}$ can be approximated by the following expressions:

$$n_{M,span,95\%} \approx 1 + (1 - e^{-k_{mean}}) \cdot CoV(k)^{1.45} \quad (42)$$

$$n_{M,span,98\%} \approx 1 + (1 - e^{-k_{mean}}) \cdot \text{CoV}(k)^{1.30} \quad (43)$$

Table 3: Coefficient of variation, 95th and 98th percentile of ratio $n_{V,end,i}$ for different mean values and coefficients of variation of the normalized stiffness k (assuming that k is normally distributed, based on 5000 realizations)

CoV($n_{V,end,i}$)					
k_{mean}	CoV(k)				
	0.10	0.15	0.20	0.25	0.30
0.5	0.004	0.007	0.009	0.011	0.013
1	0.007	0.010	0.014	0.017	0.021
1.5	0.008	0.012	0.016	0.021	0.025
2	0.009	0.013	0.018	0.023	0.028
3	0.009	0.015	0.020	0.025	0.031
5	0.009	0.014	0.020	0.025	0.031
10	0.007	0.011	0.016	0.022	0.028
15	0.006	0.010	0.013	0.018	0.024

$n_{V,end,i,95\%}$					
k_{mean}	CoV(k)				
	0.10	0.15	0.20	0.25	0.30
0.5	1.007	1.011	1.014	1.018	1.022
1	1.011	1.017	1.022	1.027	1.035
1.5	1.013	1.020	1.027	1.034	1.042
2	1.015	1.022	1.030	1.038	1.045
3	1.016	1.024	1.032	1.041	1.051
5	1.015	1.023	1.031	1.040	1.051
10	1.012	1.019	1.026	1.034	1.043
15	1.010	1.015	1.022	1.029	1.037

$n_{V,end,i,98\%}$					
k_{mean}	CoV(k)				
	0.10	0.15	0.20	0.25	0.30
0.5	1.009	1.014	1.018	1.022	1.027
1	1.014	1.020	1.028	1.034	1.043
1.5	1.017	1.026	1.033	1.043	1.052
2	1.018	1.028	1.037	1.049	1.057
3	1.020	1.031	1.042	1.055	1.066
5	1.018	1.030	1.042	1.053	1.067
10	1.016	1.024	1.035	1.046	1.061
15	1.013	1.022	1.029	1.039	1.053

The 95th/98th percentiles of $n_{V,end}$ can be approximated by the following expressions:

$$n_{V,end,95\%} \approx 1 + (0.15 - e^{-5 \cdot k_{mean}}) \cdot \text{CoV}(k) \quad (44)$$

$$n_{V,end,98\%} \approx 1 + (0.20 - e^{-5 \cdot k_{mean}}) \cdot \text{CoV}(k) \quad (45)$$

The relative difference of the 95th/98th percentiles assuming lognormal distribution of the stiffness parameter k is within 6% or less compared to the values

in Tables 1-3. This is also indicated by the distribution shape of the output variables, shown in Figure 5.

As shown in the values of Tables 1-3, the ratio $n_{M,end,i}$ (Table 1) is more affected by the variability of the stiffness parameter k . In other words, the end-moments are more sensitive to the stiffness variability compared to the span moment and the shear forces. As expected, the coefficient of variation of the stiffness parameter k results in higher variability of the output variables.

To facilitate comparison, we can consider a connection with $k_{mean} = 1.5$. For $\text{CoV}(k) = 15\%$, the 98th percentile of the end moment, the span moment and the shear force are approx. 20%, 5% and 3% higher than the reference values respectively. The corresponding 98th percentile values for $\text{CoV}(k) = 30\%$ are approx. 37%, 13% and 5%. Especially for the end moments, the 98th percentiles may reach values of the order of 20-40% higher than the reference value for reasonable input ($\text{CoV}(k) \geq 15\%$ and $k_{mean} = 1 - 5$). Such effect should be considered in the design.

4.2 FINITE ELEMENT ANALYSIS OF MOMENT-RESISTING TIMBER FRAMES

The effects of connection stiffness variability are further studied in this Section by use of Finite Element (abbr. FE) analyses of planar MRTFs. The software SAP2000 was used for the structural analysis. An algorithm was developed to perform several analyses with varying properties.

The structural model for the analysis is presented in Figure 9. The frames consisted of glulam columns and beams with cross-sectional dimensions $b_c \times h_c$ and $b_b \times h_b$ respectively. The columns were continuous. The mean modulus of elasticity was $E_{0,mean} = 13000 \text{ N/mm}^2$ and the mean shear modulus was $G_{mean} = 650 \text{ N/mm}^2$. These values correspond to strength class GL30c [16]. The beams and the columns were modelled as linear elements and the material was modelled as linear-elastic. Shear deformations of timber were taken into account in the model. All frames consisted of 3 bays with 8.0m bay length between the center-lines of the columns. Frames with 4 and 8 storeys were studied. The height of each storey was $h = 3.0 \text{ m}$.

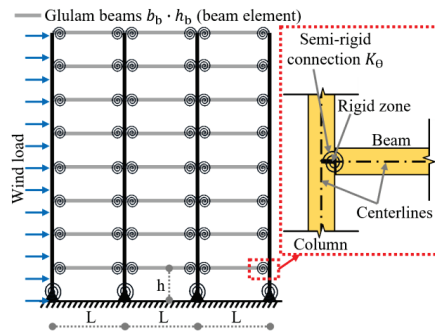


Figure 9: Structural model for FE analyses

The connections were modelled as linear-elastic rotational springs with spring constant K_θ (by use of the partial release command of SAP2000). With respect to the translational degrees of freedom, the connections were modelled as rigid. Since the columns were continuous, the connections were placed at the edge of the columns with a rigid offset of $h_c/2$ to the columns' centerline, see the detail in Figure 9. The supports of the frame were assumed rigid with respect to translations while the for the rotational degree of freedom a small rotational stiffness of 5000 kNm/rad was assumed.

Three actions were considered in the analysis: dead load ($G = 2.0 \text{ kN/m}^2$), live load ($Q = 3.0 \text{ kN/m}^2$) and the wind action W . The wind load was calculated according to EN 1991-1-4 [17] for a basic wind velocity $v_b = 26 \text{ m/s}$ and terrain category IV (urban environment). For the determination of loads on the frame and wind-induced accelerations it was assumed that the building consists of six frames equally spaced at a distance of 4.0 meters, resulting in a total width of 20 m.

To consider the connection stiffness variability, the stiffness of each beam-to-column connection was selected as a normally distributed random variable (see Eqs.(38)-(39)). Similar to the definition given by Eq.(24), the stiffness can be expressed in dimensionless form by dividing the rotational stiffness by the bending stiffness of the beams, i.e.: $k = K_\theta / (EI_b / L_b)$. Here, L_b is the net bay length. For each frame, analyses with mean dimensionless connection stiffness of $k_{mean} = 1.5$ and $k_{mean} = 2.5$ were performed. These values represent feasible connection stiffness for moment resisting connections with threaded rods (see Section 2). Moreover, they are sufficient, so that the frames fulfil the serviceability requirements with respect to wind-induced deformations and accelerations; see e.g. Figure 10 for accelerations. For each k_{mean} -value, two values of the coefficient of variation were considered: $\text{CoV}(K_\theta) = 15\%$ and 25% .

As a crude simplification, the modulus of elasticity and the shear modulus of glulam were assumed constant and equal to their mean value, i.e. their variability was not taken into account in this analysis. All other parameters (e.g. loads, mass etc.) were also kept constant. Therefore, the results of these analyses should only be considered as indicative; however, they allow for comparison with the results provided in Section 4.1. In total, 8 frames were studied (2 number of storeys \times 2 k_{mean} -values \times 2 $\text{CoV}(K_\theta)$ values). For each frame type, 3000 realizations were generated and solved by use of FE analysis (in total 24000 analyses were performed).

The following response quantities were quantified by FE analysis, for each frame:

- The internal actions were determined by use of linear-elastic analysis. The envelopes of the internal forces and moments were then determined for the fundamental Ultimate Limit State combinations according to EN1990 [18], with wind load (in both directions) being the leading variable action. The load safety factors were $\gamma_G = 1.2$ for the permanent load, $\gamma_Q = 1.5$ for the live load and $\gamma_W = 1.5$ for the wind load. The ratios between the envelope internal forces and moments for each realization divided by the

corresponding values obtained by use of analysis with mean stiffness values were determined for each frame, as specified by Eqs.(33)-(37).

- The horizontal deflections were determined for the characteristic Serviceability Limit State combination according to EN1990 [18], with wind as the leading variable load. The maximum horizontal deflection is denoted Δ and the maximum inter-storey drift is denoted IDR_{max} .
- The fundamental eigenfrequency (f) was quantified by modal analysis. The quasi-permanent load ($G + 0.3 \cdot Q$), according to EN1990 [18] was used to determine the mass.
- The wind-induced accelerations (A) on the top-floor were determined by use of the approximate method given by EN1991-1-4 [17] (Annex B). A damping ratio of $\xi = 2.0\%$ was assumed based on measurements of timber buildings [19]. The accelerations were compared to the requirements by ISO10137 [20]. To consider the smaller return period, the basic wind velocity was multiplied by $c_{prob} = 0.73$.

The results of the FE analyses are summarized in Table 4 (4 storey frames) and Table 5 (8 storey frames). The ratios $n_{M,end}$, $n_{M,span}$, $n_{V,end}$ (Eqs.(33)-(37)) were determined separately for each connection of the frame and the range is given in the Tables. As indicated by the small ranges the ratios for different connections are quite similar. The FE results can be summarized as follows:

- The end moments are -by far- the action that it is most sensitive to connection stiffness as indicated by the higher $n_{M,end}$ -values. On the other hand, the span moments and the shear forces are not very sensitive to connection stiffness as indicated by the low values of $n_{M,span}$ and $n_{V,end}$.
- The ratios $n_{M,end}$, $n_{M,span}$, $n_{V,end}$ are quite similar for 4-storey and 8-storey frames. Moreover, they are in very good agreement with the results obtained by the simple beam model in Section 4.1 (Tables 1-3). In fact, the beam model results in slightly higher values of $n_{M,end}$. Therefore, the beam model can be used to provide safe-sided predictions.
- The effect of stiffness variability on deformations, eigenfrequency and top-floor accelerations is quite small as indicated by FE results. Figure 10 shows a plot of the fundamental eigenfrequencies and top floor accelerations for all realizations of MRTFs, compared to ISO10137 [20] requirements. As shown by the results, the response of all realizations is quite similar for each frame. Therefore, the effects of the variability of connection stiffness can be neglected in the serviceability limit state.

The aim of the present -preliminary- study was to highlight the effects of connections' stiffness variability. A more detailed reliability analysis considering the variability of the loads and the material stiffness can be used to better quantify the values of ratios $n_{M,end}$, $n_{M,span}$

and $n_{V,end}$. Moreover, the presented results come solely from linear-elastic analysis; i.e. possible redistribution of moments if the connections are ductile was not considered.

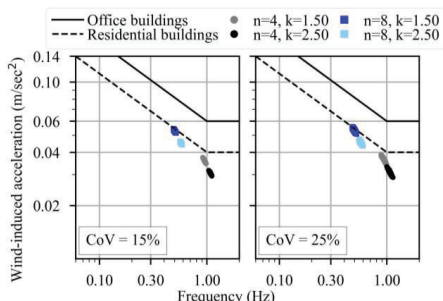


Figure 10: Fundamental eigenfrequency – top floor acceleration for all realizations of MRTFs, compared to ISO10137 [20] requirements

Table 4: FE results of 4-storey MRTFs (3000 realizations per frame)

Frame details	N = 4 storeys, h = 3.0 m, H = 12.0 m 3 bays, L = 8 m $b_c \times h_c = b_b \times h_b = 430 \times 585 \text{ mm}^2$			
	18866	18866	31443	31443
K_θ (kNm/rad)	18866	18866	31443	31443
k_{mean}	1.5	1.5	2.5	2.5
CoV(k)	15%	25%	15%	25%
CoV($n_{M,end}$)	8-9%	14-16%	6-8%	12-14%
$n_{M,end,95\%}$	1.12-1.14	1.19-1.22	1.09-1.11	1.15-1.17
$n_{M,end,98\%}$	1.15-1.17	1.23-1.27	1.11-1.14	1.18-1.21
CoV($n_{M,span}$)	≈2%	3-4%	2-3%	4-5%
$n_{M,span,95\%}$	1.03-1.05	1.06-1.09	1.04-1.05	1.08-1.10
$n_{M,span,98\%}$	1.05-1.06	1.09-1.12	1.05-1.07	1.10-1.13
CoV($n_{V,end}$)	1%	1-2%	1%	1-2%
$n_{V,end,95\%}$	1.01-1.02	1.02-1.03	1.01-1.02	1.02-1.03
$n_{V,end,98\%}$	1.02	1.03-1.05	1.02	1.03-1.05
Δ_{mean} (mm)	6.73	6.81	5.13	5.16
CoV(Δ_{max})	9%	15%	9%	16%
mean(IDR_{max}) (mm)	2.71	2.74	2.25	2.26
CoV(IDR_{max})	6%	11%	6%	11%
f_{mean} (Hz)	0.950	0.946	1.080	1.075
CoV(f)	1%	2%	1%	2%
A_{mean} (m/s ²)	0.036	0.036	0.030	0.031
CoV(A)	1%	2%	1%	2%

Table 5: FE results of 8-storey MRTFs (3000 realizations per frame)

Frame details	N = 8 storeys, h = 3.0 m, H = 24.0 m 3 bays, L = 8 m $b_c \times h_c = b_b \times h_b = 430 \times 585 \text{ mm}^2$			
	18866	18866	31443	31443
K_θ (kNm/rad)	18866	18866	31443	31443
k_{mean}	1.5	1.5	2.5	2.5
CoV(k)	15%	25%	15%	25%
CoV($n_{M,end}$)	8-9%	14-16%	6-8%	12-14%
$n_{M,end,95\%}$	1.11-1.14	1.19-1.23	1.09-1.11	1.14-1.18
$n_{M,end,98\%}$	1.14-1.17	1.23-1.27	1.11-1.13	1.17-1.22
CoV($n_{M,span}$)	≈2%	3-5%	2-3%	4-5%
$n_{M,span,95\%}$	1.03-1.06	1.07-1.12	1.04-1.07	1.08-1.13
$n_{M,span,98\%}$	1.04-1.08	1.09-1.15	1.05-1.08	1.10-1.17
CoV($n_{V,end}$)	≈1%	1-2%	≈1%	≈2%
$n_{V,end,95\%}$	1.01-1.02	1.02-1.03	1.01-1.02	1.02-1.03
$n_{V,end,98\%}$	1.02	1.03-1.04	1.02	1.03-1.04
Δ_{mean} (mm)	35.26	35.70	26.39	26.69
CoV(Δ_{max})	3%	5%	3%	5%
mean(IDR_{max}) (mm)	8.49	8.55	6.84	6.92
CoV(IDR_{max})	3%	5%	3%	5%
f_{mean} (Hz)	0.501	0.498	0.577	0.574
CoV(f)	1%	1%	1%	1%
A_{mean} (m/s ²)	0.053	0.053	0.045	0.045
CoV(A)	1%	1%	1%	1%

5 CONCLUSIONS AND FUTURE WORK

This paper provides an overview of analysis and design aspects of moment-resisting connections with inclined threaded rods. In the first part of the paper, a series of expressions that estimate the properties of such connections were provided based on recent publications. In the second part of the paper, a preliminary study on the effect of connections' stiffness variability on the structural response of timber frames was presented, based on a simple beam model and Finite Element simulations of planar frames. In common practice, structural analysis of timber structures is performed by use of mean stiffness values. However, in moment-resisting frames the magnitude and distribution of internal forces and moment is highly dependent on the stiffness of their connections. The results of this study have shown that the variability of connections' stiffness can result in great variability of the internal forces and moments. The end moments are more sensitive to this effect with 98th percentiles of the order of 20%-40% higher than the reference values obtained by analysis with mean stiffness values. Such increase should be considered in the design for the Ultimate Limit State. The Finite element results were in good agreement with the predictions obtained by use of a simple beam model

with rotational springs. When it comes to serviceability requirements, the FE models showed that the variability of connections' stiffness has small influence and may be neglected.

REFERENCES

- [1] A. Vilguts, H. Stamatopoulos, and K. A. Malo, "Parametric analyses and feasibility study of moment-resisting timber frames under service load," *Engineering Structures*, vol. 228, p. 111583, 2021/02/01/ 2021, doi: <https://doi.org/10.1016/j.engstruct.2020.111583>.
- [2] K. Lied and K. Nordal, "A conceptual study of glulam connections using threaded rods and connecting circular steel profiles," in "Master thesis," NTNU Norwegian University of Science and Technology, Trondheim, Norway, 2016.
- [3] A. Vilguts, S. Ø. Nesheim, H. Stamatopoulos, and K. A. Malo, "A study on beam-to-column moment-resisting timber connections under service load, comparing full-scale connection testing and mock-up frame assembly," *European Journal of Wood and Wood Products*, vol. 80, no. 4, pp. 753-770, 2022/08/01 2022, doi: 10.1007/s00107-021-01783-2.
- [4] H. Stamatopoulos, K. A. Malo, and A. Vilguts, "Moment-resisting beam-to-column timber connections with inclined threaded rods: Structural concept and analysis by use of the component method," *Construction and Building Materials*, vol. 322, p. 126481, 2022, doi: <https://doi.org/10.1016/j.conbuildmat.2022.126481>.
- [5] R. Steiger and E. Gehri, "Interaction of shear stresses and stresses perpendicular to grain," presented at the Proceedings of the 44th CIB-W18 meeting, Alghero, Italy, 2011.
- [6] P. Dietsch, H. Kreuzinger, and S. Winter, "Design of shear reinforcement for timber beams," presented at the Proceedings of the 46th CIB-W18 meeting Vancouver, Canada, 2013.
- [7] H. Stamatopoulos and K. A. Malo, "On strength and stiffness of screwed-in threaded rods embedded in softwood," *Construction and Building Materials*, vol. 261, p. 119999, 2020/11/20/ 2020, doi: <https://doi.org/10.1016/j.conbuildmat.2020.119999>.
- [8] H. J. Blaß and O. Krüger, *Schubverstärkung von Holz mit Holzschrauben und Gewindestangen*. Karlsruhe: KIT Scientific Publishing, 2010.
- [9] H. Stamatopoulos and K. A. Malo, "Withdrawal stiffness of threaded rods embedded in timber elements," *Construction and Building Materials*, vol. 116, pp. 263-272, 2016, doi: <http://dx.doi.org/10.1016/j.conbuildmat.2016.04.144>.
- [10] H. Stamatopoulos and K. A. Malo, "Withdrawal capacity of threaded rods embedded in timber elements," *Construction and Building Materials*, vol. 94, pp. 387-397, 2015, doi: <http://dx.doi.org/10.1016/j.conbuildmat.2015.07.067>.
- [11] H. Stamatopoulos, F. M. Massaro, and J. Qazi, "Mechanical properties of laterally loaded threaded rods embedded in softwood," *European Journal of Wood and Wood Products*, 2021/09/15 2021, doi: 10.1007/s00107-021-01747-6.
- [12] CEN, "NS-EN 1995-1-1:2004+A1:2008+A2:2014+NA:2010," in *Design of timber structures - Part 1-1: General - Common rules and rules for buildings*, ed. Brussels: European committee for standardization, 2004.
- [13] T. Laggner, G. Flatscher, and G. Schickhofer, "Combined loading of self-tapping screws," presented at the Proceedings of WCTE 2016 - World Conference on Timber Engineering, Vienna, Austria, 2016.
- [14] S. Aicher and K. Simon, "Rigid Glulam Joints with Glued-in Rods subjected to Axial and Lateral Force Action," presented at the Proceedings of the 8th INTER meeting Karlsruher Institut für Technologie (KIT), 2021.
- [15] A. Vilguts, "Moment-resisting timber frames with semi-rigid connections," Ph.D. Thesis, Department of Structural Engineering, Norwegian University of Science and Technology, Trondheim, Norway, 2021.
- [16] CEN, "EN 14080-2013: Timber structures- Glued laminated timber and glued solid timber - Requirements," ed. Brussels, Belgium: European Committee for Standardization, 2013.
- [17] CEN, "NS-EN 1991-1-4:2005+NA:2009," in *Actions on structures - Part 1-4: General actions - Wind actions*, ed. Brussels, Belgium: European Committee for Standardization, 2009.
- [18] CEN, "NS-EN 1990:2002+A1:2005+NA:2016," in *Basis of structural design*, ed. Brussels, Belgium: European Committee for Standardization, 2016.
- [19] A. Feldmann *et al.*, "Dynamic properties of tall timber structures under wind-induced vibration," presented at the Proceedings of WCTE 2016 - World Conference on Timber Engineering, Vienna, Austria, 2016.
- [20] ISO, International Organization for standardization, "ISO10137: Bases for design of Structures - Serviceability of Buildings and Walkways against Vibrations," ed. Geneva, Switzerland: ISO, 2007.

Part III
Appendices

Appendix A

Analytical modelling of moment-resisting timber connection with inclined threaded rods

Configuration A

This configuration corresponds to tests 1, 3, and 4 presented in subsection 4.3.3.

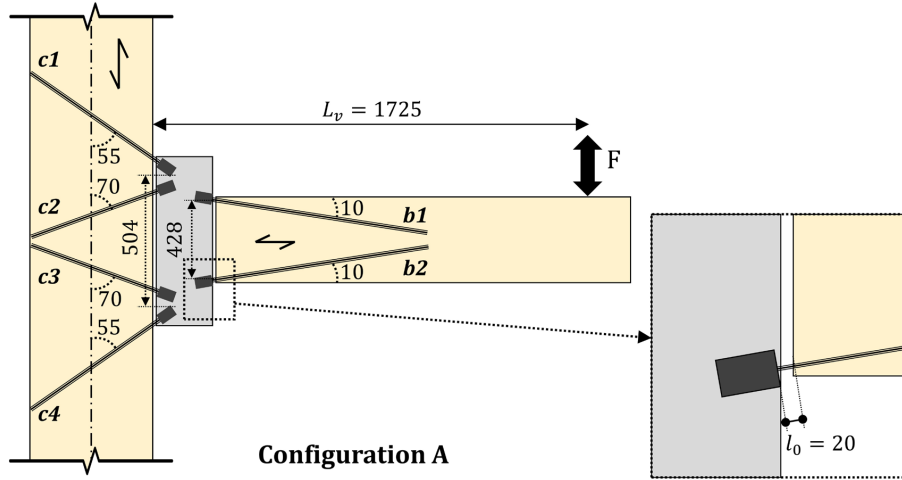


Figure III.1 Configuration A (dimensions are in mm and angles are in degrees)

The axial stiffness (K_{ax}) of the rods was taken from the results of the withdrawal tests presented in 4.4.2. As an approximation, the stiffness of rods perpendicular to grain was used for the rods in the column ($c1$, $c2$, $c3$, and $c4$), and the stiffness of rods parallel to grain was used for the rods in the beam ($b1$, $b2$).

The experiments conducted on rods inserted parallel and perpendicular to grain has shown that their axial stiffness converges beyond a penetration length of $10d$ - $15d$. Therefore, the axial stiffness of rods inserted at $20d$ was deemed representative for the longer rods used in the column and the beam.

The axial stiffness of the threaded rods under fully reversed cyclic loading was used as the axial stiffness:

$$K_{ax,c1} = K_{ax,c2} = K_{ax,c3} = K_{ax,c4} \approx 110 \text{ kN/mm} ; K_{ax,b1} = K_{ax,b2} \approx 122 \text{ kN/mm}$$

The lateral stiffness (K_v) of the threaded rods can be estimated using the following equations:

$$K_v = \frac{3 \cdot k_v \cdot l_{ch}}{\lambda_0^3 + 3 \cdot \lambda_0^2 + 3 \cdot \lambda_0 + 3} \quad (III.1)$$

$$\lambda_0 = l_0/l_{ch} ; l_{ch} = \sqrt[4]{4 \cdot E_s \cdot I_s/k_v} \quad (III.2)$$

where $I_s \approx \pi \cdot d_1^4/64$ is the 2nd moment of area and d_1 is the core diameter of the rod, E_s is the elastic modulus of the rod (210000 N/mm²), l_0 is the free length of the rod (20 mm, see Figure III.1), and k_v is the foundation modulus (i.e. stiffness per unit length) of a laterally-loaded rod.

An approximate value of 300 N/mm² can be used for the foundation modulus. This value corresponds to the foundation modulus perpendicular to the grain. It is based on an experimental study of laterally-loaded threaded rods with $d=22$ mm, embedded in glulam made of pine and spruce [1].

Substituting in Eqs. (III.1) and (III.2):

$$I_s = \pi \cdot 16.1^4/64 = 3298 \text{ mm}^4 \rightarrow l_{ch} = \sqrt[4]{4 \cdot 210000 \cdot 3298/300} = 55.1 \text{ mm}$$

$$\lambda_0 = 20/55.1 = 0.36 \rightarrow K_v = \frac{3 \cdot 300 \cdot 55.1}{0.36^3 + 3 \cdot 0.36^2 + 3 \cdot 0.36 + 3} = 10950 \text{ N/mm}$$

$$K_v \approx 11 \text{ kN/mm}$$

For *configuration A*, the required input parameters can be summarized as follows:

$z_b = 428 \text{ mm}$	$z_c = 504 \text{ mm}$	$\alpha_{c1} = \alpha_{c4} = 55^\circ$	$\alpha_{c2} = \alpha_{c3} = 70^\circ$
$\alpha_{b1} = \alpha_{b2} = 10^\circ$	$L_v = 1725 \text{ mm}$	$K_{v,b1} = K_{v,b2} \approx 11 \text{ kN/mm}$	
$K_{ax,c1} = K_{ax,c2} = K_{ax,c3} = K_{ax,c4} \approx 110 \text{ kN/mm}$			
$K_{ax,b1} = K_{ax,b2} \approx 122 \text{ kN/mm}$			

a-Beam side stiffness:

- The compliance terms for the beam side (substituting in Eqs. (I.10) and (I.11)):

$$S_{xx,b1} = S_{xx,b2} = \sin(10)^2/11 + \cos(10)^2/122 = 0.01069 \text{ mm/kN}$$

$$S_{xy,b1} = \sin(10) \cdot \cos(10) \cdot (1/11 - 1/122) = 0.01414 \text{ mm/kN}$$

$$S_{xy,b2} = \sin(10) \cdot \cos(10) \cdot (1/122 - 1/11) = -0.01414 \text{ mm/kN}$$

- The beam side stiffness (substituting in Eq. (I.9)):

$$K_{\theta,b} = \frac{428^2}{(0.01069 + 0.01069) + (-0.01414 - 0.01414) \cdot 428/(2 \cdot 1725)}$$

$$= 10249,721 \text{ kNm/rad} \rightarrow 10250 \text{ kNm/rad (1 plane of rods)}$$

$$\rightarrow 20500 \text{ kNm/rad (2 planes of rods)}$$

The measured beam side stiffness under fully reversed loading for tests 1, 3, and 4 are 29008 kNm/rad, 23916 kNm/rad, and 22113 kNm/rad, respectively. The calculated stiffness using the analytical expressions is 7%-29% softer than the measured stiffness from the full-scale tests.

- Using the simplification by Eq. (I.13):

$$K_{\theta,b} \approx \frac{428^2 \cdot 122/2}{(122/11) \cdot \sin(10)^2 + \cos(10)^2} \approx 8567,363 \text{ kNm/rad}$$

$$\rightarrow 8567 \text{ kNm/rad (1 plane of rods)}$$

$$\rightarrow 17135 \text{ kNm/rad (2 planes of rods)}$$

b-Column side stiffness:

- The compliance terms for the column side (substituting in Eqs. (I.15) and (I.16)):

$$S_{xx,c}^{(c1-c2)} = S_{xx,c}^{(c3-c4)} = \frac{\cos(55)^2/110 + \cos(70)^2/110}{(\cos(55) \cdot \sin(70) + \cos(70) \cdot \sin(55))^2} = 0.00604 \text{ mm/kN}$$

$$S_{xy,c}^{(c1-c2)} = \frac{\cos(55) \cdot \sin(55)/110 - \cos(70) \cdot \sin(70)/110}{(\cos(55) \cdot \sin(70) + \cos(70) \cdot \sin(55))^2} = 0.00201 \text{ mm/kN}$$

$$S_{xy,c}^{(c3-c4)} = \frac{\cos(70) \cdot \sin(70)/110 - \cos(55) \cdot \sin(55)/110}{(\cos(70) \cdot \sin(55) + \cos(55) \cdot \sin(70))^2} = -0.00201 \text{ mm/kN}$$

- The column side stiffness (substituting in Eq. (I.14)):

$$K_{\theta,c} = \frac{504^2}{(0.00604 + 0.00604) + (-0.00201 - 0.00201) \cdot 504/(2 \cdot 1725)}$$

$$= 22095,279 \text{ kNm/rad} \rightarrow 22095 \text{ kNm/rad (1 plane of rods)}$$

$$\rightarrow 44190 \text{ kNm/rad (2 planes of rods)}$$

The measured column side stiffness under fully reversed loading for tests 1, 3, and 4 are 42289 kNm/rad, 40160 kNm/rad, and 45607 kNm/rad, respectively. The

calculated stiffness using the analytical expressions is 3%-10% different from the measured stiffness from the full-scale tests.

- Using the simplification by Eq. (I.17):

$$K_{\theta,c} \approx \frac{504^2}{(0.00604 + 0.00604)} \approx 21027,815 \text{ kNm/rad}$$

$$\rightarrow 21028 \text{ kNm/rad (1 plane of rods)}$$

$$\rightarrow 42056 \text{ kNm/rad (2 planes of rods)}$$

c-The connection stiffness:

$$K_{\theta,con} = \left(1/K_{\theta,c} + 1/K_{\theta,plate} + 1/K_{\theta,b}\right)^{-1}$$

$K_{\theta,plate} \approx 300000 \text{ kNm/rad}$ (estimated by use of FEA and confirmed with the measured stiffness from the full-scale tests).

The stiffness of the connection considering 2 planes of rods:

$$K_{\theta,con} = \left(\frac{1}{44190} + \frac{1}{300000} + \frac{1}{20500}\right)^{-1} = 13379 \text{ kNm/rad}$$

The measured connection stiffness under fully reversed loading for tests 1, 3, and 4 are 15836 kNm/rad, 14486 kNm/rad, and 13762 kNm/rad, respectively. The calculated stiffness using the analytical expressions is 3%-16% softer than the measured stiffness from the full-scale tests.

The stiffness of the connection using the stiffness values obtained with the simplified expressions:

$$K_{\theta,con} = \left(\frac{1}{42056} + \frac{1}{300000} + \frac{1}{17135}\right)^{-1} = 11700 \text{ kNm/rad}$$

Configuration B

This configuration corresponds to test 2 presented in subsection 4.3.3.

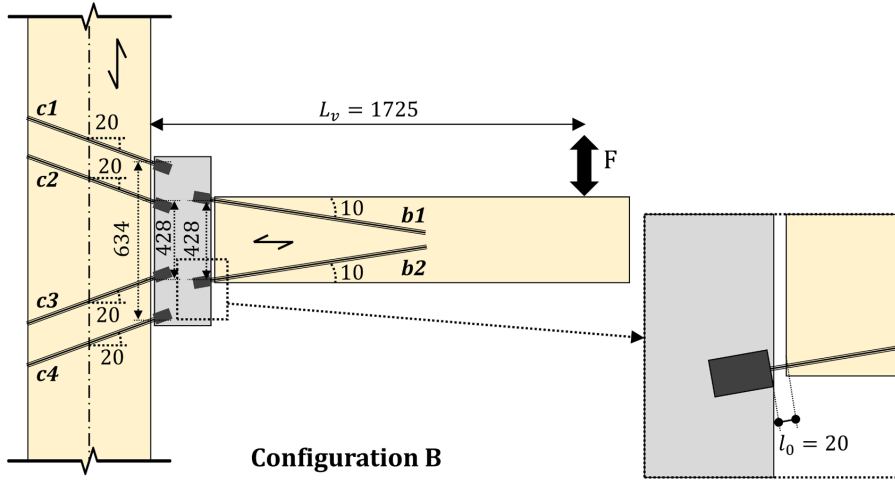


Figure III.2 Configuration B (dimensions are in mm and angles are in degrees)

The axial stiffness (K_{ax}) of the rods in the column ($c1$, $c2$, $c3$, and $c4$) and in the beam are the same as *configuration A*:

$$K_{ax,c1} = K_{ax,c2} = K_{ax,c3} = K_{ax,c4} \approx 110 \text{ kN/mm} ; K_{ax,b1} = K_{ax,b2} \approx 122 \text{ kN/mm}$$

The lateral stiffness of threaded rods in the beam is the same as *configuration A*:

$$K_{v,b1} = K_{v,b2} \approx 11 \text{ kN/mm}$$

The lateral stiffness of threaded rods in the column was calculated using a foundation modulus of 500 N/mm^2 ($l_0=20 \text{ mm}$). This value corresponds to the foundation modulus parallel to the grain. It is based on an experimental study of laterally-loaded threaded rods with $d=22 \text{ mm}$ embedded in glulam made of pine and spruce [1].

$$K_{v,c1} = K_{v,c2} = K_{v,c3} = K_{v,c4} \approx 15 \text{ kN/mm}$$

For *configuration B*, the required inputs can be summarized as follows:

$z_b = 428 \text{ mm}$	$z_{c1-c4} = 634 \text{ mm}$	$z_{c2-c3} = 428 \text{ mm}$
$L_v = 1725 \text{ mm}$	$\alpha_{b1} = \alpha_{b2} = 10^\circ$	$\theta_{c1} = \theta_{c2} = \theta_{c3} = \theta_{c4} = 20^\circ$
$K_{v,b1} = K_{v,b2} \approx 11 \text{ kN/mm}$		$K_{v,c1} = K_{v,c2} = K_{v,c3} = K_{v,c4} \approx 15 \text{ kN/mm}$
$K_{ax,c1} = K_{ax,c2} = K_{ax,c3} = K_{ax,c4} \approx 110 \text{ kN/mm}$		
$K_{ax,b1} = K_{ax,b2} \approx 122 \text{ kN/mm}$		

a-Beam side stiffness:

- The compliance terms for the beam side (substituting in Eqs. (I.10) and (I.11)):

$$S_{xx,b1} = S_{xx,b2} = \sin(10)^\circ/11 + \cos(10)^\circ/122 = 0.01069 \text{ mm/kN}$$

$$S_{xy,b1} = \sin(10) \cdot \cos(10) \cdot (1/11 - 1/122) = 0.01414 \text{ mm/kN}$$

$$S_{xy,b2} = \sin(10) \cdot \cos(10) \cdot (1/122 - 1/11) = -0.01414 \text{ mm/kN}$$

- The beam side stiffness (substituting in Eq. (I.9)):

$$K_{\theta,b} = \frac{428^2}{(0.01069 + 0.01069) + (-0.01414 - 0.01414) \cdot 428/(2 \cdot 1725)}$$

$$= 10249,721 \text{ kNmm/rad} \rightarrow 10250 \text{ kNm/rad (1 plane of rods)}$$

$$\rightarrow 20500 \text{ kNm/rad (2 planes of rods)}$$

The measured beam side stiffness under fully reversed loading for test 2 is 18725 kNm/rad. The calculated stiffness using the analytical expressions is 9% stiffer than the measured stiffness from the full-scale tests.

- Using the simplification by Eq. (I.13):

$$K_{\theta,b} \approx \frac{428^2 \cdot 122/2}{(122/11) \cdot \sin(10)^\circ + \cos(10)^\circ} \approx 8567,363 \text{ kNmm/rad}$$

$$\rightarrow 8567 \text{ kNm/rad (1 plane of rods)}$$

$$\rightarrow 17135 \text{ kNm/rad (2 planes of rods)}$$

b-Column side stiffness:

- The compliance terms for the column side (substituting in Eqs. (I.22)-(I.25)).

$$S_{xx,c1} = S_{xx,c2} = S_{xx,c3} = S_{xx,c4} = \sin(20)^2/15 + \cos(20)^2/110 = 0.01583 \text{ mm/kN}$$

$$S_{xy,c1} = S_{xy,c2} = \sin(20) \cdot \cos(20) \cdot (1/15 - 1/110) = 0.01850 \text{ mm/kN}$$

$$S_{xy,c3} = S_{xy,c4} = \sin(20) \cdot \cos(20) \cdot (1/110 - 1/15) = -0.01850 \text{ mm/kN}$$

- The column side stiffness (substituting in Eqs. (I.19)-(I.21)):

$$K_{\theta}^{(c1-c4)} = \frac{634^2}{(0.01583 + 0.01583) + (-0.01850 - 0.01850) \cdot 634/(2 \cdot 1725)}$$
$$= 16174,696 \text{ kNmm/rad} \rightarrow 16175 \text{ kNm/rad}$$

$$K_{\theta}^{(c2-c3)} = \frac{428^2}{(0.01583 + 0.01583) + (-0.01850 - 0.01850) \cdot 428/(2 \cdot 1725)}$$
$$= 6769,367 \text{ kNmm/rad} \rightarrow 6769 \text{ kNm/rad}$$

$$K_{\theta,c} = 16175 + 6769 = 22944 \text{ kNm/rad (1 plane of rods)}$$

$$K_{\theta,c} = 45888 \text{ kNm/rad (2 plane of rods)}$$

The measured column side stiffness under fully reversed loading for test 2 is 32692 kNm/rad. The calculated stiffness using the analytical expressions 40% stiffer than the measured stiffness from the full-scale tests.

- Using the simplification by Eqs. (I.28) and (I.29):

$$K_{\theta}^{(c1-c4)} \approx \frac{634^2 \cdot 110/2}{(110/15) \cdot \sin(20)^2 + \cos(20)^2} \approx 12699,234 \text{ kNmm/rad}$$
$$\rightarrow 12699 \text{ kNm/rad (1 plane of rods)}$$

$$K_{\theta}^{(c2-c3)} \approx \frac{428^2 \cdot 110/2}{(110/15) \cdot \sin(20)^2 + \cos(20)^2} \approx 5787,441 \text{ kNmm/rad}$$
$$\rightarrow 5787 \text{ kNm/rad (1 plane of rods)}$$

$$K_{\theta,c} = 12699 + 5787 = 18486 \text{ kNm/rad (1 plane of rods)}$$

$$K_{\theta,c} = 36972 \text{ kNm/rad (2 plane of rods)}$$

c-The connection stiffness:

The stiffness for the connection considering 2 planes of rods:

$$K_{\theta,con} = \left(\frac{1}{45888} + \frac{1}{300000} + \frac{1}{20500} \right)^{-1} = 13530 \text{ kNm/rad}$$

The measured connection stiffness under fully reversed loading for test 2 is 11452 kNm/rad. The calculated stiffness using the analytical expressions is 18% stiffer than the measured stiffness from the full-scale tests.

The stiffness of the connections using the values obtained with the simplified expressions:

$$K_{\theta,con} = \left(\frac{1}{36972} + \frac{1}{300000} + \frac{1}{17135} \right)^{-1} = 11269 \text{ kNm/rad}$$

For both configurations, the analytical expressions presented in subsection 4.3.4 provided reasonable estimates for the stiffness. The estimation of the stiffness was based on the axial stiffness of the threaded rods under fully reversed loading, which presumably yielded a connection stiffness value for fully reversed loading. However, it is also possible to use the axial stiffness of threaded rods under different loading conditions, such as cyclic tension/compression loading to get the corresponding connection stiffness.

References

[1] H. Stamatopoulos, F.M. Massaro, J. Qazi, Mechanical properties of laterally loaded threaded rods embedded in softwood, European Journal of Wood and Wood Products 80(1) (2022) 169-182.

Appendix B

Experimental work on rods inserted parallel to grain into the narrow face of CLT elements

This appendix is awaiting publication and is not included in NTNU Open

Appendix C

Friction shims: experimental work

This appendix is awaiting publication and is not included in NTNU Open

Appendix D

Additional journal paper published during the Ph.D.

Article

Comparative Life Cycle Analysis of Timber, Steel and Reinforced Concrete Portal Frames: A Theoretical Study on a Norwegian Industrial Building

Osama Abdelfattah Hegeir ^{1,*} , Tore Kvande ² , Haris Stamatopoulos ¹  and Rolf André Bohne ² 

¹ Department of Structural Engineering, Norwegian University of Science and Technology (NTNU), Rich. Birkelandsvei 1A, 7491 Trondheim, Norway; haris.stamatopoulos@ntnu.no

² Department of Civil and Environmental Engineering, Norwegian University of Science and Technology (NTNU), Rich. Birkelandsvei 1A, 7491 Trondheim, Norway; tore.kvande@ntnu.no (T.K.); rolf.bohne@ntnu.no (R.A.B.)

* Correspondence: osama.a.s.a.hegeir@ntnu.no; Tel.: +47-980-77404

Abstract: The construction industry is a big contributor to greenhouse gas emissions, which has a negative environmental impact. Several studies have highlighted the possibility of using timber to reduce the environmental impact of construction. Most of these studies have focused on residential buildings, but little attention has been devoted to industrial buildings. In this paper, an attempt is made to compare the environmental impact of using timber, steel, and reinforced concrete in industrial buildings using life cycle assessment. The system boundary was set to cradle-to-gate with transportation to construction site due to the limitation of data, and only the quantities of the main structural system are considered. Portal frames with variable spans were designed using the three materials to meet similar load carrying capacity. Reinforced concrete was used in the foundation of all frames. The results of the comparative study show that timber has, by a good margin, better environmental impact than reinforced concrete and steel, due to the carbon stored in the wood. The results also show that reinforced concrete and steel alternatives have similar environmental impacts. The findings of this study agree with the findings of other studies on residential buildings.

Keywords: LCA; GHG emissions; CO₂ emissions; industrial buildings; timber; concrete; steel; portal frame



Citation: Hegeir, O.A.; Kvande, T.; Stamatopoulos, H.; Bohne, R.A.

Comparative Life Cycle Analysis of Timber, Steel and Reinforced Concrete Portal Frames:

A Theoretical Study on a Norwegian Industrial Building. *Buildings* **2022**, *12*, 573. <https://doi.org/10.3390/buildings12050573>

Academic Editors: Luis Filipe Almeida Bernardo and Miguel Nepomuceno

Received: 17 March 2022

Accepted: 25 April 2022

Published: 29 April 2022

Publisher's Note: MDPI stays neutral with regard to jurisdictional claims in published maps and institutional affiliations.



Copyright: © 2022 by the authors. Licensee MDPI, Basel, Switzerland. This article is an open access article distributed under the terms and conditions of the Creative Commons Attribution (CC BY) license (<https://creativecommons.org/licenses/by/4.0/>).

1. Introduction

The world population is constantly increasing [1], implying a higher need for urbanization. However, the construction industry is a big contributor to worldwide greenhouse gas (GHG) emissions. In 2010, 19% of the total global energy-related GHG emissions were related to the construction industry [2]. GHG emissions are linked to the serious problem of climate change and its negative environmental impacts, such as extreme temperatures, heavy rains, and droughts [3]. Given the need for urbanization and the need for reducing the GHG emissions within the construction industry, the choice of construction material is of significant importance.

Timber is a good alternative to concrete and steel as a construction material, due to the high strength/weight ratio. Comparative life cycle analysis (LCA) studies highlight the positive environmental impact of using cross laminated timber (CLT) instead of reinforced concrete in multistorey buildings [4–9]. Skullestad et al. [10] performed LCA on buildings up to 21 floors and concluded that timber buildings have 34–84% lower climate change impact than reinforced concrete buildings with the same load capacity. Dodoo et al. [11] pointed out that the use of low-energy multi-storey timber buildings can further reduce carbon emissions by 8–9% compared to conventional multi-storey timber buildings. Dodoo et al. [12] studied the carbonation in the post-use phase of concrete and

concluded that it does not change the validity that timber buildings have lower carbon emissions than concrete buildings. Gong et al. [13] performed LCA on concrete, steel, and timber residential buildings, the results show that the energy consumption over the life cycle of the timber building is approximately 30% lower than the concrete and steel buildings. According to Börjesson et al. [14], the efficiency of using timber as a construction material in a building highly depends on how timber is handled after the demolition of the building.

Industrial buildings, such as factories or warehouses, are traditionally constructed using structural steel as the main structural material. The structural system of such structures can vary depending on the span of the structural system. The most commonly used systems in practice are portal frames and trusses. The truss system is preferred over the portal frame system when the cross sections of the portal frame system become very heavy and non-economic [15]. Trusses can be built using timber or steel. However, the truss system is not common if reinforced concrete is to be used, due to the difficulty of the formwork and, thus, portal frames are usually used.

Previous studies have shown that using timber as a construction material instead of structural steel or reinforced concrete can result in reduced GHG emissions and, therefore, more environmentally friendly construction [4–14]. However, the focus was mainly on multistorey residential buildings, and less focus was given to industrial buildings. The material demands for multistorey buildings are different from industrial buildings and not linearly proportional. One example is, e.g., the amount of concrete in the foundations, which depends on the number of storeys, or the weight of the structure, but not linearly. Moreover, when it comes to timber buildings, different criteria are likely to govern the structural design of multistorey buildings (serviceability limit state) [16–19] and industrial buildings (ultimate limit state). The possibility of using timber as a structural material in industrial buildings to reduce the environmental impact of the construction process has not been investigated. This paper is an attempt to highlight the possibility of reducing the environmental impact of constructing industrial buildings by using timber as a construction material.

In this paper, the environmental impact of using timber, structural steel, and reinforced concrete in the construction of industrial buildings is compared using LCA. The focus of this paper is given to the portal frame as a structural system, since it is easily constructable using all three different materials of concern. The study is conducted on an imaginary industrial building located in Oslo. The load-bearing structure is calculated for all three materials (in accordance with the relevant Eurocodes) giving material volume for the LCA.

2. Methodology

2.1. Structural System and Layout

The structural system of this study is to cover a rectangular area of $W \times L$ plan dimensions, as shown in Figure 1. The portal frame was designed based on timber, structural steel, and reinforced concrete; all the three alternatives are shown in Figure 1. All frames have concrete foundations, as shown in Figure 1. Steel dowels and bolts are used in the connections of timber frames. Illustrative drawings of the column–foundation connection, apex connection, and beam–column connection are shown in Figure 2. The out of plane spacing S between adjacent portal frames varies depending on the material to achieve economic design of each material. The slope of the roof is assumed to be 1:5 for all frames. Two variations of the span are chosen for each material, one short span of 10 m and one long span of 25 m. This is mainly to study the effect of the span and to capture any non-linearity in the results caused by the span. The dimensions are summarized in Table 1.

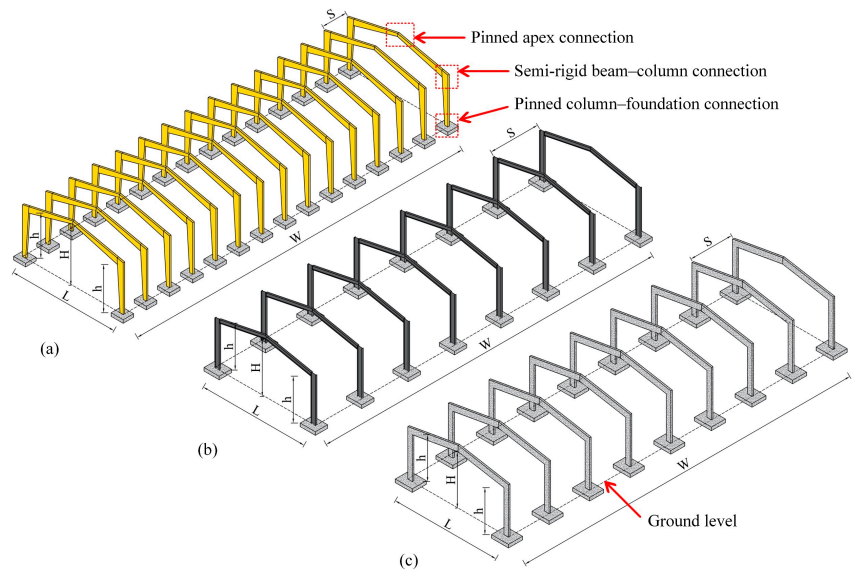


Figure 1. 3D drawing of the portal frames: (a) timber frames; (b) steel frames; (c) reinforced concrete frames.

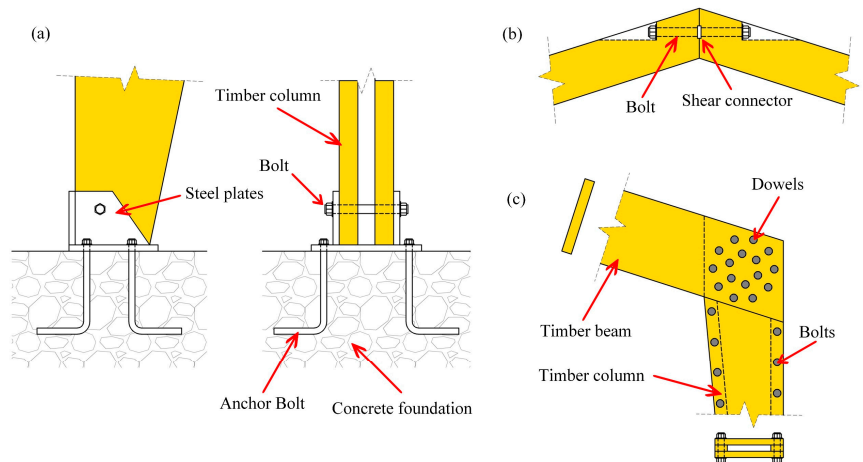


Figure 2. Illustrative drawings of connections in timber frames: (a) pinned column–foundation connection; (b) pinned apex connection; (c) semi-rigid beam–column connection.

Table 1. Summary of the dimensions of the main system.

Material	Width W (m)	Length L (m)	Spacing S (m)	Height at Apex H (m) *	Height at the Corner h (m) *
Timber	42.00	10.00/25.00	3.00	6.00/7.50	5.00
Steel	42.00	10.00/25.00	6.00	6.00/7.50	5.00
Concrete	42.00	10.00/25.00	5.25	6.00/7.50	5.00

* Measured from the ground level shown in Figure 1.

2.2. Assumptions and Simplifications

In this study, the following assumptions, simplifications, and limitations apply:

- For all frames, the design is performed such that the clear height at the corner is 5 m;
- All secondary elements were not included in the structural design; therefore, their own weight was assumed to be 0.30 kN/m² for all frames, this is to facilitate the comparison;
- All frames are subjected to a uniform live load of 0.40 kN/m² at the roof as recommended by EN1991-1-1 [20];
- The peak wind pressure is 0.65 kN/m², this corresponds to the Oslo area ($V_b = 26$ m/s) with terrain category of II as defined by EN1991-1-4 [21];
- The characteristic snow load is 2.80 kN/m², this corresponds to the Oslo area with altitude of less than 100 m EN1991-1-3 [22];
- The columns were assumed pinned to the foundations for timber, steel and concrete frames;
- The corner and apex connections of steel and concrete frames were assumed rigid. The apex connection of timber frames was assumed pinned, and the corner connection of timber frames was assumed semi-rigid (refer to Figure 2);
- The foundations of all frames are isolated footing and made of reinforced concrete;
- The concrete used in reinforced concrete frames and the foundations of all frames is C30/C37 (30 MPa cylinder strength or 37 MPa cube strength) and the reinforcing bars are of quality B500C available in the Norwegian market (500 MPa yield strength). The maximum aggregate size is 20 mm. The exposure class is XC3. The design life is 50 years. The previous assumptions result in a minimum cover of 35 mm, a maximum water content of 0.55, and a minimum cement content of 300 kg/m³ [23];
- The structural steel used in the beams and columns of the steel portal frames is of quality S460, available in the Norwegian market (460 MPa yield strength);
- The timber used in the beams and columns of the timber frames is glulam of strength class GL30c defined by EN14080 [24];
- The steel dowels and bolts used in the connections of timber frames were assumed of a strength class 8.8 (800 MPa ultimate strength and 640 MPa yield strength) as defined by ISO 898 [25];
- The structural steel used in the connections of the timber frames is of quality S460 available in the Norwegian market (460 MPa yield strength);
- The load combination used in the design of all frames is the fundamental load combination defined by equation 6.10 in EN1990 [26] ($\gamma_G = 1.20$, $\gamma_Q = 1.50$, $\psi_0 = 0.70$ for live load and snow load, and 0.60 for wind load, as defined by the Norwegian National Annex);
- The structural design for all frames was performed based on the respective Eurocode for each material, EN1995-1-1 [27] for timber, EN1993-1-1 [28] for steel, and EN1992-1-1 [29] for concrete;
- All frames of the three materials are dimensioned to meet similar load carrying capacity;
- The structural design and the calculation of quantities were performed only for the main structural system, no secondary structural elements (purlins, slabs, etc.) or covering were included.

2.3. LCA Background, Functional Unit, and System Boundaries

LCA is a standardized method used to quantify the environmental impacts of a product/service during the whole life cycle starting from material extraction up until disposal. The NS-EN ISO 14040:2006 [30] guidelines describe the principles and the framework of the LCA, while NS-EN ISO 14044:2006 [31] describes detailed requirements needed when performing LCA. For the case of buildings, NS-EN 15978:2011 [32] gives calculation methods to assess the environmental impacts of newly built and existing buildings.

The assessment of the environmental impacts is done using some environmental indicators. An environmental indicator is a numeric value that evaluates the environmental impact. According to NS-EN 15804:2012 [33], the core environmental impact indicator for climate change is the global warming potential (GWP), and the unit of the GWP is

kg CO₂-eq. The functional unit in this paper is set to kg CO₂-eq. per square meter of the area (m²), shown in Figure 1 by dotted line (*LxW*), to get a realistic comparison between the three alternatives.

According to NS-EN 15978:2011 [32], the system boundaries are divided into five stages: the product stage (A1–A3), construction process stage (A4–A5), use stage (B1–B7), end of life stage (C1–C4), and benefits and loads beyond the system boundary (D). In this paper, since the main purpose is to compare the different alternative materials and due to the poor data availability, the system boundary is set to cradle-to-gate with the option of adding A4 (transportation to construction site) as defined by NS-EN 15804:2012 [33], which represents A1–A4.

2.4. Calculation of Emissions

To calculate the GWP, environmental product declarations (abbr. EPDs) are used. The EPDs provide the value of several environmental impact indicators, including GWP, for the different stages defined in NS-EN 15978:2011 [32]. In this paper, the EPDs retrieved from the Norwegian EPD Foundation [34] were used. In all calculations, the exact EDP of each product was used [35–39]. However, for dowels and bolts which are used in the connections of timber frames, the exact EDPs were not available, therefore, the EDP of threaded steel anchors was used for both [40].

3. Structural Design and Quantities

In this section, the details of the structural analysis and design of all frames are explained. The structural analysis of all frames is performed using CSI SAP2000 [41]. The structural design and dimensioning are performed using CSI SAP2000 [41] and Excel sheets developed by the authors. The quantities of all materials are also shown.

3.1. Timber Frames

The structural design is performed assuming glulam of strength class GL30c. Due to the moderate stiffness of timber, rigid connections cannot be achieved, therefore, the corner connections were assumed as semi-rigid in the structural analysis models. The connections of the timber portal frame were designed based on dowel-type connections as shown in Figure 2; therefore, steel is used in the connections and is calculated in the quantities. The structural design is performed using Excel sheets developed by the authors, since no design of timber available in CSI SAP2000 [41]. The total quantities of the timber frames, both the 10 m span and the 25 m span are summarized in Table 2.

Table 2. Quantities of the timber frames.

Span (m)	The Portal Frame				Foundations	
	Timber CL30c (m ³)	Steel Dowels 8.8 (kg)	Steel Bolts 8.8 (kg)	Steel Plates S460 (kg)	Concrete C30/C37 (m ³)	Reinforcement B500C (kg)
10.00	37.08	390.62	672.23	1180.41	7.68	338.75
25.00	94.91	1302.29	855.69	1757.46	18.75	651.03

3.2. Steel Frames

CSI SAP2000 [41] is used to perform the design of structural elements since it performs the design based on the EN1993-1-1 [28] together with the Norwegian national annex. The total quantities of the steel frames, both the 10 m span and the 25 m span are summarized in Table 3.

Table 3. Quantities of the steel frames.

Span (m)	The Portal Frame		Foundations	
	Steel S460 (kg)	Concrete C30/C37 (m ³)	Reinforcement B500C (kg)	
10.00	7373.18	8.06	297.82	
25.00	37630.66	22.04	670.44	

3.3. Reinforced Concrete Frames

Together with Excel sheets developed by the authors, CSI SAP2000 [41] is used to perform the design of structural elements since it performs the design based on the EN1992-1-1 [29] together with the Norwegian national annex. The total quantities of the concrete frames, both the 10 m span and the 25 m span are summarized in Table 4.

Table 4. Quantities of the reinforced concrete frames.

Span (m)	The Portal Frame		Foundations	
	Concrete C30/C37 (m ³)	Reinforcement B500C (kg)	Concrete C30/C37 (m ³)	Reinforcement B500C (kg)
10.00	23.11	3776.48	10.08	374.74
25.00	120.65	22109.31	30.13	836.82

4. Results, Discussion, and Limitations

The quantities summarized in Tables 2–4 are used together with the respective EDPs provided by Norwegian EPD Foundation [34] to calculate the GWP/m² for all frames. The GWP extracted from the EDPs are summarized in Table 5. The results of the total GWP/m² are summarized in Table 6 and are shown in Figure 3.

Table 5. Summary of the GWP for different material [34].

Material	GWP (A1–A4)	Unit
Glulam (GL30c)	−597.70	kg CO ₂ -eq./m ³ timber
Steel dowels and bolts used for timber frames' connections (strength class 8.8)	2.90	kg CO ₂ -eq./kg steel
Steel plates (S460)	2.47	kg CO ₂ -eq./kg steel
Concrete (C30/C37)	212.26	kg CO ₂ -eq./m ³ concrete
Steel reinforcement (B500C)	0.40	kg CO ₂ -eq./kg steel
Structural steel I beams (S460)	1.21	kg CO ₂ -eq./kg steel

Table 6. GWP/m² for all frames.

Item	Span (m)	Timber	Steel	Concrete
		GWP (kg CO ₂ – eq./m ²)		
Main frame	10.00	−52.77	21.19	15.31
	25.00	−54.03	43.25	32.88
Foundations	10.00	4.21	4.36	5.45
	25.00	4.04	4.71	6.41
Steel fasteners and plates	10.00	14.27	0.00	0.00
	25.00	10.09	0.00	0.00
Total	10.00	−34.30	25.55	20.76
	25.00	−39.90	47.96	39.29

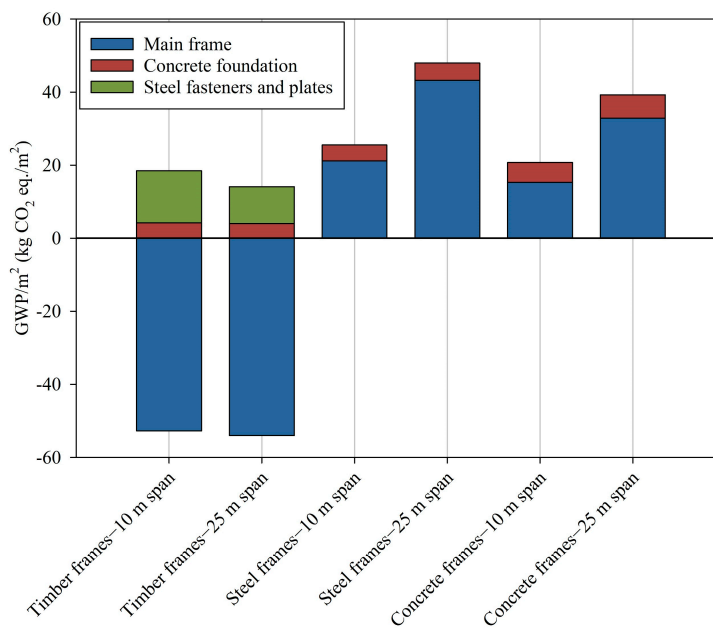


Figure 3. Comparison between the GWP/m² for all frames.

As shown in Figure 3 and summarized in Table 6, steel frames have a total GWP/m² (main frames, foundation, and steel fasteners and plates) that is higher than the concrete frames and much higher than the timber frames. This applies for both the 10-m span and the 25-m span frames. In the timber frames, although concrete is used in the foundations and steel is used in the connections, the net GWP/m² is negative due to the fact that timber stores CO₂. It is notable to mention that finetuning the design or using materials with lower GWPs, such as low-carbon concrete or recycled steel, might yield different results. However, such scenarios are not discussed in this paper. Furthermore, the end-of-life and circularity options (C and D) for timber, steel, and concrete frames should be taken into consideration.

As reinforced concrete is used for the foundation of all frames, it is also of interest to compare only the GWP/m² of the foundations. The results are shown in Table 6 and depicted in Figure 3. The foundations of timber frames have the lowest GWP/m² for both the small span and large span. This is because timber is a light material with good stiffness/weight ratio compared to steel and concrete and, hence, smaller foundations can be used. The GWP/m² for the foundations of the concrete frames are larger than the GWP/m² for the foundations of the steel frames for the small and large span frames. This is due to steel being lighter than concrete and having a higher stiffness/weight than concrete, which results in overall smaller foundations.

The use of different materials in the design and construction of the main structural system (portal frame) implies the possible use of different secondary structural elements, non-structural elements, insulation, etc. This will influence the total GWP/m² of the three alternatives (timber, steel, and concrete). However, in this paper, the focus is given to the main structural elements and other elements are assumed to be the same for the three alternatives. In some cases, and due to practical considerations, this assumption might not be valid.

5. Conclusions and Future Work

A portal frame with a small span of 10 m and a large span of 25 m was designed using timber, steel, and reinforced concrete to give the material quantities for LCA. A cradle-to-gate with the option of adding A4 (A1–A4) LCA is performed to compare the GWP of the three alternative materials. In performing the LCA, we could conclude that:

1. Considering the total GWP/m² (main frames, foundations, and steel fasteners and plates), the steel frames have a GWP/m² that is higher than the concrete frames and much higher than the timber frames for both the 10-m span and 25-span frames;
2. Considering only the foundations, the timber frames have the lowest GWP/m², while the concrete frames have the highest GWP/m² for both the 10-m span and 25-span frames.

Due to the limited data available, and to simplify the comparison, only the main structural elements were included in the LCA. This is done under the assumption that all other materials are the same, which in some cases may not be practical. There is a need for a more holistic LCA that includes the main and the secondary structural elements, and the non-structural elements to be able to fully judge the environmental impact of the different alternative materials. Furthermore, due to the limited data available for the operational conditions, demolishing, and disposal strategy, only cradle-to-gate with the option of adding A4 (A1–A4) was considered. To get a better understanding, it is worth including all stages in future studies to validate the findings of this paper. Since the focus in this study was given to portal frames, future work on different structural systems such as trusses or arches can be of interest.

Author Contributions: O.A.H., conceptualization, formal analysis, methodology, visualization, writing—original draft; T.K., H.S. and R.A.B., conceptualization, methodology, supervision, writing—review and editing. All authors have read and agreed to the published version of the manuscript.

Funding: This research received no external funding.

Data Availability Statement: The data presented in this study are available on request from the corresponding author.

Conflicts of Interest: The authors declare no conflict of interest.

References

1. Department of Economic and Social Affairs, United Nations. Population Dynamics, World Population Prospects 2019. Available online: <https://population.un.org/wpp/Graphs/Probabilistic/POP/TOT/900> (accessed on 25 January 2022).
2. IPCC. *Climate Change 2014: Mitigation of Climate Change. Contribution of Working Group III to the Fifth Assessment Report of the Intergovernmental Panel on Climate Change*; Cambridge University Press: Cambridge, UK; New York, NY, USA, 2014.
3. IPCC. *Summary for Policymakers. In Global Warming of 1.5 °C. An IPCC Special Report on the Impacts of Global Warming of 1.5 °C Above Pre-Industrial Levels and Related Global Greenhouse Gas Emission Pathways, in the Context of Strengthening the Global Response to the Threat of Climate Change, Sustainable Development, and Efforts to Eradicate Poverty*; World Meteorological Organization: Geneva, Switzerland, 2018; 32p.
4. Liu, Y.; Guo, H.; Sun, C.; Chang, W.S. Assessing cross laminated timber (CLT) as an alternative material for mid-rise residential buildings in cold regions in China—A life-cycle assessment approach. *Sustainability* **2016**, *8*, 1047. [[CrossRef](#)]
5. Guo, H.; Liu, Y.; Meng, Y.; Huang, H.; Sun, C.; Shao, Y. A Comparison of the energy saving and carbon reduction performance between reinforced concrete and cross-laminated timber structures in residential buildings in the severe cold region of China. *Sustainability* **2017**, *9*, 1426. [[CrossRef](#)]
6. Chen, Z.; Gu, H.; Bergman, R.D.; Liang, S. Comparative life-cycle assessment of a high-rise mass timber building with an equivalent reinforced concrete alternative using the athena impact estimator for buildings. *Sustainability* **2020**, *12*, 4708. [[CrossRef](#)]
7. Eliassen, A.R.; Faanes, S.; Bohne, R.A. Comparative LCA of a concrete and steel apartment building and a cross laminated timber apartment building. *IOP Conf. Ser. Earth Environ. Sci.* **2019**, *323*, 012017. [[CrossRef](#)]
8. Liang, S.; Gu, H.; Bergman, R.; Kelley, S.S. Comparative life-cycle assessment of a mass timber building and concrete alternative. *Wood Fiber Sci.* **2020**, *52*, 217–229. [[CrossRef](#)]

9. Sandanayake, M.; Lokuge, W.; Zhang, G.; Setunge, S.; Thushar, Q. Greenhouse gas emissions during timber and concrete building construction—A scenario based comparative case study. *Sustain. Cities Soc.* **2018**, *38*, 91–97. [CrossRef]
10. Skullestad, J.L.; Bohne, R.A.; Lohne, J. High-rise Timber Buildings as a Climate Change Mitigation Measure—A Comparative LCA of Structural System Alternatives. *Energy Procedia* **2016**, *96*, 112–123. [CrossRef]
11. Dodo, A.; Gustavsson, L.; Sathre, R. Lifecycle carbon implications of conventional and low-energy multi-storey timber building systems. *Energy Build.* **2014**, *82*, 194–210. [CrossRef]
12. Dodo, A.; Gustavsson, L.; Sathre, R. Carbon implications of end-of-life management of building materials. *Resour. Conserv. Recycl.* **2009**, *53*, 276–286. [CrossRef]
13. Gong, X.; Nie, Z.; Wang, Z.; Cui, S.; Gao, F.; Zuo, T. Life cycle energy consumption and carbon dioxide emission of residential building designs in Beijing: A comparative study. *J. Ind. Ecol.* **2012**, *16*, 576–587. [CrossRef]
14. Börjesson, P.; Gustavsson, L. Greenhouse gas balances in building construction: Wood versus concrete from life-cycle and forest land-use perspectives. *Energy Policy* **2000**, *28*, 575–588. [CrossRef]
15. Segui, W.T. *Steel Design*, 5th ed.; Cengage Learning: Stamford, USA, 2013.
16. Abrahamsen, R. Mjöstårnet-Construction of an 81 m tall timber building. In Proceedings of the 23 Internationales Holzbau-Forum (IHF), Garmisch-Partenkirchen, Germany, 30 November–2 December 2022.
17. Stamatopoulos, H.; Malo, K.A. Wood Frame Solutions for Free Space Design in Urban Buildings (WOODSOL). In Proceedings of the 7th Forum Wood Building Nordic, Växjö, Sweden, 27–28 September 2018.
18. Bjertnæs, M.A.; Malo, K.A. Wind-Induced Motions of “Treet”—A 14-Storey Timber Residential Building in Norway. In Proceedings of the World Conference on Timber Engineering (WCTE), Quebec City, QC, Canada, 10–14 August 2014.
19. Vilguts, A.; Stamatopoulos, H.; Malo, K.A. Parametric analyses and feasibility study of moment-resisting timber frames under service load. *Eng. Struct.* **2021**, *228*, 111583. [CrossRef]
20. *NS-EN 1991-1-1:2002+NA:2019*; Actions on Structures—Part 1-1: General Actions—Densities, Self-Weight, Imposed Loads for Buildings. European Committee for Standardization: Brussels, Belgium, 2019.
21. *NS-EN 1991-1-4:2005+AC:2010*; Actions on Structures—Part 1-4: General Actions—Wind Actions. European Committee for Standardization: Brussels, Belgium, 2010.
22. *NS-EN 1991-1-3:2003+A1:2015+NA:2018*; Actions on Structures—Part 1-3: General Actions—Snow Loads. European Committee for Standardization: Brussels, Belgium, 2018.
23. Mosley, B.; Bungey, J.; Hulse, R. *Reinforced Concrete Design to Eurocode 2*, 7th ed.; Palgrave Macmillan: London, UK, 2012.
24. *NS-EN 14080:2013+NA:2016*; Timber Structures—Glued Laminated Timber and Glued Solid Timber—Requirements. European Committee for Standardization: Brussels, Belgium, 2016.
25. *NS-EN ISO 898-1:2013*; Mechanical Properties of Fasteners Made of Carbon Steel and Alloy Steel—Part 1: Bolts, Screws and Studs with Specified Property Classes—Coarse Thread and Fine Pitch Thread. European Committee for Standardization: Brussels, Belgium, 2013.
26. *NS-EN 1990:2002+A1:2005+NA:2016*; Basics of Structural Design. European Committee for Standardization: Brussels, Belgium, 2016.
27. *NS-EN 1995-1-1:2004+A1:2008+NA:2010*; Design of Timber Structures—Part 1-1: General—Common Rules and Rules for Buildings. European Committee for Standardization: Brussels, Belgium, 2016.
28. *NS-EN 1993-1-1:2005+A1:2014+NA:2015*; Design of Steel Structures—Part 1-1: General Rules and Rules for Buildings. European Committee for Standardization: Brussels, Belgium, 2015.
29. *NS-EN 1992-1-1:2004+A1:2014+NA:2021*; Design of Concrete Structures—Part 1-1: General Rules and Rules for Buildings. European Committee for Standardization: Brussels, Belgium, 2021.
30. *NS-EN ISO 14040:2006*; Environmental Management—Life Cycle Assessment—Principles and Framework. European Committee for Standardization: Brussels, Belgium, 2006.
31. *NS-EN ISO 14044:2006*; Environmental management—Life Cycle Assessment—Requirements and Guidelines. European Committee for Standardization: Brussels, Belgium, 2006.
32. *NS-EN 15978:2011*; Sustainability of Construction Works—Assessment of Environmental Performance of Buildings—Calculation Method. European Committee for Standardization: Brussels, Belgium, 2011.
33. *NS-EN 15804:2012+A2:2019*; Sustainability of Construction Works—Environmental Product Declarations—Core Rules for the Product Category of Construction Products. European Committee for Standardization: Brussels, Belgium, 2019.
34. Norwegian EPD Foundation. Available online: <https://www.epd-norge.no/epder/> (accessed on 27 January 2022).
35. Standard Limtrejelke-Moelven Limtre AS. Available online: <https://www.epd-norge.no/epder/> (accessed on 27 January 2022). (In Norwegian)
36. Lavkarbonbetong kl. A B35-M45 D.16 Uredusert, Synk 200 mm, Standard FA-Helgeland Betong. Available online: <https://www.epd-norge.no/epder/> (accessed on 27 January 2022). (In Norwegian)
37. Bjelker og Formstål-Norsk Stål AS. Available online: <https://www.epd-norge.no/epder/> (accessed on 27 January 2022). (In Norwegian)
38. Kamstål til bruk i betong-Norsk Stål AS. Available online: <https://www.epd-norge.no/epder/> (accessed on 27 January 2022). (In Norwegian)

-
39. Varmvalsede stålplater-Norsk Stål AS. Available online: <https://www.epd-norge.no/epder/> (accessed on 27 January 2022). (In Norwegian)
 40. Permanent Bar Anchor 43 GEWI @Plus-Dywidag Norge AS. Available online: <https://www.epd-norge.no/epder/> (accessed on 27 January 2022).
 41. CSI SAP2000 Structural Analysis and Design. Available online: <https://www.csiamerica.com/products/sap2000> (accessed on 21 January 2022).

ISBN 978-82-326-7876-1 (printed ver.)
ISBN 978-82-326-7875-4 (electronic ver.)
ISSN 1503-8181 (printed ver.)
ISSN 2703-8084 (online ver.)



NTNU

Norwegian University of
Science and Technology